VINCENT KÜMMERER

STORM PROCESSES AND IMPACTS IN HIGH ENERGY GEOLOGICALLY CONTROLLED BARRIERS

Faculdade de Ciências e Tecnologia

2025

VINCENT KÜMMERER

STORM PROCESSES AND IMPACTS IN HIGH ENERGY GEOLOGICALLY CONTROLLED BARRIERS

PhD in Marine, Earth and Environmental Sciences - Geosciences

Performed under the supervision of:

Prof. Dr. Óscar Ferreira

Dr. Carlos Loureiro

Faculdade de Ciências e Tecnologia

2025

STORM PROCESSES AND IMPACTS IN HIGH ENERGY GEOLOGICALLY CONTROLLED BARRIERS

Declaration of authorship

I hereby declare to be the author of this work, which is original and unpublished. Authors and papers consulted are duly cited in the text and are listed in the included references.

Vincent Kümmerer

Date: 31/01/2025

Acknowledgments

I would like to thank my supervisors Carlos and Óscar for dedicating so much time to helping me understand coastal processes and geomorphology. Their constant availability and help made me feel supported throughout this PhD. They gave me the opportunity to freely explore and study in my own direction, while providing feedback and guidance to avoid getting lost. I will always remember waiting and checking the forecast for a powerful storm to hit the Outer Hebrides. Carlos, thank you for exploring and monitoring this beautiful and remote coastline with me. Perhaps one day we can all return to this special place together.

To my office colleagues and friends, Luísa, Jacqueline and Maziar, thank you for putting up with my jokes and supporting me when deadlines made work a bit more challenging. I would also like to thank my colleagues at CIMA for supporting me in this project.

I would also like to thank my friends Jonas, Robi, Niklas, Fabi, Emiel, Lucas, Javi, Emilia, Lahja, Franzi, Aaron and all my other windsurfing, surfing and fishing friends who reminded me that observing and analysing the coast and storms in the field is just as important as studying in front of a computer. Thanks to my childhood friends Konne, Mariano, Simi and Juli for visiting me abroad.

To my family, Elisabeth, Albrecht, Robin and Felix, who have not only inspired me to do what I most want to do, such as pursue a career in science, but have also given me the foundation to feel safe wherever I am.

To my life partners, Valeria and Tala (the dog), thank you for making me feel at home wherever I am, even when we moved 10 houses in Scotland in 6 months. Valeria, thank you for always being there for me throughout this project even though you were in the same position. You always reminded me of my strengths when I was struggling and without you this time would have been much less enjoyable.

Finally, I am grateful for how much Portugal and its people have taught me and shaped me into the person I am today.

This research was supported by the financial support:

- through the Portuguese Foundation of Science and Technology (FCT) with the Ph.D grant 2020.07497.DB
- through the British Society for Geomorphology (BSG) with the grant BSG-2022-30 for data collection.

Abstract

Coastal barriers are dynamic sedimentary landforms exposed to the impacts of coastal storms, with storm-induced erosion and shoreline retreat controlled primarily by the hydrodynamic forcing and barrier morphology. When located in storm-dominated environments, coastal barriers are typically attuned to energetic wave forcing, but extreme events can still result in significant impacts. Moreover, in geologically controlled barrier systems, less studied non-dynamic geological controls such as the underlying bedrock topography or sediment availability can also mediate the morphological response to storms. Aiming to investigate the relative importance of geological controls on storm processes and impacts in coastal barriers along high wave energy coasts, this study integrates morphological and hydrodynamic data, satellite imagery and process-based numerical modelling to explore storm response in the Outer Hebrides barriers in the northwest of Scotland. Improvements to storm identification methods, to assessment and morphodynamic modelling of morphological change at contemporary timescales, resulted in more comprehensive characterisation of storm processes and impacts in high energy, geologically controlled barriers. Results indicate that there is an increasing trend in storm duration in the western coast of Scotland, and that more than the intensity of wave forcing, water level has a critical influence on storm response in barriers with a wide and shallow nearshore profile. However, variation in foreshore configuration, particularly the presence and height of intertidal rock surfaces, can induce a shift in the primary control of storm response from the hydrodynamic forcing to the geological control. Thus, geological constraints are shown to be important controls on storm-induced morphological response in coastal barriers, leading to spatial variability in shoreline change. Overall, the results of this thesis outline that the incorporation of geological controls in storm impact assessments, particularly in the context of rising sea-levels, is critical to better understand storm-induced changes in coastal barriers on high-energy, geologically constrained coastal environments.

Keywords: Coastal Barriers; Geological Control; Coastal Storms; Morphodynamics; Process-Based Modelling.

Resumo

As barreiras sedimentares costeiras são formas de relevo dinâmicas, cuja resposta erosiva a tempestades é principalmente determinada pelo forçamento hidrodinâmico e pela morfologia litoral. Em ambientes costeiros dominados por tempestades, as barreiras sedimentares estão normalmente ajustadas à elevada energia da ondulação, mas a ocorrência de eventos extremos pode resultar em impactos significativos. Para além disso, em barreiras sedimentares controladas geologicamente, a presença de superfícies rochosas ou da disponibilidade de sedimentos pode influenciar a resposta morfológica às tempestades. Tendo como objetivo a investigação dos controlos geológicos nos processos e impactos de tempestades em barreiras sedimentares de litorais expostos a ondulação de elevada energia, este estudo integra a análise de dados morfológicos e hidrodinâmicos, imagens de satélite e modelação numérica para explorar a resposta morfodinâmica a tempestades nas barreiras das Outer Hebrides (Noroeste da Escócia). As melhorias propostas nos métodos de identificação de tempestades, na avaliação e na modelação morfodinâmica da resposta morfológica a tempestades, resultaram numa caraterização mais detalhada dos processos erosivos e dos impactos das tempestades em barreiras controladas geologicamente. Os resultados obtidos indicam um aumento na duração das tempestades na costa oeste da Escócia, e que o nível da água é mais determinante na resposta às tempestades do que a intensidade da ondulação. Contudo, a variação geomorfológica do perfil das barreiras, nomeadamente as características das superfícies rochosas na zona entremarés, pode levar à alteração no controlo da resposta às tempestades, com o domínio do forçamento hidrodinâmico a ser substituído pelo controlo geológico. Assim, verificou-se que os controlos geológicos determinam de forma significativa a resposta morfológica induzida pelas tempestades nas barreiras, promovendo uma variabilidade espacial considerável na dinâmica da linha de costa. Este trabalho evidencia que a incorporação dos controlos geológicos na análise do impacto de tempestades é fundamental para melhor compreender a dinâmica e evolução de barreiras sedimentares costeiras.

Palavras chave: Barreiras Costeiras; Controlo Geológico; Tempestades Costeiras; Morfodinâmica; Modelação Numérica.

Resumo Alargado

A investigação sobre as respostas morfológicas dos sistemas barreira às tempestades tem incidido, principalmente, em zonas costeiras sedimentares sem restrições geológicas e expostas a ondulações moderadamente energéticas. Como tal, os processos morfodinâmicos e as respostas morfológicas dos sistemas barreiras com controlo geológico e expostos a condições de ondulação de elevada energia têm sido menos estudados, havendo ainda a necessidade de melhorar a compreensão dos impactos das tempestades ao longo destas zonas costeiras. Os sistemas barreiras localizados em costas dominadas por tempestades de alta energia estão geralmente adaptados às condições energéticas vigentes. No entanto, os impactos dessas tempestades podem ser significativos quando interagem algumas condições hidrodinâmicas (ex. ondas, maré, sobrelevação). Assume-se, normalmente, que a erosão induzida por tempestades e que o recuo da linha de costa das ilhas barreira são controlados, principalmente, pela intensidade hidrodinâmica e pela morfologia da barreira. No entanto, variáveis não dinâmicas, como a topografia do leito rochoso subjacente e os afloramentos rochosos, podem interferir na resposta morfológica em sistemas de barreira com controlo geológico.

Esta tese investiga a importância relativa dos controlos geológicos nos processos e nas respostas morfológicas a tempestades em barreiras sedimentares costeiras expostas a ondulação de elevada energia. Com esta análise pretende-se melhorar a compreensão dos mecanismos de interacção morfodinâmica entre as superfícies rochosas naturais e os processos morfossedimentares durante tempestades. A investigação desenvolvida abrange várias escalas, desde a caracterização de larga escala da dinâmica climática associada à ocorrência de tempestades costeiras, até à investigação de escala local dos processos morfodinâmicos erosivos em barreiras sedimentares, e está estruturada em quatro objetivos principais: (*i*) identificação e caraterização de tempestades independentes em litorais expostos a ondulação de elevada energia; (*ii*) avaliação da resposta morfológica a tempestades extremas em barreiras sedimentares condicionadas geologicamente; (*iii*) análise do impacto de diferentes configurações geológicas do perfil de praia na variação da linha de costa a diferentes escalas temporais; (*iv*) avaliação de diferentes tipos e níveis de controlo geológico na resposta de barreiras sedimentares a tempestades e determinação da sua importância relativa em relação ao forçamento hidrodinâmico. Este trabalho explora, como estudo de caso, o litoral das ilhas-barreira das Outer Hebrides, localizadas no Noroeste da Escócia, que se distinguem pelo

elevado condicionamento geológico dos seus sistemas barreira, bem como pela exposição a um clima de ondulação extremamente energético e dominado por tempestades. Para alcançar os referidos objetivos, recorreu-se a uma vasta gama de dados e abordagens, incluindo observações de estações de monitorização costeira, dados de modelos climáticos, levantamentos de campo para obtenção de dados topográficos, hidrodinâmicos e sedimentares em barreiras costeiras, análise de imagens de satélite e ainda modelação numérica de processos morfodinâmicos.

Para investigar os processos e impactos de tempestades costeiras, foi necessário identificar e caracterizar de forma robusta os eventos de tempestade com potencial para causar impactos significativos no litoral. Os critérios para identificação de eventos de tempestade são geralmente diferentes entre autores e os limiares utilizados na definição de tempestade são normalmente selecionados de forma arbitrária, sendo frequentemente negligenciada a independência estatística e meteorológica entre eventos de tempestade. Verificou-se, ainda, que a identificação e caraterização de tempestades independentes em litorais expostos a condições de ondulação de elevada energia deve ser adaptada à ocorrência frequente e sequencial de eventos extremos. Nesse sentido, foi desenvolvido um algoritmo de identificação de tempestades especificamente adaptado a ambientes costeiros dominados por tempestades extremas e frequentes. O algoritmo incorpora critérios definidos estatisticamente para identificar eventos independentes a partir de séries temporais de ondulação, coerentes com os processos e escalas meteorológicas regionais, permitindo a individualização de eventos extremos durante períodos de sucessão rápida de tempestades e possibilitando uma caraterização objetiva e robusta das tempestades costeiras. A coerência e robustez na identificação e caracterização de tempestades é particularmente importante quando se avaliam as tendências a longo prazo na frequência e intensidade de eventos extremos. A aplicação do algoritmo de identificação de tempestades a conjuntos de dados de reanálise climática da ondulação para a costa ocidental da Escócia, exposta a condições de elevada energia e localizada no principal trajeto de tempestades do Atlântico Norte, permitiu identificar um aumento significativo da duração das tempestades nas últimas décadas, o que contribuiu para o aumento da potência da ondulação das tempestades que afetam o litoral ocidental da Escócia.

Para a avaliação da resposta morfológica a tempestades em barreiras sedimentares condicionadas geologicamente, foram monitorizadas as alterações morfológicas resultantes de um evento de tempestade extremo e efetuada a modelação da ondulação ao longo das ilhas-

barreira das Outer Hebrides. Os resultados da modelação revelaram que a propagação da ondulação sobre superfícies rochosas pouco profundas conduz a uma dissipação significativa da energia e, por conseguinte, a uma redução da energia das ondas que chega ao litoral. As alterações morfológicas observadas em diferentes barreiras das Outer Hebrides evidenciaram uma resposta morfológica genericamente moderada a baixa, mas com impactos variáveis ao longo da costa. Os impactos observados variaram entre o desenvolvimento de pequenas escarpas nas dunas e o galgamento de barreiras sedimentares. Esta variação foi determinada, essencialmente, pelas características morfológicas das barreiras, pelos declives do terraço de maré e da praia submersa, e controlada pelos afloramentos rochosos, que influenciam fortemente a transformação da ondulação junto à costa. Esta análise indica que, para ocorrerem impactos severos nas ilhas barreira das Outer Hebrides, é necessária uma combinação excecional no forçamento hidrodinâmico das tempestades, em específico, uma ondulação extrema coincidente com marés altas e que os impactos serão mais significativos em zonas com morfologia dunar deprimida e terraços de maré estreitos.

A quantificação da evolução costeira a diferentes escalas temporais exige uma determinação cuidada de indicadores da linha de costa adequados às características geomorfológicas do litoral em análise, em particular quando são utilizados métodos automáticos de deteção da linha de costa. Assim, para avaliar as alterações da linha de costa ao longo das ilhas barreira das Outer Hebrides, foi desenvolvida uma abordagem inovadora que tira partido da crescente resolução espacial e temporal de imagens de satélite. A metodologia implementada assenta na utilização de imagens PlanetScope para determinar a posição da linha de vegetação dunar como indicador da variação da linha de costa, e no seccionamento das barreiras em sectores homogéneos e espacialmente restritos, permitindo a delimitação semi-automática da linha de costa. Verificou-se que a evolução da linha de costa nas ilhas barreira das Outer Hebrides entre 2016 e 2023 se caracterizou por uma taxa de acreção média reduzida (+0.4 m/ano), mas estatisticamente significativa, que provavelmente representa uma tendência de recuperação destas barreiras sedimentares costeiras às tempestades extremas que afetaram o litoral ocidental da Europa nos invernos de 2013 a 2015. Para interpretar a influência do controlo geológicos na evolução da linha de costa, foi proposta uma classificação do tipo de controlo geológico no perfil de praia. A integração das taxas de erosão com a classificação do controlo geológico revelou que variação da linha de costa, a diferentes escalas temporais, depende não só do forçamento

hidrodinâmico e da morfologia da barreira, mas também da presença de superfícies rochosas subtidais e entre-marés ao longo das barreiras, bem como da disponibilidade de sedimentos.

Embora tenha sido demonstrado que os impactos de tempestades em barreiras sedimentares controladas geologicamente são influenciados pela heterogeneidade espacial das superfícies rochosas e pelo forçamento hidrodinâmico, o papel dos diferentes tipos e níveis de controlo geológico nas respostas morfológicas a tempestades encontra-se ainda mal definido e permanece por quantificar. Para investigar a importância relativa dos controlos geológicos e do forçamento hidrodinâmico em condições de tempestade na erosão dunar em barreiras controladas geologicamente, foi implementado o modelo numérico XBeach. Foram simulados um conjunto de cenários baseados nas características oceanográficas e morfológicas das barreiras sedimentares das Outer Hebrides, incluindo diferentes magnitudes nas condições de tempestade e perfis transversais esquemáticos representativos de diferentes tipos e níveis de controlo geológico. Os resultados obtidos com a modelação morfodinâmica demonstraram que a variação do nível máximo da água, relacionada com a sobrelevação meteorológica, tem maior influência na resposta morfológica das barreiras que a intensidade da ondulação durante tempestades. A modelação permitiu, ainda, demonstrar que a presença de superfícies rochosas na zona entre-marés pode efetivamente reduzir a erosão das dunas durante tempestades. Foi possível identificar um limiar a partir do qual o efeito de redução da erosão é mais significativo, e que está relacionado com a diferença vertical entre o nível total da água e a elevação da superfície rochosa. Abaixo desse limiar, verifica-se uma alteração na resposta morfodinâmica da barreira sedimentar, que deixa de ser dominada pelo forçamento hidrodinâmico e passa a ser dominada pelo controlo geológico. Como este limiar é determinado pela diferença entre os níveis de água de tempestade e a elevação da superfície rochosa, a subida do nível médio do mar vai ter implicações na resposta erosiva, sendo a análise desse impacto relevante para a gestão costeira de barreiras sedimentares controladas geologicamente.

Os resultados apresentados nesta tese demonstram que os controlos geológicos não dinâmicos podem ter um papel significativo na resposta das barreiras sedimentares ao impacto induzido por tempestades em locais com clima de ondas de alta energia e dominado por tempestades. Nestes ambientes, será ainda necessária uma análise mais aprofundada sobre os limiares de impacto das tempestades, incorporando o efeito combinado das condições futuras da agitação marítima e do nível do mar, para se obter uma melhor compreensão das trajetórias futuras da

evolução dessas barreiras. A quantificação da diferença entre barreiras geologicamente condicionadas e não condicionadas pode ser utilizada para desenvolver novos conceitos de resiliência adaptados a estas costas complexas, o que é essencial para melhorar a sua gestão.

Palavras chave: Barreiras Costeiras; Controlo Geológico; Tempestades Costeiras; Morfodinâmica; Modelação Numérica.

Table of Contents

List of Figures

List of Tables

List of Acronyms and Abbreviations

β	Bedrock slope
c_f	Dimensionless bed friction coefficient
$E_{W,ub}$	Total storm wave energy at the upper beach
f_w	Wave friction coefficient
$T_{impact,Dt}$	Total dune impact time
ΔEV_{dune}	Total eroded dune volume
1D	One-dimensional
2D	Two-dimensional
BODC	British Oceanographic Data Centre
BSS	Brier Skill Score
CEDA	Centre for Environmental Data Analysis
CEFAS	Centre for Environment Fisheries and Aquaculture Science
CMEMS	Northwest European Shelf Wave Hindcast provided by the Copernicus Marine Service
CSI	Coastal Storm Index
Dir_P	Peak wave direction
EMODnet	European Marine Observation and Data Network (Bathymetry Dataset)
ERA5	European Centre for Medium-Range Weather Forecasts Reanalysis v5
ESRI	Environmental Systems Research Institute, Inc.
FCT	Portuguese Foundation of Science and Technology
GPD	Generalized Pareto Distributions
$H_{m0,HF}$	High-(incident-band) frequency zero-moment wave heights
$H_{m0,LF}$	low-(infragravity) frequency zero-moment wave heights
H_{rms}	Root mean square wave height
H_S	Significant wave height
ID	Independence Duration
IT	Independence Threshold
MHWN	Mean High Water Neap
MHWS	Mean High Water Spring
MIDAS	Met Office Integrated Data Archive System
MLWN	Mean Low Water Neap

MSD	Minimum Storm Duration
MSL	Mean Sea Level
MVL	Measured Vegetation Line
NAO	North Atlantic Oscillation
NCAR	National Centre for Atmospheric Research
NDVI	Normalised Difference Vegetation Index
NOAA	National Oceanic and Atmospheric Administration
NWP	Normalised Wave Power
ONDJFM	Months of October to March
POT	Peak-Over-Threshold
R	Pearson correlation coefficient
RMSE	Root Mean Square Error
RPH_S	Significant wave height return period
RTK-DGNSS	Real Time Kinematic Differential Global Navigation Satellite System
S	Model Skill parameter
SD	Standard Deviation
SDVL	Satellite Derived Vegetation Line
SI	Scatter Index
ST	Storm Threshold
SWAN	Simulating WAves Nearshore (numerical model)
T_P	Peak wave period
UDM2	Unusable Data Mask v2 (Planet Scope product)
XBeach	Morpho-hydrodynamic processes based model
γ	Breaker index

Chapter 1

Introduction

1.1 Motivation

Beaches, situated at the interface between the ocean and the land, represent dynamic unconsolidated sedimentary systems that are exposed to a multitude of processes operating across temporal scales ranging from seconds to millennia and spatial scales extending from single sand grains to tens of kilometres (Jackson & Short, 2020). While these intricate dynamics and constant changes make beaches particularly enjoyable landforms to observe, they also reveal the difficulty on understanding the complex processes that determine their evolution.

A significant proportion of beaches are part of barrier island systems, as these occupy approximately 10% of the world's coastline (Stutz & Pilkey, 2011). Within barrier island systems, the barriers composed by the beaches and dunes function as a buffer to storm impacts and provide shelter for the species-rich back-barrier ecosystems (Otvos, 2012). It is also noteworthy that approximately 60% of barrier island systems globally are impacted by human occupation, which includes buildings and various types of infrastructure (Fenster et al., 2022). Human development on barrier islands hinders their dynamic morphological evolution and adaptability (Kombiadou et al., 2019) to drivers such as sea level rise or changes in storminess. This poses challenges for coastal management, including the maintenance of a functioning coupled human-natural system (Lazarus et al., 2016). Whether or not they are subject to human development, barrier islands are exposed to extreme disturbances such as coastal storms, which can cause substantial erosion and flooding. However, these disturbances also contribute to and determine the dynamics and evolution of barrier systems (Moore & Murray, 2018).

Barrier islands are found along a wide range of coastal areas, from the tropics to the high latitudes of the northern and southern hemispheres, occurring across a considerable range of wave, tide and sedimentary settings (Mulhern et al., 2017).

Distinct from most previously recognised barrier islands systems, Cooper et al. (2012) identified a long, almost continuous sandy coastline on the Atlantic coast of the Outer Hebrides islands in the northwest of Scotland as a barrier island system (Figure 1.1). Hebridean coasts do possess key elements of a barrier island system, but other elements, such as back-barrier lagoons and inlets, differ from Oertel's (1985) classic barrier island model. A key differentiating factor of the Outer Hebrides barrier islands is that they overlie extensive rock platforms. The fact that the barriers are placed and migrate over a gently sloping rock platform makes this system unique among barrier island systems, as the bedrock surface strongly influences barrier form and evolution (Cooper et al., 2012; Pile et al., 2019). Cooper et al. (2012) differentiate the Hebridean barriers from other barrier island systems by describing three important morpho-sedimentary implications imposed by the bedrock platform: (1) the shoreface does not supply sediment to the coast because sediment cover is limited and restricted to small depressions on the rock surface (Kenyon & Pelton, 1979), (2) sediments eroded from the beaches and dunes cannot be deposited on the shoreface because there is no accommodation space, and (3) the morphodynamic response of the barrier is mostly confined to the beach face and dunes.

In addition to the unique geomorphological context of the Hebridean barrier islands, due to its position on the North Atlantic storm track (Shaw et al., 2016), the Outer Hebrides coastline is exposed to one of the most intense wave climates in the world (Lobeto et al., 2024). Intense extratropical cyclones, generally propagating from the western to the north-east Atlantic, are the dominant meteorological system influencing the wave climate off the north-west coast of Scotland (Lodise et al., 2022). As such, this coast is storm dominated (Davies, 1980) and exposed to a very high wave energy climate that is highly seasonal (Santo et al., 2015). However, as energetic offshore waves propagate towards the inshore areas of the Hebridean barriers, they dissipate significant wave energy due to the gently sloping rock platform with offshore islands, rocky reefs, shoals and outcrops (Figure 1.1a, b) (Ramsay & Brampton, 2000). Such a wide and shallow rock platform exerts a very significant influence on coastal processes, making the Outer Hebrides barriers highly geologically constrained (Pile et al., 2019) when compared to the unconstrained sediment-rich conditions of most barrier island systems.

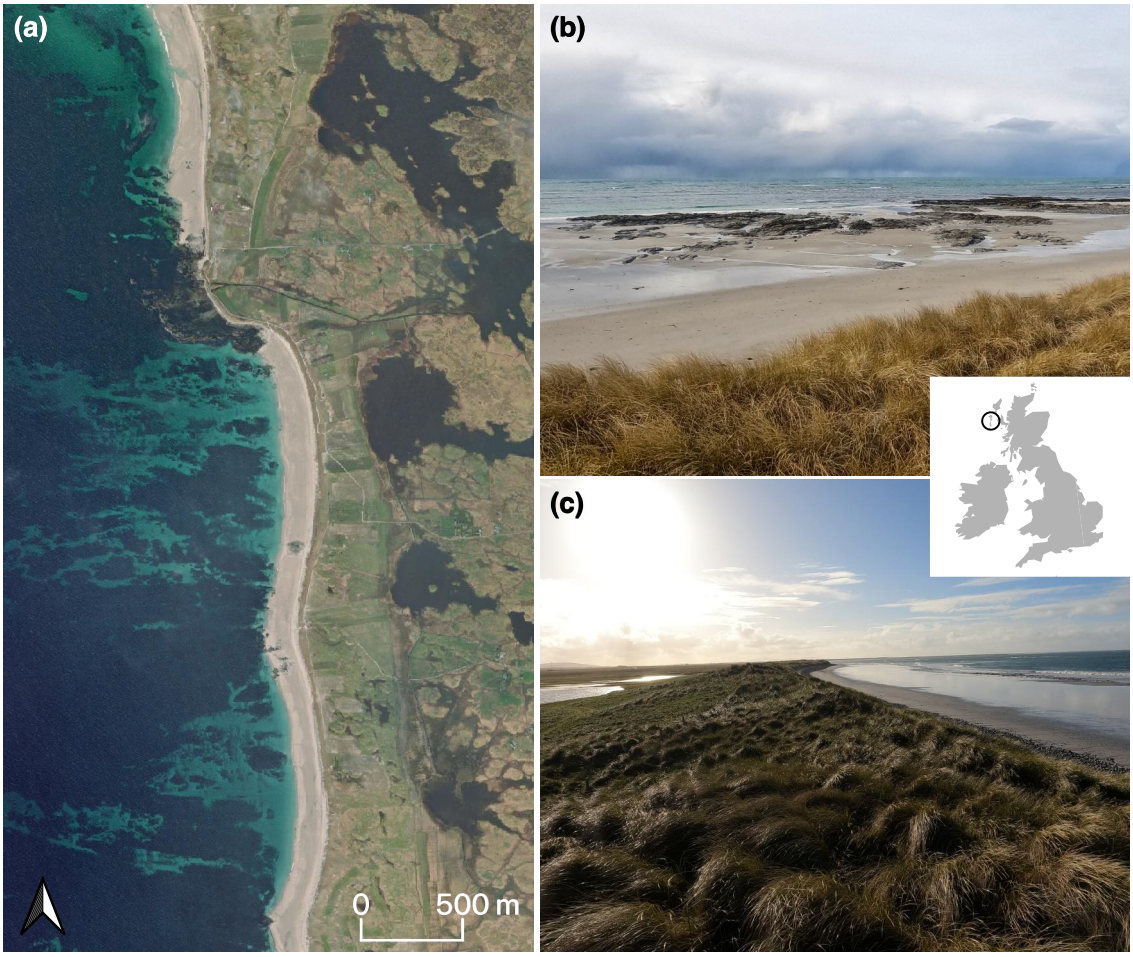

Figure 1.1 Geographical location and images of the Outer Hebrides. **(a)** Satellite image showing a Hebridean barrier island perched on bedrock with impounded lagoons. Source: ESRI world layer. **(b)** Photograph of a barrier with rock outcrops on the beach. **(c)** Photograph of a barrier with impounded lagoons.

The constraints of coastal geology on barrier morphology and hydrodynamics are referred to as 'geological controls'. These are considered as non-dynamic compared to hydrodynamic variables such as waves and tides (Cooper et al., 2018). According to Cooper et al. (2018), non-dynamic inherited geological controls include shoreline orientation, bedrock characteristics (slope, irregularity and erodibility), sediment supply and lithification. In general, unconstrained barriers have abundant sediment and extensive unconsolidated deposits between the underlying substrate or bedrock (Jackson & Cooper, 2009). On the other hand, geologically constrained barriers have limited sediment availability and thin deposits above the underlying substrate, and consequently geological controls are assumed to dominate barrier morphodynamics (Gallop et al., 2020; Jackson et al., 2005; Jackson & Cooper, 2009; Loureiro et al., 2012). In these settings, sediment transport and morphosedimentary changes are reduced and rock surfaces mediate

barrier response to storms (Cooper et al., 2004). However, the role of geological controls in barrier morphodynamics is often overlooked or oversimplified (Cooper et al., 2018). As geologically controlled barrier systems are less studied, the relationships between hydro-morphodynamic processes and the underlying geology are still poorly understood (Gallop et al., 2020; Hapke et al., 2016; Loureiro et al., 2012).

Most barrier islands are unconstrained and in their long-term evolution under rising sea levels they typically move onshore (e.g., Fitz Gerald et al., 2006). In this process, barriers might become more constrained by the presence of geological boundaries in the hinterland or antecedent topographic highs (Cooper et al., 2016; Shawler et al., 2020). As such, in the present context of rising sea levels and continued barrier transgression, previously unconstrained barriers may become geologically controlled and more similar to the Outer Hebrides barrier island system, which could be considered as an end member in terms of barrier island types (Cooper et al., 2012). Understanding geological controls on barrier morphodynamics is not only relevant at long timescales but is also relevant for small scale (< 1000 m) coastal processes influencing beach and dune morphological barrier responses to storms and sea level rise (Wernette et al., 2018). Thus, investigating geological controls can also provide useful insights about how artificial structures, that aim to mimic geological controls exerted by rock surfaces, can be used for coastal protection (e.g., Black & Andrews, 2001).

A thorough understanding of coastal processes in geologically controlled barriers, comprehensively exploring the forcing conditions and considering in detail the morphodynamic interactions between sediments and bedrock, particularly for barriers lying on bedrock (Trenhaile, 2016), is required to analyse barrier island evolution. In high-energy storm-dominated environments, barriers are typically located in rock-bounded coastlines and are adapted to energetic wave forcing (Cooper et al., 2004), and it takes a unique combination of environmental parameters to cause significant storm impacts (Guisado-Pintado and Jackson, 2018). Compared to the medium to low energy environments that are more prevalent along the world's coastline (Lobeto et al., 2024), there are few studies and observations in very high energy environments that have investigated storm processes and impacts, including less use of models to understand barrier response.

The evaluation of the relative importance of geological controls on storm processes and responses in barrier island systems is still an open question in coastal research (Hapke et al., 2016). Although challenging, as current morphodynamic formulations and models

overwhelmingly ignore geological influences and assume unlimited sediment availability (Cooper et al., 2018), this research is paramount to incorporate geological control into modelling efforts, identify limitations and propose adjustments to ensure modelling approaches can be applied to geologically controlled barriers in high-energy coastlines.

1.2 Thesis Objectives

The aim of this thesis is to *investigate the relative importance of geological controls on storm processes and impacts at coastal barriers in high wave energy coasts*. This research will deepen the understanding of how natural rock surfaces interact with sedimentary morphodynamic processes in coastal barriers. A combination of observational data, remote sensing and numerical modelling is used to disentangle the role of geological controls on storm processes and impacts in coastal barriers located in the Outer Hebrides, a high-energy and highly geologically constrained coastal system.

This study is structured around four key objectives, each aligned with the overarching aim. These objectives are structured from ocean scale storm dynamics to storm-induced morphodynamic and hydrodynamic processes at the beach, providing new insights into storm characteristics in high wave energy environments and how their interaction with the coastal geology modulates the storm response of coastal barriers.

1) *Identify and characterise independent storms in high wave energy coasts.*
   There is currently no generalised procedure for identifying independent storms in high-energy coastal environments. However, accurate storm characterisation is critical for understanding storm impacts. Wave height datasets and storm generation mechanisms are assessed to develop an improved storm definition for high wave energy climates.

2) *Assess the response of geologically constrained barriers to extreme storms.*
   Coastlines exposed to high-energy conditions are typically adapted to extreme hydrodynamic forcing. Pre- and post-storm topographic surveys, together with nearshore wave modelling, are used to examine storm-induced topographic changes

and the geological, morphological, and hydrodynamic factors that influence these changes.

3) *Evaluate the impact of varying geological foreshore configurations on shoreline change over monthly to multi-annual scales.*
   Rocky features in the nearshore zone can influence sediment availability and nearshore hydrodynamics, which, in turn, influence shoreline behaviour. Satellite-derived shorelines are analysed to identify geological controls on shoreline change behaviour from the storm to the multi-annual scale.

4) *Examine the influence of different types and levels of geological control on storm response and their relative importance compared to hydrodynamic forcing.*
   Process-based modelling is used together with different hypothetical geological control scenarios to investigate how different geological configurations and forcing conditions affect storm responses at geologically constrained barriers. The model results are used to quantify the influence of different geological controls on the morphological and hydrodynamic barrier response.

1.3 Thesis Outline

The thesis is organised into six chapters, with Chapters 2-5 addressing the four main objectives outlined above. These chapters are based on individual scientific articles that have either been published, are under review, or are in preparation for submission to peer-reviewed international journals. These chapters share the same study area and consequently some aspects of the study area description are repeated. However, each study area description is adapted to highlight information relevant to the specific objectives. Below is a brief overview of the structure of the thesis chapters:

Chapter 1 presents the motivation for the thesis by providing the context for geologically controlled barrier islands, the setting of the study area and geological controls on storm processes and impacts. This is followed by a presentation of the thesis objectives and structure.

Chapter 2 corresponds to a scientific article entitled '*Storm Identification for high-energy wave climates as a tool to improve long-term analysis*' by Vincent Kümmerer, Óscar Ferreira, Valeria Fanti and Carlos Loureiro, published in 2024 in *Climate Dynamics*.

Chapter 3 corresponds to a scientific article entitled '*Muted Morphological Response to Extreme Storms in Geologically Controlled Barrier Islands*' by Vincent Kümmerer, Carlos Loureiro and Óscar Ferreira published in the Proceedings of the Coastal Sediments 2023.

Chapter 4 corresponds to a scientific article entitled '*Distinct Shoreline Behaviour along Storm-Dominated and Geologically Controlled Coastal Barriers'* by Vincent Kümmerer, Óscar Ferreira and Carlos Loureiro, published in 2025 in *Earth Surface Processes and Landforms*.

Chapter 5 corresponds to a scientific article entitled 'Modelling the Relative Importance of Geological Controls on the Response to Storms in Coastal Barriers' by Vincent Kümmerer, Carlos Loureiro, Valeria Fanti and Óscar Ferreira, submitted to *Journal of Geophysical Research Earth Surface*.

Chapter 6 contains a summary of the thesis and the concluding remarks.

1.4 References

Black, K. P., & Andrews, C. J. (2001). *Sandy Shoreline Response to Offshore Obstacles Part 1: Salient and Tombolo Geometry and Shape*. *SPECIAL ISSUE*(29), 82–93.

Cooper, J. A. G., Green, A. N., & Loureiro, C. (2018). Geological constraints on mesoscale coastal barrier behaviour. *Global and Planetary Change*, *168*, 15–34. https://doi.org/10.1016/j.gloplacha.2018.06.006

Cooper, J. A. G., Green, A. N., Meireles, R. P., Klein, A. H. F., Souza, J., & Toldo, E. E. (2016). Sandy barrier overstepping and preservation linked to rapid sea level rise and geological setting. *Marine Geology*, *382*, 80–91. https://doi.org/10.1016/j.margeo.2016.10.003

Cooper, J. A. G., Jackson, D. W. T., Dawson, A. G., Dawson, S., Bates, C. R., & Ritchie, W. (2012). Barrier islands on bedrock: A new landform type demonstrating the role of antecedent topography on barrier form and evolution. *Geology*, *40*(10), 923–926. https://doi.org/10.1130/G33296.1

Cooper, J. A. G., Jackson, D. W. T., Navas, F., McKenna, J., & Malvarez, G. (2004). Identifying storm impacts on an embayed, high-energy coastline: Examples from western Ireland. *Marine Geology*, *210*(1–4), 261–280. https://doi.org/10.1016/j.margeo.2004.05.012

Davies, J. L. (1980). *Geographical variation in coastal development* (2nd Edition). Longman: New York.

Guisado-Pintado, E., Jackson, D.W.T., 2018. Multi-scale variability of storm Ophelia 2017: The importance of synchronised environmental variables in coastal impact. Science of The Total Environment 630, 287–301. https://doi.org/10.1016/j.scitotenv.2018.02.188

Fenster, M. S., Hughes, C. P., & Stutz, M. L. (2022). A Survey of Global Mixed-Energy and Wave-Dominated Barrier Island Distribution and Development. *Journal of Coastal Research*, *00*(0), 12.

Fitz Gerald, D. M., Buynevich, I., & Argow, B. (2006). Model of Tidal Inlet and Barrier Island Dynamics in a Regime of Accelerated Sea Level Rise. *Journal of Coastal Research*, *2*(SI 39), 789–795.

Gallop, S. L., Kennedy, D. M., Loureiro, C., Naylor, L. A., Muñoz-Pérez, J. J., Jackson, D. W. T., & Fellowes, T. E. (2020). Geologically controlled sandy beaches: Their geomorphology, morphodynamics and classification. *Science of The Total Environment*, *731*, 139123. https://doi.org/10.1016/j.scitotenv.2020.139123

Hapke, C. J., Plant, N. G., Henderson, Rachel. E., Schwab, W. C., & Nelson, T. R. (2016). Decoupling processes and scales of shoreline morphodynamics. *Marine Geology*, *381*, 42–53. https://doi.org/10.1016/j.margeo.2016.08.008

Jackson, D. W. T., & Cooper, J. A. G. (2009). Geological Control on Beach Form: Accommodation Space and Contemporary Dynamics. *Journal of Coastal Research*, *Special Issue No. 56 Special Issue No. 56. Proceedings of the 10th International Coastal Symposium ICS 2009*, 69–72.

Jackson, D. W. T., Cooper, J. A. G., & del Rio, L. (2005). Geological control of beach morphodynamic state. *Marine Geology*, *216*(4), 297–314. https://doi.org/10.1016/j.margeo.2005.02.021

Jackson, D. W. T., & Short, A. D. (2020). *Sandy beach morphodynamics*. https://www.sciencedirect.com/science/book/9780081029275

Kenyon, N. H., & Pelton, C. D. (1979). *Seabed conditions west of the Outer Hebrides* (95; p. 16). Institute of Oceanographic Sciences. https://eprints.soton.ac.uk/14378/1/14378-01.pdf

Kombiadou, K., Matias, A., Ferreira, Ó., Carrasco, A. R., Costas, S., & Plomaritis, T. (2019). Impacts of human interventions on the evolution of the Ria Formosa barrier island system (S. Portugal). *Geomorphology*, *343*, 129–144. https://doi.org/10.1016/j.geomorph.2019.07.006

Lazarus, E. D., Ellis, M. A., Brad Murray, A., & Hall, D. M. (2016). An evolving research agenda for human–coastal systems. *Geomorphology*, *256*, 81–90. https://doi.org/10.1016/j.geomorph.2015.07.043

Lobeto, H., Semedo, A., Lemos, G., Dastgheib, A., Menendez, M., Ranasinghe, R., & Bidlot, J.-R. (2024). Global coastal wave storminess. *Scientific Reports*, *14*(1), 3726. https://doi.org/10.1038/s41598-024-51420-0

Lodise, J., Merrifield, S., Collins, C., Rogowski, P., Behrens, J., & Terrill, E. (2022). Global Climatology of Extratropical Cyclones From a New Tracking Approach and Associated Wave Heights From Satellite Radar Altimeter. *Journal of Geophysical Research: Oceans*, *127*(11). https://doi.org/10.1029/2022JC018925

Loureiro, C., Ferreira, Ó., & Cooper, J. A. G. (2012). Geologically constrained morphological variability and boundary effects on embayed beaches. *Marine Geology*, *329–331*, 1–15. https://doi.org/10.1016/j.margeo.2012.09.010

Moore, L. J., & Murray, A. B. (Eds.). (2018). *Barrier Dynamics and Response to Changing Climate*. Springer International Publishing. https://doi.org/10.1007/978-3-319-68086-6

Mulhern, J. S., Johnson, C. L., & Martin, J. M. (2017). Is barrier island morphology a function of tidal and wave regime? *Marine Geology*, *387*, 74–84. https://doi.org/10.1016/j.margeo.2017.02.016

Otvos, E. G. (2012). Coastal barriers—Nomenclature, processes, and classification issues. *Geomorphology*, *139–140*, 39–52. https://doi.org/10.1016/j.geomorph.2011.10.037

Pile, J., Cooper, J. A. G., & Jackson, D. W. T. (2019). Stratigraphy and internal structure of wind-dominated barrier islands (dune and machair) of the Outer Hebrides, Scotland. *Earth Surface Processes and Landforms*, *44*(7), 1482–1493. https://doi.org/10.1002/esp.4579

Ramsay, D. L., & Brampton, A. H. (2000). *Coastal Cells in Scotland: Cells 8 & 9—The Western Isles* (150; Research, Survey and Monitoring, p. 120). Scottish Natural Heritage.

Santo, H., Taylor, P. H., Woollings, T., & Poulson, S. (2015). Decadal wave power variability in the North-East Atlantic and North Sea. *Geophysical Research Letters*, *42*(12), 4956–4963. https://doi.org/10.1002/2015GL064488

Shaw, T. A., Baldwin, M., Barnes, E. A., Caballero, R., Garfinkel, C. I., Hwang, Y.-T., Li, C., O'Gorman, P. A., Rivière, G., Simpson, I. R., & Voigt, A. (2016). Storm track processes and the opposing influences of climate change. *Nature Geoscience*, *9*(9), 656–664. https://doi.org/10.1038/ngeo2783

Shawler, J. L., Ciarletta, D. J., Connell, J. E., Boggs, B. Q., Lorenzo-Trueba, J., & Hein, C. J. (2020). Relative influence of antecedent topography and sea-level rise on barrier-island migration. *Sedimentology*, sed.12798. https://doi.org/10.1111/sed.12798

Stutz, M. L., & Pilkey, O. H. (2011). Open-Ocean Barrier Islands: Global Influence of Climatic, Oceanographic, and Depositional Settings. *Journal of Coastal Research*, *27*(2), 16.

Trenhaile, A. (2016). Rocky coasts — their role as depositional environments. *Earth-Science Reviews*, *159*, 1–13. https://doi.org/10.1016/j.earscirev.2016.05.001

Wernette, P., Houser, C., Weymer, B. A., Everett, M. E., Bishop, M. P., & Reece, B. (2018). Influence of a spatially complex framework geology on barrier island geomorphology. *Marine Geology*, *398*, 151–162. https://doi.org/10.1016/j.margeo.2018.01.011

Chapter 2

Storm Identification for High-Energy Wave Climates as a Tool to Improve Long-term Analysis

Kümmerer, V., Ferreira, Ó., Fanti, V., Loureiro, C., (2024). Storm identification for high-energy wave climates as a tool to improve long-term analysis. *Climate Dynamics* 62, (2207–2226)

Abstract

Coastal storms can cause erosion and flooding of coastal areas, often accompanied by significant social-economic disruption. As such, storm characterisation is crucial for an improved understanding of storm impacts and thus for coastal management. However, storm definitions are commonly different between authors, and storm thresholds are often selected arbitrarily, with the statistical and meteorological independence between storm events frequently being neglected. In this work, a storm identification algorithm based on statistically defined criteria was developed to identify independent storms in time series of significant wave height for high wave energy environments. This approach proposes a minimum duration between storms determined using the extremal index. The performance of the storm identification algorithm was tested against the commonly used peak-over-threshold. Both approaches were applied to 40 and 70-year-long calibrated wave reanalyses datasets for Western Scotland, where the intense and rapid succession of extratropical storms during the winter makes the identification of independent storm events notably challenging. The storm identification algorithm provides results that are consistent with regional meteorological processes and timescales, allowing to separate independent storms during periods of rapid storm succession, enabling an objective and robust storm characterisation. Identifying storms and their characteristics using the proposed algorithm allowed to determine a statistically significant

increasing long-term trend in storm duration, which contributes to the increase in storm wave power in the west of Scotland. The coastal storm identification algorithm is found to be particularly suitable for high-energy, storm-dominated coastal environments, such as those located along the main global extratropical storm tracks.

Keywords: Coastal storm; Storm independence; Wave reanalysis; Wave power; Northeast Atlantic; Western Scotland.

2.1 Introduction

Coastal storms are extreme events characterised by intense hydrodynamic forcing (such as large waves and elevated water levels) leading to beach erosion and coastal flooding, often accompanied by significant social-economic disruption (Harley, 2017). In the context of climate change, the risk associated with coastal storms is increasing due to sea-level rise (Melet et al., 2018), projected changes in coastal extreme wave conditions (Bricheno et al., 2023), and expanding coastal populations (Neumann et al., 2015). Consequently, the analysis of storm events is paramount for coastal management. Characterising past storm events allows to identify the climatic controls and trends in storminess parameters, which are needed for strategic adaptation planning and disaster preparedness in coastal areas (e.g., Garnier et al., 2018). Recent trends and future projections of extreme wave conditions are mostly assessed in global-scale studies (e.g., Young and Ribal, 2019; Timmermans et al., 2020; Lobeto et al., 2021; Morim et al., 2021; Sharmar et al., 2021; Erikson et al., 2022). These often outline different results in the magnitude and direction of historical trends because of diverse data, different assessment periods, and methodologies. For example, Sharmar et al. (2021) show differences in annual extreme wave heights (> 95th percentile) of 1.2 m between different reanalysis products for the same assessment period. Furthermore, Erikson et al. (2022) show that trends in the annual number of days where the daily-maximum significant wave height exceeds 6 m can be negative or positive for different global wave products for the period between 1980 and 2014. Findings in global scale analyses are restricted to ocean basins and are not directly transferable to the coast because nearshore bathymetry is poorly resolved in global models. Therefore, global-scale studies need to be complemented with higher-resolution regional-scale analysis that can verify and compare ocean-basin trends with coastal areas. For that, locally validated and calibrated wave data and the consideration of regional meteorological

processes are important for a robust assessment of changes in storminess. Small changes in the storm climate, at regional and local scale, can significantly enhance coastal erosion. For example, Harley et al. (2017) attributed severe coastal erosion in Southeast Australia to the anomalous storm wave direction of an extratropical cyclone. Similarly, 5° changes in the storm wave direction were found to be a main driver of heightened erosion in Northwest Spain during the winter of 2013/14 (Flor-Blanco et al., 2021). On the West coast of the U.S., changes in the storm wave period can drive large increases in the total water level and consequently storm impacts (Serafin et al., 2019). These examples highlight that detailed assessments of the storm wave climate and its variability are essential for understanding regional coastal impacts.

There are numerous approaches to identify coastal storms depending on data availability and the scope of analysis. In a review of coastal storm definitions, Harley (2017) indicated that coastal storms are created by meteorologically induced disturbances to the local maritime conditions (i.e., waves or water levels) that have the potential to alter the coastline. In contrast to a synoptic climatological approach in assessing coastal storminess that links coastal observations with regional synoptic observations such as storm tracks, statistical based climatological studies of coastal extreme wave occurrences are not able to link every storm to a particular synoptic system. However, a robust storm definition and statistically derived thresholds improve the likelihood of meteorological independence between storms (Harley, 2017). Therefore, statistical approaches typically consider a minimum duration threshold between consecutive events to determine meteorological independence between storm events (e.g., Corbella and Stretch, 2012; Loureiro and Cooper, 2018; Martzikos et al., 2021a; Amarouche et al., 2022). This minimum duration threshold has been designated as meteorological independence criterion (Harley, 2017), inter-exceedance time (Fawcett and Walshaw 2008), inter-arrival time (De Michele et al., 2007), or run parameter (Oikonomou et al., 2020). According to the definition of Harley (2017), the minimum duration threshold is linked to the average time interval between the passage of different synoptic systems (e.g., tropical or extra-tropical cyclones) that generate storms and can be used to identify meteorologically independent storm events. Using different values for the duration threshold can substantially influence storm characterisation (Sénéchal et al., 2017; Castelle and Harley, 2020) and yet, this parameter is typically selected arbitrarily or neglected in coastal storm analyses (e.g., Senechal et al., 2015; Masselink et al., 2016; Flor-Blanco et al., 2021; Vieira et al., 2021; Celedón et al., 2022).

Most regional to local coastal storm analyses have been performed in low to medium wave energy environments (e.g., Almeida et al., 2011; Mendoza et al., 2011, 2013; Dissanayake et al., 2015; Plomaritis et al., 2015; Garnier et al., 2018; Amarouche et al., 2022; Martzikos et al., 2021b), while only a few were conducted in storm-dominated (Davies, 1980) or high wave energy environments that are common in higher latitudes (e.g., Loureiro and Cooper, 2018; Wojtysiak et al., 2018). Low to medium energy wave environments are characterised by mean significant offshore wave heights below 2 m, whereas mean significant wave heights in storm dominated high-energy wave environments are above 2 m (Short, 1999). A challenging characteristic in such locations is the frequent temporal clustering of extratropical cyclones (Pinto et al., 2014; Priestley et al., 2017a, b), which further complicates the appropriate estimation of the minimum duration between consecutive storm events. These extratropical cyclone clusters can be generated by meteorological phenomena such as secondary cyclogenesis (Mailier et al., 2006) creating cyclone families (Priestley et al., 2020) or shifts in large-scale atmospheric flow characterised by an intensified jet stream (Dacre and Pinto, 2020), resulting in events that are meteorologically related. Other mechanisms can lead to the temporal clustering of storm wave events, challenging the definition of a minimum duration threshold. That was the case of a cut-off-low system that became stationary off the coast of South Africa in 2007, leading to long and intense storms that resulted in dramatic coastal erosion (Smith et al., 2010). The same can occur when tropical cyclones display irregular paths or stall for significant periods such as Hurricane Harvey in 2017 (Hall and Kossin, 2019). Therefore, processes taking place in storm-dominated environments challenge existing methods for identifying independent storm events due to the frequent temporal clustering of storms, which may be driven by related meteorological systems.

So far, no generalised storm identification procedure exists for storm-dominated or high wave energy coastal areas, which ultimately affect coastal management planning due to incorrect definition of coastal risks. This work presents a generic storm definition that is adapted to energetic wave climates and considers meteorological independence between storms based on long-term wave statistics. The storm identification algorithm is compared against the common peak-over-threshold storm identification method, with both approaches being applied to two long-term wave reanalysis datasets that have been validated and calibrated with buoy observations. To develop a storm definition suitable for high-energy wave climates this work explores wave data from the Outer Hebrides (west of Scotland) (Figure 2.1), located along the North Atlantic storm track and exposed to frequent and intense winter storms. This paper

presents a robust approach to identify storms in high wave energy coastal areas and discusses the implications for the analysis of storminess trends and storm climate variability.

2.2 Data and Methodology

2.2.1 Wave Data

Significant wave height (H_S) and peak wave period (T_P) datasets from the Outer Hebrides were used to demonstrate the storm identification approach and for presenting an application example of storm characterisation in a high wave energy coastal environment. While buoy observations are available for the last 11 years (Table 2.1), two recent and state-of-the-art reanalysis products were used to provide a continuous and extended wave time series, as well as to enable a comparison between widely used wave model products. However, when compared to in-situ observations wave reanalyses can exhibit systematic errors, such as under or over-estimation of extreme wave heights (Baordo et al., 2020). Hence, when analysing extreme events from wave reanalyses, it is paramount to correct these systematic errors by applying calibration functions obtained from the comparison with buoy data (Fanti et al., 2023). Moreover, different reanalysis products can yield differences in the magnitude and direction of long-term trends (Timmermans et al., 2020; Sharmar et al., 2021), which highlights the importance of performing a multisource analysis (Erikson et al., 2022).

Table 2.1 Synthesis of the wave data used and designation of the dataset.

	Coordinates	Sampling Interval	Period	Variables	Source	Dataset designation
Buoy	57.289° N, -7.923° W	0.5 h	2009 – 2020	H_S, T_P	CEFAS	Buoy-11
ERA5	57.29° N, -7.93° W	1 h	1950 – 2020	H_S, T_P	ECWMF	ERA5-11; ERA5-40; ERA5-70; cERA5-11; cERA5-40; cERA5-70
CMEMS	57.2973° N, -7.9091° W	3 h	1980 – 2020	H_S, T_P	Copernicus Marine Service	CMEMS-11; CMEMS-40; cCMEMs-11; cCMEMS-40

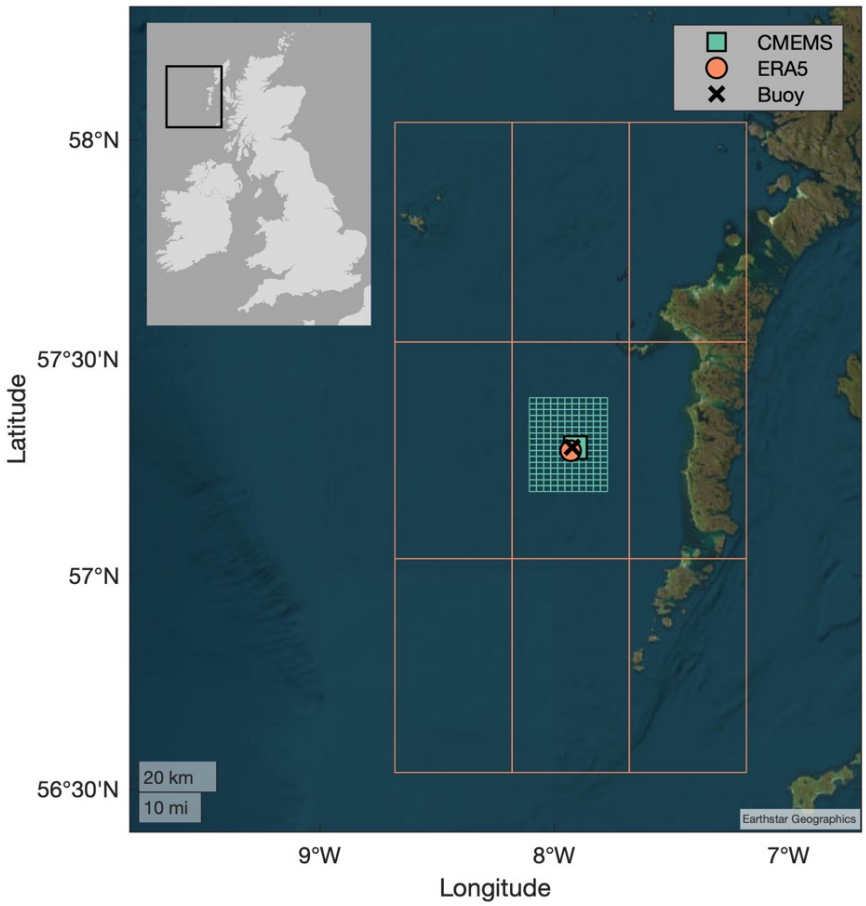

Figure 2.1 Location of the Outer Hebrides, West Scotland, wave reanalysis grid outlines (ERA5 in orange and CMEMS in green), and data output locations.

For this work, wave buoy observations were obtained from the West of Hebrides buoy, deployed and operated by CEFAS approximately 30 km offshore the Outer Hebrides in the west of Scotland (Figure 2.1) in a water depth of 100 m. Wave parameters and spectra are recorded for periods of 30 min using a Datawell Directional Waverider MkIII buoy. The modelled wave data used in this work were obtained from the ERA5 reanalysis (Hersbach et al., 2020; Bell et al., 2021), provided by the European Centre for Medium-Range Weather Forecasts, and the Northwest European Shelf Wave Hindcast, provided by the Copernicus Marine Service (hereafter CMEMS). ERA5 covers seven decades (1951–2020) with hourly data and a 0.5° × 0.5° spatial resolution, while CMEMS is restricted to four decades (1980–2020), with data every 3 h and a 0.017° × 0.017° resolution (Table 2.1).

ERA5 and CMEMS wave data were extracted for the closest point to the Outer Hebrides wave buoy (Figure 2.1). More information on the buoy and the reanalyses data and their validation against buoy observations are provided in the supplementary materials. The observations from

the Outer Hebrides wave buoy were used for validation and calibration of the two wave reanalyses. The calibration focused on the extreme values (> 95th percentile) of H_S and T_P, and transfer functions with best fits were applied to the model data (y) to better reproduce the buoy observation (x). Several transfer functions were tested, including linear, quadratic, and power functions, as well as a rotation around the mean following Fanti et al. (2023). The transfer functions used for H_S is a power function (Eq. 2.1), while for T_P a rotational function around the mean was applied (Eq. 2.2) which is derived from the rotational matrix in Eq. 2.3.

$$y' = ay^b, \tag{2.1}$$

$$y' = sin\beta(x - x_c) + cos\beta(y - y_c),\ with\ \beta = (1 - a), \tag{2.2}$$

$$\begin{bmatrix} x' \\ y' \end{bmatrix} = \begin{bmatrix} \cos(1-a) & -\sin(1-a) \\ \sin(1-a) & \cos(1-a) \end{bmatrix} \begin{bmatrix} x - x_c \\ y - y_c \end{bmatrix}, \tag{2.3}$$

The transfer functions were then applied to the long-term data set (i.e., the 70 and 40 years) assuming that deviations in the reanalysis relative to the buoy data are consistent for the entire analysis period. This resulted in the calibrated ERA5 and calibrated CMEMS wave time series and, as such, the long-term data sets are referred to as cCMEMS-40, cERA5-40, and cERA5-70, where 'c' stands for calibrated and the numbers refer to the length of the analysis period, specifically 70 years (1950–2020), 40 years (1980–2020), and 11 years for the buoy data (2009–2020).

Similarly to previous studies on the wave climate of the Northeast Atlantic (e.g., Santo et al., 2015), here the winter season is defined as the extended boreal winter comprising the months of October to March (ONDJFM). The ONDJFM extended winter considered here is also consistent with the time period when most extreme sea-level events occur in the northwest of the UK (Haigh et al., 2016). For simplicity, the winter year designation used in this work refers to the second part (JFM) of the winter season, meaning that winter 2020 refers to OND of 2019 and JFM of 2020.

2.3 Storm Identification

There are many coastal storm identification approaches based on time series, which use variables such as H_S, T_P, wave direction, and water levels (Martzikos et al., 2021a and references therein). Storm identification can be based on single, combined, or composite parameters (e.g., storm power), but the most common approaches rely on H_S time series (Harley, 2017). However, the identification of storms from H_S time series lacks a consistent methodology, as recently outlined by Harley (2017) and Martzikos et al. (2021a). Existing definitions of coastal storm events (based on H_S data) encompass several concepts, criteria, and thresholds, and are often topic specific. In storm erosion studies for example, the H_S thresholds are based on hydrodynamic conditions that result in significant morphological change (e.g., Almeida et al., 2012; Armaroli et al., 2012; Del Río et al., 2012), and the duration thresholds are based on the subsequent morphological recovery periods (e.g., Loureiro et al., 2012; Senechal et al., 2015). Consequently, storm criteria and thresholds become highly site-specific due to the varying coastal morphodynamics, wave climate characteristics and regional meteorological systems that generate the storms (Ciavola et al., 2014; Harley, 2017). Because of this, Castelle and Harley (2020) encourage generic criteria for storm identification based on long-term wave statistics, as this allows to broaden the application and compare findings from coastal storm analyses.

2.3.1 Conceptual Description

Typically, the identification of storm events for climatic analysis of storminess considers three criteria: (1) an extreme H_S threshold, hereafter storm threshold (ST), (2) a minimum storm duration (MSD), and (3) an independence duration (ID) (Ciavola et al., 2014; Harley, 2017; Martzikos et al., 2021a). However, these three storm identification criteria have been mostly applied in low to medium-energy wave environments. In storm-dominated or high wave energy environments with consecutive and rapidly succeeding storms, an additional criterion needs to be considered to ensure appropriate aggregation or separation between consecutive exceedances of the H_S storm threshold. The proposed criterion is designated as the independence threshold (IT). These four storm identification criteria are explained conceptually below and defined statistically in Sect. 2.3.2.

The ST determines if wave conditions are considered extreme and hence separates the H_S time series into storm (H_S > ST) and calm periods (H_S < ST). In the simpler situation (Figure 2.2, S1), when ST is up-crossed, it dictates the start of a storm, and likewise, when it is down-crossed it defines the end of a storm.

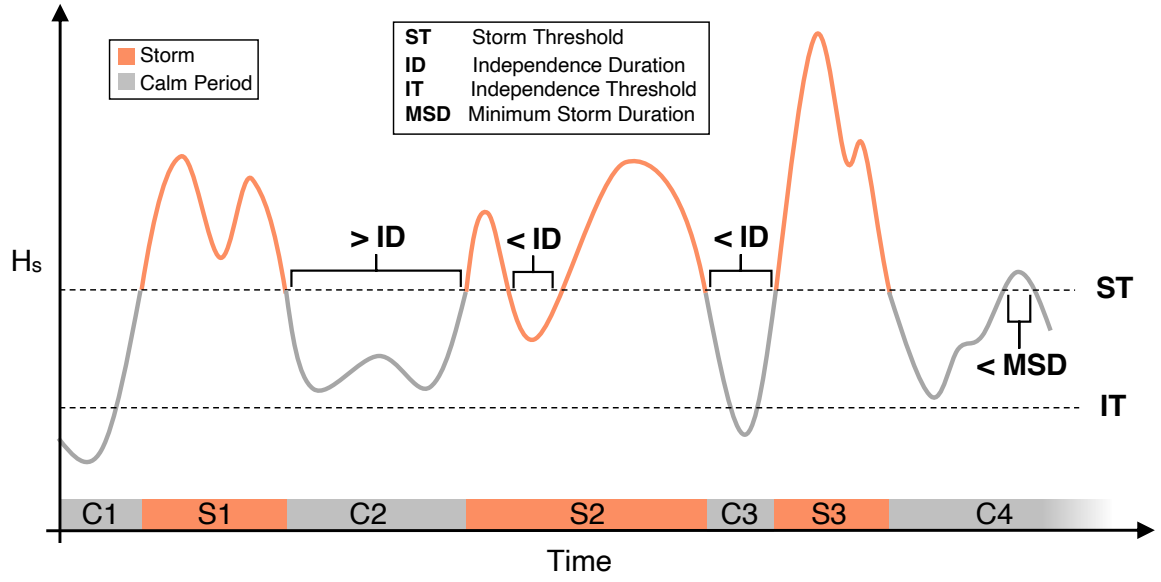

Figure 2.2 Synthetic representation of the storm identification methodology adapted to high wave energy environments. H_S is the significant wave height. C1–C4 are the calm periods between storms, and S1–S3 are individual storm events.

During storms, waves can temporarily down-cross the storm threshold, but this does not necessarily imply that a storm has ended, and as such it is necessary to also consider the length of time between successive down-crossings and up-crossings of ST. This is defined as the Independence Duration (ID) and is used to determine the meteorological and statistical independence between consecutive storm events, by combining exceedances of ST into one storm event until the inter-exceedance period is long enough to assume independence. In a meteorological or oceanographic context, ID corresponds to the average passage time of synoptic systems that drive storms over a coastal area (e.g., Harley, 2017). From a statistical perspective, a storm analysis should be conducted on an independent (and identically) distributed extreme value dataset (e.g., Lopatoukhin et al., 2000). The extreme value dataset usually consists of an extreme wave height, period, or power for each independent storm, which is then used for further statistical analysis. However, a single storm can include several H_S peaks with occasional periods of H_S < ST. Consequently, an independent storm is only considered

when the period between a downcrossing of ST and the following up-crossing is longer than ID (Figure 2.2, C2), and when the duration between consecutive up-crossings is shorter than ID the storm is extended in time (Figure 2.2, S2).

This approach enables brief crossings below ST within a single storm event by combining several H_S peaks in rapid succession that belong to the same meteorological disturbance (Harley, 2017). However, periods of rapid storm succession that are common in storm-dominated coasts in the winter season can lead to storms lasting several weeks, which are likely caused by different meteorological disturbances. Therefore, to enhance meteorological independence an additional independence threshold (IT) is defined. IT is a H_S threshold that represents storm dissipation. Consequently, IT must be smaller than ST but above the mean H_S for the coastal region. In the case of rapid storm succession (Figure 2.2, S2, S3), when the time between two consecutive storms is shorter than ID but H_S < IT (Figure 2.2, C3), two independent storm events should be considered (Figure 2.2, S2 and S3). By including IT in the storm identification, the independence between consecutive storms can be achieved in two ways: if after a down-crossing H_S remain below ST for longer than ID (Figure 2.2, C2), or if H_S falls below IT (Figure 2.2, C3).

Finally, not all records that exceed ST should be considered a storm, as storm events must have a minimum duration. Therefore, when storm duration is lower than the MSD, the event is not considered a storm (Figure 2.2, C4). The role of MSD is to filter out short-lived exceedances of ST that will have no relevant impacts on the coast (Martzikos et al., 2021a).

The performance of the proposed storm identification approach was tested against a simple Peak-Over-Threshold (POT) approach which is still widely used for the characterisation of coastal storms (e.g., Flor-Blanco et al., 2021; Vieira et al., 2021; Celedón et al., 2022; Gramcianinov et al., 2023b). In extreme value analysis, the POT approach refers to the extraction of peak H_S values from threshold exceedance clusters (e.g., Ferreira and Guedes Soares, 1998), whereas in coastal storm analysis the POT approach can also refer to the extraction of all threshold exceedances of the cluster to analyse storm characteristics such as duration and power (Harley, 2017). A simple POT approach considers ST as a stand-alone storm criterion, with each storm identified as the consecutive wave records over the ST (e.g., Weisse and Gunther, 2007; Gramcianinov et al., 2023b), but neglects MSD, ID and IT. In the example of Figure 2.2, storm S2 would be identified as two separate storms by the POT approach because no independence duration is defined. In addition, considering the POT approach, the H_S peak in C4 would be identified as an additional storm. Differences between

the proposed storm identification and the POT approach were assessed by comparing the long-term storminess metrics using the Outer Hebrides datasets as a case study (Section 2.2.1). Additionally, a sensitivity analysis of the storm criteria was performed by attributing changes in the total storm counts and storm duration to each storm criterion, given that both storm count and duration have been shown to be sensitive to changes in storm identification methods (Sénéchal et al., 2017; Castelle and Harley, 2020).

2.3.2 Statistical Definition

The two H_S thresholds, ST and IT, are estimated based on long-term H_S records. In line with most coastal storm analyses (e.g., Masselink et al., 2014; Castelle et al., 2015; Harley et al., 2017; Martzikos et al., 2021b), ST was defined as the 95th percentile of the H_S time series. IT aims to determine the conditions below which H_S is no longer associated with a storm event by considering the average conditions of the season with most storm occurrences. Based on this, IT is defined as the mean winter H_S, as it will be lower than ST but higher than the long-term mean H_S for the coastal region.

The selection of an appropriate ID is more challenging as it requires consideration of the average passage time of a meteorological or oceanographic system driving the storm (Harley, 2017). As a consequence, ID is commonly selected arbitrarily in coastal storm analyses. However, ID can be estimated statistically based on the extremal index proposed by Ferro and Segers (2003). This approach has been used previously in the estimation of return periods of extreme H_S occurrences (Oikonomou et al., 2020), extreme precipitation (Barton et al., 2016) and extreme water levels (Arns et al., 2013).

For the calculation of the extremal index, a binary parameter W_i is defined so that W_i = 1 when H_S > ST and W_i = 0 when H_S < ST, similarly to the POT approach. The total count of independent storms, Z, is given by

$$Z = \sum_{i=1}^{n} W_i(1 - W_{i+1}) \dots (1 - W_{ID+1}), \tag{2.4}$$

where n is the number of H_S data points (Smith and Weissman, 1994). Ferro and Segers (2003) demonstrate that the extremal index ($\theta, \in [0, 1]$) describes the proportion of non-zero inter-exceedance times of an extreme event and the reciprocal of the mean of the non-zero inter-

exceedance times as demonstrated by Smith and Weissman (1994). Therefore, θ can be defined as

$$\theta(ST) = \frac{2\,[\sum_{j=1}^{N-1}(T_j-1)\,]^2}{(N-1)\sum_{j=1}^{N-1}(T_j-1)(T_j-2)} \tag{2.5}$$

where T_j is the time between two consecutive ST exceedances with $j \in [1, N-1]$ and $T_j > 2$, and as an estimate of the true extremal index:

$$\theta' = Z/N, \tag{2.6}$$

corresponding to the reciprocal of the mean storm duration, where N is the number of total ST exceedances:

$$N = \sum_{i=1}^{n} W_i\,, \tag{2.7}$$

After calculating θ (Eq. 2.5) it is possible to estimate Z (Eq. 2.6) iteratively through Eq. 2.4, increasing ID values until Z is reached. ID is therefore estimated based on the H_S time series itself and explained by asymptotic theory (Ferro and Segers, 2003). When seasonality in the extreme wave climate is expected, the long intervals between consecutive storms during the calm or summer season contribute to the overestimation of ID (Oikonomou et al., 2020). Therefore, for the calculation of ID, the H_S time series is restricted to the winter season, when most extreme value exceedances occur.

The MSD was set to 6 h, which is a commonly used minimum duration for coastal storm analysis (Martzikos et al., 2021a and references therein). This MSD value assumes that storms that last at least 6 h have a high-likelihood (~ 70%) of coinciding with high-tide conditions in a semi-diurnal tidal cycle, which increases the possibility of significant storm-induced morphological impacts on the coast and minimizes the loss of extreme wave records in the storm analysis. Furthermore, the 6 h MSD ensures that a minimum of 2 storm records are used for storm identification using the CMEMS reanalysis, as this has the lowest temporal resolution (3 h) of the datasets considered (Table 2.1).

2.3.3 Long-term Analysis

Following the application of the storm identification algorithm, storm parameters were estimated to define and characterise each storm event and compute aggregated winter metrics. The storm duration describes the time between the start and end of an independent storm (Figure 2.2, S1-3), and accounts for the sampling intervals of the different wave records (Table 2.1). For the characterisation of each independent storm event, mean storm H_S (SH_S), mean storm T_P (ST_P), and the 98th percentile of SH_S and ST_P were computed. In order to compare averaged wave trends with other studies, the winter mean and 98th percentile of H_S and T_P were computed in addition to storm metrics. The storm power (SP) was calculated following Splinter et al. (2014), with

$$SP = \int_0^D \frac{\rho g^2}{64\pi} {SH_S}^2 ST_P dt, \tag{2.8}$$

where D is the storm duration, ρ is the seawater density (~ 1024.5 kg/m3), g is the gravitational acceleration (9.81 m/s^2), dt is the sampling interval and wave power represents the wave energy flux per unit of wave crest length.

The maximum H_S value of each identified winter storm was used to form an independent and identically distributed extreme value dataset and was used to determine the return period of extreme H_S conditions. However, using the POT approach that lacks the ID criteria to identify storms could violate the independence requirement for the extreme value dataset. The return periods of H_S were estimated from 1 to 100 years by fitting the Generalized Pareto Distributions (GPD) to the winter storms H_S datasets, and assuming stationarity (e.g., Coles, 2001). To meet the homogeneity requirement for the application of extreme value theory, only the storms during the ONDJFM season were considered. The GPD was fitted via numerical maximum-likelihood estimation, with return periods of maximum SH_S (RSH_S) values defined by:

$$RSH_s = TH + \frac{\sigma}{\xi}\left[\left(\frac{RL}{\lambda}\right)^{\xi} - 1\right] \text{ for } \xi \neq 0, \tag{2.9}$$

where σ is the scale parameter of the GPD, ξ is the shape parameter of the GPD, R is the return period, L is the length of the extreme value dataset, and λ is the period of the H_S time series in

years. Calculating H_S return periods for the various datasets considered in this work (Table 2.1), including the buoy and the calibrated reanalysis data, provides additional validation of the calibration as it allows to consider the results for the higher percentiles of the H_S data (Fanti et al., 2023).

Winter storm counts and storm parameters were calculated to analyse the variability and periodicity of storminess in the Outer Hebrides and to compare the proposed storm identification algorithm and the common POT approach. The significance of the long-term trends was determined using the Mann–Kendall test and the magnitude and direction of the trends were estimated using Sen's slope, following Young and Ribal (2019) and Erikson et al. (2022), as this provides robust trend estimates when data are non-normally distributed. The significance of long-term trends was tested considering 0.05 and 0.1 significance levels. Climatic control of winter storminess was explored through correlation analysis of the storm parameters with the North Atlantic Oscillation (NAO) index, which is the leading mode of climate variability in the NE Atlantic (e.g., Hurrell, 1995; Scott et al., 2021). To determine the extended winter NAO, sea level pressure data were obtained from the National Centre for Atmospheric Research (NCAR) for Lisbon (40.0N, 10.0W) and Reykjavik (65.0N, 20.0W) and used to compute the station-based NAO. The NAO was computed using a reference period from 1951 to 1980 and normalized to monthly sea level pressure following the method proposed by the Climate Research Unit (2022) for station-based NAO index estimation. For consistency with the storm analysis, the NAO index was calculated for the extended winter season (ONDJFM). The correlation between the extended winter NAO and winter storm parameters was computed with Pearson's linear correlation coefficient (R) considering a 0.05 significance level.

2.3.4 Study Site

The wave climate of the Outer Hebrides (Figure 2.1) is considered one of the most energetic globally, with a fetch of more than 6000 km for the dominant W to WNW wave direction (Ramsay and Brampton, 2000). Consequently, the Outer Hebrides have been the focus of wave energy extraction research due to the high wave power resources (e.g., Neill et al., 2017). The wave climate of the west of Scotland displays high seasonality, with very energetic conditions throughout the extended winter season from October until the end of March (Santo et al., 2015). The winter wave climate in this region is also highly correlated with the NAO, where a positive NAO index is associated with energetic winters and a negative or lower NAO index with calmer

winter conditions (Santo et al., 2015; Castelle et al., 2017; Hochet et al., 2021; Scott et al., 2021). The well-established association between positive NAO and increased winter storminess determined from wind records was linked to increasing coastal erosion in the Outer Hebrides (Dawson et al., 2004). Dawson et al. (2007) argue that winter storminess in the west of Scotland was lower in the first part of the twentieth century compared to the late nineteenth century, as evidenced by mean monthly wind velocities and monthly maximum gust velocities. Santo et al. (2015) demonstrated that offshore the Orkney islands, in the north of Scotland, the wave power climate was characterised by strong interannual and multidecadal variability between 1665 and 2005. Furthermore, extreme H_S (Castelle et al., 2018) and wave storminess (Loureiro and Cooper, 2018) have been shown to exhibit a positive long-term linear trend since 1950 in the higher latitudes of the NE Atlantic. Therefore, the intensity, frequency, and variability of storms in the Outer Hebrides make this area an ideal location to develop and test a robust storm identification for high-energy or storm-dominated environments as a basis for analysing storminess patterns.

2.4 Results

2.4.1 Reanalysis Calibration

ERA5-11 and CMEMS-11 data for H_S and T_P show an overall good performance when compared to the Outer Hebrides buoy observations, although CMEMS-11 outperforms ERA5-11 in most error metrics (section 2.7.3, Figure 2.9). The highest correlation coefficients (R = 0.98) were found for H_S in both ERA5-11 and CMEMS-11. However, both wave models show negative biases for H_S and T_P indicating a systematic underestimation particularly evident for the extreme wave conditions (section 2.7.3, Figure 2.9). For example, in the most extreme event on record, which occurred on the 1st of February 2016, the buoy records a maximum H_S = 16.4 m, while the modelled values of H_S were 14.1 m and 13.9 m for ERA5-11 and CMEMS-11, respectively. The calibration applied to the reanalysis datasets aimed to reduce the systematic underestimation, resulting in a bias improvement in H_S of 0.24 m and 0.09 m for cERA5-11 and cCMEMS-11, respectively (Figure 2.3a, b).

The calibration also improved the Root Mean Square Error (RMSE) and the Scatter Index (SI) for H_S and T_P in both ERA5 and CMEMS (Figure 2.3). While after calibration the cCMEMS-11 dataset statistically outperforms cERA5-11, it is apparent that H_S values above 12 m are

better estimated in cERA5-11, as these remain underestimated in cCMEMS-11 (Figure 2.3a, b). The calibration also improves the agreement between model data and buoy observations for T_P, including extreme T_P values. As with H_S, cCMEMS-11 also outperforms cERA5-11 in terms of error metrics for T_P (Figure 2.3c, d).

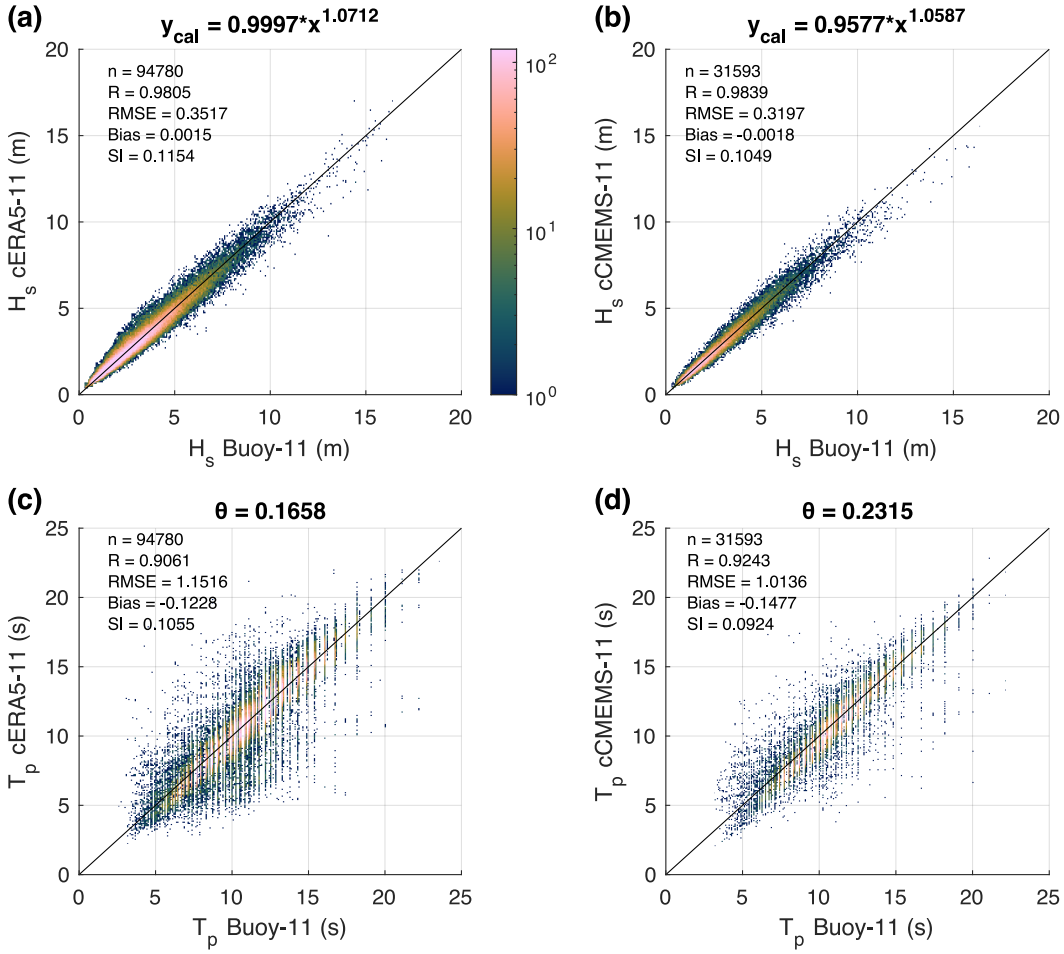

Figure 2.3 Density scatter plots of calibrated model H_S **(a, b)** and T_P **(c, d)** against buoy measurements, with the transfer function **(a, b)**, and angle of rotation **(c, d)** used for calibration. The inset boxes show the number of records (n), the correlation coefficient (R), the Root Mean Squared Error (RMSE), the bias, and the scatter index (SI). Note that the CMEMS reanalysis as a temporal resolution of 3 h, which results in fewer records compared to ERA5 that has a 1 h resolution. The density colour bar in **(a)** is representative for all subplots. For more details on the transfer functions and the statistical parameters see the supplementary material.

2.4.2 Storm Identification Criteria

The storm criteria ST, ID, and IT vary according to the dataset and the corresponding analysis period (Table 2.2). Moreover, H_S values for ST and IT also increase between the original and calibrated reanalysis data, while ID estimates are not affected by the calibration. Relative to the original datasets, the increase in ST is lower for cCMEMS (0.40 m) than for cERA5 (0.73 m on average for the two analysis periods). Likewise, IT also increases after calibration but more moderately, and differences in ST and IT between cERA540, cERA5-70 and cCMEMS-40 are reduced to less than 0.25 m.

Table 2.2 Storm identification criteria for the Outer Hebrides based on the original and calibrated reanalysis datasets.

	Dataset	ST (m)	ID (hours)	IT (m)
Original	ERA5-70	5.59	48	3.45
	ERA5-40	5.74	59	3.57
	CMEMS-40	6.13	54	3.73
Calibrated	cERA5-70	6.31	48	3.80
	cERA5-40	6.50	59	3.94
	cCMEMS-40	6.53	54	3.89

Considering the different analysis periods, the cERA570 dataset yields ~ 0.2 m lower ST and~ 0.1 m lower IT estimates than either of the 40-year datasets. A similar pattern is observed in ID, which is higher for cERA5-40 and cCMEMS-40 with 59 h and 54 h, respectively, compared to 48 h for the cERA5-70 dataset. In summary, the calibration reduced the differences in the storm identification criteria between the two reanalyses datasets, with the length of the analysis period (70 or 40 years) leading to a more significant variation in ST, ID, and IT.

As a result of the different storm definition, based on the 70-year period (cERA5-70), the total storm count is reduced from 1653 storms using the POT approach to 941 storms (43 % reduction) using the storm identification algorithm (Figure 2.4a). The vast majority of the reduction is associated with the inclusion of ID which merges H_S exceedance clusters in close temporal proximity into a single storm. Contrary to counts, duration is increased using the storm identification algorithm compared to using the POT approach (Figure 2.4b). The total storm duration in the 70-year H_S dataset using the POT is 1278 days (5 % of the time series length, ST is set to the 95th percentile of H_S) and 1650 days when using the storm identification

algorithm (6.45 % of the time series length). Thus, the implementation of the storm criteria ID, IT, and MSD increases the overall storm duration by 29 %. This pattern of change between the POT and the storm identification algorithm is also evident in the storm count and duration for the cERA5-40 and cCMEMS-40 datasets. It evidences that storm counts and duration strongly depend on the storm identification criteria used, with ID having the largest influence on total storm metrics, while the contribution of IT and MSD is much lower.

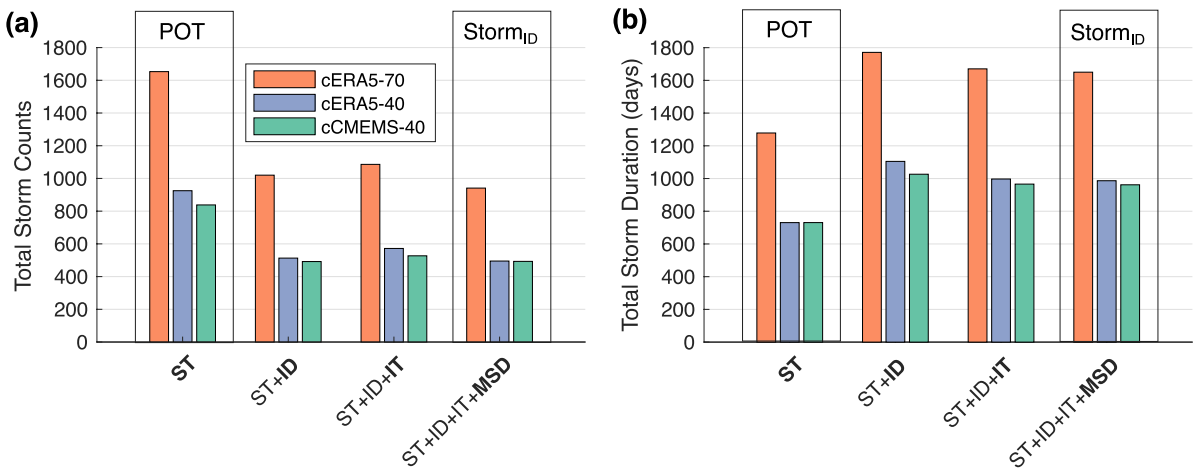

Figure 2.4 Influence of storm criteria on the total storm count **(a)** and storm duration **(b)**. Each bar group represents the progression of the storm identification algorithm (StormID) by introducing an additional storm criterion highlighted in bold. ST storm threshold, ID independence duration, IT independence threshold, and MSD minimum storm duration

A period with a rapid succession of storms between December 1992 and February 1993 illustrates the performance of the storm identification algorithm as well as the differences to the POT approach (Figure 2.5a). In this example, the storm criteria were estimated based on the cERA5-70 data, with storms identified when H_S exceeds 6.31 m (ST) for a minimum of 6 h (MSD) (Figure 2.5a). The first exceedance of H_S (10/12/1992) is not identified by the storm identification algorithm because MSD is less than 6 h.

The following storm (14/12/1992) is identified and characterised identically by the storm identification algorithm and the POT approach because H_S is below ST until the next storm (17/12/1992), which is longer than the ID of 48 h. Major discrepancies between the two storm identification methods occur between 02/01/1993 and 18/01/1993, when H_S varies considerably but remains high throughout the 16 day period. While the POT approach individualises 10 storms for this period, the storm identification algorithm identifies this period as one storm

because H_S is never below IT and ID is never exceeded. In fact, this was the most powerful storm since 1950 in the Outer Hebrides based on the storm identification algorithm and cERA5-70 data. This also demonstrates that during a storm event, H_S can fall below ST for considerable periods of time. Through the implementation of IT, this storm ends on 18/01/1994 instead of being extended until 26/01/1993. This occurs because H_S down-crosses IT on 19/02/1993, although the duration between ST exceedances is always below ID.

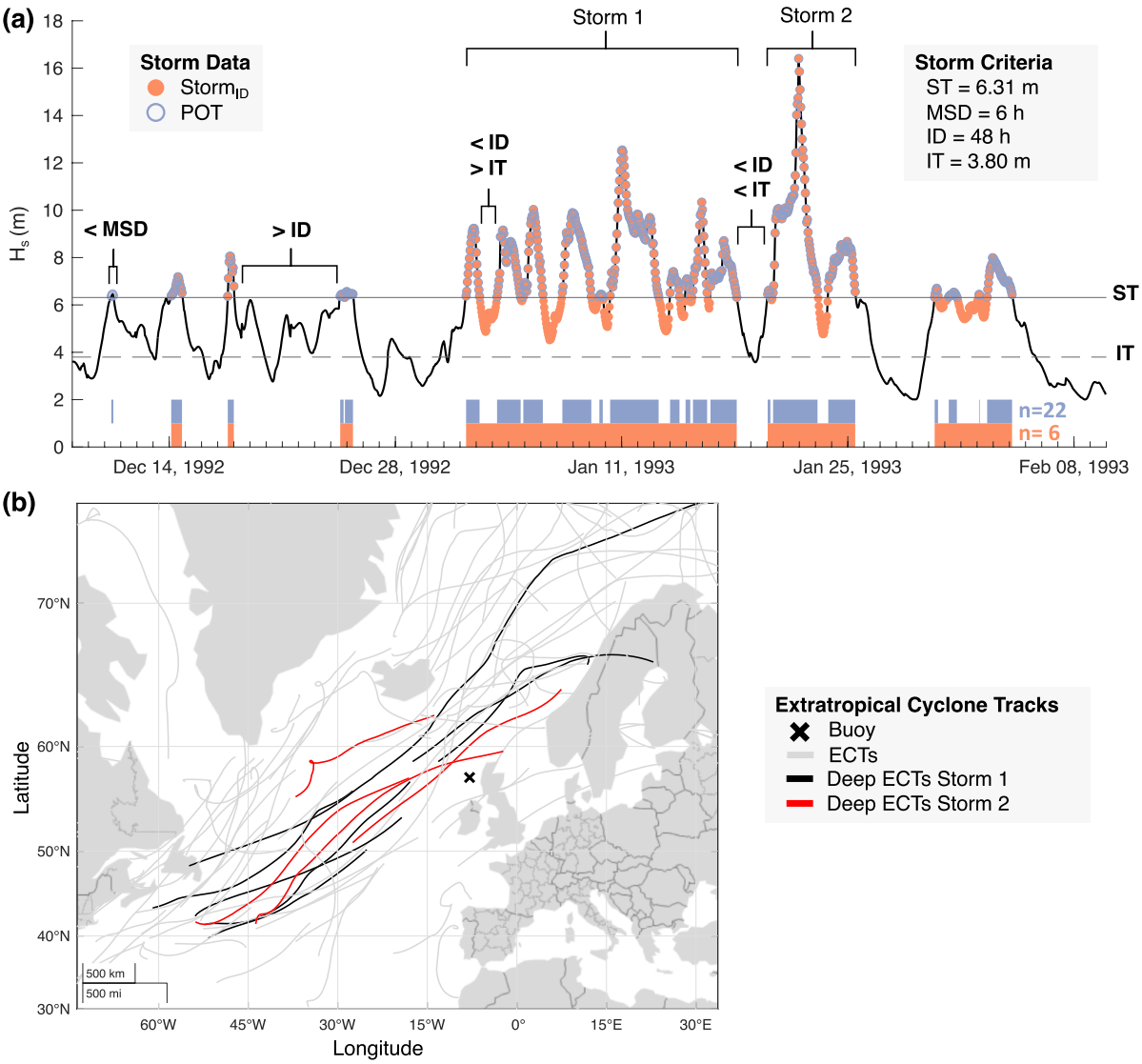

Figure 2.5 (a) Illustration of the storm identification algorithm (StormID) adapted to high wave energy environments. The four thresholds embedded in the storm identification algorithm are illustrated on an example period from the cERA5-70 H_S data. The blue rectangles indicate the storm events determined using the POT approach (n = 22) and the orange rectangles when using StormID (n = 6). ST storm threshold, MSD minimum storm duration, ID independence duration, IT independence threshold. **(b)** All extratropical cyclones tracks (ECTs) that occurred in the North Atlantic during the period considered in

(a) obtained from Lodise et al. (2022), highlighting the deep extratropical cyclones (minimum pressure below 980 hPa along the track) that occurred during Storm 1 and Storm 2 in (a).

This period of rapid storm succession is reflected by the number and path of extratropical cyclones in the North Atlantic during the same period (Figure 2.5b). During the high-energy period (02/12/1992–26/01/1993), there is a sequence of deep extratropical cyclones with similar track orientations. The stacked cyclone tracks suggest the occurrence of serial clustering of extratropical cyclones (Dacre and Pinto, 2020), which is likely to be caused by secondary cyclogenesis. The resulting family of extratropical cyclones drives a prolonged period of H_S higher than ST, with occasional short-lived downcrossings, but can be interpreted as a single storm event, with high-energy wave conditions continuously impacting the coastal area.

2.4.3 Storm Analysis

According to the cERA5-70 data, 87 % of the total storms in the Outer Hebrides occur during the extended winter season (section 2.7.3, Figure 2.10) with an average of 12 storms per winter. The winter month with the highest total storm occurrence is December with 19 % followed by January (16 %) and February (14 %). The average storm conditions are characterised by SH_S = 7.21 m (SH_S^{98} = 11.21 m) and ST_P = 14.10 s with a dominant westerly direction. Storms last on average 42 h, with a mean storm power of 15.84 MWh/m. The most powerful storms since 1950 were recorded in January of 1993 and 1994, with total storm powers above 162 MWh/m and storm duration in excess of 2 weeks (section 2.7.3, Table 2.6). The 'Great Storm' of January 2005 (e.g., Dawson et al., 2007) is recorded as the third most powerful storm since 1950 but has the second longest duration (16 days) and SH_S^{98} of 14.8 m, which is over 1 m higher than the storms in January 1993 and 1994.

In terms of return periods of extreme wave conditions, these are underestimated by more than 3 m for the 50 and 100-yr H_S return periods based on uncalibrated wave reanalyses (ERA5-11 and CMEMS-11) in comparison to the buoy data, but improve substantially following calibration (Figure 2.6a). While cERA5-11 H_S return periods are similar to those determined with the buoy data, Hs return periods based on cCMEMS-11 data remain underestimated by more than 1.5 m for return periods > 20 years. The 40 and 70-year reanalysis H_S datasets show a similar pattern in the correction after calibration, yielding slightly lower H_S return periods to those determined with the 11-year dataset (Figure 2.6b).

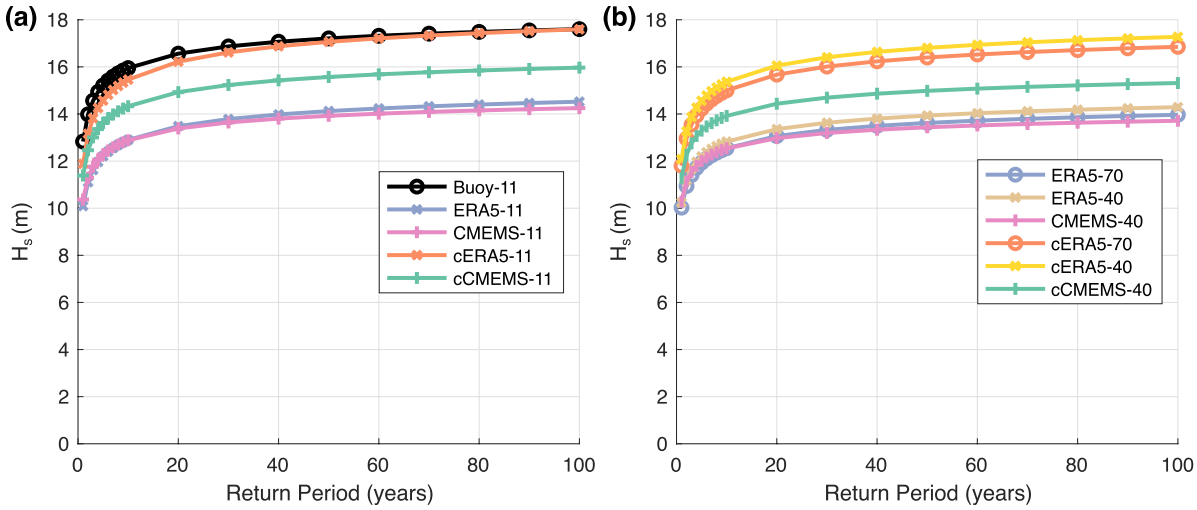

Figure 2.6 H_S return periods for the various datasets. **(a)** Return period for the buoy and the calibrated/uncalibrated wave models using the reference time of the buoy record (11 years). **(b)** Return periods for the calibrated datasets with extended analysis periods (40 and 70 years).

There is only a minor difference between the 70-year and 40-year datasets in terms of H_S return periods. In the case of cERA540 and cERA5-70, the 100-year H_S return period is 17.28 m and 16.85 m, respectively, while based on the cCMEMS-40 H_S dataset it is 15.12 m. Return values based on the POT approach were not displayed because the H_S return periods are unrealistic high, which is considered to be due to the violation of the statistical independence requirement for the extreme value dataset.

Winter storm counts, cumulative storm duration and power show clear multiannual variability and are remarkably consistent across datasets (Figure 2.7). There are, however, differences between the storm identification approaches. The storm identification algorithm produces a lower winter storm count compared to the POT approach, while for the latter total storm duration and storm power are lower (Figure 2.7). Despite the differences in value for the different storm metrics, the temporal variability in winter storminess is similar between both approaches. However, storm count variability determined with the POT approach is more pronounced, while variability in storm duration and power is slightly suppressed in the POT compared to the storm identification algorithm.

Considering specifically the winter storminess metrics in the Outer Hebrides determined using the cERA5-70 data and the storm identification algorithm proposed in this work, the winter storm counts range between a minimum of 3 storms (2013) and a maximum of 19 storms (1983 and 1992). Cumulative storm duration over the extended winter season ranges from a total of

106 h in 2001 to 1243 h in 2015, which corresponds to the least and most energetic winters with 38 MWh/m and 502 MWh/m, respectively.

In general, the storm wave climate in Western Scotland is characterised by a high multiannual variability. Compared to winter storm duration and storm power, the storm counts according to the storm identification algorithm are less variable throughout the studied period. In the early 1990's, there is a cluster of energetic winters evidenced by the maximum in the decadal moving average of the winter storm power with ~ 330 MWh/m and winter storm duration with ~ 750 h. Aside from a few energetic winters, the period between 1950 and 1980 is less energetic when compared to the period from 1980 to 2020.

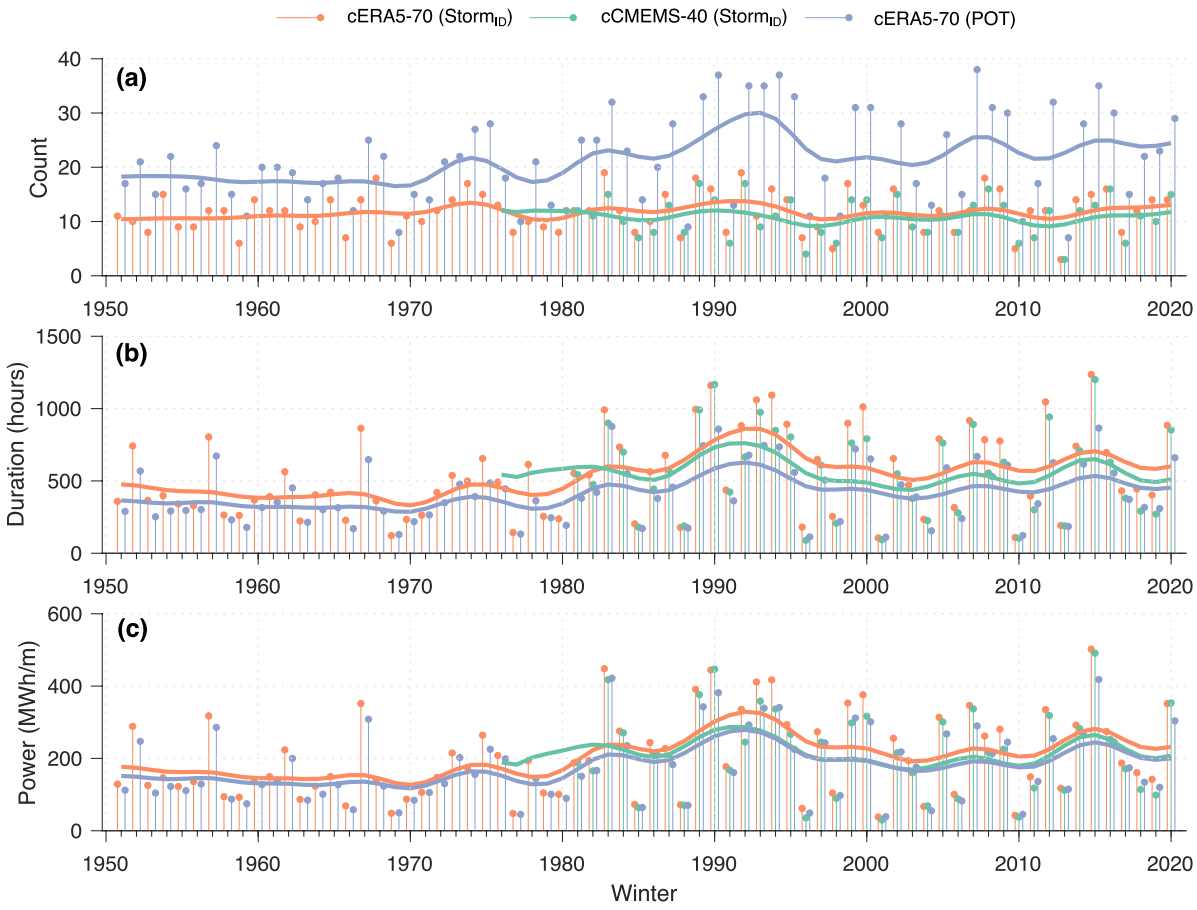

Figure 2.7 Temporal variability in winter storm count **(a)**, cumulative storm duration **(b)**, and cumulative storm power **(c)** based on two different storm data sets (cERA5-70 and cCMEMS-40) and using the storm identification algorithm and the POT approach (only for cERA5-70). Decadal moving average is indicated by thick lines.

The cumulative winter storm duration and power display statistically significant increasing trends ($p < 0.05$) since 1950 regardless of the storm identification approach (Table 2.3). Likewise, a significant increasing trend is found for the winter ST_P, while no statistically significant trend is identified for SH_S and storm counts determined using the storm identification algorithm (Table 2.3). For the storm datasets covering the last 40 years, none of the trends for the various parameters are statistically significant, although these display a tendency for negative trends in duration, power and ST_P^{98}, and positive for the other storm metrics. The change in direction and statistical significance of the trends, when considering different analysis periods, results from the grouping of very energetic winters around 1990, which affects the linear trend estimation (Figure 2.7).

Table 2.3 Winter storm trends in the Outer Hebrides. Trends are based on different wave data (calibrated ERA5 and CMEMS reanalysis), analysis periods (40 and 70 years), and storm identification approaches (Storm identification algorithm ($Storm_{ID}$) and POT). Statistically significant trends for 0.05 and 0.1 significance levels are indicated in bold and underlined, respectively.

		$\overline{SH_S}$ (mm/yr)	$\overline{ST_P}$ (ms/yr)	ST_P^{98} (ms/yr)	Counts (n/yr)	Duration (h/yr)	Power ($MWhm^{-1}/yr$)
cERA5-70	POT	1.77	**9.22**	**10.44**	**0.13**	**3.03**	**1.43**
	$Storm_{ID}$	-0.62	**5.38**	<u>8.84</u>	0.00	**4.81**	**1.82**
cERA5-40	POT	0.38	1.68	-11.18	-0.05	-1.61	-0.86
	$Storm_{ID}$	3.32	3.93	-8.07	0.00	-2.85	-1.00
cCMEMS-40	POT	2.97	0.54	-0.76	0.00	-1.23	-0.78
	$Storm_{ID}$	<u>6.50</u>	0.08	-0.21	0.00	-2.88	-0.87

The storminess trends determined using the different calibrated datasets display a general agreement, but there is a significant positive SH_S trend (6.5 mm/yr, $p < 0.1$) according to the cCMEMS-40 dataset, while for cERA5-40 or cERA70 there are no statistically significant trends for the same variable. In contrast to the winter SHs, mean winter H_S has a significant long-term (70-year) increasing trend (7 mm/ yr, $p < 0.05$), while no statistically significant trends are present in the shorter, 40-year datasets (cERA5-40 and cCMEMS-40) (Table 2.4). The winter T_P and T_P^{98} trends are only significant and positive when considering the longer 70-year dataset and winter H_S^{98} show contrasting not statistically significant magnitudes for the two different analysed periods.

Table 2.4 Winter wave trends in the Outer Hebrides. Trends are based on different wave data (calibrated ERA5 and CMEMS reanalysis) and analysis period (40 and 70 years). Statistically significant trends for 0.05 and 0.1 significance levels are indicated in bold and underlined, respectively.

	$\overline{H_S}$ (mm/yr)	$\overline{T_P}$ (ms/yr)	H_S^{98} (mm/yr)	T_P^{98} (ms/yr)
cERA5-70	**7**	**8.4**	9.9	**8.4**
cERA5-40	-3.2	5.7	-16.8	-0.9
cCMEMS-40	-5.9	0.4	-13.7	3.7

Considering the temporal variability of the NAO as the dominant mode of climate variability in the NE Atlantic, from 1950 to 2020 the extended winter NAO shows both a significant positive linear long-term trend (Figure 2.8a) and a positive correlation with winter storm parameters (Table 2.5). Negative NAO conditions are related to shorter cumulative storm duration and lower storm power, while positive NAO conditions are linked to more energetic winters in the Outer Hebrides (Figure 2.8b, c, d). Winter storm counts, cumulative duration, and power are all strongly correlated with the NAO, regardless of the storm identification approach (Table 2.5). For the mean and extreme storm parameters (SH_S, SH_S^{98}, ST_P and ST_P^{98}) correlation with the NAO is mostly weak and not statistically significant, while winter mean H_S and T_P are strongly correlated with the NAO ($R \cong 0.9$), reaffirming the role of the NAO as the overwhelming climatological control in interannual storm wave variability in the west of Scotland.

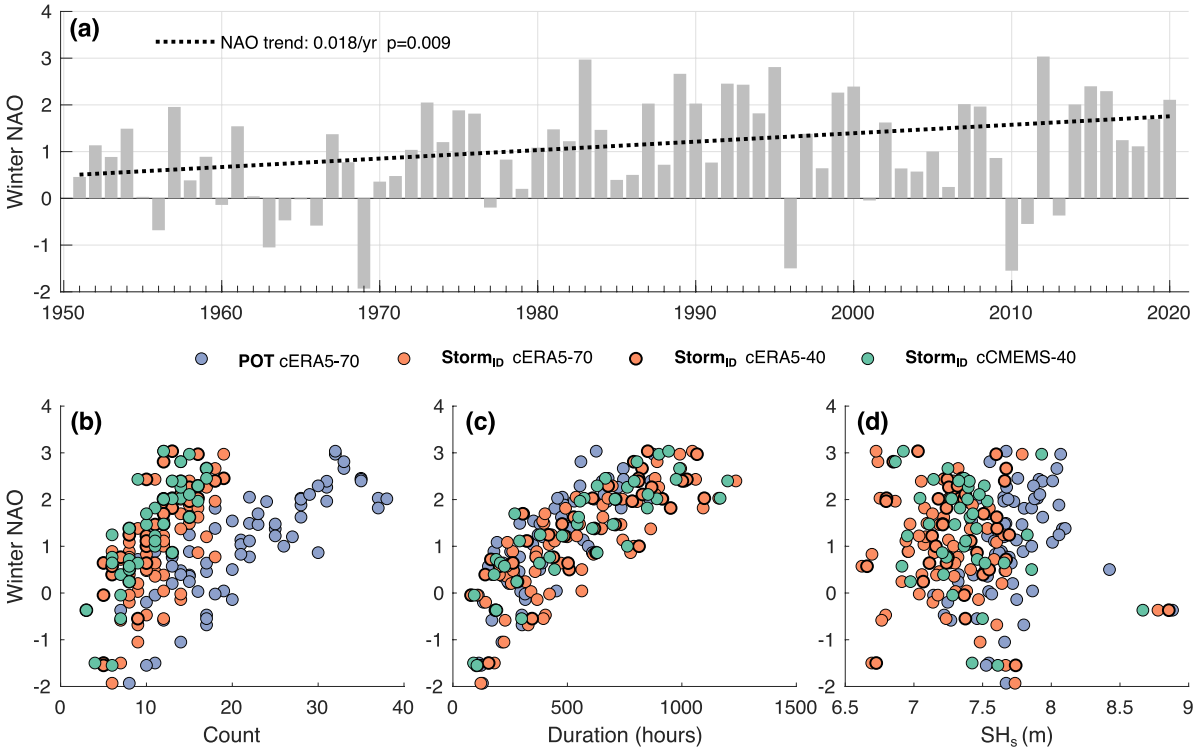

Figure 2.8 Temporal variability of the extended winter NAO **(a)** and its correlation with winter storm counts **(b)**, cumulative winter storm duration **(c)**, and mean winter storm H_S (SH_S) **(d)**. Note that the storm parameters are based on different datasets and different storm identification approaches. The value of R and statistical significance of the correlations is listed in Table 2.5.

Table 2.5 Correlation between winter storm parameters and the NAO for different datasets and the two storm identification approaches. Statistically significant correlations for p-values below 0.05 and 0.1 are indicated in bold and underlined, respectively.

		$\overline{SH_S}$	SH_S^{98}	$\overline{ST_P}$	ST_P^{98}	Count	Duration	Power
cERA5-70	POT	**0.29**	**0.27**	0.23	**0.32**	**0.81**	**0.79**	**0.77**
	$Storm_{ID}$	-0.16	0.23	0.13	**0.29**	**0.67**	**0.80**	**0.79**
cERA5-40	POT	0.18	0.12	-0.15	-0.02	**0.83**	**0.82**	**0.78**
	$Storm_{ID}$	-0.15	0.09	-0.15	-0.02	**0.81**	**0.83**	**0.8**
cCMEMS-40	POT	0.12	0.09	-0.11	0.08	**0.83**	**0.82**	**0.78**
	$Storm_{ID}$	-0.28	0.03	**-0.35**	-0.01	**0.81**	**0.82**	**0.79**

2.5 Discussion

2.5.1 Storm Identification and Characterisation

The identification of coastal storms can differ substantially according to the scope of analysis, and the choice of storm criteria, which is often arbitrary. This has been highlighted by Harley (2017) and Martzikos et al. (2021a), who reviewed the broad-scale application of statistical storm analyses and the accompanying challenges in defining a generalised storm identification approach. Both reviews concluded that ST, MSD, and ID are the most commonly used criteria to identify storms from H_S records. There is a broad consensus that ST can be determined based on the 95th percentile of the Hs time series, while a MSD of either 6 or 12 h appropriately represents the minimum duration of a coastal storm event. However, the meteorological independence between consecutive storms is poorly defined.

Independence duration can be determined based on the minimum or average time between distinct extratropical cyclones. As such, ID can display high variability according to location, ranging from 6 h on the Dutch coast (Li et al., 2014) to 336 h in Durban, South Africa (Corbella and Stretch, 2012). For western Europe, Priestley et al. (2017a, b) reported that during the exceptional 2013/14 winter season, on average, one intense extratropical cyclone affected the British Isles every 60 h. Such intense cyclones are consistently associated with extreme waves in the North Atlantic (Gramcianinov et al., 2023a), supporting the use of 60 h as an upper bound for the minimum time window between storm wave events in the higher latitudes of the North Atlantic. Importantly, the higher ID estimated by the extremal index based on the Outer Hebrides winter wave datasets indicates values close to 60 h (Table 2.2). A separation of 2.5-days (i.e., 60 h) between independent extreme windstorms affecting western Europe in 1990 and 1999 was identified by Hanley and Caballero (2012). On the other hand, the lower bound of the ID determined with the extremal index for the Outer Hebrides wave datasets indicates a minimum separation of 48 h, which aligns with the declustering window applied by Barton et al. (2022) to study extreme precipitation events over Europe. This indicates that wintertime wave, wind and precipitation extremes in western Europe driven by synoptic-scale processes can be consistently individualised by considering ID of 2–2.5 days (48–60 h). Therefore, the statistical determination of ID using the extremal index to obtain independent coastal storms from wave time series provides results that are in agreement with the meteorological timescales of extratropical cyclones in the eastern North Atlantic.

Implementing ID in high-energy wave environments can lead to storms lasting for several weeks, with repeated periods where Hs is below ST. The occurrence of serial cyclone clustering in the NE Atlantic and affecting the Outer Hebrides, causes rapid succession of winter storms, resulting in events characterised by multiple H_S peaks with intermediate H_S throughs (Figure 2.5). Serial cyclone clustering is often the result of secondary cyclogenesis creating cyclone families that are constrained by large scale flows (jet stream and Rossby wave breaking) (Dacre and Pinto, 2020). As each cyclone in the same family is not truly meteorologically independent, consecutive H_S peaks can be considered as a single storm event, even though Hs may fall below ST. In terms of coastal impacts, storms with aggregated H_S peaks can cause cumulative erosional impacts over extended periods, as there is not enough time for beach recovery in between H_S peaks (Ferreira, 2005; Splinter et al., 2014). However, it is also possible that rapidly succeeding storms are meteorologically unrelated events, possibly leading to a significant reduction in H_S between storm events. This can be captured by implementing IT as proposed in the storm identification algorithm, which assumes that if waves reach H_S values below the seasonal average, even if ID is not exceeded the following ST exceedance is considered an independent event. It is therefore strongly recommended that for statistical based climatological assessments appropriate statistically estimated ID values are considered and implemented to identify coastal storms that are associated with the driving storm meteorological mechanisms for a given coastal area.

The POT approach is a common method to define storms in coastal areas (e.g., Ciavola et al., 2014; Masselink et al., 2014, 2016; Flor-Blanco et al., 2021; Vieira et al., 2021; Celedón et al., 2022), probably due to its simplicity. However, the POT alone only defines peaks of ST exceedances without considering their independence or association with the relevant meteorological forcing. The inclusion of ID and IT can improve the ability to aggregate and distinguish exceedances of ST, improving the representation of the meteorological dynamics of coastal storm events (Harley, 2017). This allows integrating knowledge of storm-driving meteorological processes and linking their changes to possible shifts in storm wave climatology (e.g., Lodise et al., 2022; Gramcianinov et al., 2023a). In addition, the subsequent storminess analysis is physically and statistically more robust than if performed with the POT approach alone. This is particularly important for assessing long-term trends and correlating storm parameters with large scale climatic indices such as the NAO to better understand and predict coastal hazards. Compared to the POT approach, the storm identification algorithm proposed in this work has the advantage of identifying storms that better represent natural extreme events

especially in storm-dominated environments and, therefore, more correctly consider their potential consequences.

The characterisation of coastal storms is fundamental for understanding the potential impacts of storms and ultimately key to coastal risk reduction. For this purpose, wave reanalyses are an important tool, as they allow to extend observational time series in space and time, and the confidence in climatological analyses improves significantly with longer time series (e.g., Feser et al., 2020). In this work, buoy observations were compared with two wave reanalyses. ERA5, a global reanalysis, and CMEMS, a regional reanalysis with higher spatial resolution but lower temporal resolution. Both reanalyses showed very good performance for mean wave energy conditions, but underestimated observations of H_S and T_P during more energetic conditions. The systematic underestimation of extreme waves is a common limitation of several wave reanalyses, due to uncertainties in the wind forcing (Baordo et al., 2020). However, this can be improved by applying a number of calibration methods (Fanti et al., 2023). In the case of ERA5 and CMEMS, the calibration for the Outer Hebrides resulted in a significant improvement of reanalysis datasets (Figure 2.3 and Fig. 2.9 (section 2.7.3)). ERA5 was found to outperform CMEMS for storm conditions, resulting in improved agreement with the estimates of H_S return periods obtained from buoy observations (Figure 2.6), possibly due to the higher temporal resolution. Compared to its predecessor, ERA-Interim, the increase in temporal resolution from 6 h to a 1 h in ERA5, is reported to substantially improve the quality of the reanalysis product, including the representation of storm events (Hersbach et al., 2020). The very good agreement of the reanalysis datasets with the buoy observations allowed to extend the analysis period to the last 70 years and to obtain a robust assessment of the storm climatology in the Outer Hebrides, as well as to compare storm identification approaches in terms of climatological storm characterisation.

2.5.2 Long-term Storm Trends in the Outer Hebrides

In the North Atlantic, there are inconsistencies in extreme wave trends between models, buoy observations and satellite data, particularly due to the use of different analysis periods (Bricheno et al., 2023). Based on a 7-member ensemble of different global wave products covering the period from 1980 to 2014, Erikson et al. (2022) found a decreasing but not statistically significant trend in the area of the Outer Hebrides for H_S^{90} and high wave days, which are defined as the annual number of daily maximum H_S exceeding 6 m. However, when considering a longer period between 1950 and 2008, there is a significant increasing trend in H_S^{90} and T_P^{90}

for the west of Scotland (Dodet et al., 2010; Bromirski and Cayan, 2015). According to the cERA5-70 dataset, winter H_S and H_S^{98} show a long-term significant increasing trend since 1950 with 13.6 and 8.3 mm/yr, respectively, which are consistent with the trend magnitudes reported by Castelle et al. (2018) for the study area. The cERA5-40 winter SH_S determined using both storm identification approaches show no significant trend, and the cCMEMS-40 data shows an increasing trend but only at the lower confidence level ($p < 0.1$) (Table 2.3). The contrasting trends between the analysed periods (1950–2020 versus 1980–2020) demonstrate that linear trends depend strongly on the time frame of analysis due to multiannual and decadal variations in storm wave activity in the North Atlantic (Feser et al., 2020; Bricheno et al., 2023). Besides affecting linear trends, the strong variability of the wave climate in the North Atlantic challenges the selection of representative past reference periods for comparison with future wave climate projections or wave energy resource assessments (e.g., Santo et al., 2015). This reinforces the need for long-term wave time series from reanalysis that have been carefully validated and calibrated against buoy observations.

The correlation of the interannual and multidecadal variability in storm activity in the west of Scotland with the NAO is well established (e.g., Dawson et al., 2004; Santo et al., 2015). The cluster of winter seasons with increased storm activity in the 1990s (Figure 2.7) is mirrored by a prolonged and consistently positive phase of the NAO (Figure 2.8). The 1990s are characterised by frequent and intense cyclones with anomalous extreme wind speeds and shortening of the North Atlantic storm track (Feser et al., 2020). The increased storm activity between 1980 and 2020 contrasts with the less intense winters between 1950 and 1980 (Figure 2.7), which are associated with fewer and less intense positive NAO phases (Figure 2.8) and are consistent with a reduced winter storm power for this region (Santo et al., 2015). Therefore, the winter storm variability in the Outer Hebrides evidences a strong climatic control and can be confidently linked to changes in the NAO.

The increase in winter storm activity is mainly determined by changes in storm duration and storm power, rather than by changes in winter storm counts (Figure 2.7). It is important to note that the trend is unaffected by the method used to identify the storms, as this was applied consistently for all winters. While the number of winter storms determined by the POT approach shows similar patterns to the storm power calculated by the storm identification algorithm, it is possible that some spurious trends emerge from the POT approach, as this approach is still frequently used but lacks the robust independence between events obtained by the storm identification algorithm. Furthermore, both winter storm counts and duration

determined by the storm identification algorithm are strongly correlated with the NAO index, which reinforces the confidence in the results obtained by this approach. The POT approach also captures the increasing trend in winter storm duration, but also an increasing trend in the number of winter storms, thus masking the increase in storm duration. This is a shortcoming of the POT approach, questioning its ability to adequately assess storminess variability and reinforcing the need for an improved storm identification as a basis for more robust storminess trend analysis. Bromirski and Cayan (2015) found no increasing trend in storm duration in the NE Atlantic and attributed an increasing trend in storm power to the higher frequency of winter storms. However, their analysis did not consider an independence duration to identify storm events, highlighting the different results that can be obtained by using different storm identification approaches. Importantly, Amaroche et al. (2022) used a storm identification approach similar to the storm identification algorithm proposed in this work and found that changes in storm intensity in the western Mediterranean are mainly driven by changes in storm duration.

Based on the storm identification algorithm, the winter of 2015 was the most energetic during the analysis period, coinciding with the longest winter storm duration (Figure 2.7). Similarly, Loureiro and Cooper (2018) reported that this winter was the most energetic in the northwest of Ireland since 1950 due to exceptionally high SH_S. However, the POT approach does not identify the 2015 winter as the most energetic on record. Changes in storm duration have been associated with shifts in the extratropical cyclone track (Dolan et al., 1988), but recently longer storm duration has been more closely associated with the intensity of extratropical cyclones, which is controlled by the cyclone displacement speed (Gramcianinov et al., 2023a). For the North Atlantic region between 55°N and 70°N where the Outer Hebrides are located, Gramcianinov et al. (2023a) demonstrates that slower extratropical cyclone displacement speeds relative to its long-term climatology lead to longer storm duration. As storm duration is a fundamental parameter for determining the magnitude of storm impacts (e.g., Backstrom et al., 2022; Masselink et al., 2022), a robust assessment of regional changes in storm duration is crucial for coastal management. This can only be achieved by implementing robust statistical methods for identifying and characterising coastal storms.

2.6 Conclusions

A storm identification algorithm based on statistically defined criteria was developed to identify independent storms from H_S records of the Outer Hebrides (Western Scotland), a storm-

dominated, high wave energy coastal environment exposed to intense, frequent and rapidly succeeding winter storms. Storms are defined by a threshold based on the 95th percentile of H_S, but the independence of consecutive storm events is determined by a minimum duration between storm threshold exceedances or by reduction of H_S to values below the winter average H_S. To avoid arbitrarily selecting the independence duration between consecutive storms, the proposed approach implements a minimum duration between storms based on the clustering tendency of the H_S exceedances above the storm threshold determined by the extremal index. The criteria for storm independence determined by the statistical analysis are consistent with regional meteorological processes and timescales for extratropical cyclones in the eastern North Atlantic. Crucially, they allow the separation of independent winter storm events, even when they occur in rapid succession, but allow the aggregation of storm peaks associated with serially clustered extratropical cyclones, enabling an objective and robust storm characterisation. The identification algorithm is particularly suitable for high-energy, storm-dominated coastal environments, such as those located along the main global extratropical storm tracks.

To assess its performance, the storm identification algorithm was compared to the common POT approach using 40 and 70-year-long calibrated wave reanalyses datasets for Western Scotland. Whilst the POT approach captures changes in extreme H_S, it can lead to spurious trends in storminess changes, as it lacks the robust independence between events that is achieved with the storm identification algorithm. The improved physical and statistical robustness of the storms identified by the storm algorithm is critical for understanding storm hazards and associated coastal risks. In addition, changes in the storm climatology determined using the storm identification algorithm can be linked to the driving meteorological dynamics, thereby improving the predictability of storm impacts.

The storminess analysis identified a significant increase in storm duration, contributing to an increasing trend in storm power in the west of Scotland. It also shows that multiannual and decadal variability in storm wave activity in the region is strongly related to the North Atlantic Oscillation. The results of this work highlight that regional assessments of storm climate variability, based on robust statistical approaches, are essential to complement basin and global-scale studies by providing deeper insights into changes in coastal storminess that are fundamental to coastal management planning.

2.7 Supplementary Material

2.7.1 Wave Data

The observational data were obtained from the West of Hebrides wave buoy operated by the Centre for Environment Fisheries and Aquaculture Science (CEFAS). The directional wave buoy was deployed in February 2009 and in the period between 23/02/2009 – 13/02/2020, missing records account for 1.4 % of the dataset due to mooring problems in August 2010, buoy malfunctioning in February 2020, and regular maintenance operations every two years. The wave parameters are quality controlled and provided at 30 minute intervals. For comparison with the reanalysis data, the temporal resolution was decreased to hourly intervals by averaging observations within the same hour.

The ERA5 wave reanalysis is widely used and the most recent reanalysis product from the European Centre for Medium-Range Weather Forecasts (ECMWF, https://www.ecmwf.int/en/forecasts/datasets/reanalysis-datasets/era5) and provides hourly data from 1950 to the present on a 0.5° x 0.5° grid (Hersbach et al., 2020). In ERA5 the spectral wave model (WAM, WAMDI group) is coupled with the atmospheric model and runs on the ETOPO2 bathymetry data with 2 arc-minutes resolution (NOAA, 2006).

The North-West European Shelf Wave Hindcast (CMEMS) is produced by the North-West Shelf MFC (Met Office, UK) and provides 3 hourly ocean surface wave characteristics from 1980 to the present with a spatial resolution of 0.017° x 0.017°. The data is generated by the WAVEWATCH III (version 4.18) 3-1.5 km Atlantic Margin Model (Tolman, 2014) run on a bathymetry grid derived from EMODNet (http://www.emodnet-bathymetry.eu/) with 1/16 arc-minutes resolution. The wave model is forced on the hourly surface (10 m) wind data provided by the ERA5 atmospheric reanalysis. The wave model's boundary conditions are derived from a Met Office global wave model hindcast which is driven by the same ERA5 wind data. More details are available in the quality information document (https://catalogue.marine.copernicus.eu/documents/QUID/CMEMS-NWS-QUID-004-015.pdf).

2.7.2 Validation

For the validation of the reanalysis products, datasets were created to match the common periods and sampling intervals between reanalyses and buoy data. For comparison between CMEMS and buoy data, the latter was down-sampled to a 3 hour sampling interval. The reanalysis data were statistically compared against the buoy records using Pearson's correlation coefficient (R), root mean square error (RMSE), relative bias (bias), and scatter index (SI),

$$R = \frac{\sum_{i=1}^{N}(M_i-\bar{M})(O_i-\bar{O})}{\sqrt{\sum_{i=1}^{N}(M_i-\bar{M})^2\sum_{i=1}^{N}(O_i-\bar{O})^2}}, \tag{2.10}$$

$$RMSE = \sqrt{\frac{1}{N}\sum_{i=1}^{N}(M_i - O_i)^2}\,, \tag{2.11}$$

$$bias = \frac{\sum_{i=1}^{N}(M_i-O_i)}{\sum_{i=1}^{N}O_i} * 100, \tag{2.12}$$

$$SI = \frac{\sqrt{\frac{1}{N}\sum_{i=1}^{N}[(O_i-\bar{O})-(M_i-\bar{M})]^2}}{\frac{1}{N}\sum_{i=1}^{N}O_i}, \tag{2.13}$$

where O_i are the buoy observations, M_i the modeled data of the wave reanalyses, N is the number of measurements, and the overbar represents the average values. The results of the error metrics are presented in Figure 2.9.

2.7.3 Supplementary Figures and Table

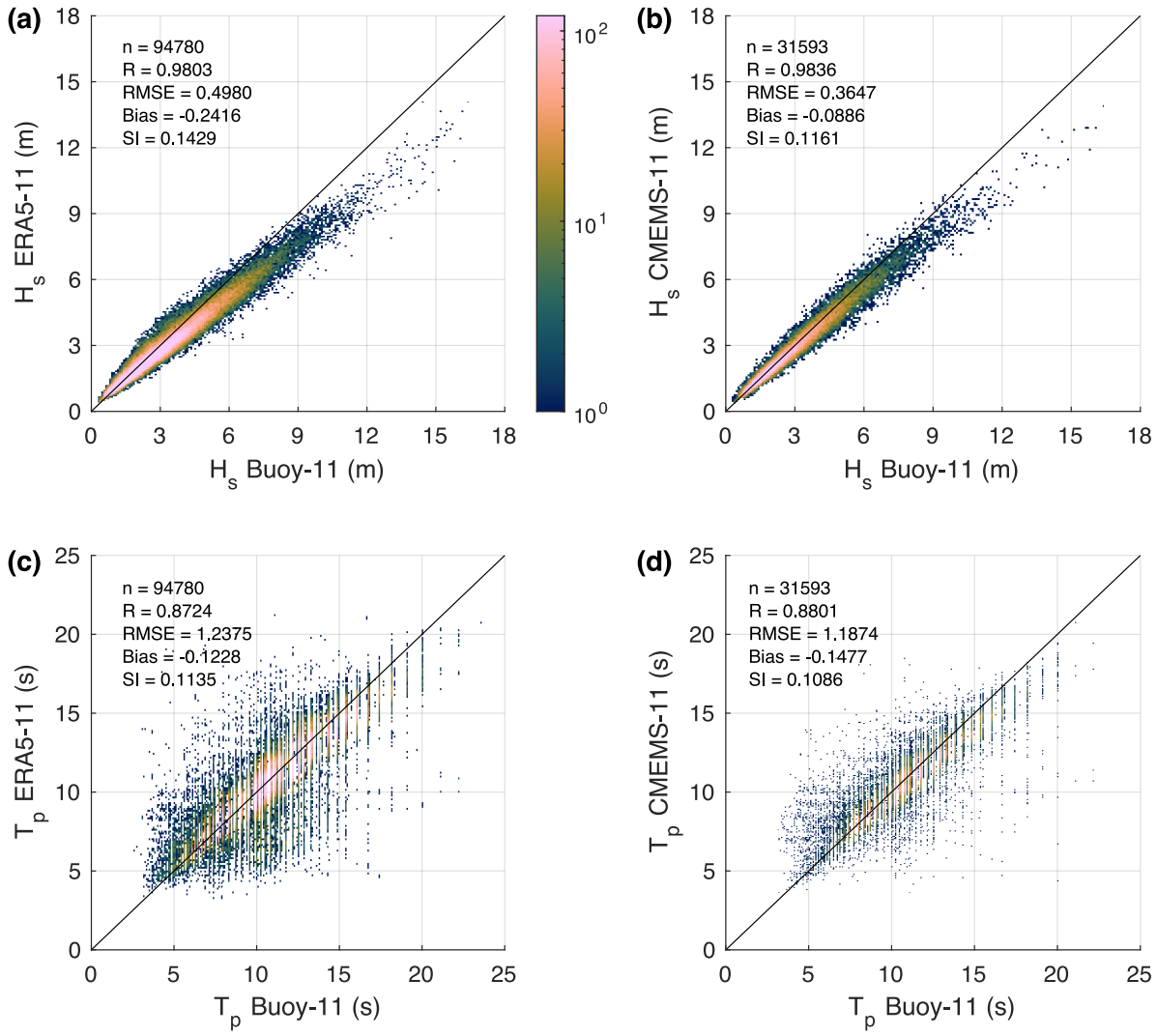

Figure 2.9 Density scatter plots of model H_s **(a,b)** and T_p **(c, d)** against buoy measurements. The inside boxes show the number of records (n), the correlation coefficient (R), the Root Mean Squared Error (RMSE), the bias, and the scatter index (SI). Note that the CMEMS reanalysis as a temporal resolution of 3 hours, which results in fewer records compared to ERA5 that has a 1-hour resolution. The density colorbar is representative for all subplots.

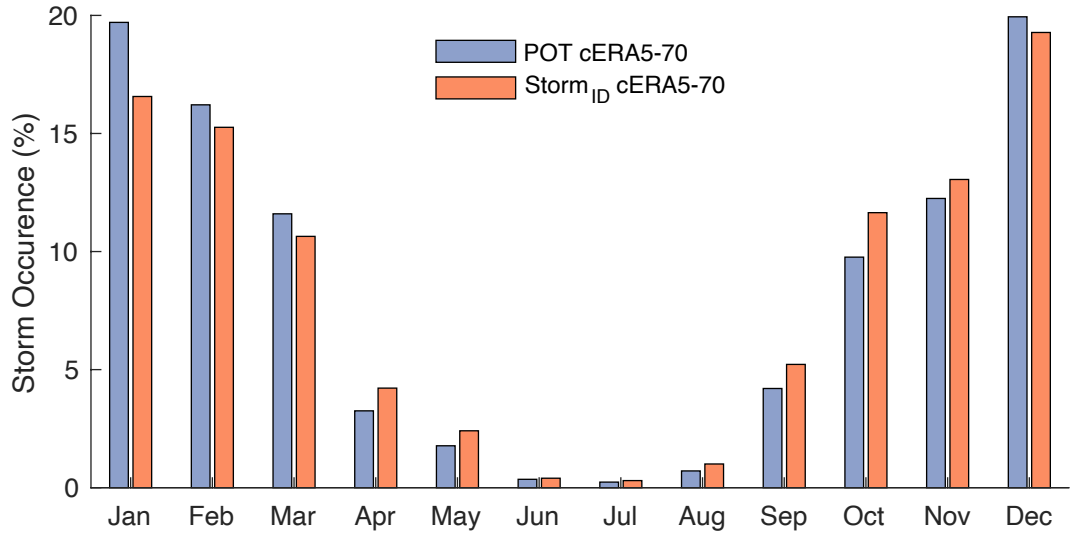

Figure 2.10 Storm counts for each month based on the cERA5-70 dataset using the storm identification approach ($Storm_{ID}$) and the POT approach.

Table 2.6 The rank of the 10 most energetic storms that occurred between 1950 and 2020 in the Outer Hebrides.

Rank	Year	$\overline{SH_S}$ (m)	SH_S^{98} (m)	$\overline{ST_P}$ (s)	ST_P^{98} (s)	Duration (h)	Power (MWh/m)
1	1993	7.50	11.35	13.61	17.08	403	162.90
2	1994	7.46	13.63	14.77	19.28	351	162.15
3	2005	7.06	14.83	13.74	16.23	389	144.16
4	1994	6.97	11.57	13.92	17.65	342	120.94
5	2015	8.38	14.33	14.80	16.58	219	117.11
6	1983	7.24	11.09	14.43	19.10	287	114.13
7	2013	7.55	10.31	14.42	17.30	273	113.23
8	2000	7.45	11.58	15.29	18.85	248	111.54
9	1986	10.16	17.09	14.73	18.83	121	106.68
10	2015	6.85	10.92	14.55	17.36	293	104.17

2.8 Acknowledgments

Vincent Kümmerer receives funding for his Ph.D. through the Portuguese Foundation of Science and Technology (FCT) grant 2020.07497.DB. This work was supported by FCT, under the projects LA/P/00069/2020 (granted to the Associate Laboratory ARNET) and UID/00350/2020 CIMA. Access to the wave data from the Outer Hebrides wave buoy was kindly provided by CEFAS Wavenet and the reanalysis products from the ECMWF and the

Copernicus Marine Service. Access to sea level pressure data was provided by the National Centre for Atmospheric Research for the sea level pressure data, and the storm tracks by was made available by John Lodise

(https://github. com/jlodise/JGR2022_ExtratropicalCycloneTracker).

2.9 References

Almeida LP, Ferreira O, Vousdoukas MI, Dodet G (2011) Historical variation and trends in storminess along the Portuguese South Coast. Nat. Hazards Earth Syst. Sci. 11(9):2407–2417

Almeida LP, Vousdoukas MV, Ferreira Ó, Rodrigues BA, Matias A (2012) Thresholds for storm impacts on an exposed sandy coastal area in Southern Portugal. Geomorphology 143–144:3–12. https:// doi.org/10.1016/j.geomorph.2011.04.047

Amarouche K, Akpınar A, Semedo A (2022) Wave storm events in the Western Mediterranean Sea over four decades. Ocean Model 170:101933. https://doi.org/10.1016/j.ocemod.2021.101933

Armaroli C, Ciavola P, Perini L, Calabrese L, Lorito S, Valentini A, Masina M (2012) Critical storm thresholds for significant morphological changes and damage along the Emilia-Romagna coastline, Italy. Geomorphology 143–144:34–51. https://doi.org/10.1016/j.geomorph.2011.09.006

Arns A, Wahl T, Haigh ID, Jensen J, Pattiaratchi C (2013) Estimating extreme water level probabilities: a comparison of the direct methods and recommendations for best practise. Coast Eng 81:51–66. https://doi.org/10.1016/j.coastaleng.2013.07.003

Backstrom JT, Loureiro C, Eulie DO (2022) Impacts of Hurricane Matthew on adjacent developed and undeveloped barrier islands in southeastern North Carolina. Regional Studies in Marine Science 53:102391. https://doi.org/10.1016/j.rsma.2022.102391

Baordo F, Clementi E, Iovino D, Masina S (2020) Intercomparison and assessement of wave models at global scale (Technical Notes No. TN0287). CMCC.

Barton Y, Giannakaki P, von Waldow H, Chevalier C, Pfahl S, Martius O (2016) Clustering of regional-scale extreme precipitation events in Southern Switzerland. Mon Weather Rev 144(1):347–369. https://doi.org/10.1175/MWR-D-15-0205.1

Barton Y, Rivoire P, Koh J, Kopp J, Martius O (2022) On the temporal clustering of European extreme precipitation events and its relationship to persistent and transient large-scale atmospheric drivers. Weather Clim Extremes 38:100518. https://doi.org/10.1016/j.wace.2022.100518

Bell B, Hersbach H, Simmons A, Berrisford P, Dahlgren P, Horányi A, Muñoz-Sabater J, Nicolas J, Radu R, Schepers D, Soci C, Villaume S, Bidlot J, Haimberger L, Woollen J, Buontempo C, Thépaut J (2021) The ERA5 global reanalysis: preliminary extension to 1950. Q J R Meteorol Soc 147(741):4186–4227. https://doi. org/10.1002/qj.4174

Bricheno LM, Amies JD, Chowdhury P, Woolf D, Timmermans B (2023) Climate change impacts on storms and waves relevant to the UK and Ireland. MCCIP Sci Rev. https://doi.org/10.14465/ 2023.reu09.str

Bromirski PD, Cayan DR (2015) Wave power variability and trends across the North Atlantic influenced by decadal climate patterns: North Atlantic Decadal Wave Variability. Journal of Geophysical Research: Oceans 120(5):3419–3443. https://doi.org/10.1002/2014JC010440

Castelle B, Dodet G, Masselink G, Scott T (2017) A new climate index controlling winter wave activity along the Atlantic coast of Europe: the West Europe Pressure Anomaly. Geophys Res Lett. 44:1384–1392. https://doi.org/10.1002/2016GL072379

Castelle B, Dodet G, Masselink G, Scott T (2018) Increased wintermean wave height, variability, and periodicity in the Northeast Atlantic over 1949–2017. Geophys Res Lett 45(8):3586–3596. https://doi.org/10.1002/2017GL076884

Castelle B, Marieu V, Bujan S, Splinter KD, Robinet A, Sénéchal N, Ferreira S (2015) Impact of the winter 2013–2014 series of severe Western Europe storms on a double-barred sandy coast: Beach and dune erosion and megacusp embayments. Geomorphology 238:135–148. https://doi.org/10.1016/j.geomorph.2015.03.006

Castelle B, Harley M (2020) Extreme events: impact and recovery. In: Sandy beach morphodynamics. https://www.sciencedirect.com/ science/book/9780081029275. Accessed 05 Nov 2022

Celedón V, Del Río L, Ferreira Ó, Costas S, Plomaritis TA (2022) Identification of risk hotspots to storm events in a coastal region with high morphodynamic alongshore variability. Nat Hazards 115(1):461–488. https://doi.org/10.1007/s11069-022-05562-x

Ciavola P, Ferreira O, Dongeren AV, de Vries JVT, Armaroli C, Harley M (2014) Prediction of storm impacts on beach and dune systems. In: Quevauviller P (ed) Hydrometeorological hazards. Wiley, New York, pp 227–52. https://doi.org/10.1002/9781118629567.ch3d

Coles S (2001) An introduction to statistical modeling of extreme values. Springer, London. https://doi.org/10.1007/978-1-4471-3675-0

Corbella S, Stretch DD (2012) Multivariate return periods of sea storms for coastal erosion risk assessment. Nat Hazard 12(8):2699–2708. https://doi.org/10.5194/nhess-12-2699-2012

Dacre HF, Pinto JG (2020) Serial clustering of extratropical cyclones: A review of where, when and why it occurs. Npj Clim Atmos Sci 3(1):48. https://doi.org/10.1038/s41612-020-00152-9

Dawson A, Elliott L, Noone S, Hickey K, Holt T, Wadhams P, Foster I (2004) Historical storminess and climate 'see-saws' in the North Atlantic region. Mar Geol 210(1–4):247–259. https://doi.org/10. 1016/j.margeo.2004.05.011

Dawson AG, Dawson S, Ritchie W (2007) Historical Climatology and coastal change associated with the 'Great Storm' of January 2005, South Uist and Benbecula Scottish outer hebrides. Scot Geograph J 123(2):135–149. https://doi.org/10.1080/14702540701623784

De Michele C, Salvadori G, Passoni G, Vezzoli R (2007) A multivariate model of sea storms using copulas. Coast Eng 54(10):734751. https://doi.org/10.1016/j.coastaleng.2007.05.007

Del Río L, Plomaritis TA, Benavente J, Valladares M, Ribera P (2012) Establishing storm thresholds for the Spanish Gulf of Cádiz coast. Geomorphology 143–144:13–23. https://doi.org/10.1016/j.geomo rph.2011.04.048

Dissanayake P, Brown J, Wisse P, Karunarathna H (2015) Effects of storm clustering on beach/dune evolution. Mar Geol 370:63–75. https://doi.org/10.1016/j.margeo.2015.10.010

Dodet G, Bertin X, Taborda R (2010) Wave climate variability in the North-East Atlantic Ocean over the last six decades. Ocean Model 31(3–4):120–131. https://doi.org/10.1016/j.ocemod.2009.10.010

Dolan R, Lin H, Hayden B (1988) Mid-Atlantic Coastal Storms. J Coastal Res 4(3):417–433

Erikson L, Morim J, Hemer M, Young I, Wang XL, Mentaschi L, Mori N, Semedo A, Stopa J, Grigorieva V, Gulev S, Aarnes O, Bidlot J-R, Breivik Ø, Bricheno L, Shimura T, Menendez M, Markina M, Sharmar V, Webb A (2022) Global ocean wave fields show consistent regional trends between 1980 and 2014 in a multi-product ensemble. Commun Earth Environ. 3(1):320. https://doi.org/10. 1038/s43247-022-00654-9

Fanti V, Ferreira Ó, Kümmerer V, Loureiro C (2023) Improved estimates of extreme wave conditions in coastal areas from calibrated global reanalyses. Commun Earth Environ 4(1):151. https://doi. org/10.1038/s43247-023-00819-0

Fawcett L, Walshaw D (2008) Bayesian inference for clustered extremes. Extremes 11(3):217–233. https://doi.org/10.1007/ s10687-007-0054-y

Ferreira JA, Guedes Soares C (1998) An application of the peaks over threshold method to predict extremes of significant wave height. J Offshore Mech Arct Eng 120(3):165–176. https://doi.org/10. 1115/1.2829537

Ferreira O (2005) Storm groups versus extreme single storms: predicted erosion and management consequences. J Coastal Res SI(42):221–227

Ferro CAT, Segers J (2003) Inference for clusters of extreme values: clusters of extreme values. J R Stat Soc Series B Stat Methodol 65(2):545–556. https://doi.org/10.1111/1467-9868.00401

Feser F, Krueger O, Woth K, van Garderen L (2020) North Atlantic winter storm activity in modern reanalyses and pressure-based observations. J Clim 34(7):2411–2428. https://doi.org/10.1175/ JCLI-D-20-0529.1

Flor-Blanco G, Alcántara-Carrió J, Jackson DWT, Flor G, FloresSoriano C (2021) Coastal erosion in NW Spain: recent patterns under extreme storm wave events. Geomorphology 387:107767. https://doi.org/10.1016/j.geomorph.2021.107767

Garnier E, Ciavola P, Spencer T, Ferreira O, Armaroli C, McIvor A (2018) Historical analysis of storm events: case studies in France, England, Portugal and Italy. Coast Eng 134:10–23. https://doi.org/ 10.1016/j.coastaleng.2017.06.014

Gramcianinov CB, de Camargo R, Campos RM, Guedes Soares C, da Silva Dias PL (2023a) Impact of extratropical cyclone intensity and speed on the extreme wave trends in the Atlantic Ocean. Clim Dyn 60(5–6):1447–1466. https://doi.org/10.1007/ s00382-022-06390-2

Gramcianinov CB, Staneva J, De Camargo R, Da Silva Dias PL (2023b) Changes in extreme wave events in the southwestern South Atlantic Ocean. Ocean Dyn 73(11):663–678. https://doi. org/10.1007/s10236-023-01575-7

Haigh ID, Wadey MP, Wahl T, Ozsoy O, Nicholls RJ, Brown JM, Horsburgh K, Gouldby B (2016) Spatial and temporal analysis of extreme sea level and storm surge events around

the coastline of the UK. Scientific Data 3(1):160107. https://doi.org/10.1038/sdata.2016.107

Hall TM, Kossin JP (2019) Hurricane stalling along the North American coast and implications for rainfall. Npj Clim Atmos Sci 2(1):17. https://doi.org/10.1038/s41612-019-0074-8

Hanley J, Caballero R (2012) The role of large-scale atmospheric flow and Rossby wave breaking in the evolution of extreme windstorms over Europe: EXTREME EUROPEAN STORMS. Geophys Res Lett. https://doi.org/10.1029/2012GL053408

Harley MD (2017) Coastal storm definition. Coastal storms: processes and impacts. John Wiley and Sons Inc., New York, pp 1–22

Harley MD, Turner IL, Kinsela MA, Middleton JH, Mumford PJ, Splinter KD, Phillips MS, Simmons JA, Hanslow DJ, Short AD (2017) Extreme coastal erosion enhanced by anomalous extratropical storm wave direction. Sci Rep 7(1):6033. https://doi.org/10.1038/s41598-017-05792-1

Hersbach H, Bell B, Berrisford P, Hirahara S, Horányi A, MuñozSabater J, Nicolas J, Peubey C, Radu R, Schepers D, Simmons A, Soci C, Abdalla S, Abellan X, Balsamo G, Bechtold P, Biavati G, Bidlot J, Bonavita M, Thépaut J (2020) The ERA5 global reanalysis. Quart J R Meteorol Soc 146(730):1999–2049. https://doi.org/10.1002/qj.3803

Hochet A, Dodet G, Ardhuin F, Hemer M, Young I (2021) Sea state decadal variability in the North Atlantic: a review. Climate 9(12):173. https://doi.org/10.3390/cli9120173

Hurrell JW (1995) Decadal trends in the North Atlantic oscillation: regional temperatures and precipitation. Science 269(5224):676679. https://doi.org/10.1126/science.269.5224.676

Li F, van Gelder PHAJM, Ranasinghe R, Callaghan DP, Jongejan RB (2014) Probabilistic modelling of extreme storms along the Dutch coast. Coast Eng 86:1–13. https://doi.org/10.1016/j.coastaleng. 2013.12.009

Lobeto H, Menendez M, Losada IJ (2021) Future behavior of wind wave extremes due to climate change. Sci Rep 11(1):7869. https:// doi.org/10.1038/s41598-021-86524-4

Lodise J, Merrifield S, Collins C, Rogowski P, Behrens J, Terrill E (2022) Global climatology of extratropical cyclones from a new tracking approach and associated wave heights from satellite radar altimeter. J Geophys Res Oceans. https://doi.org/10.1029/2022JC018925

Lopatoukhin LJ, Rozhkov VA, Ryabinin VE, Swail VR, Boukhanovsky AV, Degtyarev AB (2000) Estimation of extreme wind wave heights (WMO/TD-No. 1041 No. 9; JCOMM Technical Report No. 9, p. 70). https://repository.oceanbestpractices.org/bitstream/handle/11329/85/TR09.pdf?sequence=1. Accessed 05 Nov 2022

Loureiro C, Cooper JAG (2018) Temporal variability in winter wave conditions and storminess in the northwest of Ireland. Irish Geogr. https://doi.org/10.2014/igj.v51i2.1369

Loureiro C, Ferreira Ó, Cooper JAG (2012) Geologically constrained morphological variability and boundary effects on embayed beaches. Mar Geol 329–331:1–15. https://doi.org/10.1016/j.margeo.2012.09.010

Mailier PJ, Stephenson DB, Ferro CAT, Hodges KI (2006) Serial clustering of extratropical cyclones. Mon Weather Rev 134(8):22242240. https://doi.org/10.1175/MWR3160.1

Martzikos NT, Prinos PE, Memos CD, Tsoukala VK (2021a) Key research issues of coastal storm analysis. Ocean Coast Manag 199:105389. https://doi.org/10.1016/j.ocecoaman.2020.105389

Martzikos NT, Prinos PE, Memos CD, Tsoukala VK (2021b) Statistical analysis of mediterranean coastal storms. Oceanologia 63(1):133148. https://doi.org/10.1016/j.oceano.2020.11.001

Masselink G, Austin M, Scott T, Poate T, Russell P (2014) Role of wave forcing, storms and NAO in outer bar dynamics on a highenergy, macro-tidal beach. Geomorphology 226:76–93. https:// doi.org/10.1016/j.geomorph.2014.07.025

Masselink G, Castelle B, Scott T, Dodet G, Suanez S, Jackson D, Floc'h, F. (2016) Extreme wave activity during 2013/2014 winter and morphological impacts along the Atlantic coast of Europe. Geophys Res Lett 43(5):2135–2143. https://doi.org/10.1002/ 2015GL067492

Masselink G, Brooks S, Poate T, Stokes C, Scott T (2022) Coastal dune dynamics in embayed settings with sea-level rise—examples from the exposed and macrotidal north coast of SW England. Mar Geol 450:106853. https://doi.org/10.1016/j.margeo.2022.106853

Melet A, Meyssignac B, Almar R, Le Cozannet G (2018) Under-estimated wave contribution to coastal sea-level rise. Nat Clim Chang 8(3):234–239. https://doi.org/10.1038/s41558-018-0088-y

Mendoza ET, Jimenez JA, Mateo J (2011) A coastal storms intensity scale for the Catalan sea (NW Mediterranean). Nat Hazard 11(9):2453–2462. https://doi.org/10.5194/nhess-11-2453-2011

Mendoza ET, Trejo-Rangel MA, Salles P, Appendini CM, LopezGonzalez J, Torres-Freyermuth A (2013) Storm characterisation and coastal hazards in the Yucatan Peninsula. J Coastal Res 65:790–795. https://doi.org/10.2112/SI65-134.1

Morim J, Vitousek S, Hemer M, Reguero B, Erikson L, Casas-Prat M, Wang XL, Semedo A, Mori N, Shimura T, Mentaschi L, Timmermans B (2021) Global-scale changes to extreme ocean wave events due to anthropogenic warming. Environ Res Lett 16(7):074056. https://doi.org/10.1088/1748-9326/ac1013

Neill SP, Vögler A, Goward-Brown AJ, Baston S, Lewis MJ, Gillibrand PA, Waldman S, Woolf DK (2017) The wave and tidal resource of Scotland. Renewable Energy 114:3–17. https://doi.org/10.1016/j. renene.2017.03.027

Neumann B, Vafeidis AT, Zimmermann J, Nicholls RJ (2015) Future coastal population growth and exposure to sea-level rise and coastal flooding—a global assessment. PLoS ONE 10(3):e0118571. https://doi.org/10.1371/journal.pone.0118571

Oikonomou CLG, Gradowski M, Kalogeri C, Sarmento AJNA (2020) On defining storm intervals: extreme wave analysis using extremal index inferencing of the run length parameter. Ocean Eng 217:107988. https://doi.org/10.1016/j.oceaneng.2020.107988

Pinto JG, Gómara I, Masato G, Dacre HF, Woollings T, Caballero R (2014) Large-scale dynamics associated with clustering of extratropical cyclones affecting Western Europe. Journal of Geophysical Research: Atmospheres 119(24):13704–13719. https://doi.org/10. 1002/2014JD022305

Plomaritis TA, Benavente J, Laiz I, Del Río L (2015) Variability in storm climate along the Gulf of Cadiz: The role of large scale atmospheric forcing and implications to coastal hazards. Clim Dyn 45(9–10):2499–2514. https://doi.org/10.1007/s00382-015-2486-4

Priestley MDK, Dacre HF, Shaffrey LC, Schemm S, Pinto JG (2020) The role of secondary cyclones and cyclone families for the North Atlantic storm track and clustering over western Europe. Abstract Quart J Royal Meteorol Soc 146(728):1184–1205. https://doi.org/ 10.1002/qj.3733

Priestley MDK, Pinto JG, Dacre HF, Shaffrey LC (2017a) Rossby wave breaking, the upper level jet, and serial clustering of extratropical cyclones in western Europe: WESTERN EUROPE CLUSTERING DYNAMICS. Geophys Res Lett 44(1):514–521. https://doi.org/10.1002/2016GL071277

Priestley MDK, Pinto JG, Dacre HF, Shaffrey LC (2017b) The role of cyclone clustering during the stormy winter of 2013/2014. Weather 72(7):187–192. https://doi.org/10.1002/wea.3025

Ramsay DL, Brampton AH (2000) Coastal cells in Scotland: Cells 8 & 9—The Western Isles. Scottish Natural Heritage Research, Survey and Monitoring Report No 150. p. 120. https://www.dynamiccoa st.com/files/Ramsay_Brampton_Cell_0809.pdf

Santo H, Taylor PH, Woollings T, Poulson S (2015) Decadal wave power variability in the North-East Atlantic and North Sea: WAVE POWER VARIABILITY. Geophys Res Lett 42(12):49564963. https://doi.org/10.1002/2015GL064488

Scott T, McCarroll RJ, Masselink G, Castelle B, Dodet G, Saulter A, Scaife AA, Dunstone N (2021) Role of atmospheric indices in describing inshore directional wave climate in the United Kingdom and Ireland. Earth's Future. https://doi.org/10.1029/2020E F001625

Senechal N, Coco G, Castelle B, Marieu V (2015) Storm impact on the seasonal shoreline dynamics of a meso- to macrotidal open sandy beach (Biscarrosse, France). Geomorphology 228:448–461. https://doi.org/10.1016/j.geomorph.2014.09.025

Sénéchal N, Castelle B, Bryan K (2017) Storm clustering and beach response. Coastal storms: processes and impacts. John Wiley and Sons, Inc, New York, pp 151–174

Serafin KA, Ruggiero P, Barnard PL, Stockdon HF (2019) The influence of shelf bathymetry and beach topography on extreme total water levels: Linking large-scale changes of the wave climate to local coastal hazards. Coast Eng 150:1–17. https://doi.org/10.1016/j.coastaleng.2019.03.012

Sharmar VD, Markina MYu, Gulev SK (2021) Global ocean wind-wave model hindcasts forced by different reanalyzes: a comparative assessment. J Geophys Res Oceans 126(1):e2020JC016710. https://doi.org/10.1029/2020JC016710

Short AD (1999) Global variation in beach systems. Handbook of beach and shoreface morphodynamics. John Wiley and Sons, Inc, New York, pp 21–35

Smith RL, Weissman I (1994) Estimating the extremal index. J Roy Stat Soc: Ser B (methodol) 56(3):515–528. https://doi.org/10. 1111/j.2517-6161.1994.tb01997.x

Smith AM, Mather AA, Bundy SC, Cooper JAG, Guastella LA, Ramsay PJ, Theron A (2010) Contrasting styles of swell-driven coastal erosion: Examples from KwaZulu-Natal. South Africa Geological Magazine 147(6):940–953. https://doi.org/10.1017/S001675681 0000361

Splinter KD, Carley JT, Golshani A, Tomlinson R (2014) A relationship to describe the cumulative impact of storm clusters on beach erosion. Coast Eng 83:49–55. https://doi.org/10.1016/j.coastaleng. 2013.10.001

Timmermans BW, Gommenginger CP, Dodet G, Bidlot J-R (2020) Global wave height trends and variability from new multimission satellite altimeter products, reanalyses, and wave buoys. Geophysl Res Lett. https://doi.org/10.1029/2019GL086880

Vieira BFV, Pinho JLS, Barros JAO (2021) Extreme wave value analysis under uncertainty of climate change scenarios off Iberian Peninsula coast. Ocean Eng 229:109018. https://doi.org/10.1016/j. oceaneng.2021.109018

Weisse R, Günther H (2007) Wave climate and long-term changes for the Southern North Sea obtained from a high-resolution hindcast 1958–2002. Ocean Dyn 57(3):161–172. https://doi.org/10.1007/ s10236-006-0094-x

Wojtysiak K, Herman A, Moskalik M (2018) Wind wave climate of west Spitsbergen: seasonal variability and extreme events. Oceanologia 60(3):331–343. https://doi.org/10.1016/j.oceano.2018. 01.002

Young IR, Ribal A (2019) Multiplatform evaluation of global trends in wind speed and wave height. Science 364(6440):548–552. https:// doi.org/10.1126/science.aav952

Chapter 3

Muted Morphological Response to Extreme Storms in Geologically Controlled Barrier Islands

Kümmerer, V., Loureiro, C., Ferreira, Ó., (2023). Muted morphological response to extreme storms in geologically controlled barrier islands, In: Coastal Sediments 2023: *The Proceedings of the Coastal Sediments 2023* (pp. 44–56).

Abstract

Storm-induced erosion and shoreline retreat of barrier islands are assumed to be primarily controlled by the intensity of the hydrodynamic forcing and barrier morphology. However, less studied non-dynamic variables such as the underlying bedrock topography can mediate the morphological response in geologically controlled barrier systems. This work investigates the role of geological control on barrier island morphodynamics during an extreme storm event. Exposed to highly energetic wave conditions in the West of Scotland, a unique barrier island system developed over a gentle sloping bedrock surface along the Outer Hebrides. Morphological changes driven by an extreme storm in February 2022 were monitored along sections of the Hebridean barriers, revealing muted morphological storm response, but with alongshore variable storm impacts. These ranged from minor dune erosion to overwash of low-lying composite barriers and are linked to variation in barrier morphology and the slope of the bedrock-controlled shoreface and intertidal terrace, which strongly influence nearshore wave transformation. Results suggest that severe storm impacts in the Outer Hebrides barrier islands are only observed when there is an exceptional combination of hydrodynamic forcing (extreme storm waves with high tides and storm surges) and will be enhanced in areas with lower dune morphology and narrower geologically controlled intertidal terraces. Nearshore hydrodynamic

processes such as surfbeat and wave setup are likely to be important to understand morphological changes in such underreported geologically controlled barrier systems.

3.1 Introduction

Barrier islands are assumed to respond dynamically to storms, with erosion and shoreline retreat being controlled primarily by the intensity of the storm hydrodynamic forcing and barrier morphology (Sallenger, 2000; Ferreira et al., 2017). However, in geologically controlled barriers, non-dynamic variables such as the framework geology or net sediment supply mediate the morphological responses to storms. Untangling the role of understudied geological controls on morphological storm response is paramount for coastal management in the context of rising sea levels and changing storminess (Cooper et al., 2018). This work explores field observations and wave modelling along sections of the Outer Hebrides in Scotland (Figure 3.1) to investigate the role of geological control on barrier morphodynamics during an extreme storm event.

3.2 Study Area

A unique barrier island system in the Outer Hebrides islands in the West of Scotland (Figure 3.1) developed over a gently sloping planar bedrock surface carved during the Pliocene (Dawson et al., 2013). The bedrock surface is extensively exposed along the islands and the inner shelf but thinly covered by sand along the coast (Kenyon and Pelton, 1979). Contrarily to most common barrier island systems worldwide, the Outer Hebrides barrier islands are highly constrained in their evolution by bedrock surfaces and rocky headlands (Cooper et al., 2012).

The characteristics of the Hebridean barrier system place it at the extreme end of geological control on barrier island evolution, as the controlling factors of geomorphological variability are not directly linked to hydrodynamic factors, but instead to reduced sediment supply and the topography of the underlying bedrock surfaces (Pile et al., 2019). The irregular pre-quaternary bedrock determines distinct modes of development of the coastal barriers, which migrate landward over or between bedrock surfaces (Cooper et al., 2012). In topographic lows, like Baleshare and Gualan, typical barrier islands can develop, and include sandy shorefaces, extensive dune fields, tidal inlets, and back-barrier lagoons (Figure 3.1b, A and B), while in topographic highs like Howmore, the barriers are perched on bedrock (Figure 3.1b, C). The back-barrier lagoons in these perched barriers are often elevated due to agricultural practices and only remnants of the lagoon systems are present.

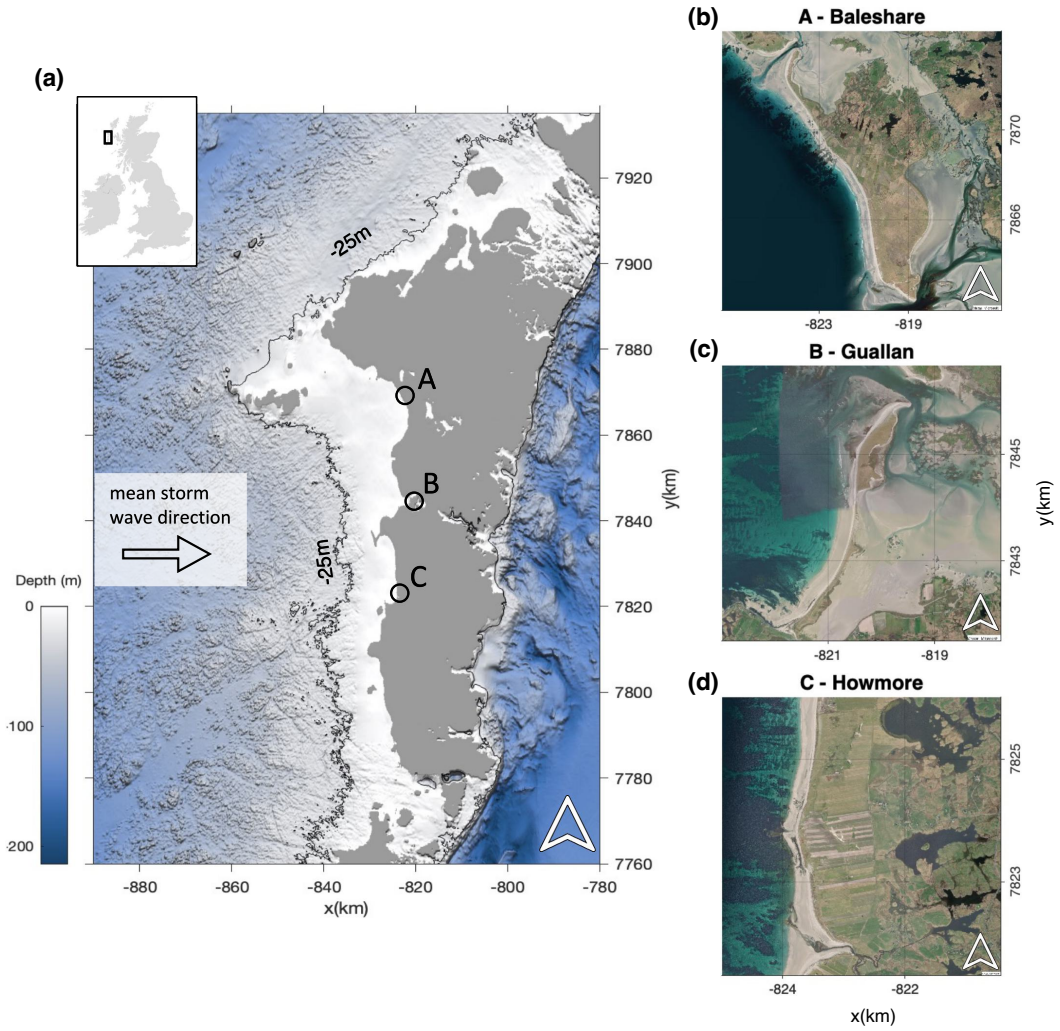

Figure 3.1 Location and bathymetry of the Outer Hebrides barrier system **(a)** and the three study sites **(b)**. Sources: EMODnet bathymetry (a) and Maxar satellite images from Esri World Layer (b).

Alongshore variability in morphology and sediment type are also observed in the Hebridean barriers, which can range from fully sandy systems with high foredunes to composite barriers with sandy dissipative intertidal terraces, gravel to cobble berms and low-elevation foredunes (Cooper et al., 2012). Overwash and breaching occasionally occur in these barriers, as observed in Gualan (Dawson et al., 2012).

The wave climate in the NW of Scotland is extremely energetic, with significant wave height (H_S) frequently exceeding 10 m during storm events, and the tide regime is mesotidal with mean spring tidal range of 4.1 m. The coastline position along the Outer Hebrides has been generally stable in the past decades (Gómez et al., 2014; Hansom et al., 2017). However, winter storms

can drive episodic dune erosion or lead to localized coastal change, as observed following an exceptional storm in January 2005 (Dawson et al., 2007; Angus and Rennie, 2014).

Due to its characteristics and setting, the barrier islands of the Outer Hebrides provide the ideal opportunity to investigate the understudied role of geological control on barrier resilience, enabling new insights into the geomorphological behaviour of geologically controlled barrier islands and beaches.

3.3 Methodology

In order to assess the morphological response of the Outer Hebrides barrier islands to an extreme winter storm in February 2022, event-based field surveying was conducted and complemented by nearshore wave modelling. Pre- and post-storm topographic surveys were performed using a Leica RTK-DGNSS to monitor morphological changes in three distinct locations along the barrier island system (Figure 3.1). The surveys included cross-shore beach profiles performed at low tide, extending from the low tide terrace to the dune crest or back-barrier margin, supplemented by alongshore surveying of the vegetation line and overwash extent. The cross-shore profiles were located away from any tidal inlets or stream outlets to exclude morphological processes related to these landforms. The storm hydrodynamic forcing was characterized using offshore wave observations from the West of Hebrides buoy (located ~30 km offshore from the study sites and in 100 m water depth) and coastal water levels recorded in the Stornoway tide gauge (~100 km North of the study sites). The surveying was performed over a period of approximately 48 hours and coincided with spring tide conditions, with surveys performed immediately prior to and after the storm peak (Figure 3.2).

To analyse nearshore wave conditions, offshore waves were propagated to the coast using SWAN v41.41 (Simulating WAves Nearshore; Booij et al. 1999; Ris et al., 1999). SWAN was run in third generation, 2D stationary mode and implemented using a 200 m regular grid with water depth determined from the EMODnet bathymetry (EMODnet Bathymetry Consortium, 2020). Two runs were performed with SWAN to simulate the wave field at both high and low tide during the peak of the storm event (Table 3.1). The default settings were used for all simulations, except for depth-induced wave breaking which was determined using the dβ-kd model for surf-breaking due to the complex and shallow shoreface bathymetry (Salmon and Holthuijsen, 2015).

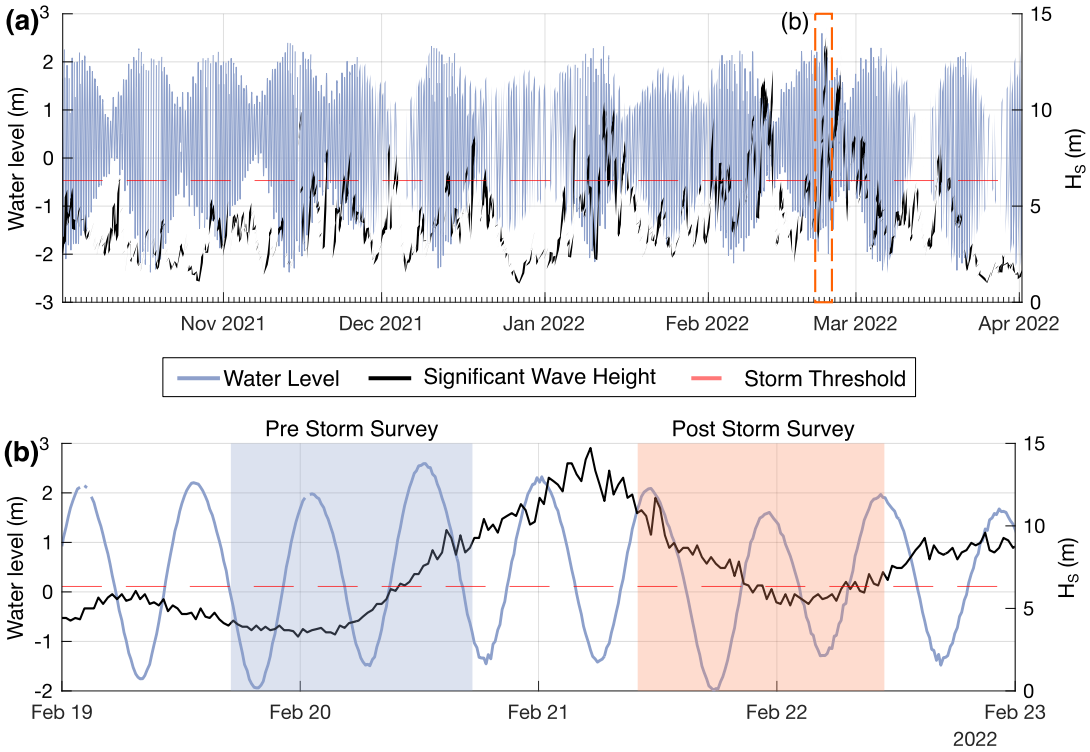

Figure 3.2 Offshore wave heights and water levels during the 2021/22 winter season **(a)**, and during the February 2022 storm event **(b)**. The storm threshold is 6.33 m according to Kümmerer et al. (2021).

Table 3.1 Forcing conditions for SWAN runs. Significant wave height (H_S), peak wave period (T_P), peak wave direction (Dir) and spread, and water level (WL) referenced to Mean Sea Level (MSL).

SWAN run	H_S (m)	T_P (s)	Dir (°)	spread (°)	WL (m, MSL)
High Tide	11.9	18.2	276	34	2.2
Low Tide	14.7	20.0	273	32	-1.4

3.4 Results

The storm of 21st February 2022 analysed in this work was the most energetic storm event of the 2021/22 winter season, with offshore significant wave heights reaching close to 15 m and peak wave periods of 20 s (Figure 3.2 and Table 3.1). Such extreme wave conditions coincided with spring tides and storm surge values up to 0.62 m. Despite the extreme magnitude of the

hydrodynamic forcing and the shore normal exposure of the surveyed barriers (Figure 3.1), the observed morphological changes in barrier topography were limited (Figure 3.3).

Most of the surveyed area displayed minimal morphological changes, but topographic changes with impacts ranging from overwash and minor dune erosion to no measurable change were observed (Figure 3.3). The beach profile in Baleshare showed no measurable change (Figure 3.3a), while minor dune erosion was observed in Howmore (Figure 3.3b). More extensive changes occurred in Gualan, where the low-lying composite barrier was lowered due to overwash of the barrier crest and washover deposition in the back barrier margin (Figure 3.3c and Figure 3.4d).

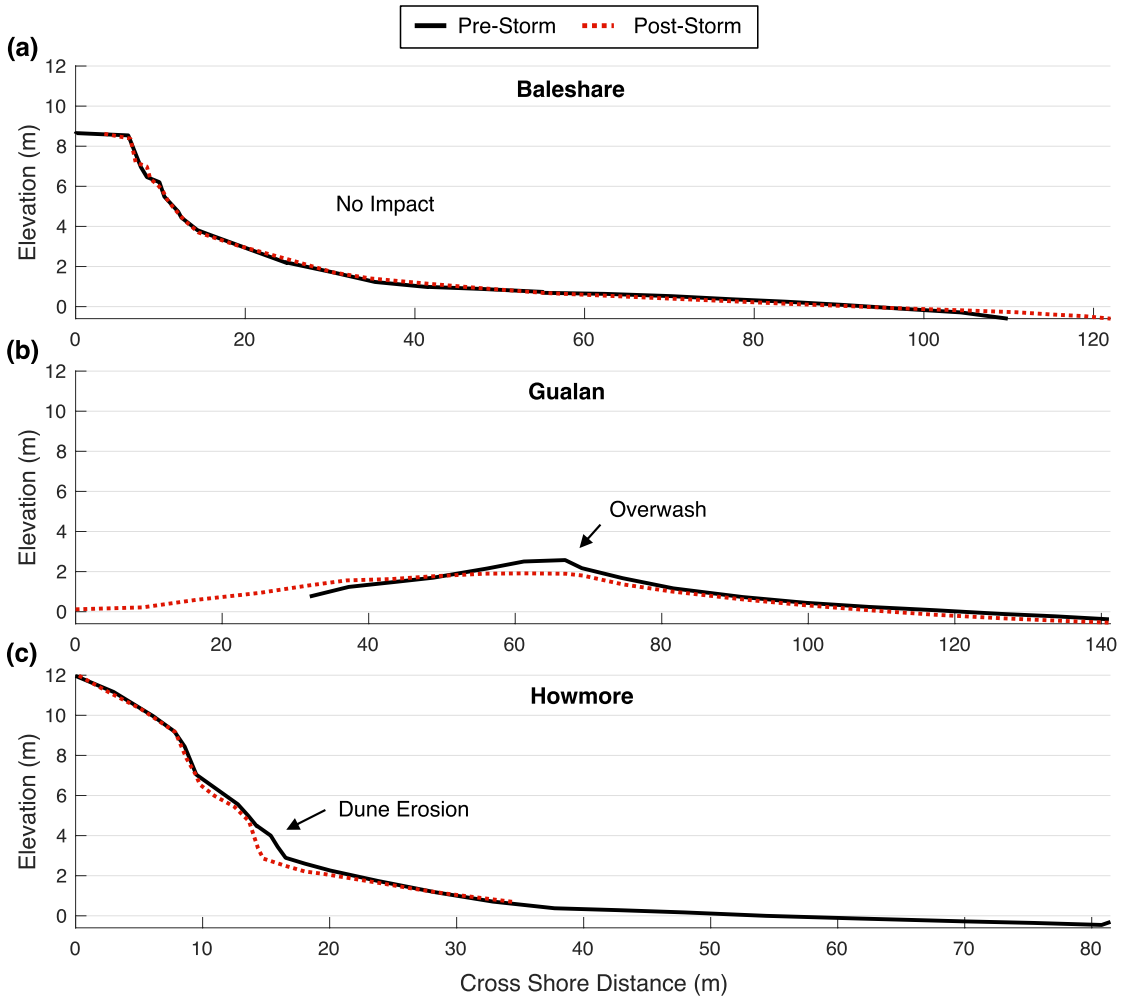

Figure 3.3 Representative pre- and post-storm beach profiles in the study sites.

The morphology of all three barriers surveyed is characterized by a flat dissipative intertidal terrace and a steep beach face that is either composed of cobbles or exhibits a cobble core. The

intertidal terrace in Baleshare, especially the section of the profile between Mean Sea Level (MSL) (0 m) and +2 m, is very wide (~70 m), more than double compared to Howmore, where it is only ~30m wide (Figure 3.3a, c).

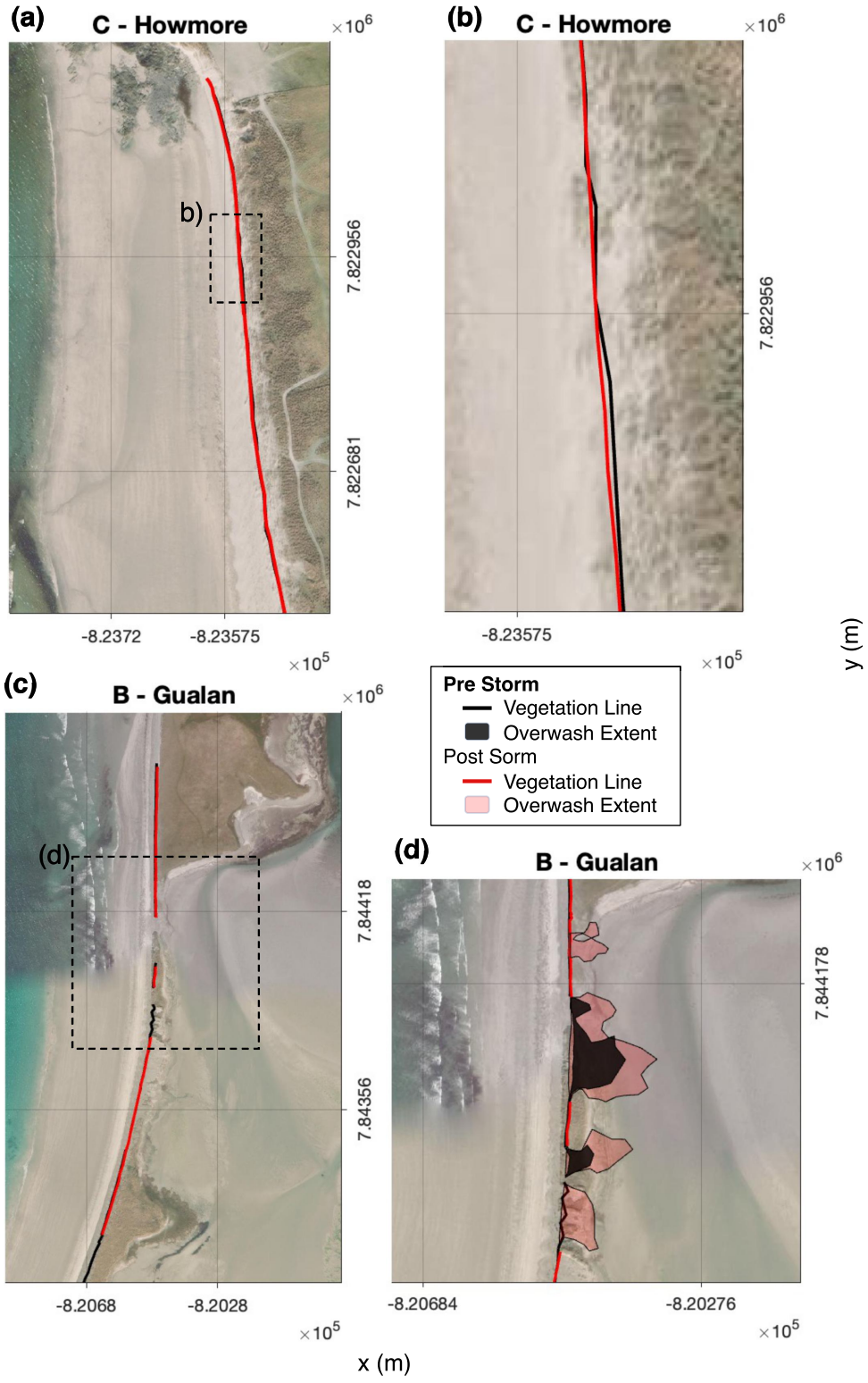

Figure 3.4 Pre- and post-storm vegetation lines overlayed on ESRI world imagery at Howmore **(a,b)** and Gualan **(c,d)**. At Gualan pre- and post-storm overwash extent is displayed **(d)**.

The vegetation lines surveyed in Howmore and Gualan indicate minimal to inexistent storm-induced shoreline change (Figure 3.4a, b, c), except for the section along Gualan that was extensively overwashed (Figure 3.4d). This area had been experiencing overwash prior to the surveys, which measured overwash extent by mapping the limits of fan-like superficial cobble deposits before and after the storm peak. The total overwash extent tripled after the storm peak storm to ~ 6500 m2 (Figure 3.4d).

Modelling of the storm wave conditions with SWAN revealed extensive wave energy dissipation induced by the wide and gently sloping bedrock-dominated shoreface (Figure 3.5). H_S is considerably reduced as waves propagate shoreward, with H_S values in excess of 10 m along the western boundary (Figure 3.5a, b) reducing to H_S between 2 and 5 m close to the beach. While bottom friction dissipation is important (Figure 3.5c), more energy is dissipated due to depth induced surf breaking, which takes place about 2 km offshore with occasional secondary breaking further inshore in areas with shallower bedrock (Figure 3.5d). At low tide, H_S is reduced even further, despite the forcing conditions at low tide being more energetic than at high tide (Table 3.1; Figure 3.5b).

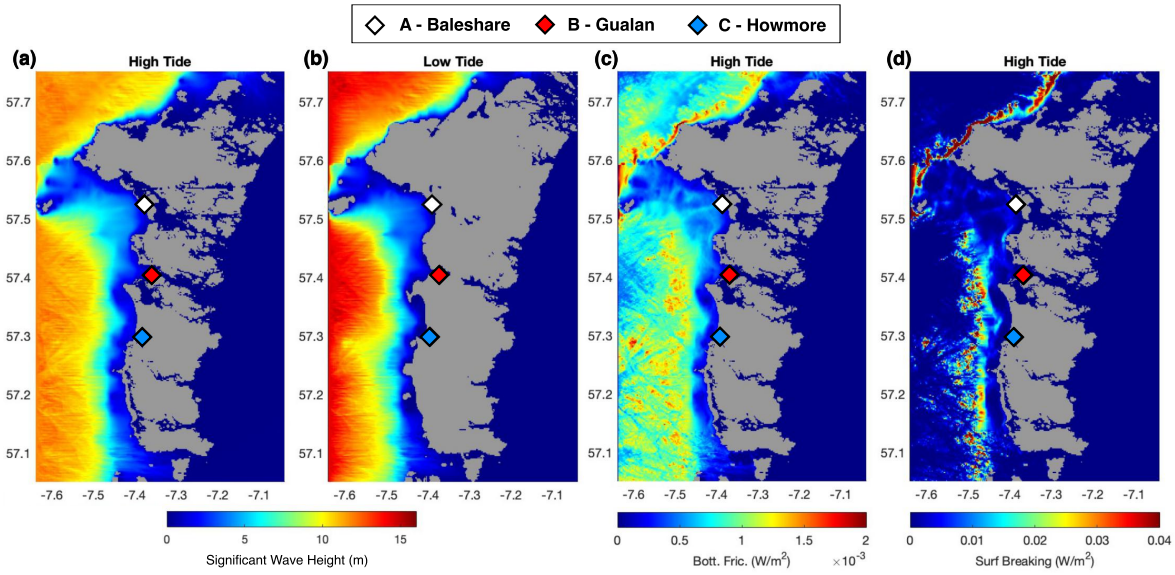

Figure 3.5 Modelled wave height during the storm at high tide **(a)** and low tide **(b)**. Wave energy dissipation due to bottom friction **(c)** and surf breaking **(d)** at high tide.

3.5 Discussion

Most of the surveyed areas in the Outer Hebrides barriers had limited or no detectable storm-induced morphological changes. This muted morphological response contrasts with the extreme hydrodynamic forcing during the storm peak. In most barrier settings, much lower wave forcing can cause substantial topographic changes (e.g. Malvarez et al., 2021; Backstrom et al., 2022). However, high-energy coastal environments are generally attuned to extreme conditions and require the combination of energetic waves, high spring tides, and substantial storm surges for storm impacts to be significant (Cooper et al., 2004). The large reduction in wave height, and consequently wave energy, close to the shore is decisive for the muted morphological response to the February 2022 extreme storm in the study area. In addition, although extreme, the storm peak was relatively short-lived, and this limited the period over which more energetic waves were able to reach the beaches and dunes, reinforcing the notion that storm peak duration has an important role in determining the magnitude of storm impacts (e.g. Masselink et al., 2022; Backstrom et al., 2022).

The substantial wave energy dissipation across the shoreface is dominated by depth-induced surf breaking while the role of bottom friction dissipation is much lower. Similar patterns of energy dissipation were identified in a comprehensive analysis of wave transformation across sloping rock shore platforms by Poate et al. (2018), which contrasts with rougher coral reef settings where bottom friction is more important (e.g. Lowe et al., 2005). However, energy dissipation by bottom friction is a function of physical and biological roughness and the extensive kelp fields that exist along the bedrock-dominated shoreface of the study area are likely to augment the wave dissipation and attenuation (Angus and Rennie, 2014). This has not been considered in the present wave model implementation but requires further investigation.

The varying storm-induced morphological changes observed between the study sites can be explained by the differences in intertidal terrace morphology. A wide intertidal terrace is more effective at dissipating nearshore wave energy and preventing storm waves from impacting the barriers. The cobble core of the barrier system further increases the resilience to storm-induced changes compared to purely sandy barrier systems, by increasing the resistance of the barrier to wave action. However, when this cobble core is low-lying, as is the case at Gualan, the barrier can be overwashed during periods of elevated water level, due to high tides and storm surges. While the barrier morphology is crucial for storm impact resilience, the varying morphological changes between Baleshare (no change) and Howmore (dune erosion) in this specific storm

event are primarily related to the differences in the width of the intertidal terrace. However, the intertidal slope is primarily controlled by the topography of the underlying bedrock surfaces rather than by morphodynamics. Overall, the bedrock controls energy dissipation in the shoreface and intertidal terrace, determining the magnitude of the hydrodynamic forcing, and consequently the extent of storm impacts in the Hebridean barrier islands.

3.6 Conclusion

In most of the barriers in the study area, a flat dissipative intertidal terrace and a steep beach face composed of cobbles buffer storm impacts. Significant morphological changes in the Outer Hebrides barriers driven by the February 2022 storm occurred only during periods of elevated water levels and in areas where the wave energy was not highly dissipated across the bedrock-controlled shoreface and intertidal terrace. This suggests that severe storm impacts in the Outer Hebrides barrier islands are only observed when there is an exceptional combination of hydrodynamic forcing (extreme storm waves with high tides and storm surges) and will be enhanced in areas with lower dune morphology and narrower geologically controlled intertidal terraces. Nearshore hydrodynamic processes such as surfbeat and wave setup are likely to be important to understand morphological changes in such underreported geologically controlled barrier systems.

3.7 Acknowledgements

Vincent Kümmerer receives funding for his Ph.D. through FCT grant 2020.07497.BD. This work is supported by FCT through the grant UID/00350/2020/CIMA and ARNET – Aquatic Research Network (LA/P/00069/2020). Access to the wave data from the Outer Hebrides buoy was kindly provided by CEFAS Wavenet and the Stornoway tide gauge data was retrieved from the British Oceanographic Data Centre (BODC).

3.8 References

Angus, S., & Rennie, A. (2014). “An Ataireachd Aird: The storm of January 2005 in the Uists, Scotland,” Ocean & Coastal Management, 94, 22–29.

Backstrom, J. T., Loureiro, C., & Eulie, D. O. (2022). “Impacts of Hurricane Matthew on adjacent developed and undeveloped barrier islands in southeastern North Carolina,” Regional Studies in Marine Science, 53, 102391.

Booij, N., Ris, R. C., & Holthuijsen, L. H. (1999). "A third-generation wave model for coastal regions: 1. Model description and validation," Journal of Geophysical Research: Oceans, 104(C4), 7649–7666.

Cooper, J. A. G., Green, A. N., & Loureiro, C. (2018). "Geological constraints on mesoscale coastal barrier behaviour," Global and Planetary Change, 168, 15–34.

Cooper, J. A. G., Jackson, D. W. T., Dawson, A. G., Dawson, S., Bates, C. R., & Ritchie, W. (2012). "Barrier islands on bedrock: A new landform type demonstrating the role of antecedent topography on barrier form and evolution," Geology, 40(10), 923–926.

Cooper, J. A. G., Jackson, D. W. T., Navas, F., McKenna, J., & Malvarez, G. (2004). "Identifying storm impacts on an embayed, high-energy coastline: Examples from western Ireland," Marine Geology, 210(1–4), 261–280.

Dawson, A. G., Dawson, S., Cooper, J. A. G., Gemmell, A., & Bates, R. (2013). "A Pliocene age and origin for the strandflat of the Western Isles of Scotland: A speculative hypothesis," Geological Magazine, 150(2), 360–366.

Dawson, A. G., Dawson, S., & Ritchie, W. (2007). "Historical Climatology and coastal change associated with the 'Great Storm' of January 2005, South Uist and Benbecula, Scottish Outer Hebrides," Scottish Geographical Journal, 123(2), 135–149.

Dawson, A. G., Gómez, C., Ritchie, W., Batstone, C., Lawless, M., Rowan, J. S., Dawson, S., McIlveny, J., Bates, R., & Muir, D. (2012). "Barrier Island Geomorphology, Hydrodynamic Modelling, and Historical Shoreline Changes: An Example from South Uist and Benbecula, Scottish Outer Hebrides," Journal of Coastal Research, 285, 1462–1476.

Ferreira, Ó., Plomaritis, T. A., & Costas, S. (2017). "Process-based indicators to assess storm induced coastal hazards," Earth-Science Reviews, 173, 159167.

Gómez, C., Wulder, M. A., Dawson, A. G., Ritchie, W., & Green, D. R. (2014). "Shoreline Change and Coastal Vulnerability Characterization with Landsat Imagery: A Case Study in the Outer Hebrides, Scotland," Scottish Geographical Journal, 130(4), 279–299.

Hansom, J. D., & Angus, S. (2005). "Machair nan Eilean Siar (Machair of the Western Isles)," Scottish Geographical Journal, 121(4), 401–411.

Hansom, J. D., Fitton, J. M., Rennie, A. F. (2017). "Dynamic Coast – National Coastal Change Assessement: Cell 8 and 9 – The Western Isles", CRW2014/2.

Kenyon, N.H., and Pelton, C.D. (1979). "Seabed conditions west of the Outer Hebrides: Report 95," Tech. Rep., Institute of Oceanographic Sciences, Godalming, Surrey, UK, 16 p.

Kümmerer, V., Loureiro, C., Ferreira, O., & Fanti, V. (2021). "Multidecadal Variability in Winter Wave Storminess off the Outer Hebrides (Northwest Scotland)," AGU 2021 Fall Meeting Abstracts, OS33B-04.

Lowe, R. J., Falter, J. L., Koseff, J. R., Monismith, S. G., & Atkinson, M. J. (2007). "Spectral wave flow attenuation within submerged canopies: Implications for wave energy dissipation," Journal of Geophysical Research, 112(C5), C05018.

Masselink, G., Brooks, S., Poate, T., Stokes, C., & Scott, T. (2022). "Coastal dune dynamics in embayed settings with sea-level rise – Examples from the exposed and macrotidal north coast of SW England," Marine Geology, 450, 106853.

Malvarez, G., Ferreira, O., Navas, F., Cooper, J. A. G., Gracia-Prieto, F. J., & Talavera, L. (2021). "Storm impacts on a coupled human-natural coastal system: Resilience of developed coasts," Science of The Total Environment, 768, 144987.

Pile, J., Cooper, J. A. G., & Jackson, D. W. T. (2019). "Stratigraphy and internal structure of wind-dominated barrier islands (dune and machair) of the Outer Hebrides, Scotland," Earth Surface Processes and Landforms, 44(7), 14821493.

Poate, T., Masselink, G., Austin, M. J., Dickson, M., & McCall, R. (2018). "The Role of Bed Roughness in Wave Transformation Across Sloping Rock Shore Platforms: Bed roughness on wave transformation," Journal of Geophysical Research: Earth Surface, 123(1), 97–123.

Ris, R. C., Holthuijsen, L. H., & Booij, N. (1999). "A third-generation wave model for coastal regions: 2. Verification," Journal of Geophysical Research: Oceans, 104(C4), 7667–7681.

Sallenger, A. H. (2000). "Storm Impact Scale for Barrier Islands," Journal of Coastal Research, 16, 6.

Salmon, J. E., Holthuijsen, L. H., Zijlema, M., van Vledder, G. Ph., & Pietrzak, J. D. (2015). "Scaling depth-induced wave-breaking in two-dimensional spectral wave models," Ocean Modelling, 87, 30–47.

Chapter 4

Distinct Shoreline Behaviour along Storm-Dominated and Geologically Controlled Coastal Barriers

Kümmerer V., Ferreira Ó., Loureiro, C. (2025). Distinct shoreline behaviour along storm-dominated and geologically controlled coastal barriers. *Earth Surfaces Processes and Landforms, 50(4), e70042.*

Abstract

Contemporary shoreline change is driven by a complex combination of factors, and as such is often highly variable along the coast. While differences in beach morphology can explain some of the variability in shoreline change, the geological constraints imposed by the coastal geology are often overlooked. This work examines the influence of foreshore configurations with varying degrees of non-dynamic geological control, which are analysed in combination with hydrodynamic forcing to investigate seasonal to multiannual shoreline evolution along five coastal barriers in the Outer Hebrides, Western Scotland. These barriers are characterised by strongly geologically constrained evolution and are exposed to a storm-dominated wave climate. Monthly averaged vegetation lines from 2016 to 2023 were derived from Planet Scope satellite imagery as a shoreline position indicator using an automated approach validated by visual inspection. The satellite-derived vegetation lines have a sub-pixel accuracy with a root mean square error of 3 m. Changes in shoreline position are statistically correlated with extreme storm conditions, characterised by both extreme water levels and wave conditions. However, the control exerted by the variable geological configuration along the barriers results in distinct inter- and intra-site shoreline change behaviour, with lower shoreline variability observed in barrier sectors fronted by rocky foreshores, compared to sediment-rich foreshores. The observed multiannual shoreline change from 2016 to 2023 is characterised by a small but

statistically significant accreting trend (mean 0.4 m/yr), likely representing the recovery of the barriers from extreme winter storms that impacted northern European coasts from 2013 to 2015. The results demonstrate that considering variable geological controls in shoreline change assessments improves the understanding of shoreline variability along coastal barriers, allowing to identify distinct storm-driven shoreline behaviour according to the degree of geological control.

Keywords: Geological Control; Shoreline Change; Vegetation Line; Foreshore; Satellite Imagery; Planet Scope; Coastal Storm; Extreme Storm; Western Scotland.

4.1 Introduction

Coastal barriers are dynamic landforms that buffer the impacts of coastal storms. In the context of climate change and increasing anthropogenic pressures on the coast, it is critical to understand how barriers respond to storms in order to predict their morphological trajectories at a management scale.

Current morphodynamic models, when calibrated, can confidently predict storm-driven changes in sediment-rich, geologically unconstrained coastlines (e.g., Stockdon et al., 2023), but are often poorly suited to sediment-limited coastlines that are geologically constrained by rocky features (e.g. outcrops, shore platforms, headlands) that complicate nearshore morphodynamics (Cooper et al., 2018; Gallop et al., 2020). Therefore, there is a need to assess the influence of geological controls on contemporary morphological change to enhance the understanding of barrier evolution, which is crucial for coastal adaptation planning (Gallop et al., 2015). Geological controls on barrier evolution are exerted mainly through the supply of sediment and the geological framework on which the sediment rests and moves according to the contemporary hydrodynamic processes (Hapke et al., 2016; Riggs et al., 1995). The geological framework segments the alongshore sediment dynamics by headlands and the cross-shore by irregularities in the bedrock topography, resulting in local constrains on sediment supply (Cooper et al., 2012; Short, 2010; Wernette et al., 2018). Geological features additionally influence coastal processes, resulting in alongshore variable wave heights, nearshore processes, storm response and recovery (Bastos et al., 2022; Fellowes et al., 2022; Gallop et al., 2012, 2013, 2015; Loureiro et al., 2012, 2014; Muñoz-Perez and Medina, 2010;

Robinet et al., 2020; Suanez et al., 2012; Velegrakis et al., 2016). For example, geological controls such as the degree of embayment indentation (Fellowes et al., 2022), the underlying bedrock topography (Hapke et al., 2016; Robinet et al., 2020; Short, 2010; Wiles et al., 2022) or coral reef structures (Laigre et al., 2023; Mulcahy et al., 2016) control, at least partially, the shoreline variability by locally modulating the forcing conditions at the foreshore. These controls are rarely considered in morphodynamic models (Cooper et al., 2018; Gallop et al., 2020), which often reflects the general absence of observations of geologicallycontrolled morphodynamics necessary to feed process-based models. While differences between sediment-rich and adjacent geologically constrained areas with rocky features have been demonstrated (Gallop et al., 2012; Muñoz-Perez and Medina, 2010; Simeone et al., 2021; Wiles et al., 2022), modelling and understanding the coastal processes leading to these differences along the coast are complex and challenging to resolve numerically (Gallop et al., 2013; Robinet et al., 2020; Velegrakis et al., 2016).

Assessing coastal change in geologically constrained beaches allows to quantify differences in morphodynamic behaviour between unconstrained and constrained barrier systems, thus contributing to an improved understanding of these complex and understudied coastlines. A common approach for assessing coastal change is the temporal analysis of the position of the shoreline, the physical interface between ocean and land (Boak and Turner, 2005). Time series of shoreline positions reflect changes in beach profile and volume and are used to quantify beach erosion and accretion (e.g., Barnard et al., 2011). Time series of shoreline positions can be obtained using in-situ instrumentation or remote sensing, including satellite imagery (Doherty et al., 2022; Pardo-Pascual et al., 2024; Rogers et al., 2021; Vos et al., 2019), aerial photography (e.g., Dawson et al., 2012), ground-based video (Velegrakis et al., 2016) and smartphone photography (Harley et al., 2019). Multispectral satellite imagery, in particular, provides a cost-effective data source to infer shoreline change, but is limited by temporal coverage and spatial resolution (Turner et al., 2021). Because it achieves lower spatial accuracy than video cameras or drone imagery, it limits the detection of short-term coastal change (Angnuureng et al., 2022). However, openly available satellite imagery and image processing algorithms can be applied at global scale and are readily available, allowing analysis of coastal change in remote locations and at larger spatial scales (e.g., Mentaschi et al., 2018). In addition, commercial satellite imagery, as provided by Planet Scope, with higher spatial and temporal resolution, allows accurate detection of storm-driven coastal change (Doherty et al., 2022; Rogers et al., 2021; Turner et al., 2021). Nevertheless, in-situ observations remain essential to

calibrate and then validate satellite derived shorelines (Turner et al., 2021). Regardless of the source of shoreline position data, geological controls are rarely considered in shoreline change assessments of coastal barriers, despite being essential for predicting future coastal change at management scales (Cooper et al., 2018). This work investigates the influence of foreshore configurations with varying degrees of non-dynamic geological control, which are considered alongside hydrodynamic forcing to characterise seasonal (monthly) to multiannual shoreline evolution. The analysis explores seven years of satellite-derived shoreline change along five geologically constrained barriers in the Outer Hebrides (Northwestern Scotland), a highly geologically constrained coastal system (Cooper et al., 2012) and exposed to a storm-dominated wave climate.

4.2 Study Area and Methods

4.2.1 Study Area

Located in the NE Atlantic, the Outer Hebrides barrier system is exposed to very energetic wave conditions (Figure 4.1) and experiences a mean spring tidal range of 4.1 m. The wave climate has a marked seasonality and is strongly correlated to the North Atlantic Oscillation (NAO) (Kümmerer et al., 2024; Santo et al., 2015). The evolution of this barrier system is subject to extensive geological control by the underlying gently sloping bedrock (Cooper et al., 2012), which extends offshore and substantially dissipates storm wave energy (Kümmerer et al., 2023). In addition, nearshore wave attenuation is enhanced by extensive kelp beds (Angus and Rennie, 2014). The bedrock is frequently exposed along the islands and the inner shelf and occasionally covered with a thin sediment layer (Kenyon and Pelton, 1979). Coastal sediments have been mainly supplied from offshore calcareous sands produced by breakdown of marine organisms, which are supplemented by coarse siliceous sediments eroded from glacial deposits along the Outer Hebrides islands (Gilbertson et al., 1999). The reduced sediment supply and the spatially varying bedrock surfaces control coastal geomorphological variability in the Outer Hebrides (Pile et al., 2019), placing these barriers at the extreme end of geological control on barrier island evolution, as recognised by Cooper et al. (2012).

Although most of the coastline in the Outer Hebrides evidences long-term landward retreat, the shoreline position has been generally stable in the last decades (Gómez et al., 2014; Hansom et al., 2017). Winter storms, such as an exceptional event in January 2005, can lead to localised

erosional impacts (Dawson et al., 2007). However, geomorphological changes are generally muted along the coastline, as the barriers have adjusted to the extreme hydrodynamic forcing conditions during storm events.

Five barriers were selected based on varying degrees of embaymentisation, shoreline length and orientation, and therefore presenting a range of geomorphic characteristics (Figure 4.1). In addition, they also evidence different degrees of geological control on contemporary morphodynamics, from fully sandy barriers to beaches with presence of extensive rock surfaces and outcrops. The barriers selected all have well vegetated dunes, which is common along most of the Outer Hebrides barrier systems.

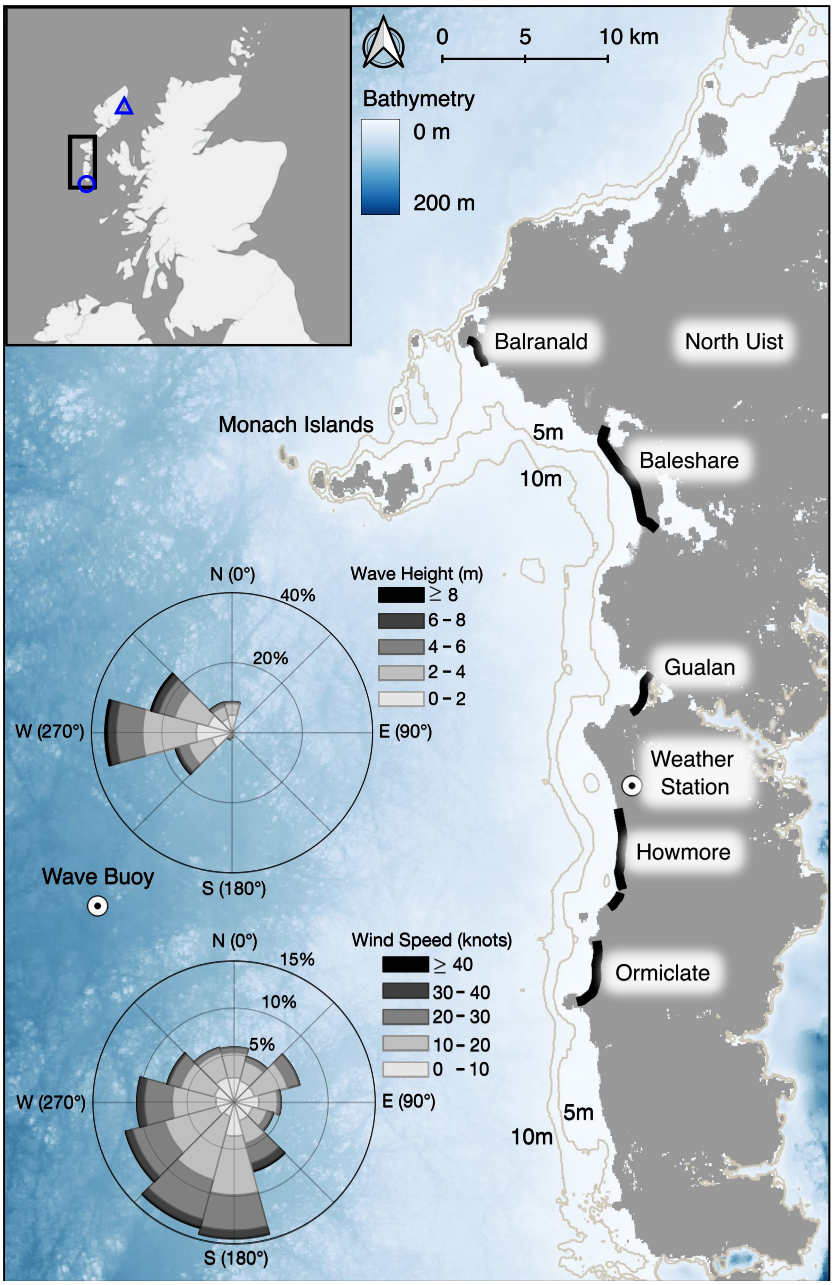

Figure 4.1 Study area in the Outer Hebrides, Western Scotland. Location (inset) and bathymetry (referenced to MSL), including the 5 m and 10 m bathymetric contours. Location and extent of the study sites (black lines), offshore wave buoy (57.289°N, 7.923°W), weather station (57.366°N, 7.383°W), with corresponding rose diagrams showing the dominant wave and wind direction and magnitude. The location of the tidal gauges of Eriskay (blue circle) and Stornoway (blue rectangle) are indicated in the inset figure.

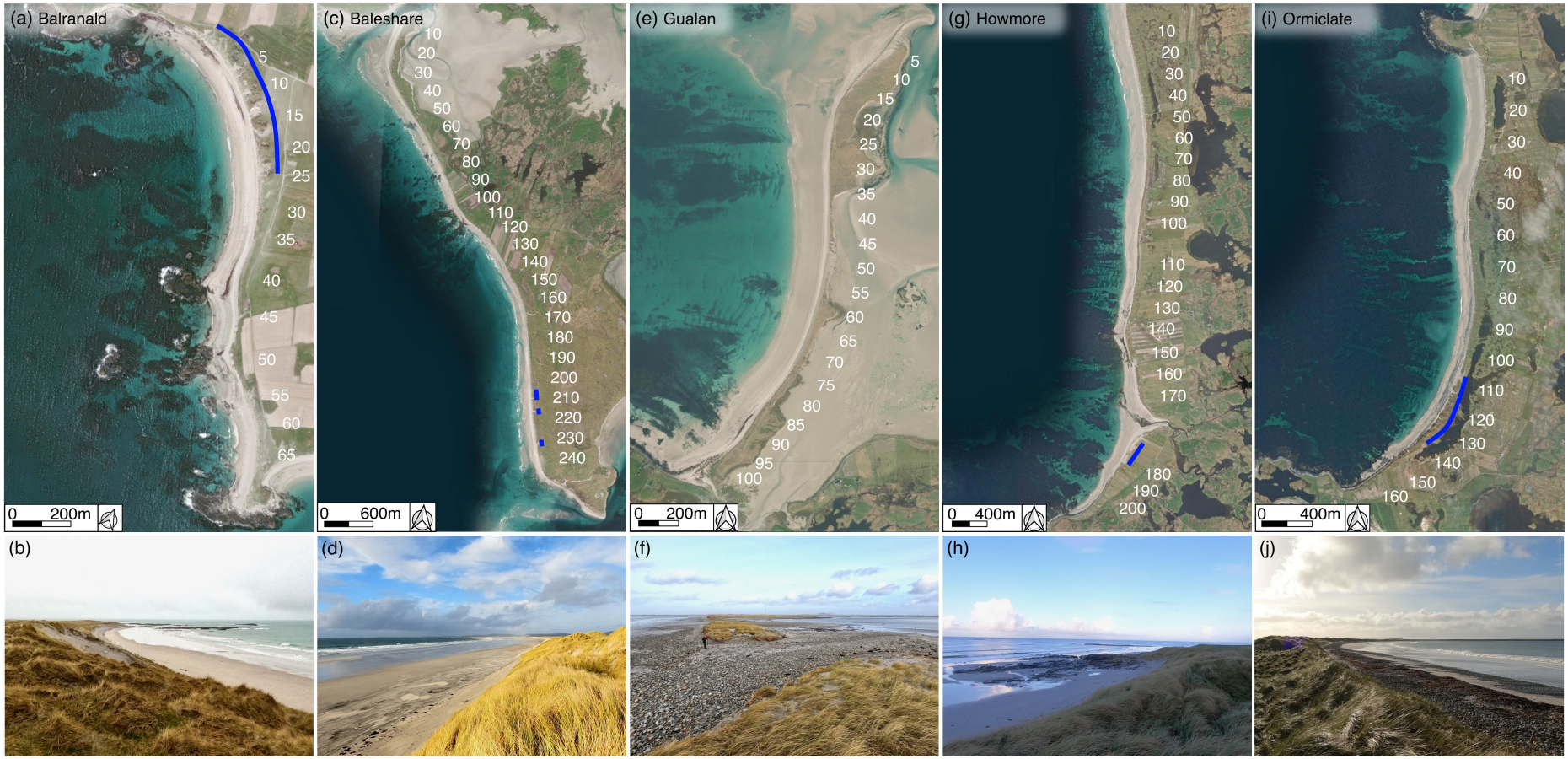

Figure 4.2 Overview images and photos of the study sites. **(a,c,e,g,i)** Aerial images of the study sites from the ESRI world imagery layer. Locations with extensive dune blowouts are marked with a blue line. Note: The difference in scales between sites and the gap after transect 100 at Howmore (g) is because the dune is interrupted by agricultural land in this site, preventing the identification of a reliable vegetation-based shoreline. **(b)** High dunes with blowouts and rock outcrops in the southern beach section of Balranald (16/02/2022). **(d)** High dunes and a wide low tide terrace at Baleshare (08/11/2022). **(f)** Frequently overwashed barrier at Gualan (21/02/2022) with low dunes on top of a shingle barrier (ocean is to the left). **(h)** Rock outcrops in front of scarped high dunes at Howmore (06/11/2023). **(j)** Mixed sand and gravel upper beach at Ormiclate (06/11/2022).

Balranald, a small headland-bay beach, and the barrier island of Baleshare are NW-SE orientated, while Gualan, Howmore, and Ormiclate are N-S orientated (Figure 4.1 and Figure 4.2a, c, e, g, i). The beaches are generally dissipative with a wide intertidal terrace and the barrier composition ranges from completely sandy (Figure 4.2b, d) to mixed sand and gravel (Figure 2f, j), as well as gravel and shingle with frequent seaweed (wrack) accumulations that contribute to the sediment matrix (Randall, 1997). The beaches are typically backed by densely vegetated foredunes, dominated by marram grass (Huiskes, 1979). Dune morphology ranges from 18 m high foredunes, with extensive blowouts in Balranald (Figure 4.2a, b), to small 2 m high dunes in Gualan (Figure 4.2f). Foredunes are generally characterised by scarped and steep seaward facing slopes, often with ramp foredune accumulations. At Gualan, a lowlying offshore sand-capped shingle barrier island, overwash events erode the foredunes, depositing washover fans in the backbarrier (Figure 4.2f).

4.2.2 Planet Scope Imagery

For this work Planet Scope imagery was used because of its higher spatial and temporal resolution than openly available satellite imagery, such as those obtained from the Landsat 8 and Sentinel 2 missions. Although Planet Scope is a commercial product, the imagery can be used for academic research at no cost.

Planet Scope imagery has a daily to sub-daily sampling interval with a spatial resolution of 3.7 m at nadir, resampled to a fixed resolution of 3 m (Planet Team, 2023). As cloud cover is high in the Outer Hebrides, the daily temporal resolution increases the number of available cloud-free images when compared to more commonly used satellite imagery sources with revisit time of several days (5 to 15 days for Sentinel 2 and Landsat 8, respectively). Furthermore, the higher spatial resolution of 3 m increases precision in the satellite-derived shoreline position in relation to other openly available but coarser (10 – 30 m) resolution satellite imagery (Doherty et al., 2022; Rogers et al., 2021), allowing smaller changes down to the storm event scale to be detected. It is important to note that Planet Scope imagery is only available since 2016, while Landsat 8 and Sentinel 2 are available since 2013 and 2015, respectively.

The pre-processing of the Planet Scope imagery was performed using the open-source CoastSat.PlanetScope python toolkit developed by Doherty et al. (2022). Following their approach, the four-band (red, green, blue and near infrared) analytical orthoscence Planet Scope products were considered for the analysis. The shoreline monitoring period is restricted to the

last 7 years as the first four-band orthoscence products for the Outer Hebrides have only become available from December 2016. A total of 1790 images were downloaded for the 5 beaches within the period between December 2016 and May 2023 (Table 4.1). This included manually selecting the images with less clouds, cloud shadows or haze using the Planet Explorer online tool in the case of multiple acquisitions for the same day, and also avoiding the use of images with very high cloud cover (> 90 %).

Table 4.1 Number of images after each pre-processing step.

Pre-processing steps	Balranald	Baleshare	Gualan	Howmore	Ormiclate
Downloaded images	306	350	263	521	350
UDM2 filtering	299	332	245	493	339
Co-registration†	298	330	244	486	336
Image merging†	226	250	211	335	283
CoastSat filtering†	224	243	210	316	277

† Steps performed using the CoastSat.PlanetScope toolkit developed by Doherty et al. (2022).

The Planet Scope images are orthorectified and resampled with digital number values corresponding to the radiance detected by the sensor. After the initial visual check for manually selecting images to download, an additional pre-processing step was introduced before using the CoastSat.PlanetScope toolkit, as this algorithm does not use the updated Unusable Data Mask 2 (UDM2) files that are provided alongside each image. The UDM2 files contain information on sensor errors, data loss, and indicators for image distortions such as cloud cover, snow, or haze. This additional pre-processing step masked areas that are classified as 'clear' but have < 50 % sensor confidence or as 'cloud' with > 50% sensor confidence. Furthermore, images that have > 30 % of the image masked were discarded in this step (Table 4.1, UDM2 filtering). Then, the remaining UDM2-masked images were processed with the CoastSat.PlanetScope pre-processing algorithm and converted to top of the atmosphere radiance using the information provided by the supplementary Planet Scope files. The native accuracy of the orthorectification by Planet Scope of < 10 m (Planet Team, 2023) was then reduced to ~ 0.9 m by the image co-registration step (Doherty et al., 2022) (Table 4.1, co-registration). The images were merged if the Planet Scope scene boundary was within the beach area (Table 4.1, image merging). Full details of the CoastSat.PlanetScope image pre-processing algorithms for radiometric conversion and co-registration are provided in Doherty et al. (2022).

4.2.3 Satellite-Derived Vegetation Line

The Satellite Derived Vegetation Line (SDVL), which marks the seaward edge of the foredune vegetation and is indicative of shoreline dynamics (Boak and Turner, 2005), was extracted from the pre-processed Planet Scope imagery using a semi-automated approach. The SDVL was chosen over the commonly used waterline shoreline indicator because the combination of high-energy waves and large tidal ranges (~4 m) with a very low gradient complex nearshore bathymetry (Figure 4.1) significantly affects the horizontal accuracy of the shoreline position derived from the waterline (Castelle et al., 2021; Konstantinou et al., 2023; Vos et al., 2023; Zhang et al., 2024). Furthermore, Pollard et al. (2020) demonstrated that, out of a variety of shoreline indicators, the vegetation line is most effective in recording and preserving storm erosion in mixed gravel and sand barriers in the UK east coast. The dense and fast-growing dune vegetation (Figure 4.2) at the study sites (Huiskes, 1979) reinforces the choice of the vegetation line as a more robust shoreline indicator, with the temporal lag in vegetation growth as the main limitation (Boak and Turner, 2005).

Following image pre-processing, the Normalised Difference Vegetation Index (NDVI) was calculated for each image according to distinct barrier sections. These sections (see Figure 4.3a as example) were defined based on the difference in vegetation color caused by variation in vegetation characteristics, water table, agricultural practices, and large accumulations of seaweed generally located at the northern and southern ends of the beaches. As the barrier sections were spatially restricted to a small alongshore band covering the vegetated foredune and upper beach, the NDVI pixel value distribution is strongly bi-modal (Figure 4.3b) and, therefore, suitable for automatic image thresholding using Otsu's method (Otsu, 1979). This widely used method is based on the identification of a threshold that maximises the inter-class variance for distinct pixel classes. The SDVL position was then extracted as the NDVI contour determined with a dedicated Otsu threshold (see Figure 4.3b as example) that best describes the interface between sediment and vegetation for each barrier section and image.

The automatic calculated and temporally and spatially variable NDVI threshold improves the SDVL extraction compared to a fixed NDVI threshold segmentation because the NDVI values are variable according to season, atmospheric conditions, and different Planet Scope imagery sensors (Planet Team, 2023). In this study, images from three generations of Planet Scope micro satellite sensors (PS2, PS2.SD, and PSB.SD) are used, which can result in differing spectral signatures even for the same day (e.g., Keay et al., 2023).

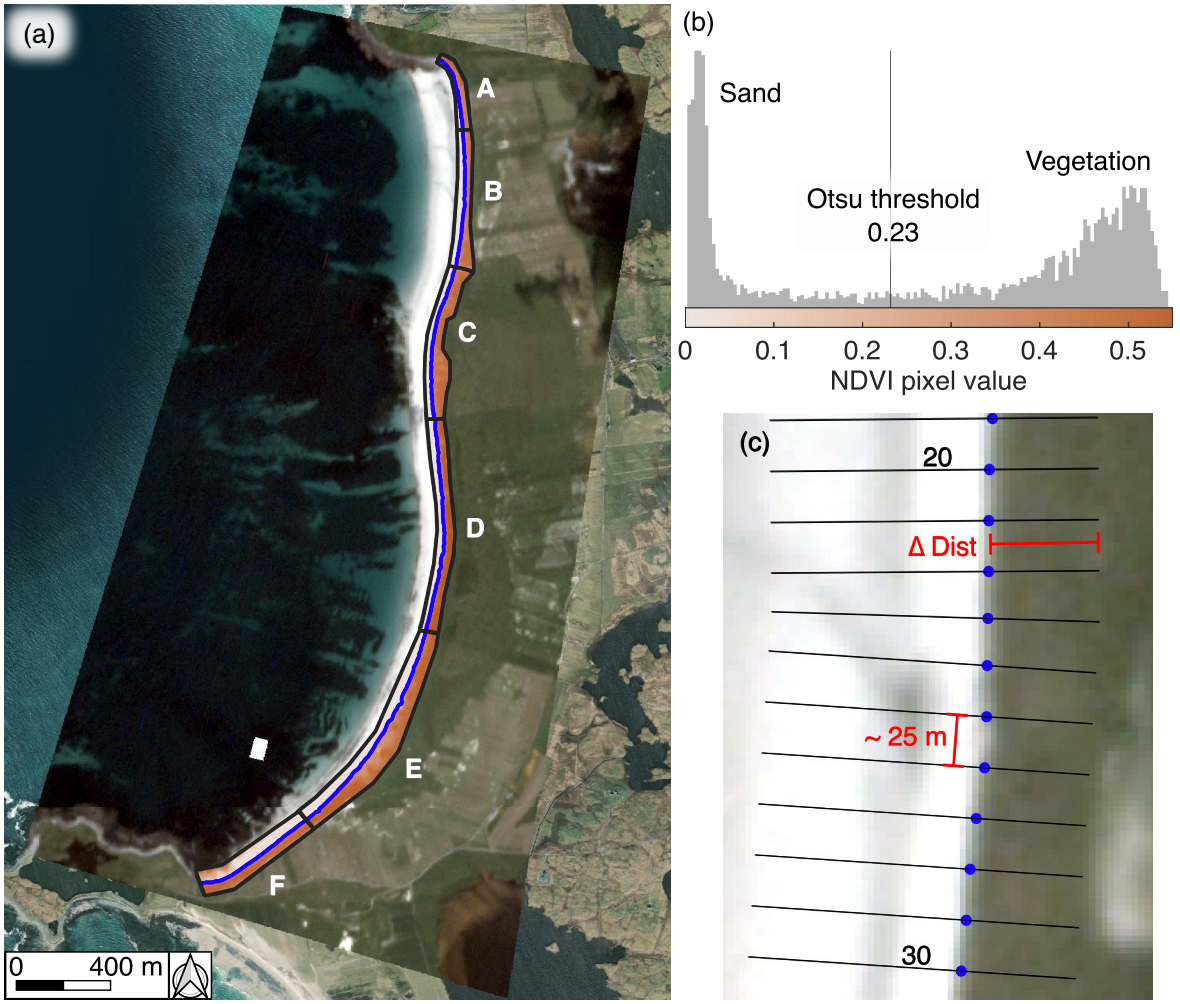

Figure 4.3 SDVL extraction at Ormiclate on 02/08/2019. **(a)** Pre-processed Planet Scope image with NDVI images for each barrier section (A-F – black lines) and SDVL (blue line) overlaid on ESRI world imagery. **(b)** NDVI pixel histogram of barrier section B and the calculated Otsu threshold for SDVL extraction. Lower NDVI pixels values (< 0.23) are classified as sediment while higher NDVI pixels (>0.23) are classified as vegetation. **(c)** Barrier perpendicular transects at 25 m intervals, used as a reference for estimating the position of the SDVL, defined as the distance between the end of the transect and the intersection of the transect with the SDVL (blue points).

The automated approach was then validated by visual inspection of each SDVL to remove misinterpreted shorelines due to undetected poor image quality or interferences from seaweed deposits near the dune. As the barriers are divided into relatively small sections (Figure 4.3a), each section with a wrongly extracted SDVL was manually discarded from further analysis. Shoreline changes were determined from the intersection of the valid SDVLs with shore-

perpendicular transects at a 25 m spacing and the SDVL position was defined as the distance from the transect intersection point to the baseline of the transect (Figure 4.3c).

The positional accuracy of SDVLs was evaluated against Measured Vegetation Lines (MVL) obtained from RTK-DGNSS field surveys during the 2022-23 winter season. In the field, positions of the seaward dune vegetation edge were surveyed always by the same RTK-DGNSS operator considering the morphology of the dune and the presence of vegetation in a density that could be detectable from Planet Scope satellite imagery. However, in cases of very steep dunes where the dune vegetation edge is located in the middle of the seaward slope and of difficult access, MVLs were measured as close as possible to the dune toe. This can introduce a small landward deviation between the SDVL and the MVL, but only in very specific areas. Distances from the end of each transect to the intersection with the MVL were then statistically compared with their temporally closest SDVL position distance using Pearson's correlation coefficient (R), Root Mean Square Error (RMSE), and relative bias (bias):

$$\mathrm{R} = \frac{\sum_{\mathrm{i}=1}^{\mathrm{N}}(\mathrm{M_i}-\bar{\mathrm{M}})(\mathrm{O_i}-\bar{\mathrm{O}})}{\sqrt{\sum_{\mathrm{i}=1}^{\mathrm{N}}(\mathrm{M_i}-\bar{\mathrm{M}})^2 \sum_{\mathrm{i}=1}^{\mathrm{N}}(\mathrm{O_i}-\bar{\mathrm{O}})^2}}, \tag{4.1}$$

$$\mathrm{RMSE} = \sqrt{\frac{1}{\mathrm{N}}\sum_{\mathrm{i}=1}^{\mathrm{N}}(\mathrm{M_i}-\mathrm{O_i})^2}, \tag{4.2}$$

$$\mathrm{bias} = \frac{\sum_{\mathrm{i}=1}^{\mathrm{N}}(\mathrm{M_i}-\mathrm{O_i})}{\sum_{\mathrm{i}=1}^{\mathrm{N}}\mathrm{O_i}} * 100, \tag{4.3}$$

where O_i are the MVL positions, M_i are the SDVL positions, N is the number of data points (available transects for MVL and SDVL data), and the overbar represents average values.

After validation, the vegetation-based shorelines were averaged to monthly SDVL positions to improve the temporal consistency in the analysis due to the existence of long periods of cloud cover. Shoreline change was then evaluated as the deviation from the mean SDVL position during the monitoring period (December 2016 to May 2023). Additionally, a moving average of 100 m (4 transects) was used to reduce the noise in the alongshore SDVL position. The SDVL changes were also spatially averaged to obtain the mean shoreline change in each study

site. An error range around the mean SDVL positions equal to twice the RMSE between the MVL and SDVL positions is assumed to account for uncertainties in small SDVL deviations.

4.2.4 Classification of Foreshore Configuration

To analyse the influence of the geological control exerted by the underlying bedrock topography on shoreline change, the foreshore configuration of the five barriers were classified according to the presence of intertidal and subtidal rocky features. Foreshore configurations with higher presence of rocky features and consequently lower sediment volume indicate a higher degree of geological control (Figure 4.4a) (Gallop et al., 2012, 2020; Jackson and Cooper, 2009).

Here the offshore limit of the foreshore was defined as 500 m from the vegetation line, corresponding to ~ 6 m below mean sea level and thus including part of the upper shoreface. Three foreshore classes were defined:

(1) Sediment: Areas covered by loose sediment including sand, mixed-sand and gravel and shingle.
(2) Sub-tidal rock surface: Outcropping rock surfaces in the subtidal shore area.
(3) Rock Outcrop surface: Outcropping rock surfaces in the intertidal and upper-tidal shore area.

The foreshore classes were mapped over a reference Planet Scope image with the lowest water level record at the Eriskay gauge for the period analysed (Figure 4.4b). Where there were gaps in the foreshore area due to the image pre-processing operations (i.e. removal of clouds or haze), the image with the second lowest associated water level was selected as the reference image. In addition to the Planet Scope images, information from field observations and higher-resolution Google Earth imagery were used to aid the foreshore mapping. Based on visual inspection of the Planet Scope imagery, it was possible to confirm that the spatial patterns of sediment cover on the foreshore remained identical through time (Figure 4.16, section 4.6.4). The foreshore configuration was classified proportionally, with percentages representing the cover of each class at locations corresponding to the 25 m-spaced transects used for the SDVL position extraction (Figure 4.4c). To have consistent foreshore classification transect lengths, these begin at the mean SDVL position and extend 500 m offshore, perpendicular to the shore. Like

the monthly SDVL positions, the percentage cover of the foreshore configuration was alongshore averaged using a 100 m moving mean.

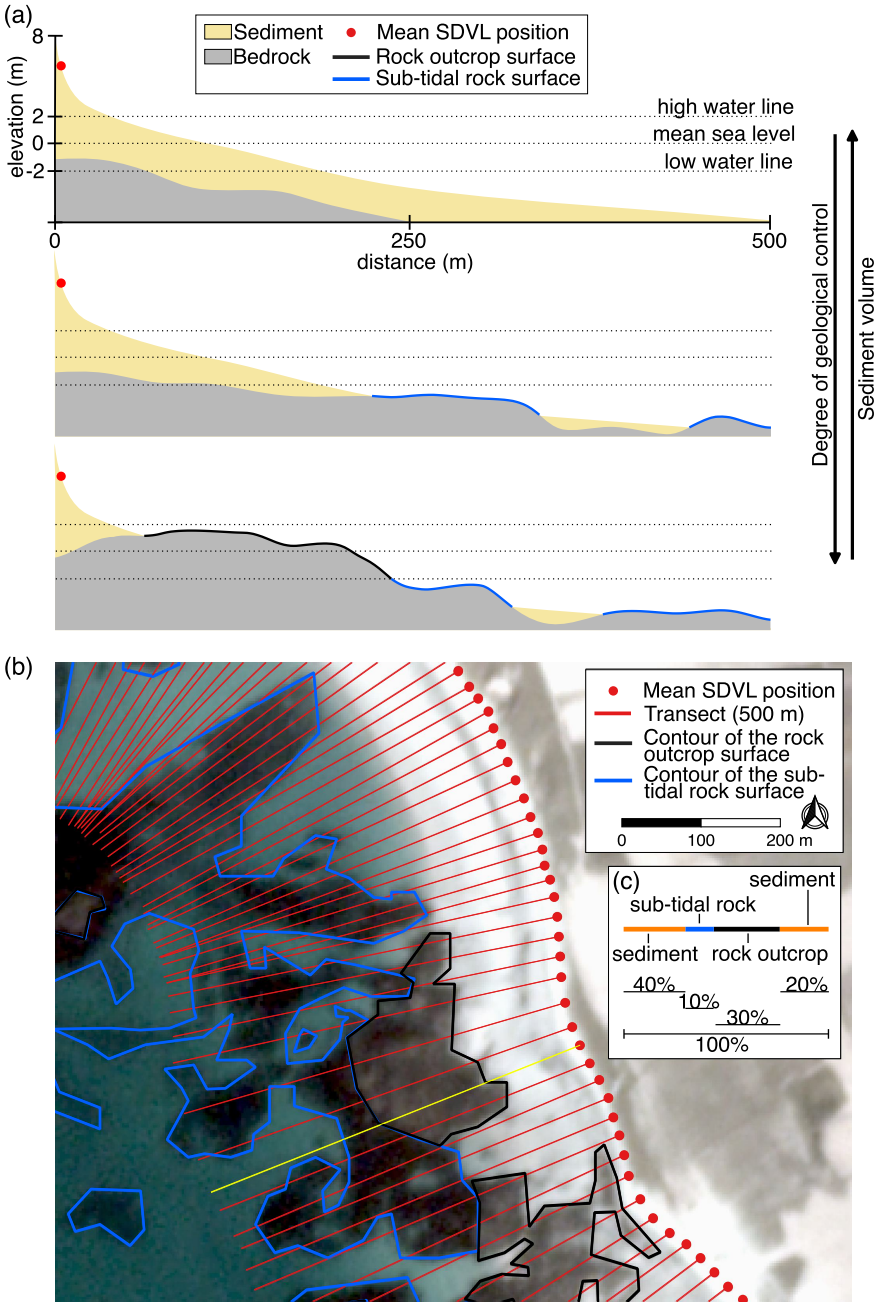

Figure 4.4 Foreshore configuration. **(a)** Conceptual model of cross-shore profiles with varying degrees of geological control. **(b)** Example of foreshore configuration mapping at Balranald using the Planet Scope image (18/04/2019, 11:14 am) with the lowest associated water level during the monitoring period. The transects begin at the mean SDVL position and have a consistent length of 500 m. **(c)** Illustration of the foreshore configuration classification for the yellow transect in (b) expressed as a percentage cover of each class.

4.2.5 Correlation between Shoreline Change and Forcing

The relationships between site-averaged monthly-mean SDVL positions and monthly averaged ocean and atmospheric forcing parameters were investigated. This included the characterisation of the coastal storms identified for the period between January 2012 and May 2023, which includes the SDVL monitoring period (2016 to 2023) but also an earlier period (2012-2016) that allows the coastal evolution to be analysed in the context of the recent coastal storm climate (before and during the SDVL monitoring period) in the Outer Hebrides.

Hourly mean wind speed data were downloaded from the CEDA archive for MIDAS weather station 18903 (South Uist Missile Range), located between Howmore and Gualan (Figure 4.1), which are provided by the British Atmospheric Data Centre (Met Office, 2006). The hourly mean wind speed data were converted to monthly means. Observed water levels at 15-minute intervals were obtained from the British Oceanographic Data Centre (BODC) for the Stornoway tide gauge, located on the NE coast of the Outer Hebrides. A previous comparison between water levels recorded at the Stornoway tide gauge and water levels at the Eriskay tide gauge located on the West coast of the Outer Hebrides showed only minor differences (R = 0.93, RMSE = 0.41 m). Therefore, the Stornoway record was used in this work because of fewer data gaps within the analysis period. Water level data were converted from Chart Datum to the Ordnance Datum corresponding to mean sea level (-2.71 m) and values flagged as suspect by the BODC quality control were excluded from the dataset. Gaps in the water level record before 2018 were filled with model data from the Global Tide and Surge Model (GTMS - (Muis et al., 2020) version 3.0 forced with ERA5 reanalysis (Hersbach et al., 2020). The GTSM3.0 model effectively replicates the water level records for the Outer Hebrides (R = 0.98, RMSE = 0.21 m). Significant wave height (H_S) and peak wave period (T_P) observations were obtained from the West of Hebrides buoy, operated by the Centre for Environment Fisheries and Aquaculture Science (CEFAS), and deployed in 100 m water depth ~30 km offshore the study area (Figure 1). The wave data is provided at 30-minute intervals and quality controlled by CEFAS.

The hydrodynamic forcing conditions driving relevant morphological changes in the study area are characterised by the coincidence of high wave energy events with elevated water levels (Kümmerer et al., 2023; Young, 2015), as the beaches have a wide dissipative low-tide terrace and are generally in equilibrium with energetic forcing. This causes the waves to dissipate all of their energy before reaching the foredune through wave breaking and bore collapse at lower water levels. Therefore, to integrate the wave and water level components in a single parameter, the normalised wave power was calculated following Morris et al. (2001). By normalising the

daily wave power by the daily water level range, higher values of wave forcing are obtained during high water levels, indicating a higher wave erosion potential, and lower erosion potential during low water levels. First, the daily offshore mean wave power (MWP_0) was calculated following Splinter et al. (2014) as:

$$MWP_O = \frac{\rho g^2}{64\pi} {H_S}^2 T_P, \quad (4.4)$$

where ρ is the seawater density (~ 1024.5 kg/m^3), g is the gravitational acceleration (9.81 m/s^2) and wave power represents the wave energy flux per unit of wave crest length. Then the normalised wave power (NWP) was calculated as:

$$NWP = MWP_O(\eta_{dwlr}/\eta_{mwlr}), \quad (4.5)$$

where η_{dwlr} is the daily water level range and η_{mwlr} is the maximum water level range. As for the other forcing parameters, daily NWP values were averaged to monthly values.

In addition to the monthly forcing parameters, coastal storms that combine extreme waves and water levels were also identified to catalogue extreme events with a high likelihood of causing relevant shoreline changes. First, wave storms were extracted from the H_S timeseries following the approach of Kümmerer et al. (2024) who developed a robust wave storm identification for high-energy wave climates. Then, to discard events with lower water levels and consequently lower likelihood of beach erosion, only storm events that coincided with extreme water levels (> 99.5th percentile of water levels) were retained. These events are hereafter referred to as extreme coastal storms. To correlate the occurrence of extreme coastal storms with monthly SDVL position changes an additional parameter, the Coastal Storm Index (CSI), was calculated as the normalised monthly sum of the extreme coastal storm wave power maxima (i.e., peak power of storm waves that coincide with water levels exceeding the 99.5th percentile).

The climatic control on monthly shoreline variability was evaluated by comparison with the North Atlantic Oscillation (NAO) index. The NAO is the dominant mode of climate variability in the NE Atlantic (Hurrell, 1995), and it is strongly correlated with winter and storm wave activity in the Outer Hebrides (Kümmerer et al., 2024; Scott et al., 2021) and with shoreline variability along the Atlantic coast of Northern Europe (Castelle et al., 2024; Masselink et al.,

2023). Monthly NAO data, derived from monthly mean standardized 500-mb height anomalies, were obtained from the National Oceanic and Atmospheric Administration (NOAA) Climate Prediction Center.

Finally, the correlation between forcing parameters and shoreline change was established using beach averaged monthly SDVL deviations and the monthly averaged forcing parameters. Statistical correlations were calculated using R (Eq. 4.1) with a significance level of 0.05 and 0.1. The magnitude and significance of shoreline change trends were determined using Sen's slope and the Mann-Kendall test, respectively.

4.3 Result

4.3.1 SDVL Validation

The comparison between the MVL with the temporally closest SDVL shows a very good agreement (Figure 4.5a), evidenced by a strong positive correlation (R = 1.00) and a RMSE of 3.01 m across all sites (Figure 4.5b and Table 4.2), which corresponds to a sub-pixel error (considering the native 3.7 m resolution of Planet Scope imagery).

The best agreement between MVLs and SDVLs is observed at Ormiclate, with the highest correlation (R = 0.99) and lowest RMSE (2.34 m). Baleshare displays the highest RMSE with 3.84 m although with a strong correlation of R = 0.98. For all sites except Balranald, SDVL positions are consistently located seaward of their corresponding MVL, with a mean bias of 0.9 m but always lower than 1.33 m. Maximum deviations between MVL and SDVL can reach values of 12 m at Howmore and Baleshare (Figure 4.5b), with the latter site showing the highest scatter between MVL and SDVL positions. At Baleshare, areas with high deviation between MVL and SDVL are characterised by higher dunes with dune blowouts or areas of the barrier composed by gravel. In these cases, lowdensity vegetation patches near the barrier crest were not identified by the automated SDVL extraction algorithm but were measured as the vegetation line in the field. At Ormiclate, the surveyed area has the clearest and more consistent vegetation line, and this is reflected in the lower error metrics (Table 4.2). Most deviations between MVL and SDVL positions are therefore a result of the difference in the interpretation of the vegetation limit in the field and the image analysis. An additional source of error that cannot be accounted in the validation is the time gap between SDVL and MVL surveys, which ranges between 0 and 20 days with a mean time gap of 12 days across all sites (Table 4.2). However, a longer time

gap does not necessarily result in a weaker correlation or higher error, as it is the case for Balranald.

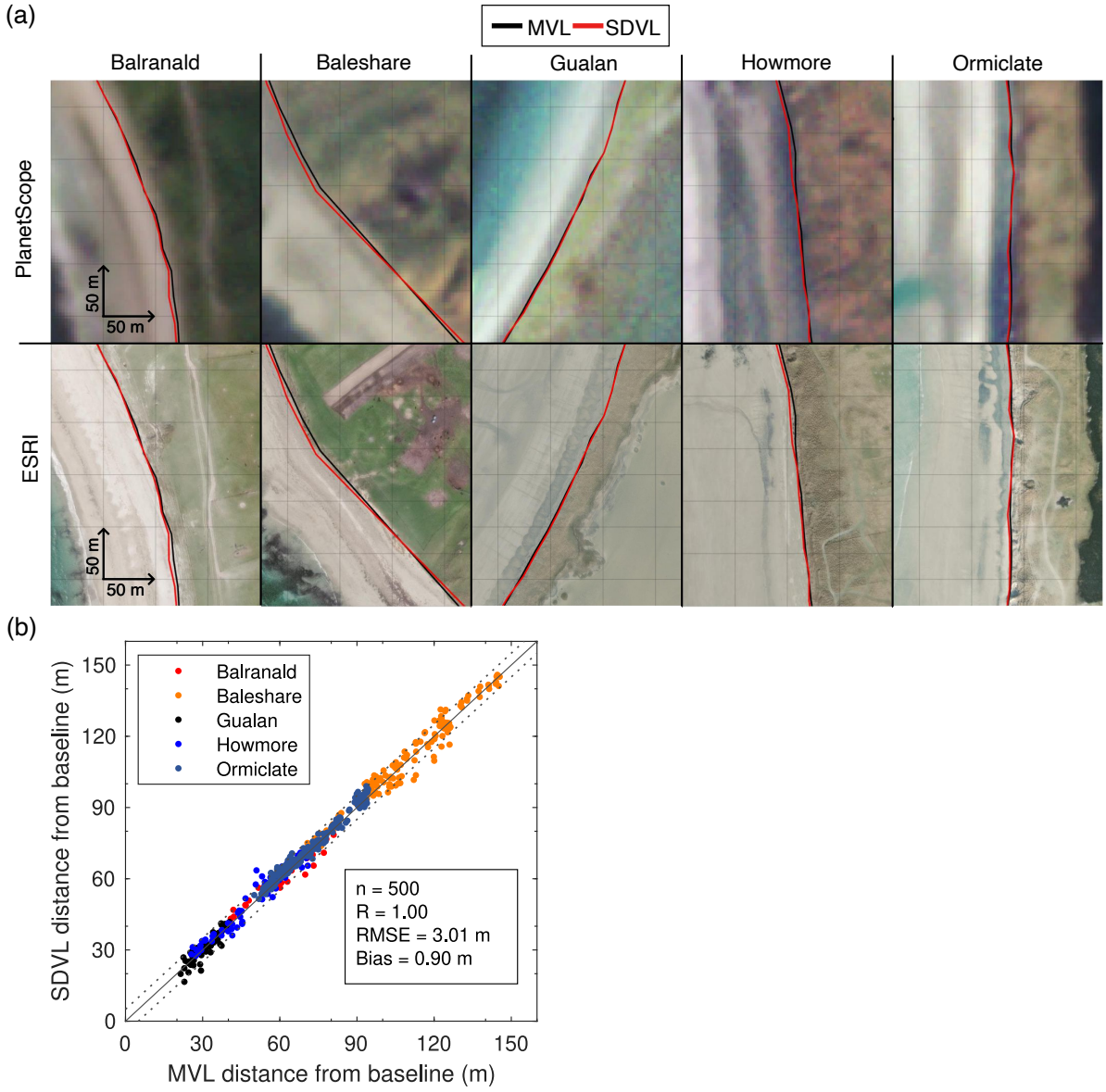

Figure 4.5 SDVL validation. **(a)** Comparison of MVLs (black lines) with their temporally closest SDVL (red lines) overlayed on north-oriented Planet Scope and higher-resolution satellite images available through the ESRI World Imagery Layer. **(b)** Scatter plot of SDVL and MVL distances from baseline and error metrics. The dotted lines represent ± 3 m error levels.

Table 4.2 Timing and error metrics between MVL and temporally closest SDVL. 'Time gap' is the number of days between MVL and SDVL survey dates and 'n' is the number of data points (i.e., 25 m spaced transects). A positive (negative) bias indicates a systematic seaward (landward) position of the SDVL compared to the MVL.

Site	MVL date	SDVL date	Time gap (days)	n	R	RMSE (m)	Bias (m)
Balranald	2022-11-05	2022-10-16	20	33	0.97	3.10	-0.43
Baleshare	2022-11-08	2022-11-08	0	138	0.98	3.84	1.01
	2023-02-17	2023-02-07	10				
	2023-02-24	2023-03-10	14				
Gualan	2022-11-07	2022-10-30	8	80	0.91	2.32	0.12
	2023-02-18	2023-01-31	18				
	2023-02-24	2023-03-10	14				
Howmore	2022-11-06	2022-11-13	7	61	0.97	3.42	1.03
	2023-02-18	2023-01-31	18				
	2023-02-22	2023-03-07	13				
Ormiclate	2022-11-06	2022-11-13	7	188	0.99	2.34	1.33
	2023-02-18	2023-01-31	18				
	2023-02-22	2023-03-10	16				
Mean	-	-	13	500	1.00	3.01	0.90

4.3.2 Forcing Conditions

Forcing conditions before and during the SDVL monitoring period are presented to provide a wider context of coastal storms that can influence multiannual shoreline dynamics. Winter storms can have extreme H_S (Figure 4.6a), which do not necessarily coincide with water levels above the 99.5th percentile as in the 2021/22 winter (Figure 4.6b). However, all observed extreme coastal storm events, i.e. storms with coinciding extreme H_S and water levels, occurred exclusively during winter months. In the pre-monitoring period (2012-2016), a cluster of extreme coastal storms occurred during the 2013/14 winter, which included the most powerful storm since January 2012. The first part of the monitoring period, from 2016 to 2020, is characterised by more frequently occurring extreme storm events when compared to the second part of this period (2021-2023). Considering only the shoreline monitoring period (2016-2023), the most extreme events occurred during the 2019/20 winter season. Only in winters 2013/14, 2019/20 and 2022/23 water levels exceeded 3 m above mean sea level, which was not reached in any other analysed winter (Figure 4.6b). The 2021/22 winter is exceptional due to the lack of storm events that coincided with water levels exceeding the 99.5th percentile, despite the occurrence of very energetic wave conditions. A catalogue with the key forcing parameters of each of the extreme coastal storms (Table 4.4, section 4.6.4) and graphical representation of

wave power and water level during each event are provided in the supplementary information (Figure 4.18-41, section 4.6.4).

As a result of the strong seasonality in extreme H_S and extreme water levels (Figure 4.6), the normalised wave power is higher during the winter months, indicating an increased erosion potential between October and March (Figure 4.7a). Monthly mean wind speeds are high throughout the year with an average of ~30 ms-1. The highest monthly wind speeds coincide with months of strong hydrodynamic forcing, which results in extreme winter forcing conditions (Figure 4.7b). A positive monthly NAO is generally linked to winter months coinciding with stronger forcing conditions in the Outer Hebrides.

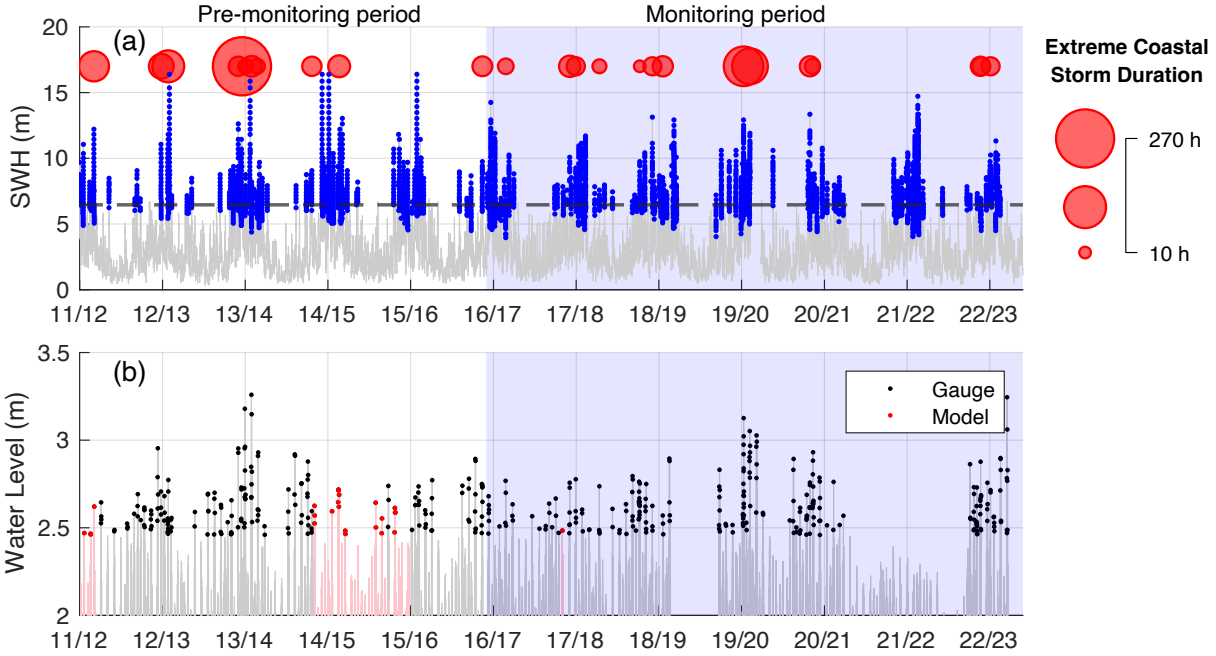

Figure 4.6 Storm event forcing before and during the SDVL monitoring period. **(a)** H_S in 30 min intervals. Blue dots indicate significant wave height during storms, and the horizontal dashed line indicates the 95th percentile of H_S. The red circles indicate extreme storm events with coinciding water levels above the 99.5th percentile for the Stornoway tide gauge and the circle size is scaled in relation to the storm duration. **(b)** Water levels above 2 m recorded at the Stornoway tide gauge (grey) and from the GTSM 3.0 model (red). Black and red dots indicate peaks that exceed the water level 99.5th percentile for the gauge and model, respectively.

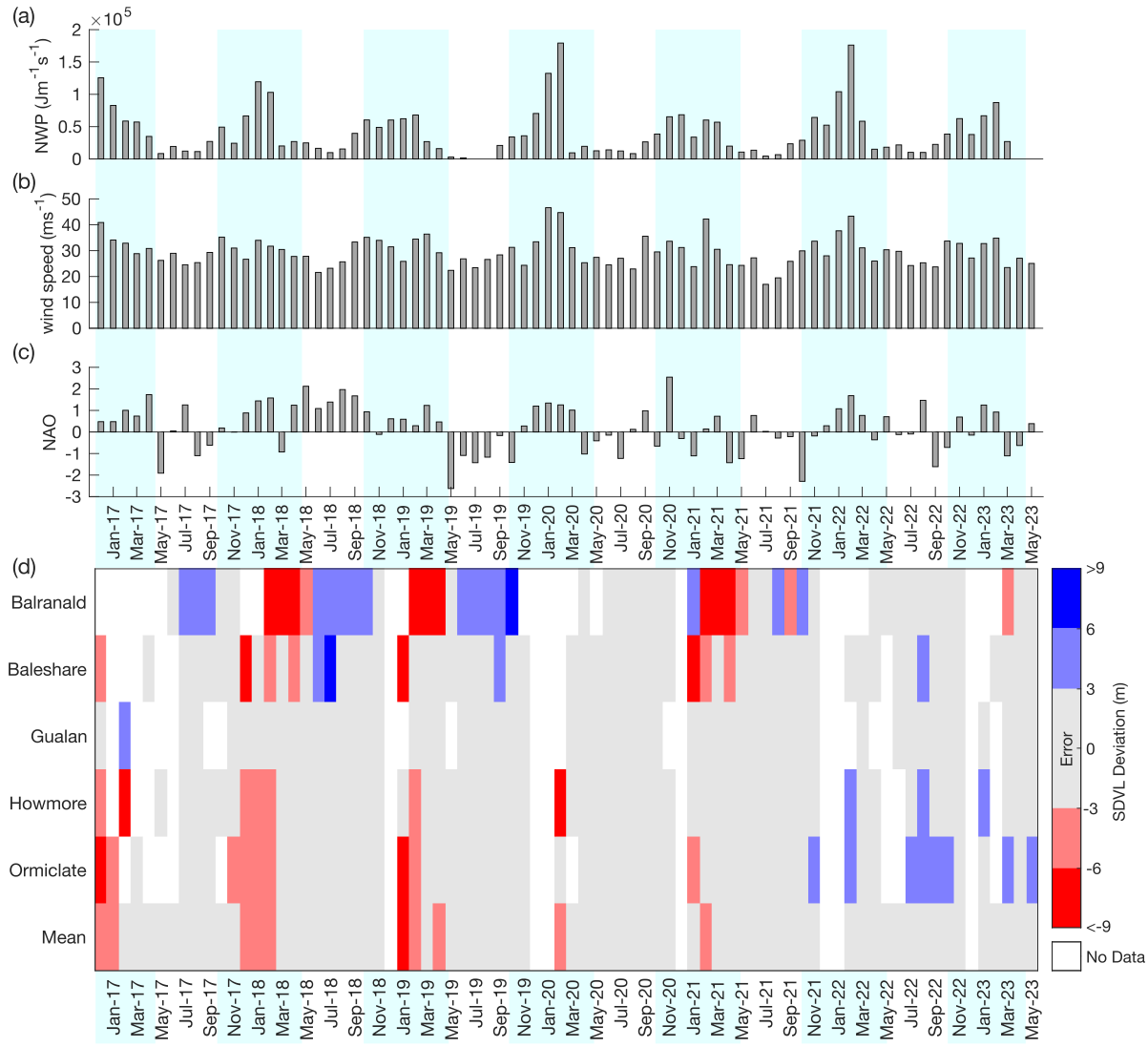

Figure 4.7 Site averaged monthly mean SDVL deviation and monthly forcing parameters between December 2016 and May 2023. Light blue vertical bars highlight winter months. **(a)** Normalised wave power (NWP). **(b)** Wind speed. **(c)** North Atlantic Oscillation (NAO). **(d)** Variability in site averaged monthly mean SDVL position relative to the mean for the period analysed. Light grey colour for values between ± 3 m corresponds to values within the SDVL extraction error range.

4.3.3 Inter-site Shoreline Behaviour

Similarities in shoreline behaviour can be observed from the site averaged monthly mean SDVL positions, which show a clear seasonal variability over the last 7 years. This is characterised by shoreline retreat typically occurring in winter (October – April) and shoreline advance in summer (May – September) (Figure 4.7d and Figure 4.8). The seasonality in shoreline changes is in line with the seasonal varying wave forcing conditions, but the higher magnitude in winter

wave forcing does not directly result in higher shoreline retreat. The highest monthly normalized wave power during the analysis period was observed in February 2022 (Figure 4.7a), combined with strong monthly wind speed (Figure 4.7b), which indicate an elevated erosional potential. However, shoreline retreat was not observed during this month, which also lacked extreme water level events (Figure 4.6). Similarly, shoreline retreat in the 2019/20 winter is relatively small considering the magnitude of the forcing, but this is likely masked by the lack of cloud free PlanetScope images over the winter months (Figure 4.17, section 4.6.4), particularly December and January, for which no images were available across the entire study area (Figure 4.7d). However, the general pattern of shoreline behaviour changes after the 2020/21 winter, with a higher shoreline variability before and lower variability after this winter season for the mean site-averaged SDVL deviation (Figure 4.8f). The absence of winter shoreline retreat after the 2020/21 winter (Figure 4.7d) agrees with the absence of extreme storms during this period (Figure 4.6), with the exception of Balranald.

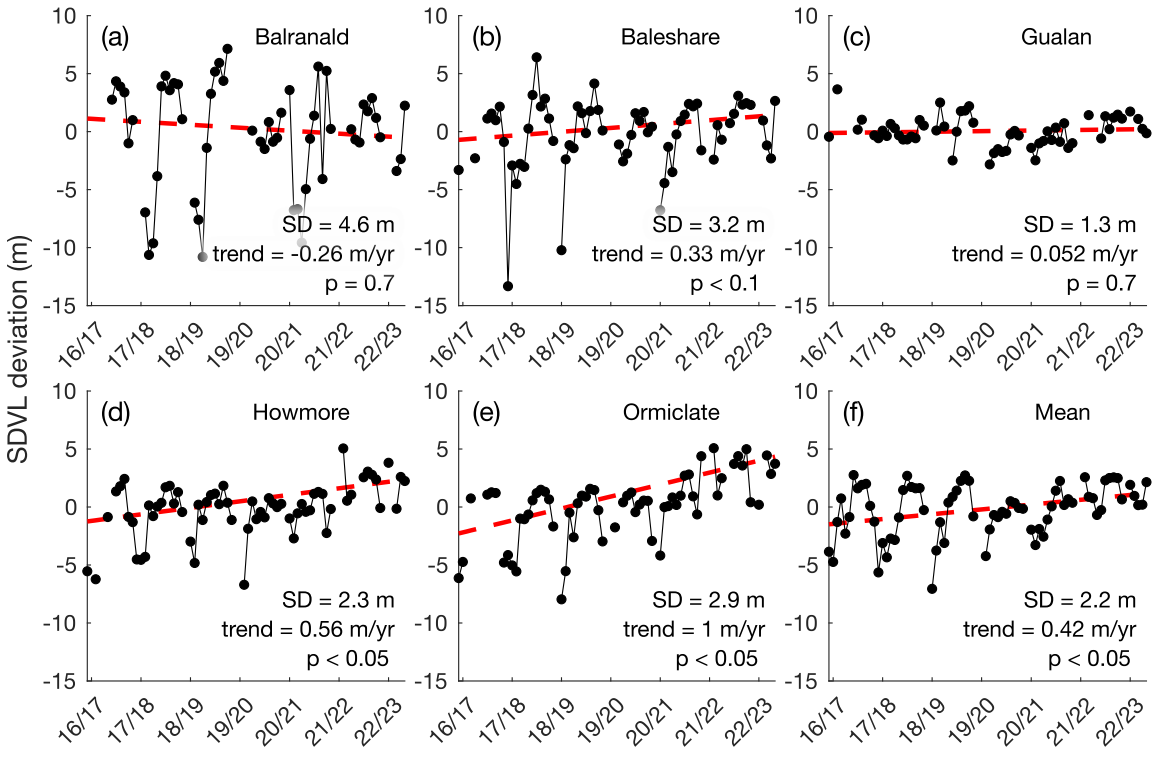

Figure 4.8 Multiannual trends (red lines) and standard deviation (SD) of site-averaged monthly mean SDVL position (black lines) relative to the mean for the whole period analysed. The dots represent data points for each month and the black line is interrupted where data gaps are longer than one month.

Differences in shoreline behaviour can be observed in the trends and the variability of the site-averaged monthly mean SDVL positions. There is a statistically significant multiannual (7-year) trend of shoreline advance at 3 out of the 5 beaches (Baleshare, Howmore and Ormiclate), superimposed on the seasonal variability in shoreline position (Figure 4.8b, d, e). The mean advancing shoreline position trend is 0.42 m/yr, and this is statistically significant at a 0.05 significance level, indicating that overall and during the study period, barriers in the Outer Hebrides display an accretionary trend (Figure 4.8f). The highest rate of shoreline advance is observed at Ormiclate with 1 m/yr, while Balranald and Gualan show no statistically significant trend in shoreline position.

Higher variability in shoreline position is found on the NW-SE orientated barriers (Balranald and Baleshare) compared to barriers with a N-S orientation (Gualan, Howmore and Ormiclate) (Figure 4.7d and Figure 4.8). The highest shoreline variability is observed at Balranald, indicated by the highest standard deviation (SD = 4.6 m) in site-averaged monthly mean SDVL positions and a maximum seasonal difference during the monitoring period of 18 m (Figure 4.8). Similar high variability and magnitude of seasonal shoreline position change were observed at Baleshare but with a lower SD of 3.2 m. While Howmore and Ormiclate have lower shoreline variability compared to Balranald and Baleshare with SDs of 2.3 m and 2.9 m, respectively, Gualan shows a muted shoreline variability with a SD of 1.3 m (Figure 4.8). Here, the change in SDVL position rarely exceeds the error range (Figure 4.7d and Figure 4.8c).

The analysis of auto-correlation in shoreline change demonstrates further differences in seasonal shoreline behaviour between sites (Figure 4.9). Except for Gualan, the site-averaged monthly mean SDVL positions show a pronounced peak at 12 months that indicates seasonal differences between winter and summer shoreline behaviour. An additional distinct peak at 6 months is shown for Balranald and Baleshare barriers. This peak indicates that the site-averaged shoreline position is both advancing and retreating over the mean shoreline position in summer and winter, respectively (Figure 4.7d). This differs from the behaviour of the barriers at Gualan, Howmore and Ormiclate that have no distinct peak at 6 months in the auto-correlation function, which indicates that the shoreline is either retreating in winter and subsequently advancing to the mean position or advancing in summer and subsequently retreating to the mean position in winter. This muted inter-seasonal shoreline behaviour results in an overall lower SDVL variability for Gualan, Howmore and Ormiclate.

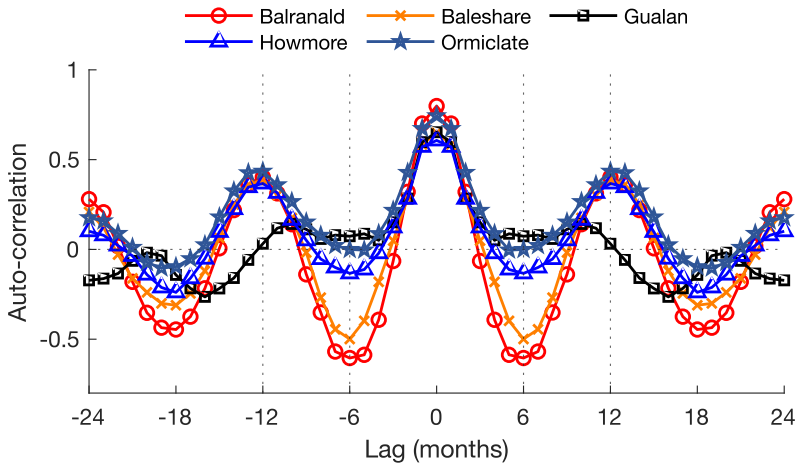

Figure 4.9 Auto-correlation of the site-averaged monthly SDVL deviations between December 2016 and May 2023.

In terms of forcing conditions, based on the parameters tested, CSI and NWP evidence higher inverse correlation to the monthly mean SDVL positions, as shown by statistically significant negative values of R = 0.41 and R = -0.38 (for a p-value of 0.05), respectively (Table 4.3). In contrast, monthly wind speed and NAO values show no statistically significant correlation when considering all sites combined. A negative correlation indicates that stronger forcing is associated with shoreline retreat and weaker forcing with shoreline advance. However, wind speed is significantly negatively correlated with SDVL positions at Balranald, Howmore and Ormiclate. Furthermore, the correlation between wind speed and SDVL is weaker compared to the correlation between NWP and SDVL positions, except for Balranald where wind speed has a higher negative correlation. The monthly NAO index is not significantly correlated with monthly shoreline positions in any of the sites. Site averaged mean SDVL deviation at Gualan has no statistically significant correlation with any of the forcing parameters considered.

Table 4.3 Correlations between site-averaged monthly mean SDVL deviation and monthly forcing parameters. Statistically significant correlations for p-values below 0.05 are indicated in bold.

	Balranald	Baleshare	Gualan	Howmore	Ormiclate	Mean
NWP	- 0.23	**- 0.42**	0.16	**-0.42**	**-0.34**	**-0.38**
Wind Speed	**-0.27**	-0.18	0.10	**-0.35**	**-0.25**	-0.29
CSI	-0.13	**-0.37**	0.14	**-0.51**	**-0.36**	**-0.41**
NAO	-0.11	-0.07	0.07	-0.12	-0.19	-0.15

4.3.4 Intra-Site Shoreline Behaviour

At the finer scale of individual barriers, distinct intra-site shoreline change can be observed, with varying shoreline behaviour between beach sectors with different types of foreshore configuration (Figure 4.10 and Figure 4.11-15). The two southernmost barriers, Howmore and Ormiclate, have substantially less sediment cover on the foreshore when compared to the other three barriers (Figure 4.10a). These barriers are characterised by transects with ~ 50 % of sub-tidal rock surfaces within 500 m offshore from the mean SDVL position.

Beach sectors fronted by a sediment-rich foreshores show a consistently higher variability in shoreline position (Figure 4.10b) than sectors fronted by a rocky foreshore (Figure 4.10c, d). This shoreline behaviour pattern is observed for Balranald (Figure 4.10e), Baleshare (Figure 4.10f) and Gualan (Figure 4.10g) but not evident at Howmore (Figure 4.10h) and Ormiclate (Figure 4.10i), which have greater geological control due to a higher percentage of sub-tidal rock surfaces (Figure 4.10a). Other deviations from this shoreline behaviour are associated with the presence blowouts on the foredune that are responsible for the higher variability on the SDVL position (Figure 4.10b, c, i). However, there are no blowouts at transects fronting foreshores with higher rock outcrop percentages (Figure 4.10d).

The lowest SDVL variability is generally observed along sectors exhibiting rock outcrops on the beach. In these sectors, such as between transects 35 and 52 at Balranald (Figure 4.11) and between transects 75 and 120 at Baleshare (Figure 4.12), the change in shoreline position generally does not exceed ± 5 m, which contrasts with the higher variation in adjacent sectors with lower geological control. The only exception to this shoreline behaviour is observed at Howmore, where the sector with a rock outcrop north of the river outlet between transect 130 and 155 (Figure 4.14) has a higher SDVL variability when compared to the area north of transect 130 that although characterized by high proportion of rocky foreshore (> 50% sub-tidal rock surfaces), does not have outcropping rocks (Figure 4.14b). Varying foreshore configuration also affects the length of the recovery period after winter shoreline retreat at Balranald (Figure 4.11) and Baleshare (Figure 4.12). Following the shoreline retreat in the 2020/21 winter, the recovery period until the shoreline switches to mean position advance is longer (~1 year) in sectors fronted by rocky foreshore and rock outcrops when compared to adjacent sectors fronted by sedimentrich foreshores, where recovery is faster (~6 months).

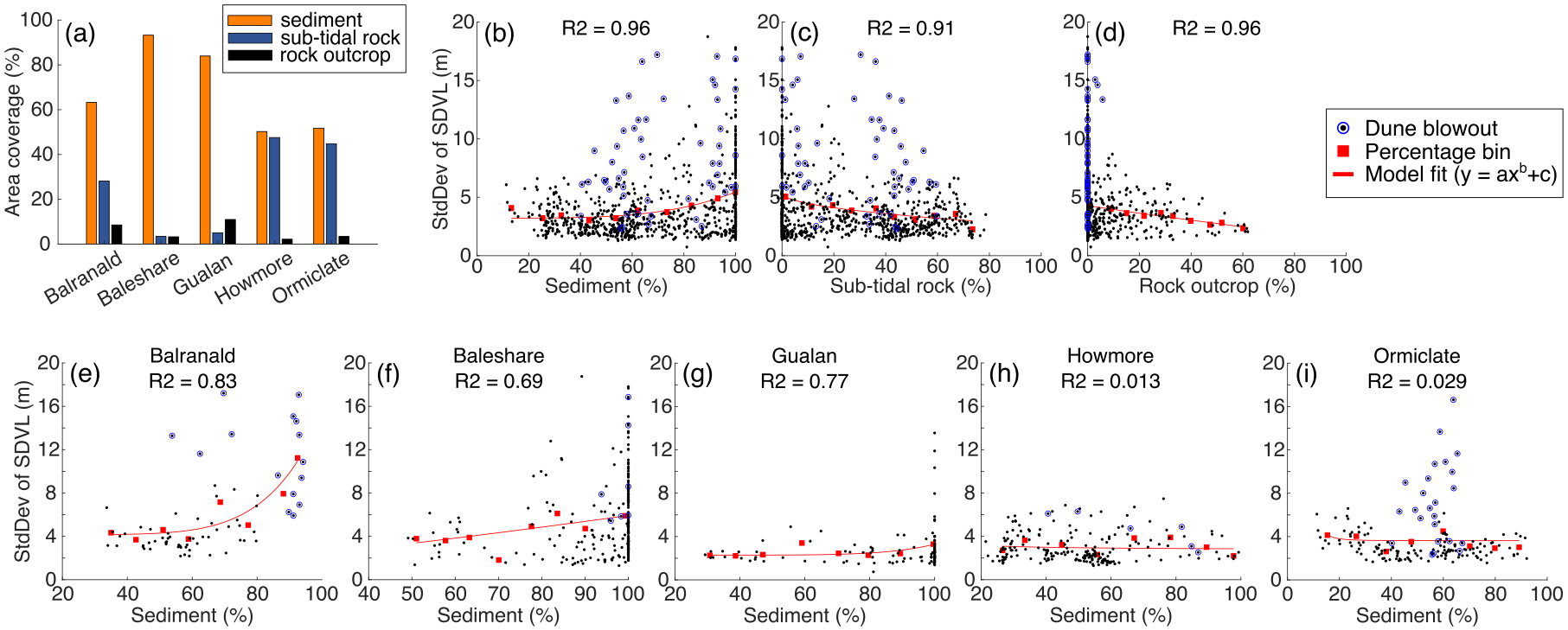

Figure 4.10 Geological control on shoreline behaviour. (a) Coverage of the three foreshore classes for each beach. (b-d) Sediment, sub-tidal rock and rock outcrop coverage against the standard deviation of monthly SDVL positions for each transect at all sites, respectively. (e-i) Sediment coverage against standard deviation of monthly shoreline positions for each transect at each site. The R^2 for each relationship was determined based on a bin-averaged polynomial model that better captures the curvilinear pattern of the data clouds. Note that transects where blowouts were identified are marked with a blue circle.

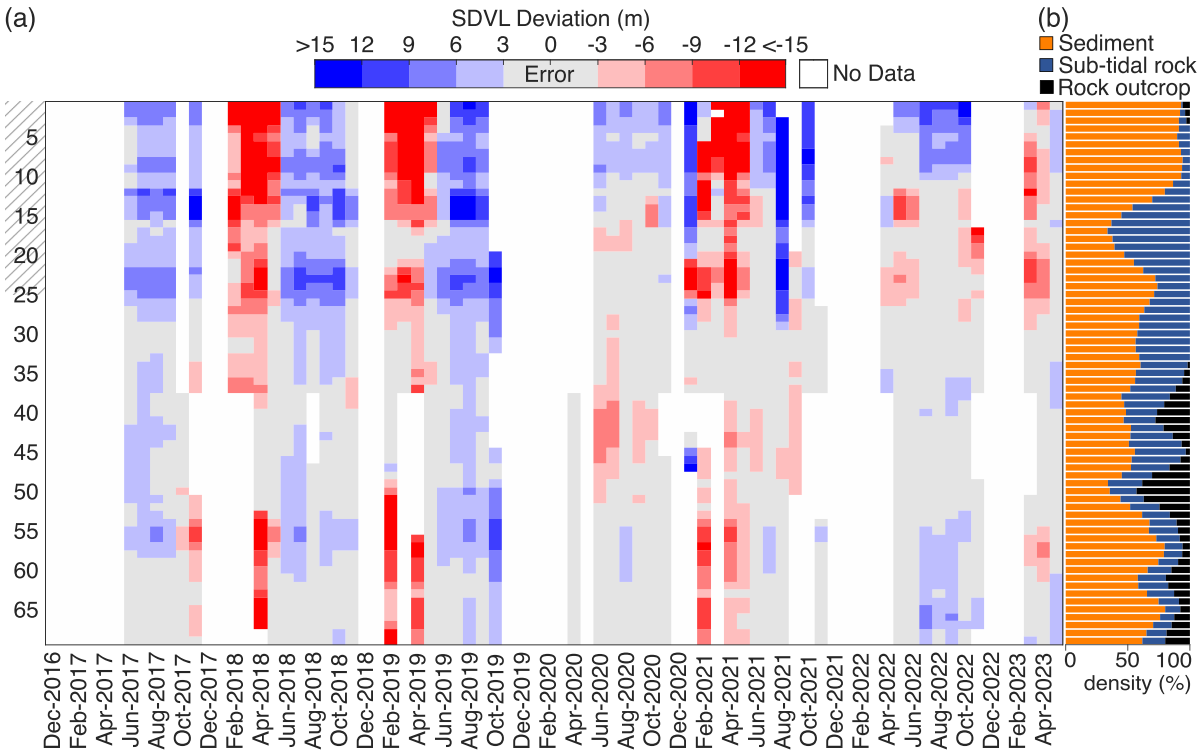

Figure 4.11 Monthly averaged SDVL deviation and foreshore configurations at Balranald. **(a)** Monthly averaged SDVL position relative to the mean for the whole period analysed for each transect. Values are averaged alongshore with a moving mean of 4 transects (100 m). Light grey colour for values between ±3 m indicates the SDVL extraction error range and white indicates absence of images for the corresponding month due to extensive cloud cover. Dashed transect numbers mark transects crossing extensive foredune blowouts. **(b)** Foreshore configuration as percentage coverage for each foreshore class at each transect.

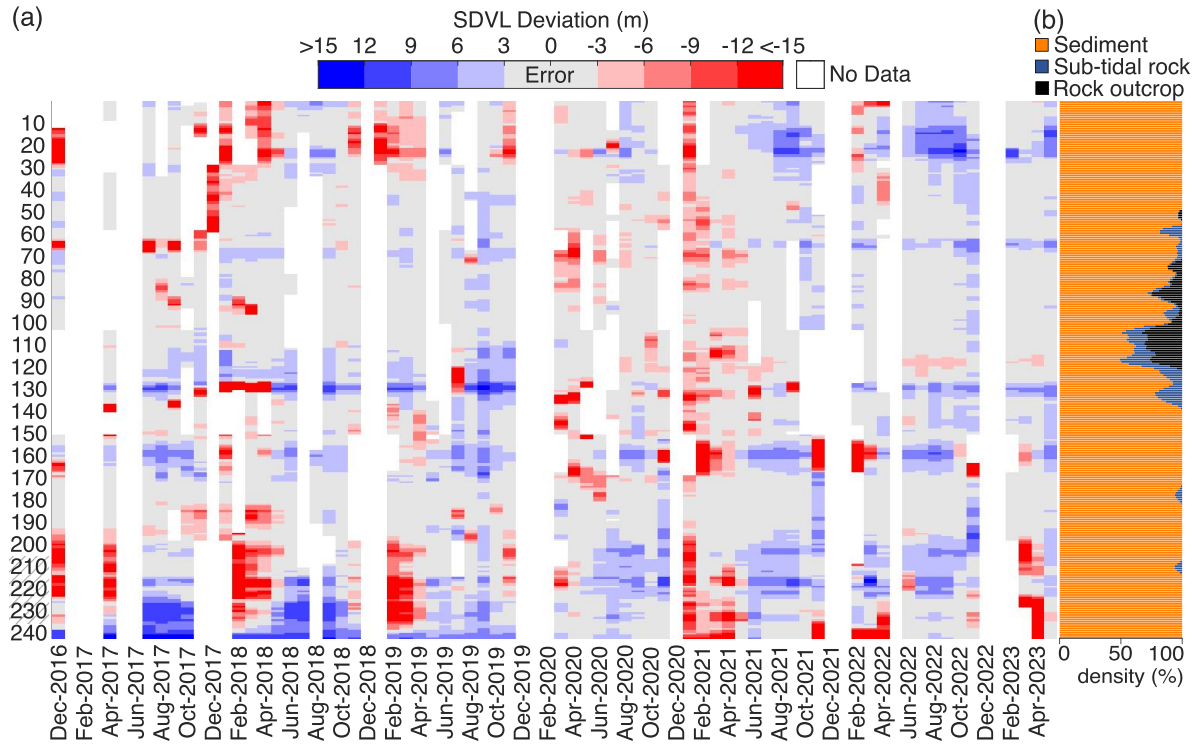

Figure 4.12 Monthly averaged SDVL deviation and foreshore configurations at Baleshare. (see Figure 11 for description of figure caption).

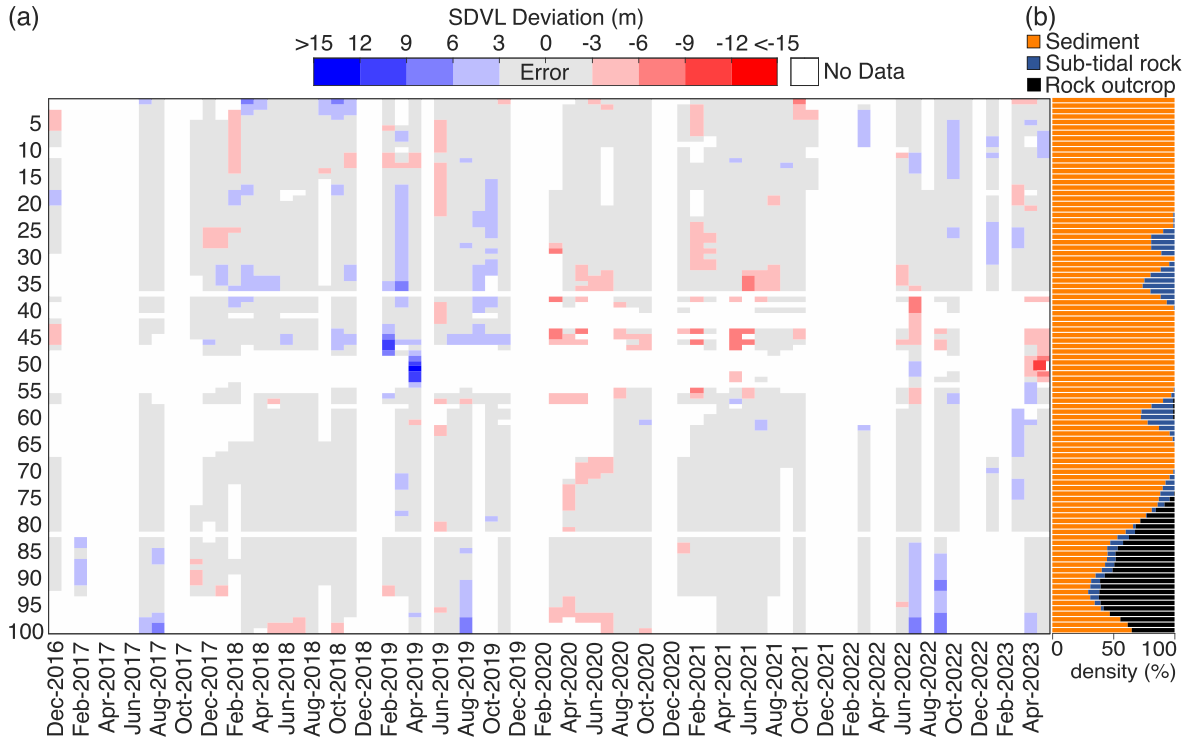

Figure 4.13 Monthly averaged SDVL deviation and foreshore configurations at Gualan (see Figure 11 for description of figure caption). Note: Between transect 38 and 55 occasionally there is no SDVL data, either because of the lack of satellite images or the interruption of the vegetation line due to overwash events that completely eroded the dune, including its vegetation.

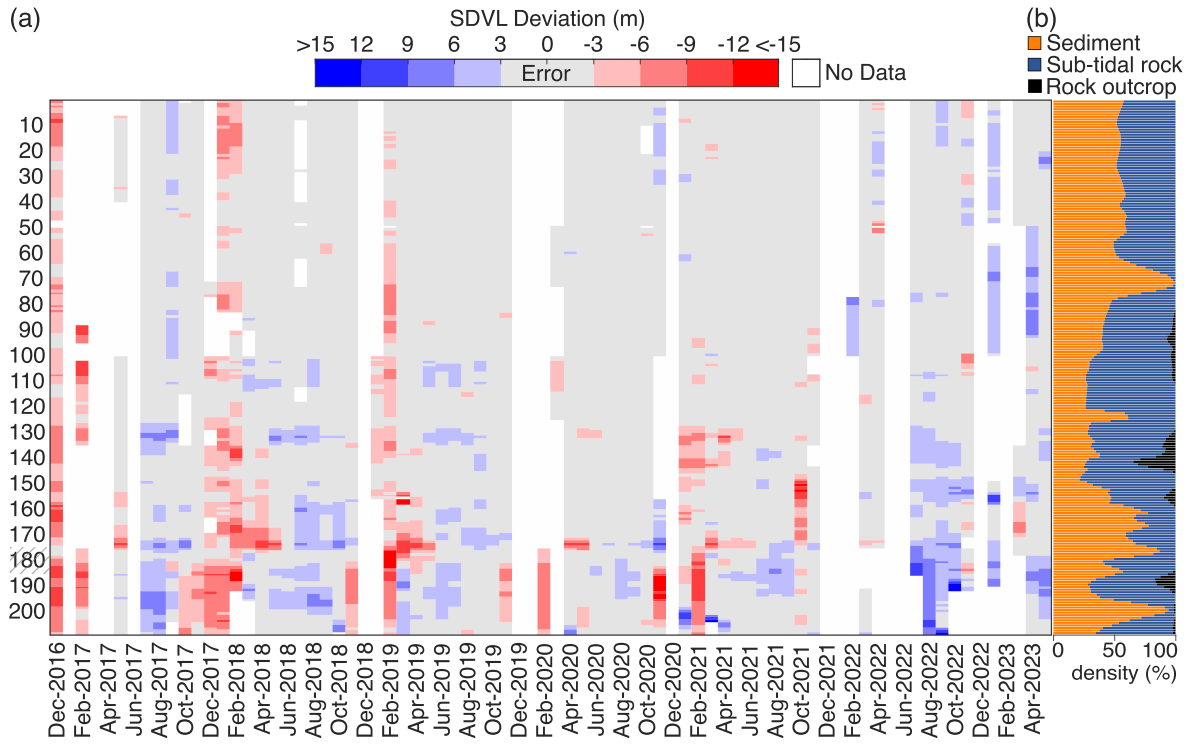

Figure 4.14 Monthly averaged SDVL deviation and foreshore configurations at Howmore. (see Figure 11 for description of figure caption).

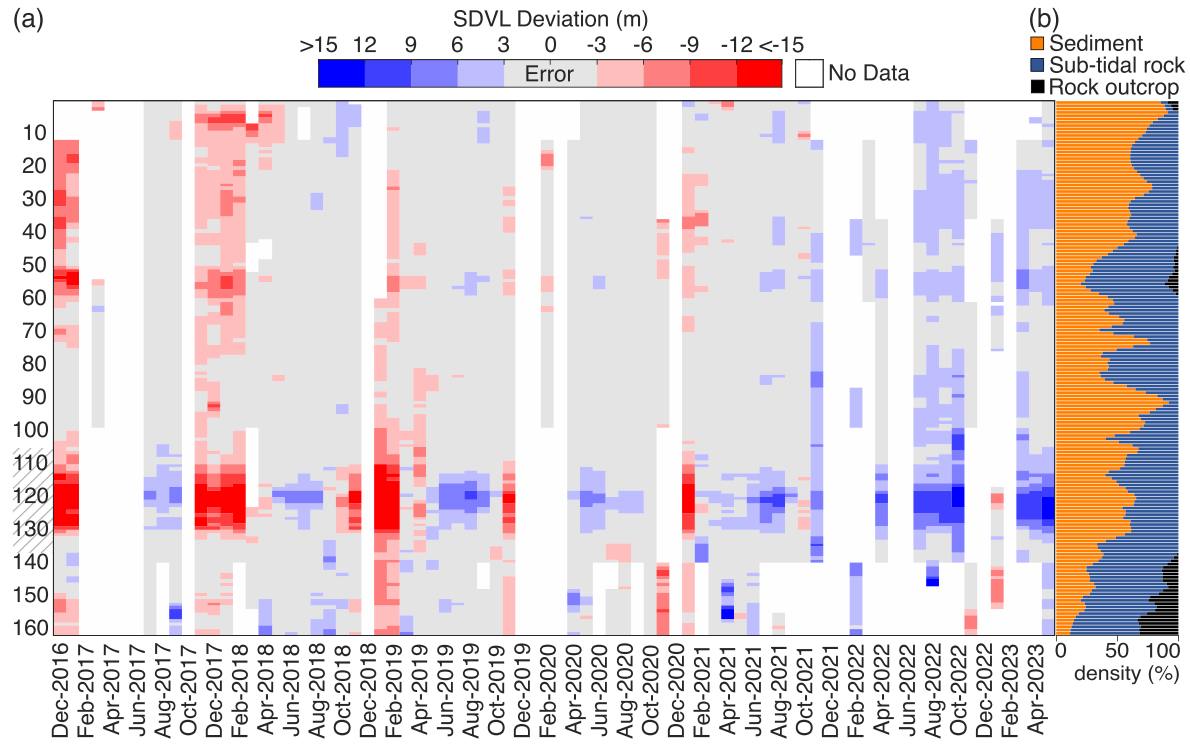

Figure 4.15 Monthly averaged SDVL deviation and foreshore configurations at Ormiclate (see Figure 11 for description of figure caption).

4.4 Discussion

4.4.1 Satellite Derived Shoreline Mapping in Complex Coastlines

Satellite-derived shorelines commonly obtained from publicly available satellite imagery have horizontal accuracy in the order of 10 m in microtidal sites, which worsens as tidal range increases (Vos et al., 2023). Similarly, integration of different satellite imagery products with very high (3 m) to moderate resolutions (10-30 m) for mapping coastal vegetation edges results in horizontal accuracy in the order of 19 m (Muir et a., 2024). However, consistently using a higher spatial resolution dataset such as Planet Scope imagery (3.7 m) substantially improves the accuracy of satellite-derived shoreline positions to values of a few meters (>5 m) (Figure 4.5) (Doherty et al., 2022; Rogers et al., 2021). The potential of the Planet Scope imagery for shoreline mapping is further reinforced by the shorter revisit time (daily to sub-daily) that improves the usability of satellite imagery, especially in coastal regions with extensive and frequent cloud cover.

Shoreline changes derived from satellite imagery are commonly assessed using the instantaneous waterline shoreline position (McAllister et al., 2022). However, this indicator has significant limitations in coastlines characterised by high-energy wave conditions, gentle shoreface slopes and large tidal variation (Castelle et al., 2021; Graffin et al., 2023; Konstantinou et al., 2023; Vos et al., 2023; Zhang et al., 2024). This limitation arises from the need to horizontally correct the waterline shoreline position according to the vertical variation in water level and intertidal beach slopes at the satellite fly-over time. Furthermore, energetic waves and gentle sloping beaches substantially increase the uncertainty in the horizontal correction (Castelle et al., 2021; Zhang et al., 2024). The vegetation line position, however, requires no horizontal correction and therefore prevents the errors induced by changes of the beach slope and by tidal and swash driven aliasing. Furthermore, the vegetation line was found to be a better indicator of storm driven erosion compared to other shoreline proxies in mixed gravel-sand barriers, including the waterline (Pollard et al., 2020). The intertidal shoreline position can recover within days after the peak of a minor storm (e.g., Vousdoukas et al., 2012), while the vegetation line is able to preserve storm impacts for a longer period due to the relatively slow recolonisation of the dune vegetation. For example, the overall lack of satellite imagery during winter may mask undetected erosion caused by winter storms as both December and January are characterised by energetic forcing that result in shoreline retreat (Figure 4.7a). However, storm-induced erosion during these months would be visible in the February SDVL

as dune vegetation growth is slow during winter in the Outer Hebrides (Huiskes, 1979). Therefore, although there is a temporal lag in the vegetation growth which may limit the accurate detection of post-storm beach recovery (Boak and Turner, 2005), the vegetation line enables better detection of storm event erosion using satellite-derived shorelines because it is less sensitive to the time gap between the storm peak and the satellite pass. SDVL accuracy can also be impacted by dune scarping events that lead to a false accumulation signal when large, vegetated dune blocks avalanche causing a possibly seaward shift of the SDVL. However, these tend to be localized features with limited impact when aliasing the vegetation line with a moving average, as performed here.

The combination of Planet Scope imagery and the vegetation line as shoreline indicator was previously used by Rogers et al. (2021). Their SDVL extraction tool VEdge_Dectector is based on a fully automated algorithm using a convolutional neural network. Their approach performs well for straight sandy coastlines (RMSE = 2.37-7.97 m) but faces issues in more complex coastlines with the presence of outcropping rocks. While automated approaches are faster and applicable to larger areas, higher accuracy (RMSE = 2.32-3.84 m, Table 4.2) can be achieved by incorporating a brief manual inspection of the SDVLs into the workflow, as implemented in this work. Advances in satellite products and algorithms using machine learning or artificial intelligence will further improve shoreline extraction (Turner et al., 2021). Yet, at the current stage of algorithm development, including a visual inspection of the automatically derived shorelines greatly improves the accuracy of satellite-derived shoreline positions in more complex coastal areas. Choosing an appropriate shoreline indicator according to coastline type further increases the information obtained from satellite-derived shorelines.

4.4.2 Shoreline Response to Forcing

Changes in shoreline position are mainly driven by oceanographic and meteorological forcing, which is evidenced by the statistically significant correlations between forcing parameters and SDVL changes (Table 4.3). The seasonal shoreline variability in the Outer Hebrides is related to the strong seasonality in the wave climate (Kümmerer et al., 2024; Santo et al., 2015) and storm surge forcing (Haigh et al., 2016) in the NE Atlantic. This generally results in winter shoreline retreat and summer shoreline advance along the Hebridean coast. Superimposed on the seasonal signal, multiannual shoreline trends are often the result of exceptional storm-driven erosion (e.g., Suanez et al., 2023), with subsequent beach recovery taking place over several

years (Burvingt and Castelle, 2023; Houser et al., 2015; Konstantinou et al., 2021). Along the Outer Hebrides, the assessment of shoreline changes since 1970 are limited to local erosional hotspots and the shoreline position is generally stable for most of the coastline (Gómez et al., 2014; Hansom et al., 2017). Thus, the mean advancing trend in shoreline position between 2017 and 2023 in the Outer Hebrides barriers (Figure 4.8f) is likely associated with a multiannual recovery phase from energetic winter conditions that occurred prior to the monitoring period (i.e. winters of 2013/14 and 2014/15). A similar pattern of multiannual barrier recovery has recently been observed in several beaches along the Atlantic coast of Europe and was found to be initiated after the extreme storm conditions recorded in the winter of 2013/14 (Burvingt and Castelle, 2023). The 2013/14 winter was characterised by several extreme storm events in fast succession (Figure 4.6) that caused severe erosion of beaches and dunes along the Atlantic coast of Europe (Castelle et al., 2015; Kandrot et al., 2016; Masselink et al., 2016a, 2016b). While wave conditions in the Outer Hebrides were more energetic during the following 2014/15 winter (Figure 4.6) (Kümmerer et al., 2024), these extreme wave conditions coincided with lower water levels compared to the 2013/14 winter. It is important to note that Masselink et al. (2016a) show that for Portrush beach in Northern Ireland, the subaerial beach volume was more significantly reduced during the 2014/15 winter than in the 2013/14 winter. As this is the northernmost beach with regular beach surveys, and the 2014/15 winter had higher storm power at higher latitudes than the previous winter, it is possible that the Hebridean barriers were similarly affected during this winter. It is therefore likely that the observed multiannual recovery of the barriers only began after the combined effect of the extreme storms of these two winters.

For seasonal to multiannual timeframes, the monthly SDVL data allows to better characterise spatial variability in shoreline position and its relation with the hydrodynamic conditions causing shoreline change at the management scale (~ 10 years). Wind and hydrodynamic forcing are significantly correlated with SDVL changes and the storm event history contributes to improved understanding of interannual shoreline mobility in the Outer Hebrides barriers. Storm events that occur during low water level conditions do not typically result in relevant morphological impacts in coastlines in equilibrium with high-energy conditions (Cooper et al., 2004), as observed along the Outer Hebrides. As the European Atlantic coast is not surge dominated (Haigh et al., 2016), the severity of storm impacts depends on the coincidence with spring tide conditions (e.g., Levoy et al., 2023). Furthermore, geologically constrained beaches in high-energy environments are adapted to extreme forcing and, thus, shoreline retreat only

occurs during extreme coastal storm events with coinciding high-water levels, extreme wave power and extreme wind speeds (Cooper et al., 2004; Guisado-Pintado and Jackson, 2018; Suanez et al., 2023). In the Outer Hebrides, where the dissipative and geological constrained beaches are adapted to high-energy conditions, only rare extreme wave conditions associated with high water levels cause coastal storm impacts (Dawson et al., 2007; Kümmerer et al., 2023). Therefore, the duration above a critical water level is a key variable determining the severity of beach erosion, as observed for other barriers in the UK (Masselink et al., 2022) and Ireland (Kandrot et al., 2016; Williams et al., 2015). Kümmerer et al. (2024) identified an increasing trend in storm duration in the NE Atlantic coast during the past 70 years, and longer storms increase the likelihood of coinciding high water levels and intense wave forcing (Rulent et al., 2021), resulting in increased erosion potential.

4.4.3 Geological Controls on Shoreline Behaviour

While dynamic forcing conditions drive shoreline change, the geological framework exerts a major control on the shoreline evolution of coastal barriers (Hapke et al., 2016). The geomorphological variability of the Hebridean barriers is mediated by the topography of the underlying and frequently exposed bedrock surfaces and the limited sediment supply (Cooper et al., 2012; Pile et al., 2019). Previous modelling of shoreline variability with and without the influence of rocky features at Narrabeen Beach (SE Australia) demonstrated their strong influence on contemporary shoreline dynamics (Robinet et al., 2020). In the Outer Hebrides barriers, the control exerted by the varying foreshore configuration is also evident in the contemporary shoreline dynamics at the inter and intra-site spatial scale.

At the finer spatial scale of individual beaches, distinct intra-site shoreline change patterns can be observed, with varying shoreline behaviour between beach sectors with different types of foreshore configuration (Figure 4.10b-d). Rock fronted sectors with higher geological control show a consistently lower variability in shoreline position than sectors fronted by higher percentages of sediment and thus lower geological control. However, this behaviour is restricted to beach sectors with a general higher availability of sediment in the foreshore, as it is not observed along the barriers of Howmore and Ormiclate. Both barriers have a substantially higher percentage of sub-tidal rock surfaces in the foreshore and, therefore, are subjected to a higher geological control and consequently dampened response to hydrodynamic forcing. This is also indicated by their generally muted shoreline variability ($> \pm 5$ m) compared to the higher

shoreline variability of the more northern barriers (Figure 4.10e-i). Thus, the results from the Outer Hebrides barriers indicate that when the overall geological control is very high, the muted response will be similar alongshore, even if there are smaller sectors where sediment is more prevalent in the foreshore. When geological control is lower, the alongshore variability in shoreline response is higher and more directly related to the proportion of rock and sediment cover for each transect. Similar muted shoreline behaviour in higher geologically constrained sectors with rocky features compared to less constrained, sediment-rich sectors was found in other coastlines such as Victoria beach (Cadiz, Spain) (Muñoz-Perez and Medina, 2010) Yanchep beach (SW Australia) (Gallop et al., 2012), Sinis Peninsula (Sardinia, Italy) (Simeone et al., 2021) and Mossel Bay (South Africa) (Wiles et al., 2022). At these locations, the lower shoreline variability results in longer recovery periods after storm erosion, which is also observed in the Outer Hebrides. One hypothesis for a muted shoreline behaviour is that the sediment-starved foreshore of these beach sectors limits cross-shore sediment transport, and the non-erodible surface consistently dissipates wave energy, resulting in limited morphological exchange (Gallop et al., 2012; MuñozPerez and Medina, 2010; Robinet et al., 2020). The hydrodynamic processes responsible for these differences in shoreline behaviour are difficult to resolve through hydrodynamic modelling because of a general lack of in-situ wave measurements and bathymetric data in complex and highly energetic surf zones, especially considering the sloping nearshore bedrock surfaces and extensive kelp beds present in the Outer Hebrides. However, beach sectors with high geological control are not always associated with a muted shoreline response. While sediment-rich beaches can switch beach states according to the variation in wave forcing conditions, beaches with rocky lower profiles lack this readjustment mechanism (Jackson and Cooper, 2009). Thus, if a threshold is reached in terms of water elevation above the rocky surface or erosion of the reef structures, shorelines can reach a tipping point and rapidly erode under specific hydrodynamic conditions and possibly result in complete removal of the beach (Davidson et al., 2021) or extreme shoreline retreat.

At the larger spatial scale, there is a clear difference in shoreline behaviour between the northern barriers of Balranald and Baleshare and the southern barriers of Howmore and Ormiclate, characterised by seasonal SDVL variability with higher and lower magnitudes, respectively. As mentioned, the northern barriers have lower proportions of foreshore rocky surface (> 28 %), which indicates a higher sediment availability and possibly sediment volume. A similar finding was postulated by Ritchie (1971), who argued that there is more sediment available along North Uist due to the Lewisian gneiss bedrock topography. The typically northwest to southeast

bedrock ridges and the continuous shallow reef to the Monach Islands (Figure 4.1) facilitateed sediment deposition in local depressions. The inter-site shoreline behaviour difference may be also related to differences in shoreline orientation between the northern barriers, with a NW-SE orientation, and the southern barriers, with a N-S orientation. The seasonal advance of the vegetation line depends on the growth of foredunes in the seaward margin of the barriers, which provides conditions for the recolonisation of dune vegetation. While foredune growth is strongly linked to local sediment availability and fetch distance, the angle between the main wind direction and shoreline orientation can exert a major control on foredune development (Delgado-Fernandez and Davidson-Arnott, 2011; Dłużewski et al., 2023). The main wind direction is more frequently shore-parallel at the southern beaches resulting in less sediment transport to the foredunes compared to general onshore winds at Balranald and Baleshare (Figure 4.1). Therefore, the potential for foredune development is higher in the northern beaches with NW-SE shoreline orientation compared to the southern beaches with N-S orientation, resulting in a higher seasonal shoreline advance. Similarly, the variation in foredune development potential can explain the muted seasonal shoreline advance in rock fronted beach sectors, as in such cases there is also a limit to the supply of sediment for onshore aeolian sediment transport leading to reduced foredune development. A marked muted behaviour is observed at Gualan, with an overall low shoreline variability during the monitored period compared to the other sites. The location of Gualan island between two headlands and the higher embaymentisation compared to the other barriers may increase wave attenuation and reduce the exposure to energetic wave action.

Dune blowouts are an additional factor influencing vegetation-based shoreline variability. Transects crossing extensive foredune blowouts show consistently higher shoreline variability (Figure 4.10b-i), but along the studied barriers, dune blowouts were not observed in transects with relevant percentages of rock outcrops. However, as the formation and evolution of blowouts and their effect on shoreline variability is a wind driven process, their study is beyond the scope of this work.

Further field and modelling efforts are required to disentangle the influence of the geological framework on shoreline changes. Pre- and post-storm beach surveys and in-situ nearshore wave, wind and water level measurements are fundamental to identify differences in nearshore forcing characteristics, beach and dune volume changes and hence shoreline behaviour between barriers and beach sectors with varying degrees of geological control. In addition, process-based modelling of idealised barrier profiles with differing geological control is likely to reveal

processes that lead to the reduced shoreline variability observed in beach sectors fronted by rocky foreshores compared to sandy foreshores.

4.5 Conclusions

This work assessed monthly SDVLs as an indicator of shoreline position on strongly geologically controlled coastal barriers in western Scotland between December 2016 and May 2023, which were identified using Planet Scope imagery based on a newly developed semi-automated approach. The combination of high-resolution Planet Scope imagery, vegetation lines as shoreline indicator, and the inclusion of a brief visual inspection of the automatically derived shorelines improved the accuracy of the satellite-derived shoreline positions resulting in sub-pixel errors (RMSE = 3 m). The approach presented is particularly suited for assessing monthly to multiannual shoreline change in coastal areas with a well-defined transition between beach and vegetated dune, regardless of beach slope and tidal range.

In the Outer Hebrides, seasonal shoreline mobility is statistically correlated with the seasonality of storm forcing, with a general shoreline retreat in winter and shoreline advance in summer. The superimposed multiannual trend of advancing shoreline position (0.4 m/yr) is likely associated with a widespread pattern of barrier recovery in the Atlantic coast of Europe after strong winter storm impacts between 2013 and 2015. Similar to other beaches in the UK and Ireland, the coincidence of extreme water levels with extreme wave conditions results in shoreline erosion in the Outer Hebrides. However, in addition to the hydrodynamic forcing, the alongshore varying geological configuration results in distinct inter- and intra- site shoreline change behaviour. Barrier sectors fronted by a sediment-rich foreshore showed consistently higher seasonal variability in shoreline position than areas fronted by a rocky foreshore or rocky outcrops. Limited morphological exchange for rocky foreshore configurations is considered to result from the sediment-starved conditions and the wave energy dissipation along the non-erodible surface. Differences in the magnitude of site-averaged shoreline variability can also be explained by the local sediment budget and likelihood of foredune development, which are both higher on the beaches with NW-SE shoreline orientation compared to those with N-S orientation. This results in higher and lower seasonal shoreline variability, respectively.

Overall, in addition to wind and hydrodynamic forcing parameters, nondynamic geological variables exert a strong control on shoreline behaviour along coastal barriers at event, seasonal

and multiannual timescales. This allows the identification of distinct storm-driven shoreline behaviour according to the degree of geological control.

4.6 Supplementary Material

4.6.1 Sediment cover on the foreshore

For the transect based classification of the foreshore configuration it is assumed that the spatial changes in the sediment cover on the foreshore and upper shoreface (500 m offshore from the mean SDVL position) are limited throughout the shoreline change analysis period (December 2016 – May 2023). This is evident from the visual inspection of various Planet Scope imagery (Figure 4.16, section 4.6.4).

4.6.2 Monthly Image Counts

There are long periods of cloud cover in the Outer Hebrides which compromises the extraction of satellite derived shoreline positions. Therefore, to improve the temporal consistency, the SDVL positions were averaged to monthly composites. The number of SDVL positions (i.e., number of available images) that were averaged varied between months with a general lower available number of SDVL positions during winter months (Figure 4.17, section 4.6.4). This can lead to masking of shoreline retreat during winter such as during the 2019/20 winter.

4.6.3 Extreme Coastal Storm Events

Extreme events with the combined occurrence of extreme water levels (99.5^{th} percentile) and extreme wave conditions were identified to provide a context for the interannual shoreline mobility in the Outer Hebrides barriers. Extreme water levels do not necessarily coincide with the strongest waves during the storm (Table 4.4, Figure 4.18-41, section 4.6.4).

4.6.4 Supplementary Figures and Table

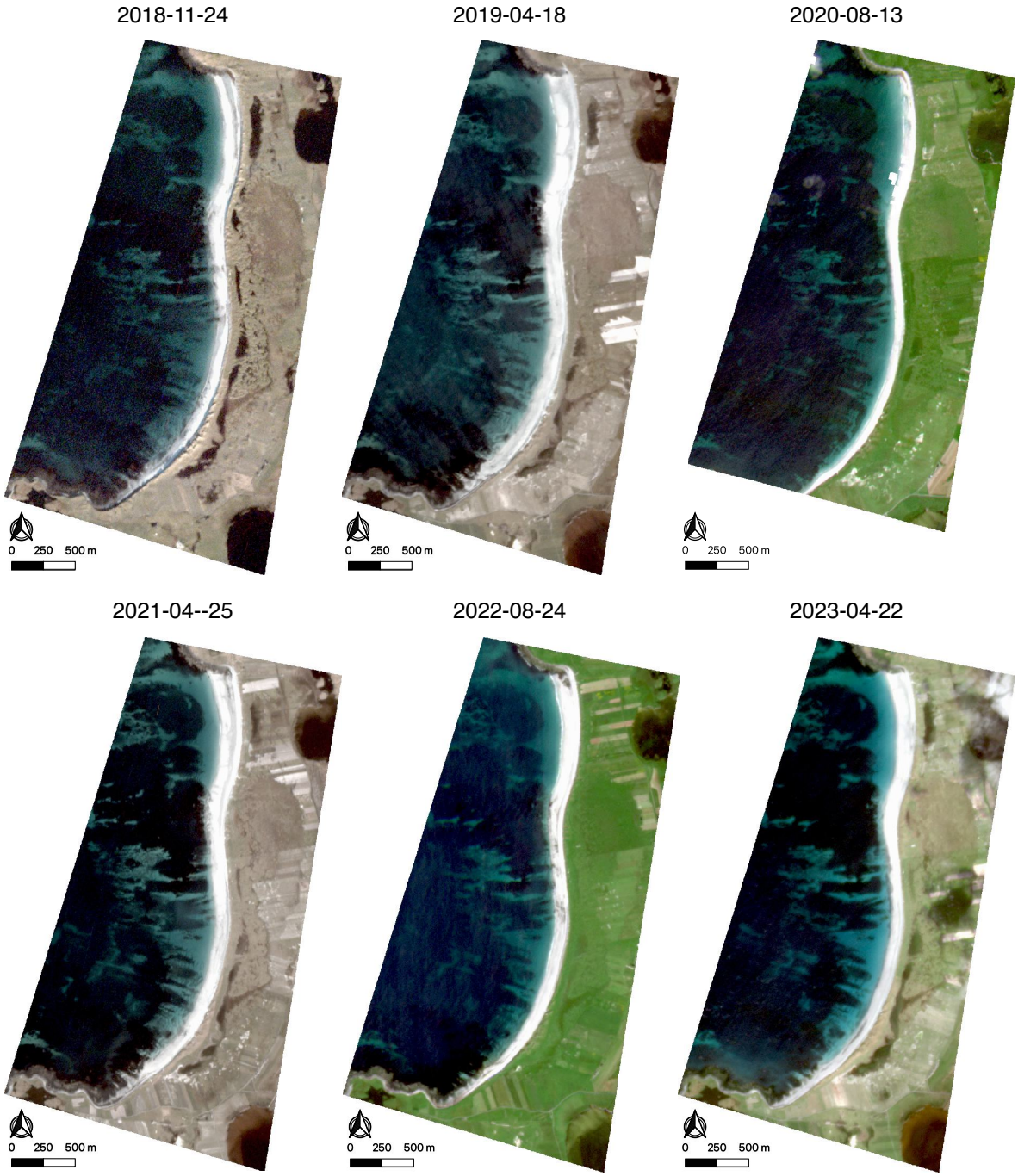

Figure 4.16 Time series of pre-processed Planet Scope imagery of Ormiclate. The horizontal lines indicate the Planet Scene overlap.

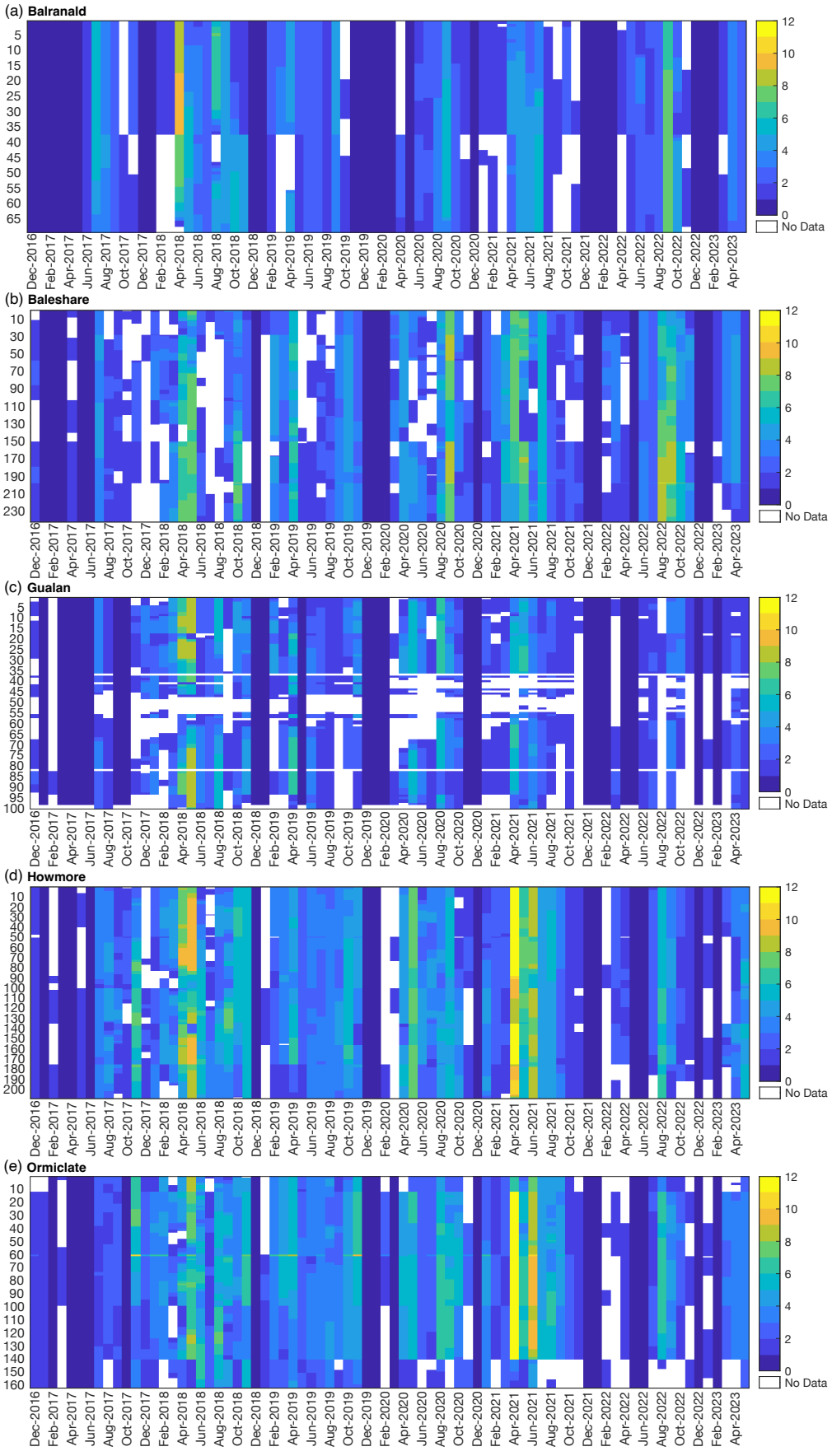

Figure 4.17 Number of averaged SDVL positions per month at each barrier and transect.

Table 4.4 List of storm characteristics of the identified extreme coastal storm events. The date corresponds to the peak wave power of the event.

Date	Peak water level (m)	Peak power associated with 3 h window around peak water level (MWh/m)	Peak Power (MWh/m)	H_S at peak power (m)	T_P at peak power (s)	Dir_P at peak power (°)
08/03/2012	2.62	0.27	1.50	12.21	20.6	293
30/12/2012	2.71	0.51	0.98	11.06	16.4	293
29/01/2013	2.77	0.35	1.03	11.44	16.1	253
05/12/2013	2.95	1.01	1.19	12.62	15.2	293
21/12/2013	2.73	0.56	1.12	10.70	20.0	264
02/02/2014	3.26	0.46	0.52	8.19	15.8	264
28/02/2014	2.53	0.32	0.43	6.92	18.3	281
26/10/2014	2.60	0.45	0.60	9.06	15.0	281
23/02/2015	2.69	0.66	1.12	10.70	20.0	253
16/11/2016	2.72	0.68	0.78	9.75	16.7	297
28/02/2017	2.55	0.25	0.30	6.84	13.3	304
07/12/2017	2.76	0.48	0.71	10.08	14.3	318
03/01/2018	2.78	0.55	0.79	8.97	20.0	262
17/04/2018	2.46	0.33	0.43	7.58	15.4	249
12/10/2018	2.75	0.46	0.88	9.91	18.2	253
07/12/2018	2.63	0.41	1.12	13.13	13.3	233
22/01/2019	2.57	0.45	0.56	8.25	16.7	315
14/01/2020	3.03	0.73	1.35	12.29	18.2	252
11/02/2020	3.00	0.40	1.26	11.90	18.2	205
01/11/2020	2.76	0.70	1.46	13.35	16.7	271
13/11/2020	2.62	0.33	0.67	8.67	18.2	284
24/11/2022	2.85	0.24	0.40	6.96	16.7	277
28/11/2022	2.65	0.26	0.33	6.61	15.4	250
08/01/2023	2.72	0.64	0.79	10.25	15.4	245

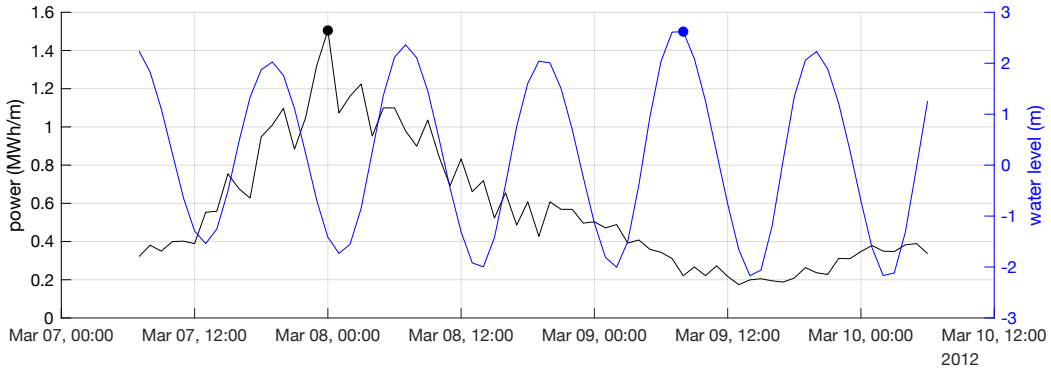

Figure 4.18 Wave power and water level during the extreme coastal storm event on 08/03/2012.

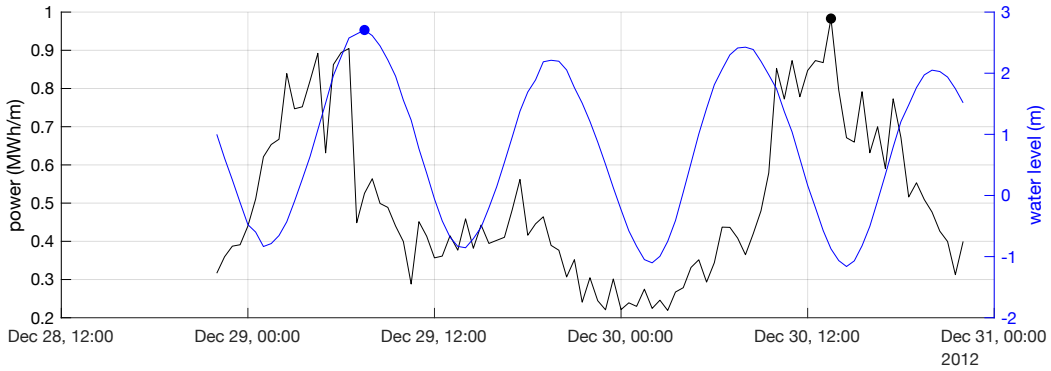

Figure 4.19 Wave power and water level during the extreme coastal storm event on 30/12/2012.

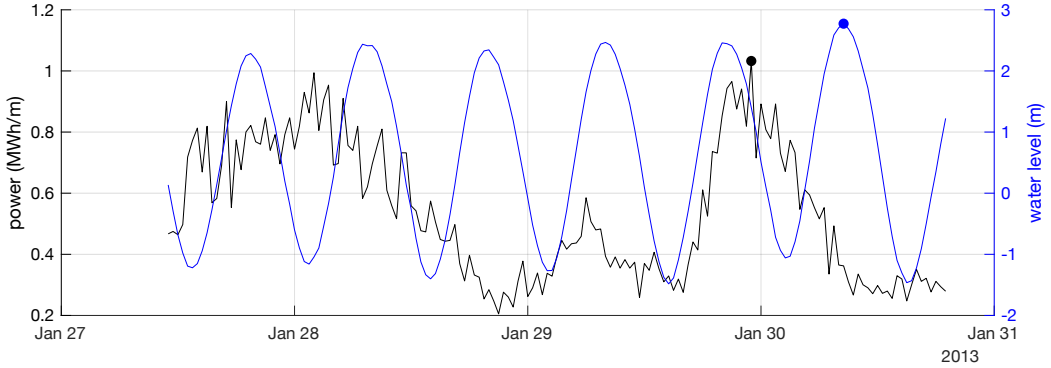

Figure 4.20 Wave power and water level during the extreme coastal storm event on 29/01/2013.

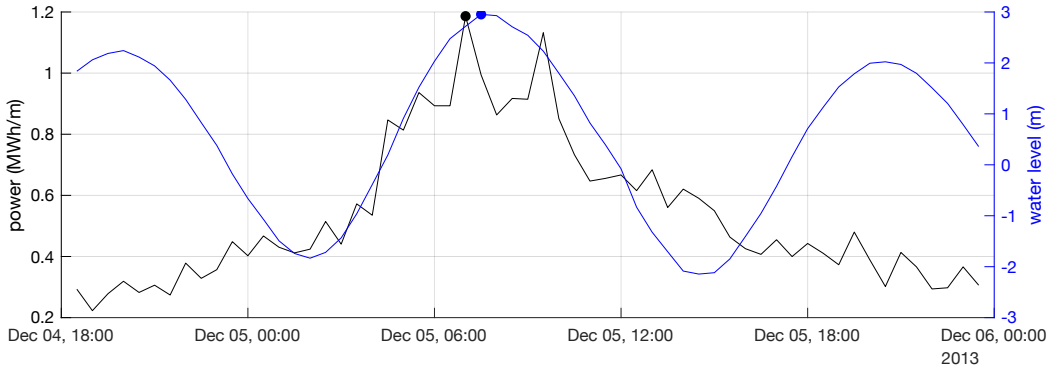

Figure 4.21 Wave power and water level during the extreme coastal storm event on 05/12/2013.

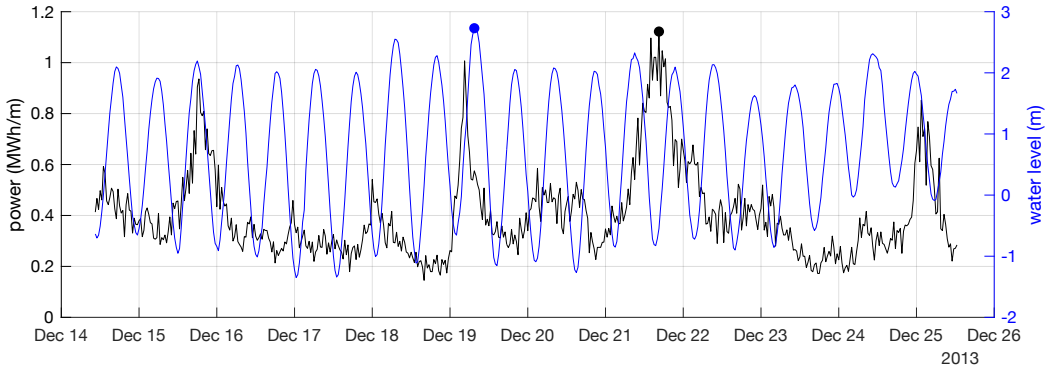

Figure 4.22 Wave power and water level during the extreme coastal storm event on 21/12/2013.

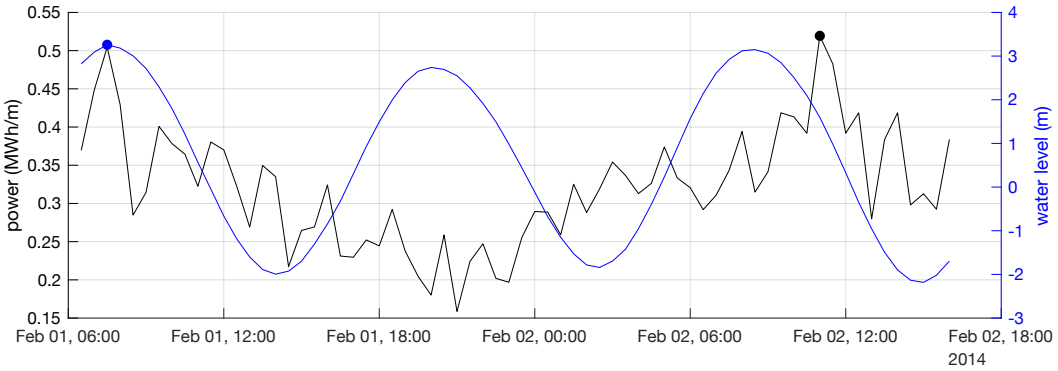

Figure 4.23 Wave power and water level during the extreme coastal storm event on 02/02/2014.

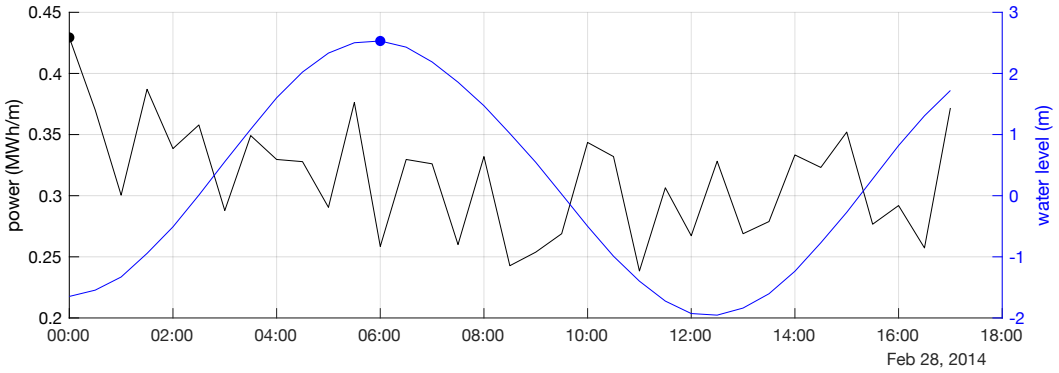

Figure 4.24 Wave power and water level during the extreme coastal storm event on 28/02/2014.

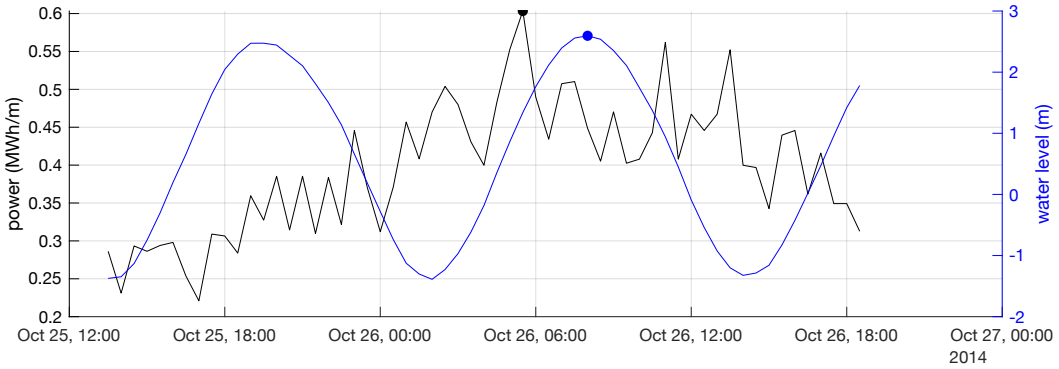

Figure 4.25 Wave power and water level during the extreme coastal storm event on 26/10/2014.

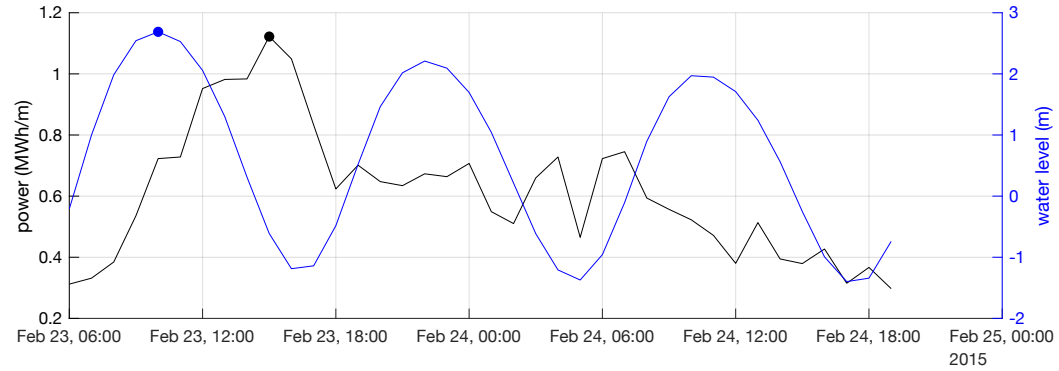

Figure 4.26 Wave power and water level during the extreme coastal storm event on 23/02/2015.

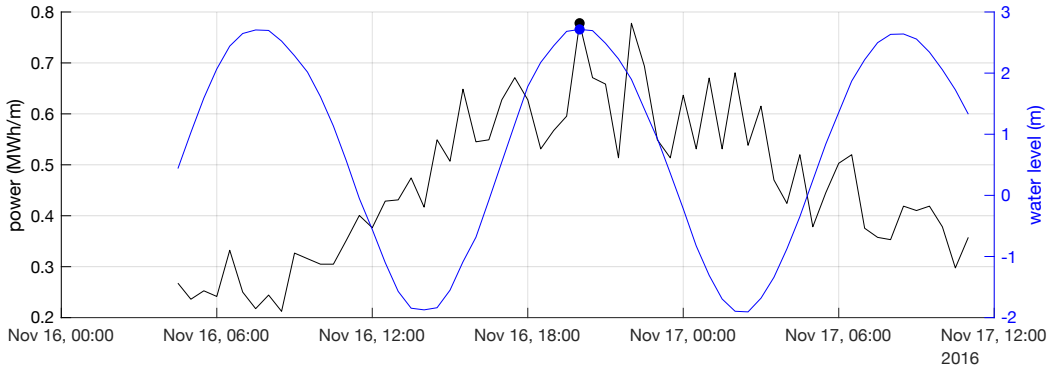

Figure 4.27 Wave power and water level during the extreme coastal storm event on 16/11/2016.

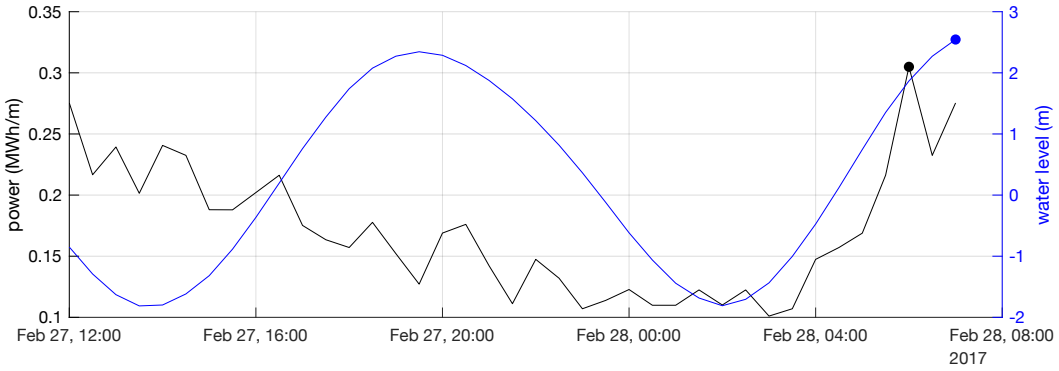

Figure 4.28 Wave power and water level during the extreme coastal storm event on 28/02/2017.

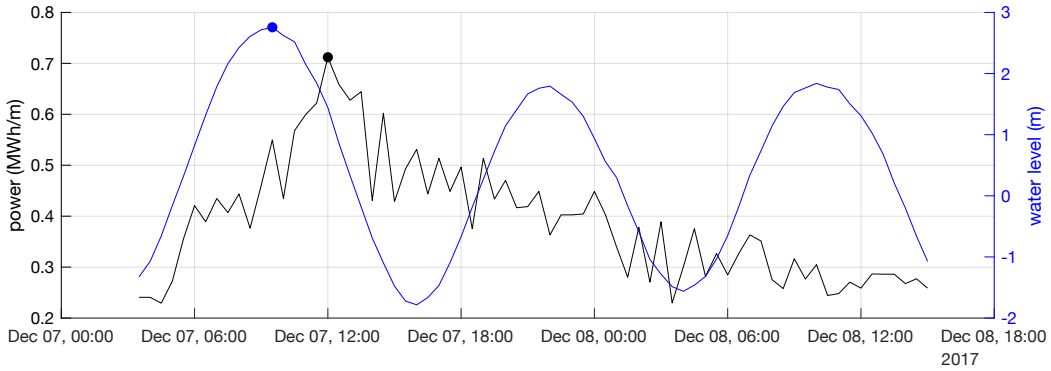

Figure 4.29 Wave power and water level during the extreme coastal storm event on 07/12/2017.

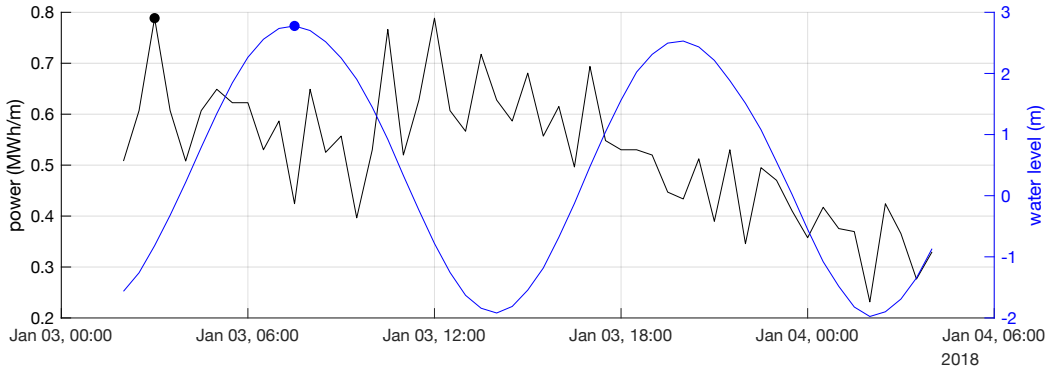

Figure 4.30 Wave power and water level during the extreme coastal storm event on 03/01/2018.

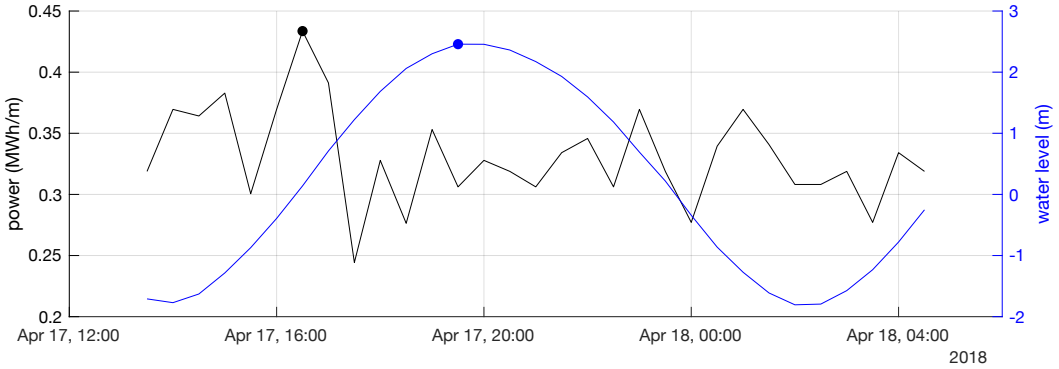

Figure 4.31 Wave power and water level during the extreme coastal storm event on 17/04/2018.

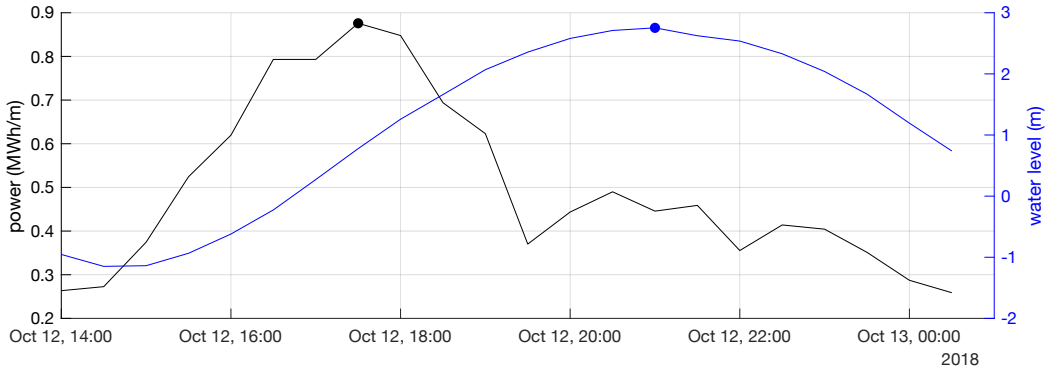

Figure 4.32 Wave power and water level during the extreme coastal storm event on 12/10/2018.

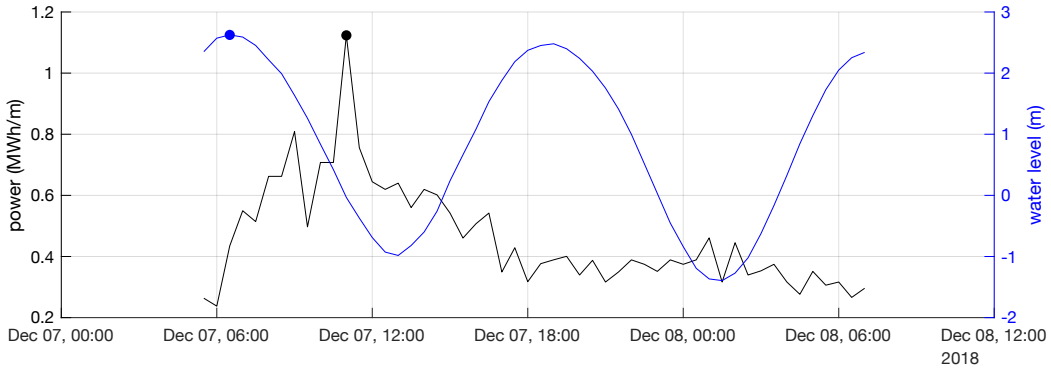

Figure 4.33 Wave power and water level during the extreme coastal storm event on 07/12/2018.

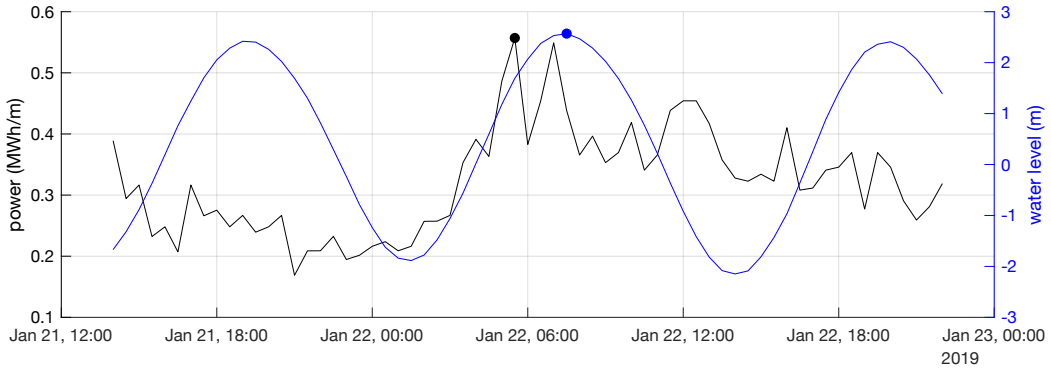

Figure 4.34 Wave power and water level during the extreme coastal storm event on 22/01/2019.

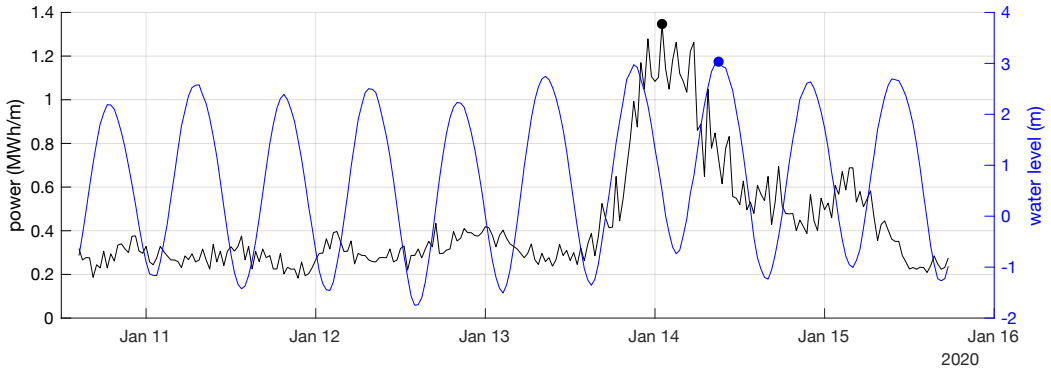

Figure 4.35 Wave power and water level during the extreme coastal storm event on 14/01/2020.

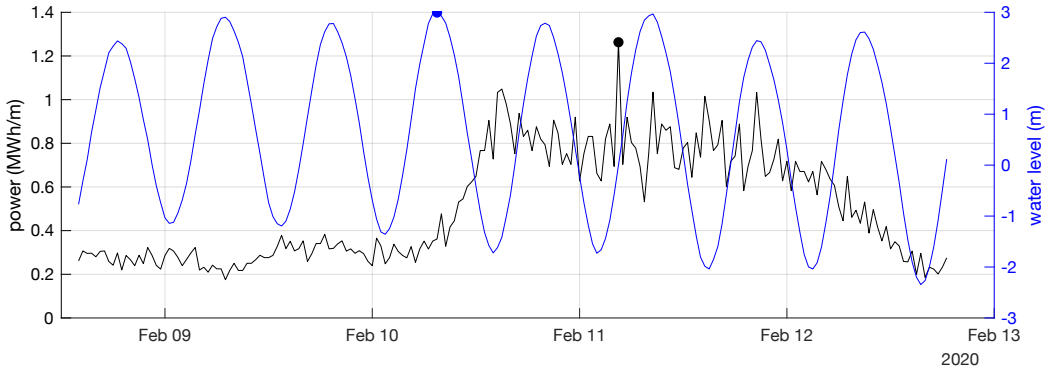

Figure 4.36 Wave power and water level during the extreme coastal storm event on 11/02/2020.

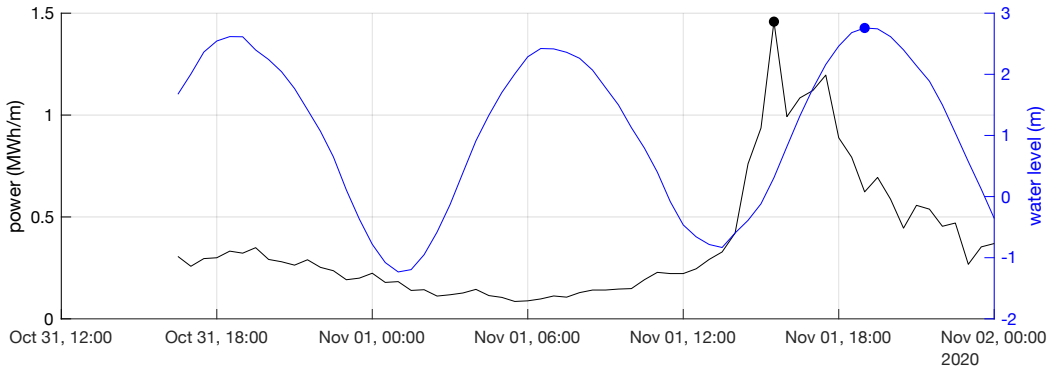

Figure 4.37 Wave power and water level during the extreme coastal storm event on 01/11/2020.

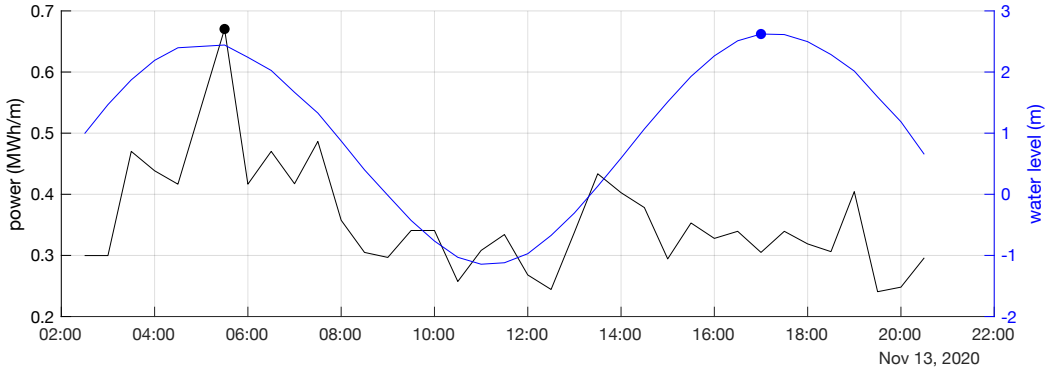

Figure 4.38 Wave power and water level during the extreme coastal storm event on 13/11/2020.

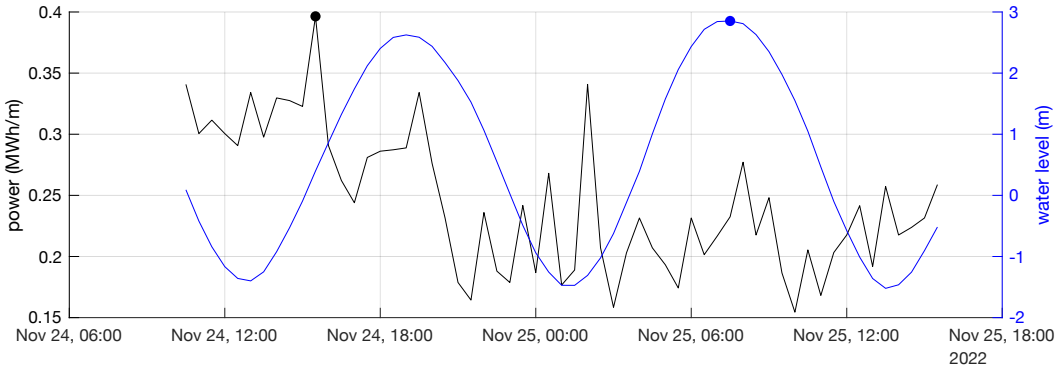

Figure 4.39 Wave power and water level during the extreme coastal storm event on 24/11/2022.

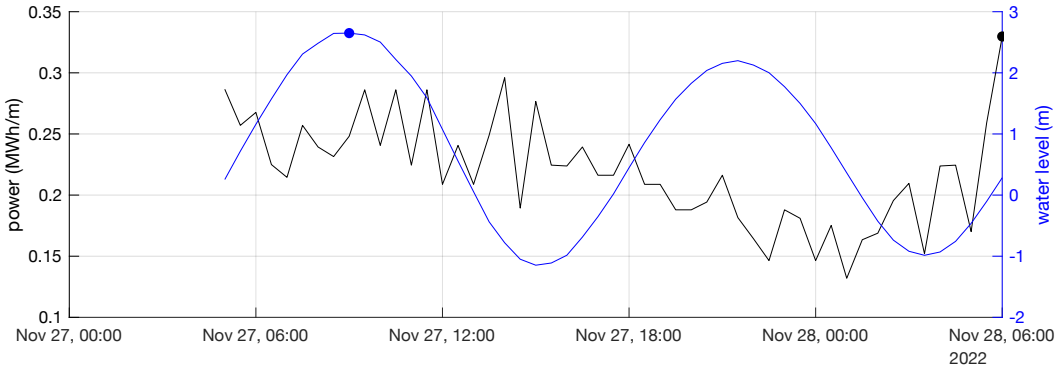

Figure 4.40 Wave power and water level during the extreme coastal storm event on 28/11/2023.

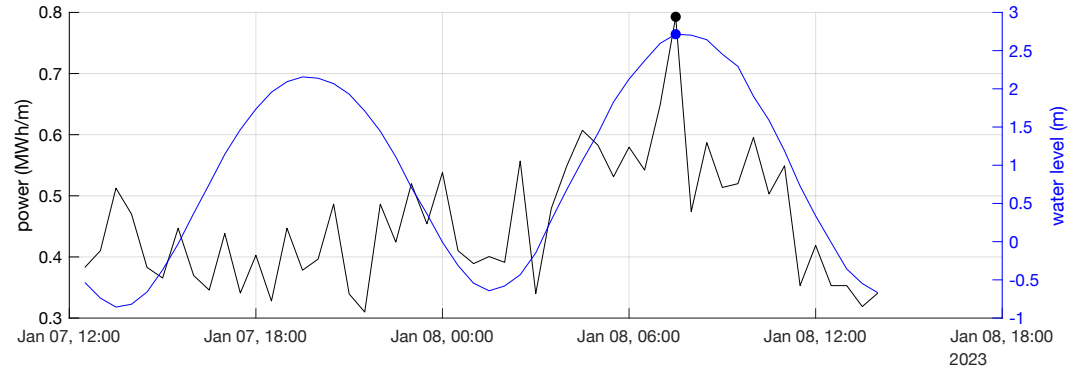

Figure 4.41 Wave power and water level during the extreme coastal storm event on 08/01/2023.

4.7 Acknowledgements

Vincent Kümmerer receives funding for his Ph.D. through the Portuguese Foundation of Science and Technology (FCT) grant 2020.07497.BD and from the British Society for Geomorphology BSG-2022-30. This work was additionally supported by FCT, under the

projects LA/P/00069/2020 (granted to the Associate Laboratory ARNET) and UID/00350/2020 CIMA.

4.8 Data Availability Statement

Planet Scope imagery was provided by Planet Labs Inc. (https://www.planet.com) through a standard research license and the planet imagery pre-processing toolbox CoastSat.PlanetScope by Yarran Doherty (https://github.com/ydoherty/CoastSat.PlanetScope). Access to the wave data from the Outer Hebrides wave buoy is provided by CEFAS Wavenet (https://wavenet.cefas.co.uk). Wind speed data of the MIDAS weather station 18903 in South Uist are provided by the British Atmospheric Data Centre (BADC) through the CEDA Archive (https://data.ceda.ac.uk). Water level data recorded by the Stornoway gauge are available from the British Oceanographic Data Centre (BODC, https://www.bodc.ac.uk) and the modelled water level data from the Copernicus Data Store (CDS) at https://doi.org/10.24381/cds.a6d42d60. Access to the NAO data are provided by the National Oceanic and Atmospheric Administration (NOAA) Climate Predication Center (www.cpc.ncep.noaa.gov).

4.9 References

Angnuureng DB, Brempong KE, Jayson-Quashigah PN, Dada OA, Akuoko SGI, Frimpomaa J, Mattah PA, Almar R. 2022. Satellite, drone and video camera multi-platform monitoring of coastal erosion at an engineered pocket beach: A showcase for coastal management at Elmina Bay, Ghana (West Africa). Regional Studies in Marine Science 53 : 102437. DOI: 10.1016/j.rsma.2022.102437

Angus S, Rennie A. 2014. An Ataireachd Aird: The storm of January 2005 in the Uists, Scotland. Ocean & Coastal Management 94 : 22–29. DOI: 10.1016/j.ocecoaman.2014.02.013

Barnard PL, Allan J, Hansen JE, Kaminsky GM, Ruggiero P, Doria A. 2011. The impact of the 2009-10 El Niño Modoki on U.S. West Coast beaches: EL NIÑO IMPACT ON USA WEST COAST BEACHES. Geophysical Research Letters 38 : n/a-n/a. DOI: 10.1029/2011GL047707

Bastos AP, Taborda R, Silva AN, Lira CP, Andrade C, Calvão JM. 2022. A punctuated equilibrium model for storm response of geologically controlled beaches: Application to western Portuguese beaches. Geomorphology 404 : 108184. DOI: 10.1016/j.geomorph.2022.108184

Boak EH, Turner IL. 2005. Shoreline Definition and Detection: A Review. Journal of Coastal Research 214 : 688–703. DOI: 10.2112/03-0071.1

Burvingt O, Castelle B. 2023. Storm response and multi-annual recovery of eight coastal dunes spread along the Atlantic coast of Europe. Geomorphology 435 : 108735. DOI: 10.1016/j.geomorph.2023.108735

Castelle B, Kras E, Masselink G, Scott T, Konstantinou A, Luijendijk A. 2024. Satellite-derived sandy shoreline trends and interannual variability along the Atlantic coast of Europe. Scientific Reports 14 : 13002. DOI: 10.1038/s41598-024-63849-4

Castelle B, Marieu V, Bujan S, Splinter KD, Robinet A, Sénéchal N, Ferreira S. 2015. Impact of the winter 2013–2014 series of severe Western Europe storms on a double-barred sandy coast: Beach and dune erosion and megacusp embayments. Geomorphology 238 : 135148. DOI: 10.1016/j.geomorph.2015.03.006

Castelle B, Masselink G, Scott T, Stokes C, Konstantinou A, Marieu V, Bujan S. 2021. Satellite-derived shoreline detection at a high-energy meso-macrotidal beach. Geomorphology 383 : 107707. DOI: 10.1016/j.geomorph.2021.107707

Cooper JAG, Green AN, Loureiro C. 2018. Geological constraints on mesoscale coastal barrier behaviour. Global and Planetary Change 168 : 15–34. DOI: 10.1016/j.gloplacha.2018.06.006

Cooper JAG, Jackson DWT, Dawson AG, Dawson S, Bates CR, Ritchie W. 2012. Barrier islands on bedrock: A new landform type demonstrating the role of antecedent topography on barrier form and evolution. Geology 40 : 923–926. DOI: 10.1130/G33296.1

Cooper JAG, Jackson DWT, Navas F, McKenna J, Malvarez G. 2004. Identifying storm impacts on an embayed, high-energy coastline: examples from western Ireland. Marine Geology 210 : 261–280. DOI: 10.1016/j.margeo.2004.05.012

Davidson SG, Hesp P, Miot Da Silva G. 2021. Rapid shoreline erosion and dunefield Change, Salmon Hole, South Australia. Science of The Total Environment 767 : 145406. DOI: 10.1016/j.scitotenv.2021.145406

Dawson AG, Dawson S, Ritchie W. 2007. Historical Climatology and coastal change associated with the ‘Great Storm’ of January 2005, South Uist and Benbecula, Scottish Outer Hebrides. Scottish Geographical Journal 123 : 135–149. DOI: 10.1080/14702540701623784

Dawson AG, Gómez C, Ritchie W, Batstone C, Lawless M, Rowan JS, Dawson S, McIlveny J, Bates R, Muir D. 2012. Barrier Island Geomorphology, Hydrodynamic Modelling, and Historical Shoreline Changes: An Example from South Uist and Benbecula, Scottish Outer Hebrides. Journal of Coastal Research 285 : 1462–1476. DOI: 10.2112/JCOASTRES-D-11-00184.1

Delgado-Fernandez I, Davidson-Arnott R. 2011. Meso-scale aeolian sediment input to coastal dunes: The nature of aeolian transport events. Geomorphology 126 : 217–232. DOI: 10.1016/j.geomorph.2010.11.005

Dłużewski M, Dłużewska JR, Hesp PA, Tomczak JO, Dubis L. 2023. Impact of coastline orientation on the dynamics of fordune growth (Łeba Barrier, south Baltic Sea coast, Poland). Miscellanea Geographica Regional Studies on Development

Doherty Y, Harley MD, Vos K, Splinter KD. 2022. A Python toolkit to monitor sandy shoreline change using high-resolution PlanetScope cubesats. Environmental Modelling & Software 157 : 105512. DOI: 10.1016/j.envsoft.2022.105512

Fellowes TE, Vila-Concejo A, Gallop SL, Harley MD, Short AD. 2022. Wave shadow zones as a primary control of storm erosion and recovery on embayed beaches. Geomorphology 399 : 108072. DOI: 10.1016/j.geomorph.2021.108072

Gallop SL, Bosserelle C, Eliot I, Pattiaratchi CB. 2012. The influence of limestone reefs on storm erosion and recovery of a perched beach. Continental Shelf Research 47 : 16–27. DOI: 10.1016/j.csr.2012.08.001

Gallop SL, Bosserelle C, Eliot I, Pattiaratchi CB. 2013. The influence of coastal reefs on spatial variability in seasonal sand fluxes. Marine Geology 344 : 132–143. DOI: 10.1016/j.margeo.2013.07.016

Gallop SL, Bosserelle C, Haigh ID, Wadey MP, Pattiaratchi CB, Eliot I. 2015. The impact of temperate reefs on 34 years of shoreline and vegetation line stability at Yanchep, southwestern Australia and implications for coastal setback. Marine Geology 369 : 224–232. DOI: 10.1016/j.margeo.2015.09.001

Gallop SL, Kennedy DM, Loureiro C, Naylor LA, Muñoz-Pérez JJ, Jackson DWT, Fellowes TE. 2020. Geologically controlled sandy beaches: Their geomorphology, morphodynamics and classification. Science of The Total Environment 731 : 139123. DOI: 10.1016/j.scitotenv.2020.139123

Gilbertson DD, Schwenninger J-L, Kemp RA, Rhodes EJ. 1999. Sand-drift and Soil Formation Along an Exposed North Atlantic Coastline: 14,000 Years of Diverse Geomorphological, Climatic and Human Impacts. Journal of Archaeological Science 26 : 439–469. DOI: 10.1006/jasc.1998.0360

Gómez C, Wulder MA, Dawson AG, Ritchie W, Green DR. 2014. Shoreline Change and Coastal Vulnerability Characterization with Landsat Imagery: A Case Study in the Outer Hebrides, Scotland. Scottish Geographical Journal 130 : 279–299. DOI: 10.1080/14702541.2014.923579

Graffin M, Taherkhani M, Leung M, Vitousek S, Kaminsky G, Ruggiero P. 2023. Monitoring interdecadal coastal change along dissipative beaches via satellite imagery at regional scale. Cambridge Prisms: Coastal Futures 1 : e42. DOI: 10.1017/cft.2023.30

Guisado-Pintado E, Jackson DWT. 2018. Multi-scale variability of storm Ophelia 2017: The importance of synchronised environmental variables in coastal impact. Science of The Total Environment 630 : 287–301. DOI: 10.1016/j.scitotenv.2018.02.188

Haigh ID, Wadey MP, Wahl T, Ozsoy O, Nicholls RJ, Brown JM, Horsburgh K, Gouldby B. 2016. Spatial and temporal analysis of extreme sea level and storm surge events around the coastline of the UK. Scientific Data 3 : 160107. DOI: 10.1038/sdata.2016.107

Hansom JD, Fitton JM, Rennie AF. 2017. Dynamics Coast - National Coastal Change Assessment: Cells 8 and 9 - The Western Isles . CRW2014/02 [online] Available from: https://www.dynamiccoast.com/files/reports/NCCA%20%20Cells%208%20and%209%20-%20The%20Western%20Isles.pdf

Hapke CJ, Plant NG, Henderson RachelE, Schwab WC, Nelson TR. 2016. Decoupling processes and scales of shoreline morphodynamics. Marine Geology 381 : 42–53. DOI: 10.1016/j.margeo.2016.08.008

Harley MD, Kinsela MA, Sánchez-García E, Vos K. 2019. Shoreline change mapping using crowd-sourced smartphone images. Coastal Engineering 150 : 175–189. DOI: 10.1016/j.coastaleng.2019.04.003

Hersbach H et al. 2020. The ERA5 global reanalysis. Quarterly Journal of the Royal Meteorological Society 146 : 1999–2049. DOI: 10.1002/qj.3803

Houser C, Wernette P, Rentschlar E, Jones H, Hammond B, Trimble S. 2015. Post-storm beach and dune recovery: Implications for barrier island resilience. Geomorphology 234 : 54–63. DOI: 10.1016/j.geomorph.2014.12.044

Huiskes AHL. 1979. Biological Flora of the British Isles. The Journal of Ecology 67 : 363. DOI: 10.2307/2259356

Hurrell JW. 1995. Decadal Trends in the North Atlantic Oscillation: Regional Temperatures and Precipitation. Science 269 : 676–679. DOI: 10.1126/science.269.5224.676

Jackson DWT, Cooper JAG. 2009. Geological Control on Beach Form: Accommodation Space and Contemporary Dynamics. Journal of Coastal Research : 69–72.

Kandrot S, Farrell E, Devoy R. 2016. The morphological response of foredunes at a breached barrier system to winter 2013/2014 storms on the southwest coast of Ireland. Earth Surface Processes and Landforms 41 : 2123–2136. DOI: 10.1002/esp.4003

Keay L, Mulverhill C, Coops NC, McCartney G. 2023. Automated Forest Harvest Detection With a Normalized PlanetScope Imagery Time Series. Canadian Journal of Remote Sensing 49 : 2154598. DOI: 10.1080/07038992.2022.2154598

Kenyon NH, Pelton CD. 1979. Seabed conditions west of the Outer Hebrides . Institute of Oceanographic Sciences: Godalming, Surrey, UK [online] Available from: https://eprints.soton.ac.uk/14378/1/1437801.pdf

Konstantinou A, Scott T, Masselink G, Stokes K, Conley D, Castelle B. 2023. Satellite-based shoreline detection along high-energy macrotidal coasts and influence of beach state. Marine Geology 462 : 107082. DOI: 10.1016/j.margeo.2023.107082

Konstantinou A, Stokes C, Masselink G, Scott T. 2021. The extreme 2013/14 winter storms: Regional patterns in multi-annual beach recovery. Geomorphology 389 : 107828. DOI: 10.1016/j.geomorph.2021.107828

Kümmerer V, Ferreira Ó, Fanti V, Loureiro C. 2024. Storm identification for high-energy wave climates as a tool to improve long-term analysis. Climate Dynamics 62 : 2207–2226. DOI: 10.1007/s00382-023-07017w

Kümmerer V, Loureiro C, Ferreira Ó. 2023. Muted morphological response to extreme storms in geologically controlled barrier islands. presented at the Coastal Sediments 2023. New Orleans, LA, USA. 44–56 pp. April

Laigre T, Balouin Y, Villarroel-Lamb D, De La Torre Y. 2023. Seasonal to Multi-Decadal Shoreline Change on a Reef-Fringed Beach. Coasts 3 : 240–262. DOI: 10.3390/coasts3030015

Levoy F, Monfort O, Anthony EJ. 2023. Multi-decadal shoreline mobility of a managed sandy tidal coast (Normandy, France): Behavioural variability in a context of sea-level rise and increasing storm intensity. Regional Studies in Marine Science 62 : 102973. DOI: 10.1016/j.rsma.2023.102973

Loureiro C, Ferreira Ó, Cooper JAG. 2012. Geologically constrained morphological variability and boundary effects on embayed beaches. Marine Geology 329–331 : 1–15. DOI: 10.1016/j.margeo.2012.09.010

Loureiro C, Ferreira O, Cooper JAG. 2014. Non-uniformity of storm impacts on three high-energy embayed beaches. Journal of Coastal Research 70 : 326–331. DOI: 10.2112/SI70-055.1

Masselink G, Brooks S, Poate T, Stokes C, Scott T. 2022. Coastal dune dynamics in embayed settings with sea-level rise – Examples from the exposed and macrotidal north coast of SW England. Marine Geology 450 : 106853. DOI: 10.1016/j.margeo.2022.106853

Masselink G, Castelle B, Scott T, Dodet G, Suanez S, Jackson D, Floc'h F. 2016a. Extreme wave activity during 2013/2014 winter and morphological impacts along the Atlantic coast of Europe. Geophysical Research Letters 43 : 2135–2143. DOI: 10.1002/2015GL067492

Masselink G, Castelle B, Scott T, Konstantinou A. 2023. Role of Atmospheric Indices in Describing Shoreline Variability Along the Atlantic Coast of Europe. Geophysical Research Letters 50 : e2023GL106019. DOI: 10.1029/2023GL106019

Masselink G, Scott T, Poate T, Russell P, Davidson M, Conley D. 2016b. The extreme 2013/2014 winter storms: hydrodynamic forcing and coastal response along the southwest coast of England. Earth Surface Processes and Landforms 41 : 378–391. DOI: 10.1002/esp.3836

McAllister E, Payo A, Novellino A, Dolphin T, Medina-Lopez E. 2022. Multispectral satellite imagery and machine learning for the extraction of shoreline indicators. Coastal Engineering 174 : 104102. DOI: 10.1016/j.coastaleng.2022.104102

Mentaschi L, Vousdoukas MI, Pekel J-F, Voukouvalas E, Feyen L. 2018. Global long-term observations of coastal erosion and accretion. Scientific Reports 8 : 12876. DOI: 10.1038/s41598-018-30904-w

Met Office. 2006. MIDAS: UK Hourly Weather Observation Data [online] Available from: https://catalogue.ceda.ac.uk/uuid/916ac4bbc46f7685ae9a5e10451bae 7c (Accessed 2 July 2023)

Morris BD, Davidson MA, Huntley DA. 2001. Measurements of the response of a coastal inlet using video monitoring techniques. Marine Geology 175 : 251–272. DOI: 10.1016/S0025-3227(01)00144-X

Muis S, Apecechea MI, Dullaart J, de Lima Rego J, Madsen KS, Su J, Yan K, Verlaan M. 2020. A High-Resolution Global Dataset of Extreme Sea Levels, Tides, and Storm Surges, Including Future Projections. Frontiers in Marine Science 7 : 263. DOI: 10.3389/fmars.2020.00263

Mulcahy N, Kennedy DM, Blanchon P. 2016. Hurricane-induced shoreline change and post-storm recovery: northeastern Yucatan Peninsula, Mexico. Journal of Coastal Research 75 : 1192–1196. DOI: 10.2112/SI75-239.1

Muñoz-Perez JJ, Medina R. 2010. Comparison of long-, medium- and short-term variations of beach profiles with and without submerged geological control. Coastal Engineering 57 : 241–251. DOI: 10.1016/j.coastaleng.2009.09.011

Otsu N. 1979. A Tlreshold Selection Method from Gray-Level Histograms. IEEE transactions on systems, man, and cybernetics 9 : 62–66.

Pardo-Pascual JE, Almonacid-Caballer J, Cabezas-Rabadán C, FernándezSarría A, Armaroli C, Ciavola P, Montes J, Souto-Ceccon PE, PalomarVázquez J. 2024. Assessment of satellite-derived shorelines automatically extracted from Sentinel-2 imagery using SAET. Coastal Engineering 188 : 104426. DOI: 10.1016/j.coastaleng.2023.104426

Pile J, Cooper JAG, Jackson DWT. 2019. Stratigraphy and internal structure of wind-dominated barrier islands (dune and machair) of the Outer Hebrides, Scotland. Earth Surface Processes and Landforms 44 : 1482–1493. DOI: 10.1002/esp.4579

Planet Team. 2023. Planet Application Program Interface: In Space for Life on Earth [online] Available from: https://api.planet.com

Pollard JA, Spencer T, Brooks SM, Christie EK, Möller I. 2020. Understanding spatio-temporal barrier dynamics through the use of multiple shoreline proxies. Geomorphology 354 : 107058. DOI: 10.1016/j.geomorph.2020.107058

Randall RE. 1997. Chapter 3.3. Vegetated shingle structures and shorelines. In Coasts and seas of the United Kingdom - Regions 15 & 16 North-west Scotland: The Western Isles and west Highland , . Joint Nature Conservation Committee: Peterborough;

Riggs SR, Cleary WJ, Snyder SW. 1995. Influence of inherited geologic framework on barrier shoreface morphology and dynamics. Marine Geology 126 : 213–234. DOI: 10.1016/0025-3227(95)00079-E

Ritchie W. 1971. The Beaches of Barra and the Uists: A Survey of the Beach, Dune & Machair Areas of Barra, South Uist, Benbecula, North Uist & Berneray . Department of Geography, University of Aberdeen

Robinet A, Castelle B, Idier D, Harley MD, Splinter KD. 2020. Controls of local geology and cross-shore/longshore processes on embayed beach shoreline variability. Marine Geology 422 : 106118. DOI: 10.1016/j.margeo.2020.106118

Rogers MSJ, Bithell M, Brooks SM, Spencer T. 2021. VEdge_Detector: automated coastal vegetation edge detection using a convolutional neural network. International Journal of Remote Sensing 42 : 48054835. DOI: 10.1080/01431161.2021.1897185

Rulent J, Bricheno LM, Green JAM, Haigh ID, Lewis H. 2021. Distribution of coastal high water level during extreme events around the UK and Irish coasts. Natural Hazards and Earth System Sciences 21 : 33393351. DOI: 10.5194/nhess-21-3339-2021

Santo H, Taylor PH, Woollings T, Poulson S. 2015. Decadal wave power variability in the North-East Atlantic and North Sea. Geophysical Research Letters 42 : 4956–4963. DOI: 10.1002/2015GL064488

Scott T, McCarroll RJ, Masselink G, Castelle B, Dodet G, Saulter A, Scaife AA, Dunstone N. 2021. Role of Atmospheric Indices in Describing Inshore Directional Wave Climate in the United Kingdom and Ireland. Earth's Future 9 DOI: 10.1029/2020EF001625 [online] Available from: https://onlinelibrary.wiley.com/doi/10.1029/2020EF001625 (Accessed 6 October 2021)

Short AD. 2010. Role of geological inheritance in Australian beach morphodynamics. Coastal Engineering 57 : 92–97. DOI: 10.1016/j.coastaleng.2009.09.005

Simeone S, Palombo L, Molinaroli E, Brambilla W, Conforti A, De Falco G. 2021. Shoreline Response to Wave Forcing and Sea Level Rise along a Geomorphological Complex Coastline (Western Sardinia, Mediterranean Sea). Applied Sciences 11 : 4009. DOI: 10.3390/app11094009

Splinter KD, Carley JT, Golshani A, Tomlinson R. 2014. A relationship to describe the cumulative impact of storm clusters on beach erosion. Coastal Engineering 83 : 49–55. DOI: 10.1016/j.coastaleng.2013.10.001

Stockdon HF, Long JW, Palmsten ML, Van Der Westhuysen A, Doran KS, Snell RJ. 2023. Operational forecasts of wave-driven water levels and coastal hazards for US Gulf and Atlantic coasts. Communications Earth & Environment 4 : 169. DOI: 10.1038/s43247-023-00817-2

Suanez S, Cariolet J-M, Cancouët R, Ardhuin F, Delacourt C. 2012. Dune recovery after storm erosion on a high-energy beach: Vougot Beach, Brittany (France). Geomorphology 139–140 : 16–33. DOI: 10.1016/j.geomorph.2011.10.014

Suanez S, Yates ML, Floc'h F, Accensi M. 2023. Using 17 years of beach/dune profile monitoring to characterize morphological dynamics related to significant extreme water level events in North Brittany (France). Geomorphology 433 : 108709. DOI: 10.1016/j.geomorph.2023.108709

Turner IL, Harley MD, Almar R, Bergsma EWJ. 2021. Satellite optical imagery in Coastal Engineering. Coastal Engineering 167 : 103919. DOI: 10.1016/j.coastaleng.2021.103919

Velegrakis AF, Trygonis V, Chatzipavlis AE, Karambas Th, Vousdoukas MI, Ghionis G, Monioudi IN, Hasiotis Th, Andreadis O, Psarros F. 2016. Shoreline variability of an urban beach fronted by a beachrock reef from video imagery. Natural Hazards 83 : 201–222. DOI: 10.1007/s11069-016-2415-9

Vos K et al. 2023. Benchmarking satellite-derived shoreline mapping algorithms. Communications Earth & Environment 4 : 345. DOI: 10.1038/s43247-023-01001-2

Vos K, Harley MD, Splinter KD, Simmons JA, Turner IL. 2019. Sub-annual to multi-decadal shoreline variability from publicly available satellite imagery. Coastal Engineering 150 : 160–174. DOI: 10.1016/j.coastaleng.2019.04.004

Vousdoukas MI, Almeida LPM, Ferreira Ó. 2012. Beach erosion and recovery during consecutive storms at a steep-sloping, meso-tidal beach. Earth Surface Processes and Landforms 37 : 583–593. DOI: 10.1002/esp.2264

Wernette P, Houser C, Weymer BA, Everett ME, Bishop MP, Reece B. 2018. Influence of a spatially complex framework geology on barrier island geomorphology. Marine Geology 398 : 151–162. DOI: 10.1016/j.margeo.2018.01.011

Wiles E, Loureiro C, Cawthra H. 2022. Shoreline variability and coastal vulnerability: Mossel Bay, South Africa. Estuarine, Coastal and Shelf Science 268 : 107789. DOI: 10.1016/j.ecss.2022.107789

Williams JJ, Esteves LS, Rochford LA. 2015. Modelling storm responses on a high-energy coastline with XBeach. Modeling Earth Systems and Environment 1 : 3. DOI: 10.1007/s40808-015-0003-8

Young EJ. 2015. Variation and trends in the sensitivity of machair soils and coastal landforms to erosion, South Uist, Outer Hebrides, University of Dundee [online] Available from: https://discovery.dundee.ac.uk/en/studentTheses/variations-andtrends-in-the-sensitivity-of-machair-soils-and-coa

Zhang X, Wu C, Hu R, Xu S, Xu Z, Yang Z. 2024. Can Satellite-Derived Beach Images Resolve the Responses to Human Activities? Journal of Geophysical Research: Earth Surface 129 : e2023JF007339. DOI: 10.1029/2023JF00733

Chapter 5

Assessment of Geological Controls on the Storm Response of Coastal Barriers

Kümmerer, V., Loureiro, C., Fanti, V., Ferreira, Ó., (submitted). Modelling the Relative Importance of Geological Controls on the Response to Storms in Coastal Barriers. *Journal of Geophysical Research Earth Surface*.

Abstract

The coastal geology modulates the morphology and evolution of coastal barriers, but its role on storm-induced erosion is still poorly understood. In a context of shoreline transgression under rising sea levels, but also reduced sediment supply in many coastal areas, geological control may become more significant for barrier morphodynamics. As such, it is crucial to better understand how the response of coastal barriers to storm events depends on the underlying geology. This study explores the use of the process-based model XBeach to investigate the relative importance of geological controls and storm forcing on nearshore hydrodynamics and dune erosion in rock-fronted coastal barriers. A range of realistic scenarios were modelled, based on morphological and oceanographic conditions of geologically constrained barriers exposed to energetic wave conditions in NW Scotland. The conditions implemented in XBeach include varying storm forcing and schematic cross-shore profiles with different types and levels of geological control (different bedrock slopes, outcrop elevations and rock platform positions and elevations). The variation in maximum water level, driven by storm surge, was found to have higher influence on the wave energy at the upper beach and in the duration of wave impact on dunes, when compared to other hydrodynamic factors (e.g. offshore wave height). The critical influence of water levels on storm responses can be explained by the saturated surfzone environment, typical of shallow rock- and reef-fronted coastlines. Considering the different

geological control configurations tested, results indicate that the variation on the subtidal shoreface slope exerted minimal control on the storm response, similarly to outcrops and rock platforms at lower elevations. However, a shift in the primary control of storm response from the hydrodynamic forcing to the geological control is observed when the difference between the rock surface elevation (outcrops and rock platforms) and the maximum water level is less than 2 m. For those cases, geological controls were highly effective in reducing dune erosion. Improved understanding of the role of geological controls and their relationship to storm forcing, and particularly water level, is fundamental to the future management of geologically controlled barriers under future sea level rise scenarios.

5.1 Introduction

Most barriers globally are likely to be impacted to some extent by geological controls as 75% of the world's coastline is rocky (MacMahan et al., 2024). However, there is limited understanding of how geological aspects define barrier evolution in rock-fronted beaches as the coastal geology is vastly overlooked in contemporary morphodynamic analysis (Cooper et al., 2018; Gallop et al., 2020). In addition, coastal sediment limitations through anthropogenic reduction of sediment supply to the coast (Syvitski et al., 2022), alongside expansion of coastal infrastructure and hard engineering interventions to mitigate erosion hazards (Nawarat et al., 2024) could potentially shift unconstrained beaches into becoming structurally or geologically constrained (Gallop et al., 2020). Therefore, understanding the influence of geological controls on storm-induced beach morphodynamics is critical for understanding and predicting future changes in coastal barriers.

Geological controls on barrier evolution are exerted through a wide range of local to regional factors including basement slope, basement irregularities such as rock/reef platforms or outcrops, and also sediment supply (Cooper et al., 2018). In contrast to unconstrained beaches where contemporary hydrodynamics explain most of the variability in morphological change, the morphodynamic behaviour of geologically constrained beaches can be dominated by non-dynamic geological controls (Jackson et al., 2005; Loureiro et al., 2013, 2012; Short, 2010). It is widely recognised that the bedrock topography defines the accommodation space and availability for beach sediments and thus determines the long-term evolution of sandy beaches in response to changes in hydrodynamic conditions (e.g., McCarroll et al., 2021; Taborda and

Ribeiro, 2015; Trenhaile, 2004). However, it has also been demonstrated that geological variations along the coast can result in distinct storm-driven beach morphodynamics (Bastos et al., 2022; Bitterwolf et al., 2024; Fellowes et al., 2022; Gallop et al., 2013, 2012; Kümmerer et al., 2023; Loureiro et al., 2014, 2012; McIntire and Walker, 1964; Muñoz-Perez and Medina, 2010; Suanez et al., 2012; Velegrakis et al., 2016). Generally, beach sections fronted by rock/reef platforms and outcrops experience reduced morphological change in response to storms compared to unconstrained sections (Bitterwolf et al., 2024; Gallop et al., 2012; McIntire and Walker, 1964; Muñoz-Perez and Medina, 2010; Velegrakis et al., 2016; Kümmerer et al., 2025). Moreover, topographically complex intertidal areas with intermittent rock and reef outcrops lead to spatial variability in nearshore hydrodynamics (e.g., Dissanayake et al., 2021; Velegrakis et al., 2016) and hence sediment transport (Bosserelle et al., 2021).

Modelling the influence of intertidal rock and reef platform morphology, their roughness and position relative to the shoreline on nearshore hydrodynamics has provided new insights on how the geological configuration controls wave transformation along rock- and reef-fronted coastlines (Buckley et al., 2022; Lavaud et al., 2022; Marshall and Stephenson, 2011; Ogawa et al., 2015; Poate et al., 2020, 2018; Portch et al., 2023; Savige et al., 2021). However, few studies have modelled the morphodynamic response of naturally perched beaches, where the sand is located landwards of rock- or reef-platforms. Process-based morphodynamic models such as XBeach (Roelvink et al., 2009) that predict erosional response based on sediment transport gradients and avalanching were designed for unconstrained and sediment-rich coasts. For such coastlines morphodynamic models have been extensively applied and validated (Sherwood et al., 2022). However, while morphodynamic modelling of reef-fronted sandy coastlines has been the focus of recent research (e.g. Masselink et al., 2020, 2021; Xu et al., 2023; Yao et al., 2025), there is still limited work on the modelling of morphological storm responses in rock-fronted coasts. Consequently, uncertainties in the prediction of morphological changes in rock-fronted beaches remain higher when compared to unconstrained and sediment-abundant barriers.

While it has been demonstrated that the morphological response of rock-fronted beaches to storms is complicated by the spatial heterogeneity of rock surfaces and nearshore hydrodynamics, the role of different types and levels of geological control on storm-induced morphological change is less clear and remains often unquantified. To address this limitation, this work implements the process-based model XBeach to investigate the relative importance of different geological controls on dune erosion and nearshore hydrodynamics in rock-fronted

coastal barriers. This will be achieved by exploring storm response under different storm conditions and a range of types and levels of geological control. Three main hypotheses of how geological control and storm characteristics determine storm response in rock-fronted barriers are tested with scenario-based simulations:

(H1) *The steeper the bedrock slopes, the lower the wave dissipation and consequently the stronger the storm response.*

(H2) *The higher the elevation of the intertidal rock structures, the higher the wave dissipation and consequently the more muted the storm response.*

(H3) *The higher water levels during a storm, the higher the wave energy that reaches the shore and consequently the stronger the storm response.*

To develop a range of realistic scenarios that include varying storm forcing and schematic cross-shore profiles with different types and levels of geological control, the morphological and oceanographic conditions of the Outer Hebrides barrier islands, in the NW of Scotland, are taken in consideration. The combination of frequent high-energy wave conditions (Kümmerer et al., 2024) and the various and distinct geological controls in the Outer Hebrides barriers (Cooper et al., 2012) provide an ideal environment to explore geological controls on storm responses.

5.2 Material and Methods

5.2.1 Study Area

The coastline of the Outer Hebrides in NW Scotland is exposed to some of the world's more energetic wave conditions with frequent and extreme coastal storms (Lobeto et al., 2024). The wave climate along this coastline is highly seasonal (Santo et al., 2015) with approximately 90% of the storms occurring in the extended winter season from October to March (Kümmerer et al., 2024). Average winter storm conditions last for 48 hours with significant wave heights (H_S) exceeding 10 m (Kümmerer et al., 2024). The area is exposed to mesotidal conditions, with a mean spring tidal range of ~4 m.

Along this coastline, a chain of barrier islands developed on a gently sloping undulated bedrock platform (Cooper et al., 2012). The bedrock is composed mainly by Lewisian Gneiss that

extends with a gentle slope (between 1:500 to 1:100) up to 50 km offshore and 100 m water depth and can be considered as unerodable at contemporary timescales (Figure 5.1a). The bedrock is thinly covered by autochthonous carbonate sands in its topographic lows (Kenyon and Pelton, 1979). The bed roughness of the rock platform is very high and has an isotropic relief with some regional lineation of the greater (> 5 m) roughness elements (Kenyon and Pelton, 1979). The energetic waves along this coastline are considerably dissipated by the submerged bedrock, which results in nearshore wave conditions dominated by depth-induced surf breaking with additional bottom friction dissipation due to the high bed roughness (Kümmerer et al., 2023).

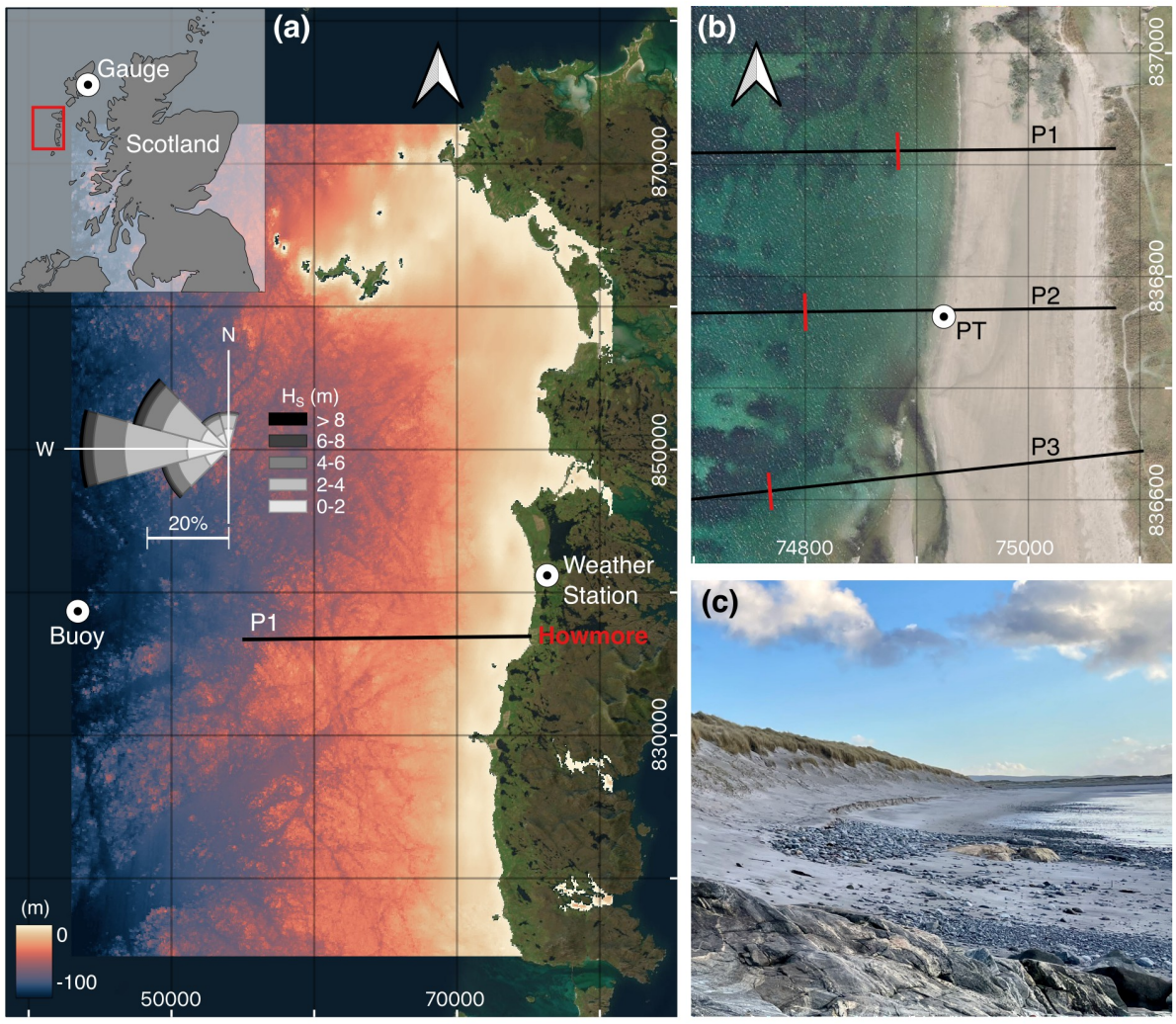

Figure 5.1 Study area. **(a)** Satellite image of the Outer Hebrides with overlaid EMODnet bathymetry and wave rose. Locations of the wave buoy, the weather station, Howmore barrier and baseline profile. The inset shows the location of the Outer Hebrides and Stornoway tidal gauge. **(b)** Satellite image of Howmore barrier and the 3 cross-shore beach profile locations P1-3, the pressure transducer (PT)

location and the sediment layer extent (red marks). **(c)** Photo of the dune and upper beach in Howmore barrier. The domain for the SWAN model is represented by the extent of the EMODnet bathymetry data, while the XBeach profile domain is indicated by the P1 profile in (a). Satellite imagery is from the ESRI World Imagery Layer.

The Hebridean barriers represent an end-member in geologically controlled barrier evolution both in terms of recognised tidal amplitude for barrier islands (Cooper et al., 2012) and limited sediment availability (Pile et al., 2019). Geological controls in the area include both large (kilometres) and smaller (10-1000 m) features that act on annual to storm timescales. The sub-tidal nearshore area is extensively controlled by the bedrock relief as the sand layer extends only a few hundreds of meters from the dune (Figure 5.1b). Varying storm-induced morphological changes between different barrier sectors are partly explained by the variable geologically controlled foreshore configuration (Kümmerer et al., 2023). Intermittent rock outcrops act as unerodable obstacles for sediment movement and their coverage along the beach determines the monthly shoreline variability (Kümmerer et al., 2025).

The study site selected as a basis for the modelling schematization is a geologically controlled sandy barrier located at Homwore (Figure 5.1b, c), along the Hebridean coastline. The barrier (Figure 5.1b) is characterised by a dissipative beach predominantly composed by fine to medium sands (D50 = 0.25 mm, D90 = 0.45 mm), with intermittent rock outcrops and some coarse gravel accumulations (Figure 5.1c). The dune has a steep stoss slope and reaches a maximum elevation of 12.5 m. The upper beach, located between the dune toe and Mean High Water Spring (MHWS), has a slope of 0.14. The intertidal terrace between Mean Low Water Neap (MLWN) and MHWS elevation is ~200 m wide with a slope of 0.02. The study site served as the basis for the design of schematic profiles with varying degrees of geological control, which can be representative of rocky coasts worldwide.

5.2.2 Field Data Acquisition and Analysis

For the implementation of the numerical modelling, hydrodynamic and topo-bathymetric data were obtained from existing datasets and also from dedicated field surveys of storm-induced topographic changes and nearshore hydrodynamics in Howmore.

5.2.2.1 Hydrodynamic Data

Water levels (tidal level and surge), wave conditions (significant wave height (H_S), peak period (T_P), and peak wave direction (Dir_P)), and mean wind speed and direction were obtained from the Stornoway tidal gauge, the West of Hebrides wave buoy, and the MIDAS weather station 18903 (South Uist Missile Range), respectively (Figure 5.1a). The buoy is deployed in 100 m water depth and is located ~30 km offshore from the study site, while the tidal gauge is located at Stornoway, which is approximately 115 km to the North of the study site (Figure 5.1a).

For characterizing hydrodynamic conditions at the beach, water levels were monitored during a spring high tide cycle in February 2023 using a pressure transducer (Figure 5.2a, c). During the monitoring period the offshore wave heights were relatively moderate for the area, with H_S of approximately 5 m. The pressure transducer (In-Situ Level TROLL 700 Data Logger) was deployed at 1 m below Mean Sea Level (MSL) during low tide and recorded at 2 Hz for 10 hours. The measured absolute pressure was converted to hydrostatic pressure and restricted to records above 0.5 m water depth. Using spectral analysis, and following Karimpour and Chen (2017), the changes in water depth were converted to low-(infragravity) and high-(incident-band) frequency zero-moment wave heights ($H_{m0,HF}$ and $H_{m0,LF}$) using bursts of 15 minutes with an infragravity cut-off frequency at 0.05 Hz and removing very low frequencies (<0.005 Hz).

5.2.2.2 Topo-bathymetric Data

The bathymetric data was obtained from EMODnet (EMODnet Bathymetry Consortium, 2022) and is referenced to MSL. For this work, a regular grid that extents ~40 km offshore (Figure 5.1a) and has a spatial resolution of ~ 200 m was used. Topographic surveys were performed at Howmore using a Real-Time Kinematic -Differential Global Navigation Satellite System (RTK-DGNSS) in February 2022 to measure 3 pre- and post-storm cross-shore profiles (P1-3), spaced 100 m alongshore (Figure 5.1b). The storm monitored was the most energetic event in the winter seasons between 2021 and 2023, with peak storm H_S of 14.7 m and still water levels reaching 2.6 m above MSL (Figure 5.2b).

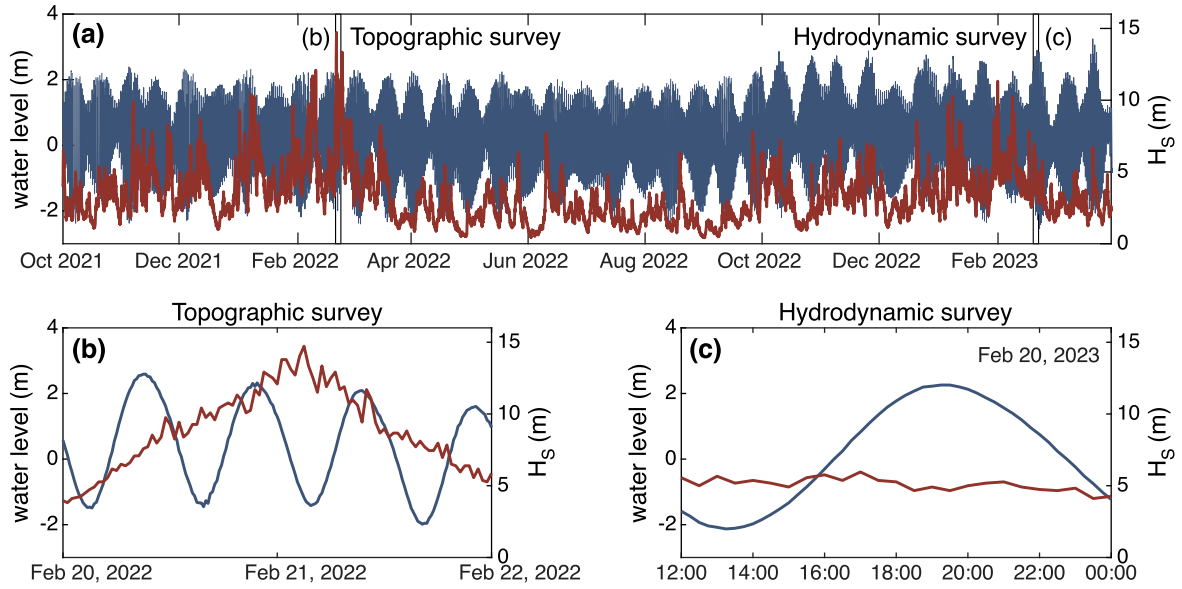

Figure 5.2 (a) Observations of water level (blue lines) and H_S (red lines) between October 2021 and April 2024 with the vertical black lines showing the timing of the topographic and hydrodynamic surveys. Detail of the water level and H_S during the topographic **(b)** and hydrodynamic survey **(c)**.

5.2.3 Model Setup

A nested modelling approach was implemented to simulate storm-induced nearshore hydrodynamics and topographic changes in Howmore. The phase-averaged wave model SWAN (Simulating Waves Nearshore; Booij et al., 1999; Ris et al., 1999) was used to propagate deepwater waves to the offshore boundary of XBeach (Figure 5.1a). SWAN (v41.41) was run in third generation and two-dimensional (2D) stationary mode and implemented with the EMODnet bathymetric grid. The model was forced with the time-varying observations of offshore waves, still water levels and wind velocities as well as the synthetic storm forcings at the west-facing offshore boundary (Figure 5.1a). The surf-breaking was determined using the β-kd scaling (Salmon et al., 2015) due to the complex and shallow shoreface bathymetry. All other settings were set to default, but white capping and quadruplets were turned off for the synthetic storm scenarios as they were forced without wind input.

XBeach (v1.24) was forced with the SWAN derived spectral wave conditions and water level outputs at the XBeach offshore boundary and run in one-dimensional (1D) surfbeat mode. This mode resolves short waves at the wave group time scale and is coupled with the non-linear shallow water equations to resolve infragravity waves and mean currents. Resulting sediment transport is modelled using a depth-averaged approach with morphological change calculated at a 15-minute time step.

The 1D cross-shore profiles used for implementation of XBeach were derived from the integration of EMODnet bathymetric data with the surveyed pre-storm barrier profiles (Figure 5.3a). The cross-shore spatial resolution of the profiles varies from 1 m to 56 m, with finer resolution in the subaerial and intertidal beach sections. The control exerted by natural and schematic bedrock surfaces (described in section 5.2.5.1) was implemented numerically by setting the exposed rock section of the profile as unerodable. In addition, the sand layer thickness was defined as the difference between the bed elevation and the bedrock surface. The bedrock surface beneath the sand layer was derived by extrapolating the mean bedrock surface gradient (Figure 5.3a). To obtain seamless topo-bathymetric data integration, an equilibrium profile based on Dean (1991) was used following the approach proposed by Fanti et al. (2025). This approach assumes that the connecting part between the topographic bathymetric data is sandy, which might not be the case in the Hebridean barriers. However, as nearshore bathymetric data is very sparse, this approach avoids the use of a simple linear interpolation between datasets. The bathymetry data was smoothed to remove the stepped relief, which is a result of the coarse spatial resolution of the EMODnet data. This is informed by the findings of McCall et al. (2017), who demonstrated that smoothing the sub-tidal bed levels and increasing the bed friction (see 5.2.4 Model Calibration) provide more accurate wave transformation with XBeach in surfbeat mode when bedrock rugosity data is limited.

5.2.4 Model Calibration and Validation

Rocky seabed has higher bottom roughness and thus higher wave dissipation when compared to sandy shores (e.g., Lavaud et al., 2022). As such, to calibrate the XBeach model the wave transformation parameters on bedrock surfaces were adjusted following the approach of McCall et al. (2017) and using observations from the hydrodynamic and topographic surveys at profile P1. The calibrated model was validated by evaluating modelled morphological changes against observations at the two alongshore adjacent profiles P2 and P3 (Figure 5.1b).

McCall et al. (2017) used 1D-XBeach in surfbeat mode to replicate observed wave data collected on rocky platforms during energetic wave conditions and calibrated three parameters: (1) wave friction coefficient (f_w), (2) breaker index (γ), and (3) dimensionless bed friction coefficient (c_f). In XBeach the short-wave related wave friction (D_f) is part of the wave action balance equation, described as:

$$\langle D_f \rangle = 0.21 \rho f_w u_{orb}^3, \tag{5.1}$$

where ρ is the water density and u_{orb} the orbital velocity magnitude. The wave breaking is modelled according to Roelvink (1993), where γ is the threshold that relates the wave height at breaking with the water depth. The bed shear stress τ_{bx}^E is part of the non-linear shallow water equation and calculated following Ruessink et al. (2001):

$$\tau_{bx}^E = c_f \rho u_E \sqrt{(1.16 u_{rms})^2 + (u_E)^2}, \tag{5.2}$$

where u_{rms} is the root mean square orbital velocity and u_E is the Eulerian velocity.

In this work, for the sandy parts of the profiles, f_w, γ and c_f were set to default values, which are 0.00, 0.55, and 0.003, respectively, while the calibration of the three parameters for the bedrock surfaces was conducted in two steps. In the first calibration step, f_w was calibrated by an optimization routine through the comparison of modelled and observed $H_{m0,HF}$ in the intertidal beach. The estimation of the modelled $H_{m0,HF}$ is detailed in the supplementary material (Figure 5.9, section 5.6.3). The optimal value of f_w was defined using the model skill parameter S defined as:

$$S(x) = \frac{1}{2}(1 - SI(x) + p(x)), \tag{5.3}$$

where SI is the scatter index, p is the Pearson linear correlation coefficient, and higher S values indicate better model skill.

In the second calibration step, various combinations of γ and c_f values were simultaneously evaluated by comparing predicted and observed morphological changes at profile P1 during the February 2022 storm (Figure 5.2b). To identify the optimal parameter value combination, the pre- and post-storm profiles of each simulation were compared to the observations using the Brier Skill Score (BSS):

$$BSS = 1 - \frac{\langle (Z_{measured} - Z_{modelled})^2 \rangle}{\langle (Z_{measured} - Z_{inital})^2 \rangle}, \tag{5.4}$$

where Z is the bed elevation.

5.2.5 Geological Control Scenario

Barrier response to storms under different geologically controlled foreshore configurations and storm forcings were explored by scenario-based simulations utilising the calibrated and validated model set up. For this, a range of schematic profiles with varying degrees of geological control and different synthetic storm forcing conditions were developed, aiming to test the relationships between geological and hydrodynamic controls on storm response.

5.2.5.1 Schematic Profiles

To test the hypotheses about the role of geological control on the cross-shore response of coastal barriers and explore the influence of varying geologically controlled foreshore configurations on barrier erosion, 12 different schematic profiles were developed. These profiles are variations of P1 (baseline profile) and represent different types and levels of geological control. They are based on the alongshore variable geologically controlled foreshore configurations found in the Hebridean barriers and replicate natural morphological variability in the cross-shore domain (Figure 5.10, section 5.6.3). The different foreshore configurations represented in the schematic profiles are divided into 3 cases: (1) bedrock slopes, (2) intertidal rock platforms, and (3) intertidal rock outcrops (Figure 5.3b, c, d).

The first set of schematic profiles ($PS_{1\text{-}4}$) differ in the mean bedrock slope (β) between the offshore boundary and the intertidal sandy part of the profile (Figure 5.3b) and is designed to test H1. The hypothesis tested in these cases is that the steeper the slopes, the lower the wave energy dissipation and consequently stronger storm response. To modify β but maintain the baseline profile shape, the baseline bedrock profile was tilted around the offshore limit of the sediment layer using increments of 0.002° with $PS_{1\text{-}2}$ characterized by steeper slopes and $PS_{3\text{-}4}$ by milder slopes in respect to the baseline (P1). The offshore depth was kept constant at 30 m, which required extending or shortening the profiles using the mean bedrock slope.

The second and third cases represent intertidal rocky features with quasi planar platforms and dome-shaped outcrop morphologies, respectively, and are designed to test H2. The second set

of schematic profiles (PS_{5-8}) contain intertidal rock platforms with varying positions in the cross-shore profile according to different tidal levels (Figure 5.3c). The platform geometry was kept constant with a length of 50 m and a seaward slope of 15%. The third set of schematic profiles (PS_{9-12}) contains rock outcrops that vary in length and height but have a constant cross-shore position with the highest point centred at MSL position in the baseline profile (Figure 5.3d). The configuration of the rock outcrop is defined as a parabolic shape with a ratio of 0.2 between the height and width of the outcrop above MSL.

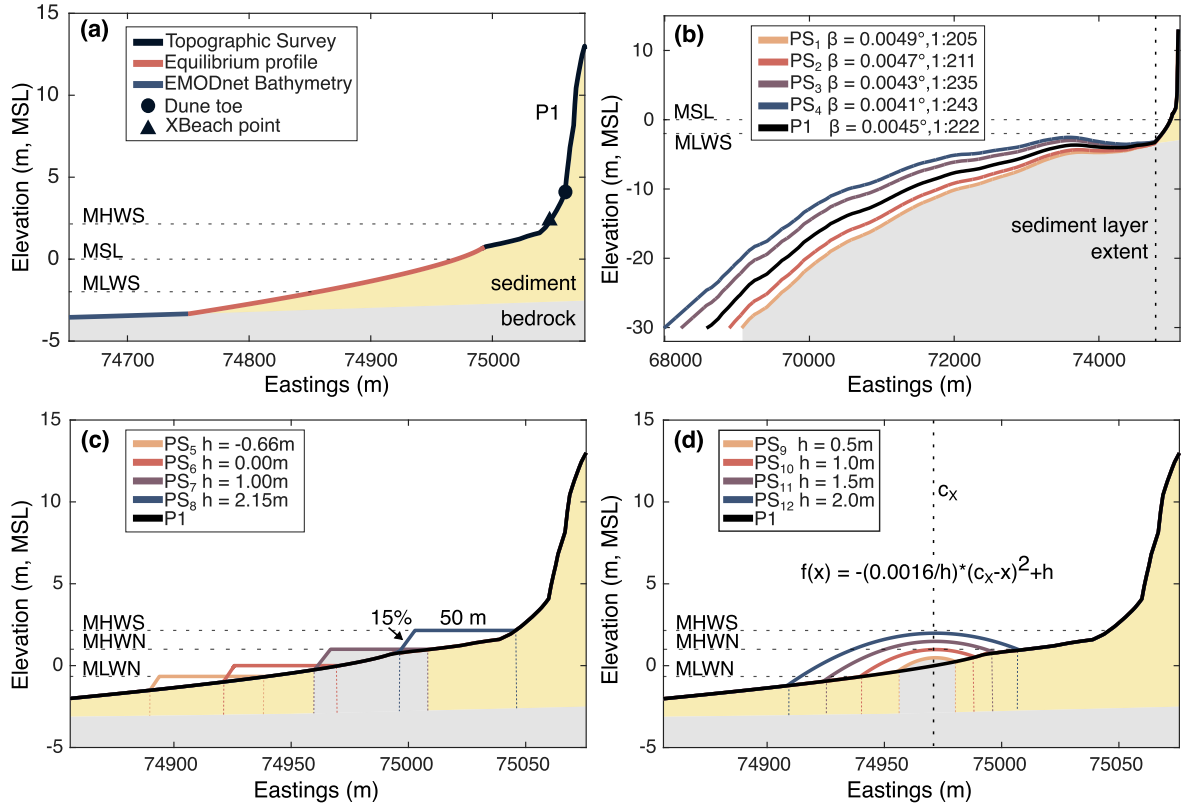

Figure 5.3 XBeach cross-shore profile set up and schematic profile configurations. **(a)** Profile setup for P1 (baseline profile) showing the profile data composition, the erodible (sediment) and non-erodible layers (bedrock), dune toe position and location for the high frequency XBeach outputs. **(b)** Schematic profiles (PS_{1-4}) with varying bedrock slope (β). **(c)** Schematic profiles (PS5-8) with different intertidal rock platforms where h is the rock platform elevation relative to MSL. **(d)** Schematic profiles (PS_{9-12}) with different intertidal rock outcrops. The parabolic shape of the outcrop is defined by the equation where h is the outcrop height relative to MSL and cX the cross-shore position of the outcrop centre.

5.2.5.2 Synthetic Forcing

The synthetic storm forcing conditions used in the scenario-based modelling were designed as a combination of 3 different wave and water level conditions and used as input for SWAN. The resulting 9 synthetic storms allow to distinguish the influence of varying wave forcing and water level on storm impacts and test H3. The synthetic storms were created following the approach of Fanti et al. (in review) that uses storm return periods determined for H_S, combining this with wave and water level parameters to design the synthetic storm time series. The wave and water level parameters used to create the synthetic storms were obtained from the Outer Hebrides wave buoy (2009-2024) and the Stornoway tide gauge (1981-2024), respectively. A de-clustering algorithm was applied to the H_S timeseries to identify independent storm events (Kümmerer et al., 2024). The synthetic storm shape was defined as the averaged shape of all storm events with a H_S return period greater than 2 years, aligned to the storm peak. To represent the temporal variation in T_P and surge, the shape determined for H_S is used, but scaled to each of the parameters. The storm duration, maximum storm T_P and surge levels associated to specific return periods are derived from linear relationships with the maximum storm H_S. Synthetic storm forcing was defined for 1-, 5-, and 25-year H_S return periods (RPH_S). The synthetic storm Dir_P was set to 277° with a spread of 30°, which represent the average storm conditions for the study area.

The 3 different water levels considered are the combination of the mean spring tidal cycle with (1) no surge, (2) 1-year return period surge level, and (3) the 25-year return period surge level. The peak wave forcing and maximum water level were aligned to obtain synthetic storms that are more likely to result in a morphological response of the barrier, which is justified by the fact that storm impacts in the Hebridean barriers are only observed when the storm wave forcing coincides with elevated water levels (Kümmerer et al., 2023).

5.2.5.3 Storm Impact Metrics

The eroded dune volume (ΔEV_{dune}), obtained from the XBeach simulations will be used as the main morphological storm response indicator. The ΔEV_{dune} is defined as the volumetric change between the initial (pre-storm) and the final (post-storm) profile, considering only the section above the pre-storm dune toe elevation (~4.10 m, MSL, Figure 5.3a). For representing the intensity of the hydrodynamic forcing, the proxy used is the total storm wave energy at the

upper beach ($E_{W,ub}$, Figure 5.3a). This is determined by the sum of the energy at every second in the XBeach point location, considering the entire duration of each storm (Figure 5.3a). In addition, the total dune impact time ($T_{impact,Dt}$) was also calculated, and this was defined as the time that the runup elevation exceeds the pre-storm dune toe elevation. This was done using the runup gauge output in XBeach.

5.3 Results

5.3.1 Model Calibration and Validation

The results of the calibration of the short wave-related bed friction revealed that f_w values between 0.08 and 0.15 have generally very good skill, with S above 0.9 (Figure 5.4a). The model skill S peaks at 0.913 when f_w is set to 0.105 (Figure 5.4a) indicating excellent agreement of the modelled and measured $H_{m0,HF}$. In the second calibration step, BSS values indicate that combinations of c_f values between 0.01 and 0.02 and γ between 0.32 and 0.4 result in better model performance. The parameter combination of γ = 0.35 and c_f = 0.015 result in modelled morphological changes closest to the observed post-storm profile, as indicated by a BSS of 0.74 (Figure 5.4b).

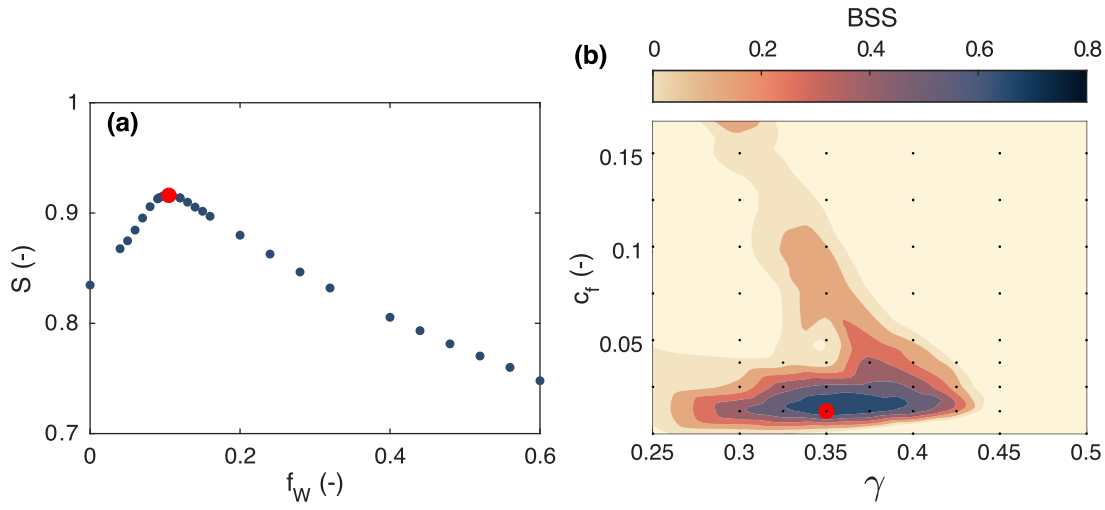

Figure 5.4 XBeach parameter calibration. The red dots indicate the optimal parameter value. **(a)** Short wave-related friction coefficient f_w against the model skill S. The blue dots indicate all the simulated f_w values. **(b)** BSS for simulations of different γ and c_f combinations. The black dots indicate simulated combinations used for the interpolation.

Using the best performing f_w, γ and c_f parameters, the validation simulations were performed and demonstrate that the morphological response, in particular the absence of dune erosion (muted response) in P2 and P3, was correctly modelled (details of the validation results are presented in the supplementary information (Figure 5.9, section 5.6.3)).

5.3.2 Geological Control on Storm Impacts

5.3.2.1 Variation in Hydrodynamic Forcing

A total of 9 synthetic storm scenarios were created from the combination of 3 different RPH_S and surge levels (Figure 5.5). The peak H_S (T_P) is 13.2 m (17.3 s), 15.6 m (18.6 s), and 17.3 m (19.6 s) according to the 1-year, 5-year and 25-year H_S return periods, respectively. The storm duration for these return periods is 44 h, 58 h and 67 h, respectively. The generated synthetic H_S, surge levels, and T_P (not shown) have a triangular shape with a rapid increase and a subsequent slower decrease. The maxima of the 3 different water level scenarios are 2.23 m, 2.92 m, and 3.14 m above MSL. The latter two have an added surge component of 0.69 m and 0.90 m, corresponding to an associated 5-year and 25-year return period storm surge, respectively. As the duration of the synthetic storms increases with return period, the1-year RPH_S scenarios include 4 tidal cycles, the 5-year RPH_S 4.5 cycles and the 25-year RPH_S 5 cycles.

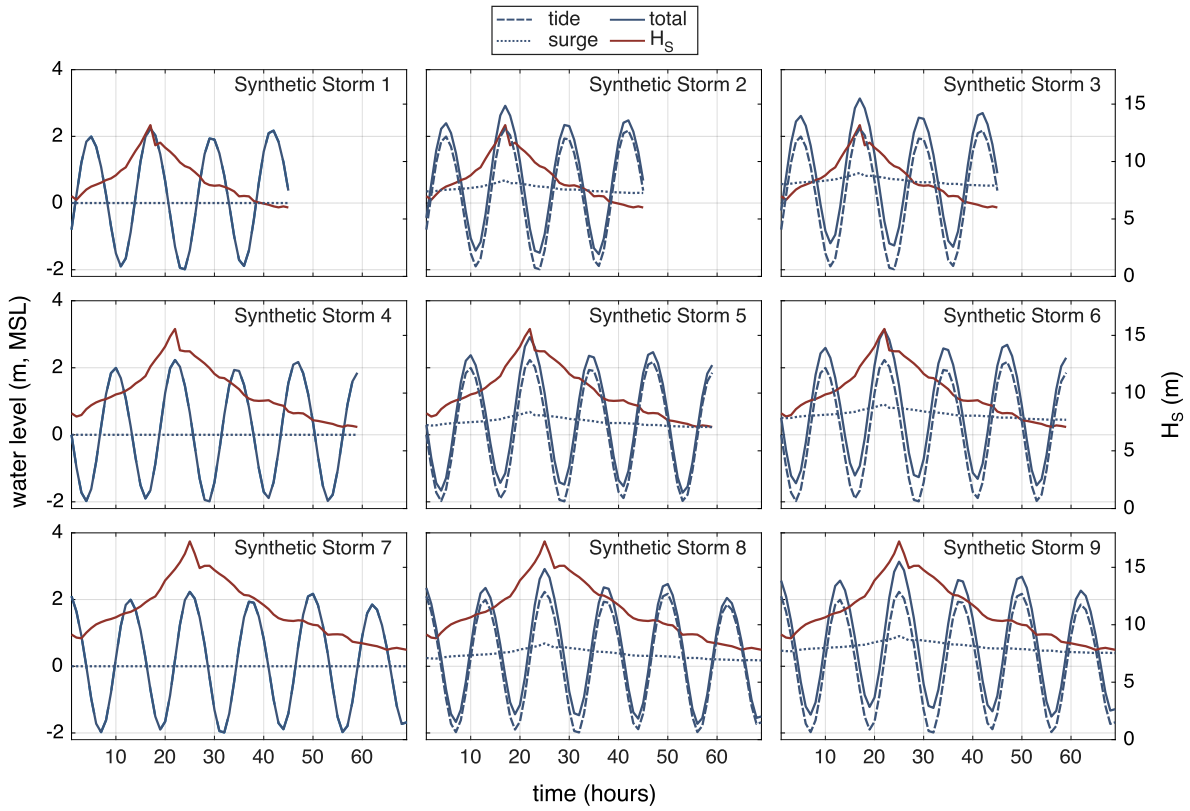

Figure 5.5 Time series of the 9 synthetic storms with varying storm forcing. The total water level corresponds to the combination of the tide and the surge components.

The increasing intensity of the hydrodynamic forcing conditions in the synthetic storms result in more energetic nearshore hydrodynamics as determined by the total wave energy in the upper beach ($E_{W,ub}$). Higher waves and water levels associated with longer return periods lead to higher $E_{W,ub}$ (Figure 5.6a, b) and $T_{impact,Dt}$ (Figure 5.6c, d**)**. For the baseline simulation, $E_{W,ub}$ ranges from 0.67 MJ/m^2 to 6.19 MJ/m^2 according to the different storm forcing scenarios (Figure 5.6a). There is a wider variability in $E_{W,ub}$ when considering the variation in water level than the increasing return periods of the wave forcing. This is evidenced by a $E_{W,ub}$ standard deviation of 2.25 MJ/m^2 for scenarios with varying water levels, while it is only 0.53 MJ/m^2 for scenarios with varying wave forcing. Thus, the influence of the water level variation on $E_{W,ub}$ is ~ 4 times higher when compared to the changes induced by the variation in the wave forcing. This indicates that, for example, a storm with a 1-year RPH_S and a maximum water level of 3.14 m (tide and surge) results in higher $E_{W,ub}$ than a storm with a 25-year RPH_S and a maximum water level of 2.23 or 2.92 m.

Regarding the total dune impact time, values are negligible ($T_{impact,Dt}$ < 1 minute) for the scenarios with a spring tide cycle but without a surge component (Figure 5.6c,d). The maximum $T_{impact,Dt}$ (about 80 minutes) was obtained for the baseline simulation combining the highest water level and the 25-year return period wave forcing. Standard deviation of $T_{impact,Dt}$ for simulations with varying water levels is 31 minutes, while for variable wave forcing it is of only 13 minutes. This indicates that the influence of the maximum water level to $T_{impact,Dt}$ is ~ 2.5 times higher than the influence of the wave forcing. These results reveal that $T_{impact,Dt}$ (Figure 5.6c) is more sensitive to changes in the magnitude of the wave forcing when compared to $E_{W,ub}$ (Figure 6a), but that maximum water level is more significant for the variability in both proxies.

Considering the averaged $E_{W,ub}$ (Figure 5.6b) and $T_{impact,Dt}$ (Figure 5.6d) for all the schematic profile simulations (these are considered individually in section 5.3.2.2), the results evidence the same pattern observed with the baseline simulation, but in most cases with slightly lower values. The reduction is on average 3.0 % for $E_{W,ub}$ and 4.6% for $T_{impact,Dt}$.

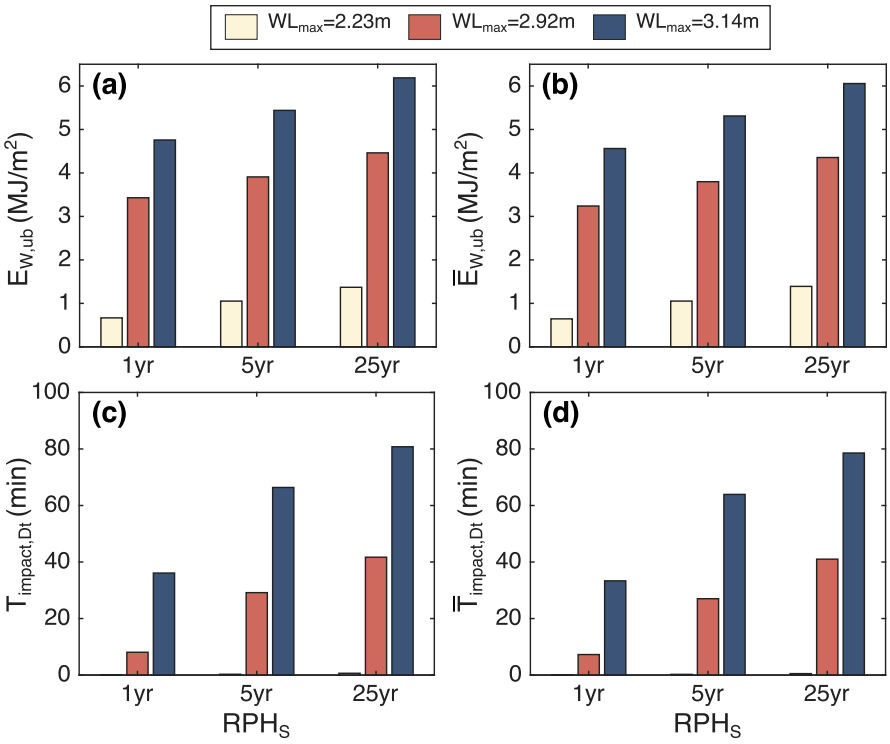

Figure 5.6 Hydrodynamic forcing for different synthetic storm conditions. (**a**,**b**) Predicted total energy in the upper beach ($E_{W,ub}$) and (**c**,**d**) predicted total dune impact time ($T_{impact,Dt}$) for the baseline profile (**a**,**c**) and the average for all schematic profiles (**b**,**d**).

5.3.2.2 Variation in Morphological Response

All simulations using the baseline profile and the varying synthetic storm forcing resulted in dune erosion through dune face scarping and avalanching (Figure 5.7a). For the baseline simulations, ΔEV_{dune} increases with more intense forcing conditions and in a stepwise pattern according to maximum water levels, ranging from 1.2 m^3/m to 22.5 m^3/m for the less (1-year RPH$_S$; no surge) and more intense (25-year RPH$_S$ and surge return period) storm forcing scenario, respectively (Figure 5.7b).

Similar to the results from the hydrodynamic forcing, morphological response represented by ΔEV_{dune} increases with higher water levels and to lesser extent with more intense wave forcing. The standard deviation of ΔEV_{dune} is 8.6 m^3/m for the same wave forcing conditions but varying water level scenarios. For varying wave conditions and the same water levels, the standard deviation is 2.3 m^3/m. This indicates that the influence of the water level variation to ΔEV_{dune} is ~ 4 times higher than the influence of the variation in wave forcing. As observed with the nearshore hydrodynamic variables, the baseline simulation with a 25-year RPH$_S$ and a

2.92 m maximum water level (including a 1-year return period surge) results in similar ΔEV_{dune} as the scenario with a 1-year RPH_S and 3.24 m storm surge (including a 25-year return period surge).

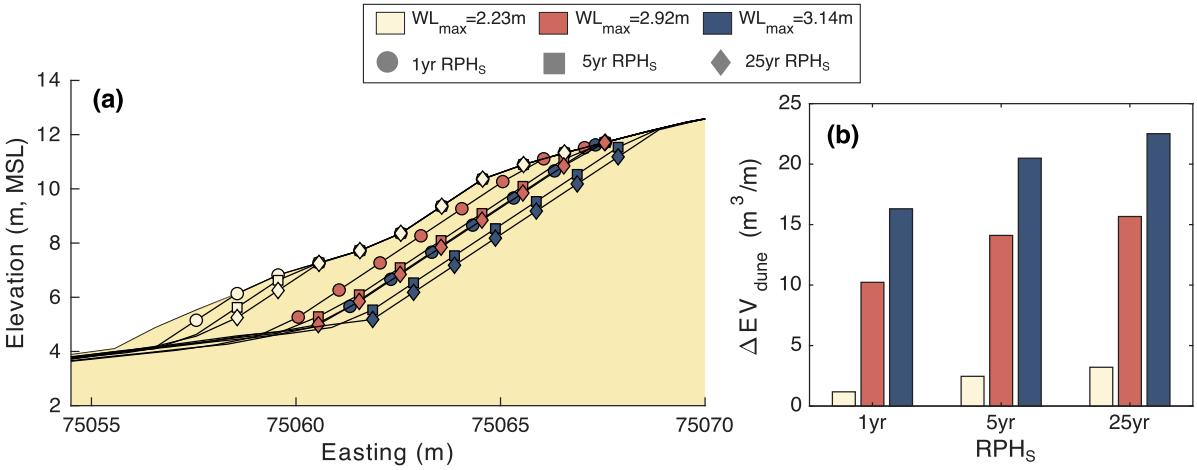

Figure 5.7 Dune erosion modelled in the baseline simulations. **(a)** Predicted post-storm profiles and **(b)** eroded dune volume (ΔEV_{dune}).

The incorporation of a range of different geological control configurations is shown to affect dune erosion, as determined by ΔEV_{dune} (Figure 5.8). Steeper sloping bedrock reliefs generally result in higher ΔEV_{dune} (Figure 5.8a). However, these changes are minor and don't exceed 2.1 m^3/m between the mildest (1:243) and steepest (1:205) slopes tested. Therefore, there is limited variability in ΔEV_{dune} between the different bedrock slopes. The influence of bedrock slope in erosional response also decreases as the storm forcing increases (Figure 5.8a).

The simulations with intertidal rock platforms and with rock outcrops indicate a clear variation in ΔEV_{dune} (Figure 5.8b, c). Differences in ΔEV_{dune} between the lowest and the highest cases for the rock platform and for the rock outcrop are 12.7 m^3/m and 11.6 m^3/m, respectively. This represents a variation in eroded volumes that is one order of magnitude higher when compared with the variation associated to the bedrock slope (~2 m^3/m). The variability between the different cases tested for the rock platform and the rock outcrop increases mostly with the water levels, and to a minor extent with the wave forcing conditions (Figure 5.8b, c). The largest variations in ΔEV_{dune} are observed for rock platforms and rock outcrops that are located 1 m above MSL or higher, which corresponds to elevations equal or above MHWN. When rock platforms or outcrops do not exceed this threshold the differences to the baseline simulation (Figure 5.8a) are minimal. The averaged morphological response to all forcing conditions

modelled indicates that rock platforms with a height of 2 m above MSL reduce ΔEV_{dune} by ~60%. For rock outcrops, a 1.5 m outcrop height reduces the averaged ΔEV_{dune} by 20% and a 2 m outcrop height up to 55% when compared to the baseline simulation.

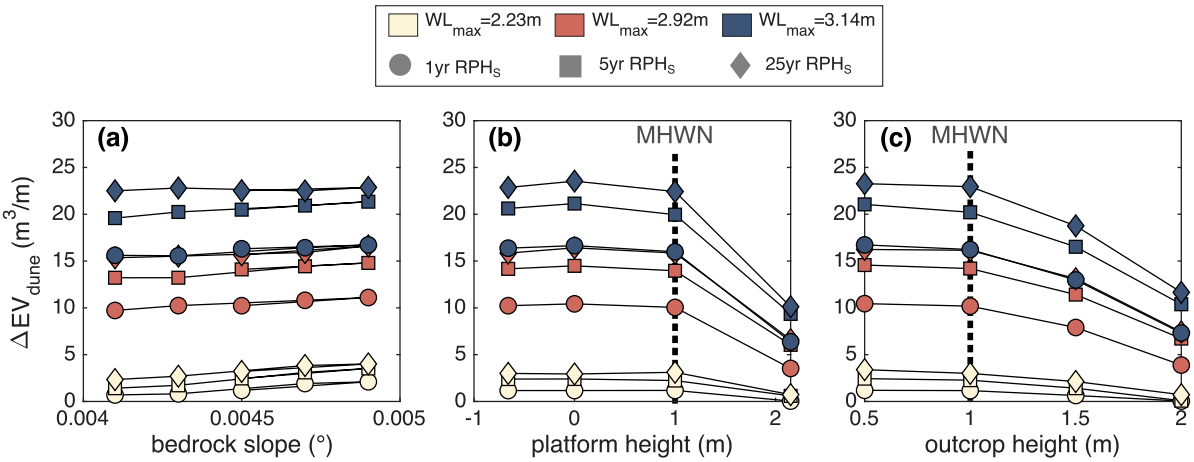

Figure 5.8 Geological control on eroded dune volumes. **(a)** ΔEV_{dune} for scenarios with varying bedrock slopes, including the baseline scenario (corresponding to the 0.0045° slope). **(b)** ΔEV_{dune} for scenarios with different intertidal rock platforms. **(c)** ΔEV_{dune} for scenarios with different intertidal rock outcrops. Mean High Water Neap (MHWN) water level is indicated as this is shown to correspond to threshold for reduction in dune erosion due to the presence of intertidal rocky features.

5.4 Discussion

5.4.1 Model Skill and Assumptions

It has been demonstrated that intertidal rock features, such as rocky reefs or submerged engineered structures, strongly influence nearshore hydrodynamics, leading to alongshore variability in morphological response (Bosserelle et al., 2021; Da Silva et al., 2023; Gallop et al., 2013; Segura et al., 2018). In this study, the absence of detailed nearshore bathymetric data prevented the 2D implementation of XBeach, which would be preferable to resolve alongshore variation in nearshore forcing and response. Therefore, a 1D simplified modeling approach was used. Modelling coastal processes in geomorphological complex settings has inherent limitations due to assumptions that are needed to simplify the description of the processes (Sherwood et al., 2022). However, calibrating key processes using field data as performed in this study supports the implementation of the model and allows to assess the outputs with higher confidence.

Using default XBeach values for key parameters related to wave transformation led to substantial overprediction of dune erosion (not shown). However, as demonstrated in this work, adjustment of wave dissipation across bedrock surfaces results in 'good' to 'excellent' model skill (as defined by Van Rijn et al., 2003), correctly reproducing the morphological changes in the cross-shore profiles used for validation (BSS > 0.72). The best performing values for the parameters calibrated in this study (f_w, γ and c_f) fall within the range of values reported in hydrodynamic studies of coral reef- (Drost et al., 2019; Pearson et al., 2017; Quataert et al., 2020) and rock-fronted (Bosserelle et al., 2021; McCall et al., 2017) coastlines using XBeach. The calibrated 1D model setup skilfully captured morphological changes along different profiles and, importantly, allowed to explore the key erosional responses in the cross-shore domain, which are more relevant due to the dominance of cross-shore hydrodynamics and sediment transport processes during storms (Masselink and van Heteren, 2014). Despite the limited range of conditions used for the calibration in the present study, the results provide further support to the use of XBeach for investigating storm impacts along rock-fronted barriers.

5.4.2 Control on Storm Response

The results obtained from the baseline and the scenario-based simulations of storm response with XBeach demonstrate that water level plays a dominant role in controlling the nearshore wave energy and the duration of storm wave impacts on dunes, while wave forcing has a relevant but secondary role. For the conditions modelled, the influence of the water level is 4 times greater than wave forcing on $E_{W,ub}$ and 2.5 times greater on $T_{impact,Dt}$. These ratios may even be underestimated, as higher RPH_S results in longer synthetic storm duration, which means that one additional high tide cycle is included in the 25-year RPH_S scenarios (Figure 5.5) and that should increase $E_{W,ub}$ for higher RPH_S scenarios.

The dominant control of water level on $E_{W,ub}$, which represents wave energy in the upper beach, can be attributed to the depth-limited and saturated surf zone (Sallenger and Holman, 1985; Thornton and Guza, 1982) in gently sloping nearshore environments (Marshall and Stephenson, 2011; e.g., Ogawa et al., 2015; Poate et al., 2018), such as those found in the Outer Hebrides barriers. In such environments, nearshore wave height is a linear function of local water depth, which is strongly modulated by tide and surge levels. A similar dominant role of water level on

$E_{W,ub}$ has been observed in reef-fronted coastlines (Costa et al., 2016; Zimmerman et al., 2024) and across rock platforms (Ogawa et al., 2011). However, wave transformation across sloping reef- and rock fronted coastlines is highly dependent on the site-specific nearshore bathymetry (Buckley et al., 2022; Lavaud et al., 2022; Poate et al., 2020; Savige et al., 2021), which can lead to variation in nearshore storm forcing.

As mentioned above, the influence of the water level is also dominant on $T_{impact,Dt}$, but less so than for $E_{W,ub}$ (Figure 5.6). This results from the fact that the duration of wave impacts above the dune toe is strongly dependent on wave-driven water level increases, which in gently sloping nearshores are largely governed by infragravity waves (e.g., Pearson et al., 2017; Thornton and Guza, 1982). On rock platforms, the extent to which infragravity wave energy can be transmitted to the shoreline is determined by the combined influence of offshore wave height, water level and platform width (Ogawa et al., 2015).

As demonstrated for $E_{W,ub}$, water level also has 4 times more influence than wave forcing on dune erosion, represented by ΔEV_{dune}. This suggests that wave energy in the upper beach may be a better indicator of dune erosion than impact time above the dune toe. A similar dominant role of water levels in morphological change has been observed in seasonal beach response at a rock-bounded platform beach in Portugal (Bastos et al., 2022) and at reef-fringed beaches in the Caribbean (Laigre et al., 2023) and Western Australia (Segura et al., 2018).

Simulation of the erosional response in the scenarios with gentler bedform slopes were associated with marginally lower dune erosion than steeper slopes, as hypothesised. This is consistent with findings of Cohn et al. (2019), that tested the influence of inner shelf (-50 m to -12 m) and nearshore (-12 m to 2 m) slopes on dune erosion using schematic profiles representative of dissipative beaches from the high wave energy Pacific Northwest coast of the USA. They found that steeper inner shelf slopes decrease erosion, but steeper nearshore slopes increase erosion and attributed this difference to competing influences of effects of infragravity, wave shoaling and breakpoint induced bound long waves. This distinction between inner shelf and nearshore also highlights that slope effects on beach erosion are dependent on the spatial setting considered in the analysis. Comparing the minor influence of bedrock slopes on storm response with the effects of intertidal rock platforms and outcrops, the results obtained for the various scenarios evidence that the most significant geological controls are restricted to the intertidal zone.

The average of all schematic profile configurations with varying geological controls shows only slightly reduced storm impacts (< 5 %), but importantly the presence of geological controls at

higher elevations of the intertidal zone can reduce dune erosion by up to 60 % compared to the baseline configuration. This indicates a shift in the primary control of storm response from the dynamic forcing (mostly related to water levels) to the geological control or to a combination between them (relative ratio between water levels and geological control elevation). This shift is only triggered when intertidal rock platform or outcrop height is above MHWN (1 m above MSL in the tested cases), which marks a threshold for effective geological control on storm response. Once this threshold is reached, the presence of geological controls is substantially more effective in reducing dune erosion, and this is valid for all tested storm scenarios.

The MHWN threshold is in line with critical thresholds for wave transmission over reef structures observed by Costa et al. (2016). They demonstrated that below a critical threshold of 2 m between the reef structure and the water level, transmitted waves are independent of the incident wave conditions (seaward of the structure) and hence less erosive. Similarly, a substantial reduction in eroded dune volumes is observed for scenarios were the difference between the maximum water level and the platform/outcrop height is less than 2 m. For example, in the scenario with a maximum water level of 3.14 m and a rock platform height of 2.15 m this difference is ~1 m and below the 2 m critical threshold for effective wave transmission resulting in reduced dune erosion. If the rock platform height is lowered to 1 m, the difference to the maximum water level becomes 2.14 m and above the critical water depth threshold, resulting in no significant reduction in dune erosion.

The strong control of the platform and outcrop height on dune erosion identified in this work is related to the dominant dynamic control of the water level in saturated nearshore environments. The intertidal geological control only becomes relevant in reducing erosional response when rock features are positioned at higher elevations, and thus restrict the control exerted by water level on the nearshore wave energy. Therefore, thresholds for geological control are dependent on the interaction between hydrodynamic forcing and nearshore morphology. This relationship will determine when and why the cross-shore geological controls are effective in reducing storm impacts along rock-fronted coastlines.

5.4.3 Implications for Coastal Management

Considering that sea levels are rising, the relative height of intertidal rock features in relation to MSL will change, potentially altering how geological controls impact barrier morphodynamics. Rock outcrops and platforms that are currently positioned around MHWN or above and provide effective protection for dunes, will eventually provide lower control on the

morphological response to storms as the background water level increases. This will enhance erosional response of dunes to storms and potentially force barriers to transgress over the bedrock surface if there is enough accommodation space landward or disintegrate if there are geological restrictions to the landward progression.

This has direct implications for coastal management in the Outer Hebrides and other areas where barriers and beaches are located in front or underlying rock surfaces. For the west coast of the Outer Hebrides, a sea level rise of up to 0.2 (0.5) m is predicted by 2050 (2100) for the high-emission RCP8.5 scenario (Fox-Kemper et al., 2021; Garner et al., 2021; Kopp et al., 2023). Thus, rock platforms and outcrops currently with an elevation of 1 m above MSL (corresponding to MHWN) will be at an equivalent elevation of 0.8 (0.5) m above MSL by 2050 (2100), leading to increased susceptibility to storm-induced dune erosion, as the protection offered by intertidal geological control is lowered by higher water levels. In similar depth-limited nearshore environments, this highlights potential limitations of using sub and intertidal rock structures as long-term nature-based solutions for adaptation of coastal areas to storms under higher sea levels.

5.5 Conclusion

The hydrodynamic and morphological response of geologically controlled sandy barriers to storms was analysed using the process-based numerical model XBeach 1D in surfbeat mode to assess the impact of different types and levels of cross-shore geological controls. Following the calibration and validation of the model setup, scenario-based simulations were performed with schematic cross-shore profiles with varying degrees of geological control, based on the natural morphological setting of the Outer Hebrides in NW Scotland, and a range of synthetic storm forcing conditions.

Results from the model calibration evidence the high sensitivity of storm-induced morphological changes to bed friction, highlighting the critical role of wave transformation processes over rock surfaces in accurately modelling storm impacts in geologically constrained barriers. Compared to the intensity of the wave forcing, variation in maximum water level, driven by storm surge magnitude, was found to have higher influence on both the amount of wave energy in the upper beach and the period during which the dune is exposed to wave impact, thereby determining the morphological response of the barrier. This dominant influence of water levels on storm response is explained by the coastal environmental setting, where a wide and shallow nearshore results in a saturated surfzone and depth-limited wave breaking

typical of rock- and reef-fronted coastlines. In such environments, the total storm energy at the upper beach is a better indicator of dune erosion than the impact time above the dune toe.

Changes in the subtidal bedrock slope were found to exert minimal control on storm responses, while intertidal rocky features can largely influence the magnitude of storm impacts. Intertidal rock platforms or outcrops can reduce dune erosional response by up to 60%, exerting a dominant control on barrier morphological change. The effectiveness on reducing storm erosion by intertidal rock features is determined by the difference between their elevation and the maximum water level. A difference of approximately 2 m is indicated as a critical threshold for reducing (or not) dune erosion. When differences are smaller(higher) than 2 m intertidal rock platforms or outcrops are effective (not effective) in reducing dune erosion. This threshold is consistent with effective wave transmission across fringing reefs and confirms that higher intertidal rock outcrops and platforms can limit the dominant role of hydrodynamic forcing in storm response.

Understanding and modelling the role of geological controls and their relation to storm forcing can be used as a tool for informing adaptation to sea level rise and management of geologically or structurally controlled barriers.

5.6 Supplementary Materials

5.6.1 Details of Model Calibration and Validation

In order to compare the observed and modelled wave heights, the water level (zs) and the root mean square wave height (H_{rms}) were obtained from XBeach at the same location as the pressure transducer with a frequency of 2 Hz. As there is a residual high frequency component in the zs spectrum in Xbeach, the zs output was converted to obtain the high-frequency (incident-band) zero-moment wave height component ($H_{m0,HF,zs}$). Prior to combining the $H_{m0,HF,zs}$and H_{rms} components, H_{rms} was converted to $H_{m0,HF,Hrms}$ by multiplying with a factor of 1.42. Finally, the high-frequency components were combined using Eq. 5.5 to obtain model outputs that are comparable to the pressure transducer observations.

$$H_{mo,HF,modelled} = \sqrt{H^2_{m0,HF,Hrms} + H^2_{m0,HF,zs}}, \quad (5.5)$$

Following the calibration of the model, it was validated by comparison of modelled and observed profiles from two alongshore adjacent profiles (P2 and P3) located within 300 m south of P1 (Figure 5.1b). The model predicted the dune erosion at P1 and the absence of any dune erosion at P2 and P3 with, in line with the observations (BSS > 0.72) (Figure 5.9, section 5.6.3).

5.6.2 Examples of Rock Platform and Rock Outcrop in the Intertidal Beach

Barriers in the Outer Hebrides are often fronted by intertidal rock platforms and outcrops of different shapes, sizes and elevations depending on the bedrock topography (Figure 5.10, section 5.6.3). This provides an ideal basis for schematising profiles with varying levels and types of geological control exerted by rocky features in the foreshore in order to test their influence on storm response.

5.6.3 Supplementary Figures

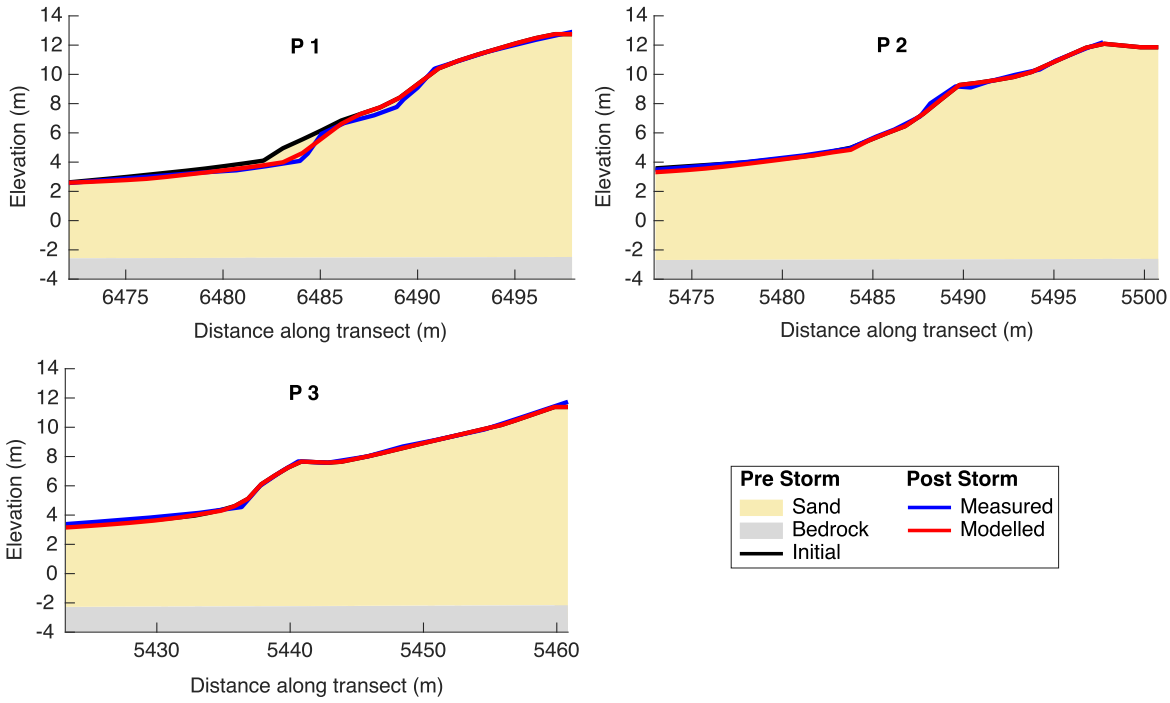

Figure 5.9 Validation of morphological changes modelled at the three profiles (P1-3).

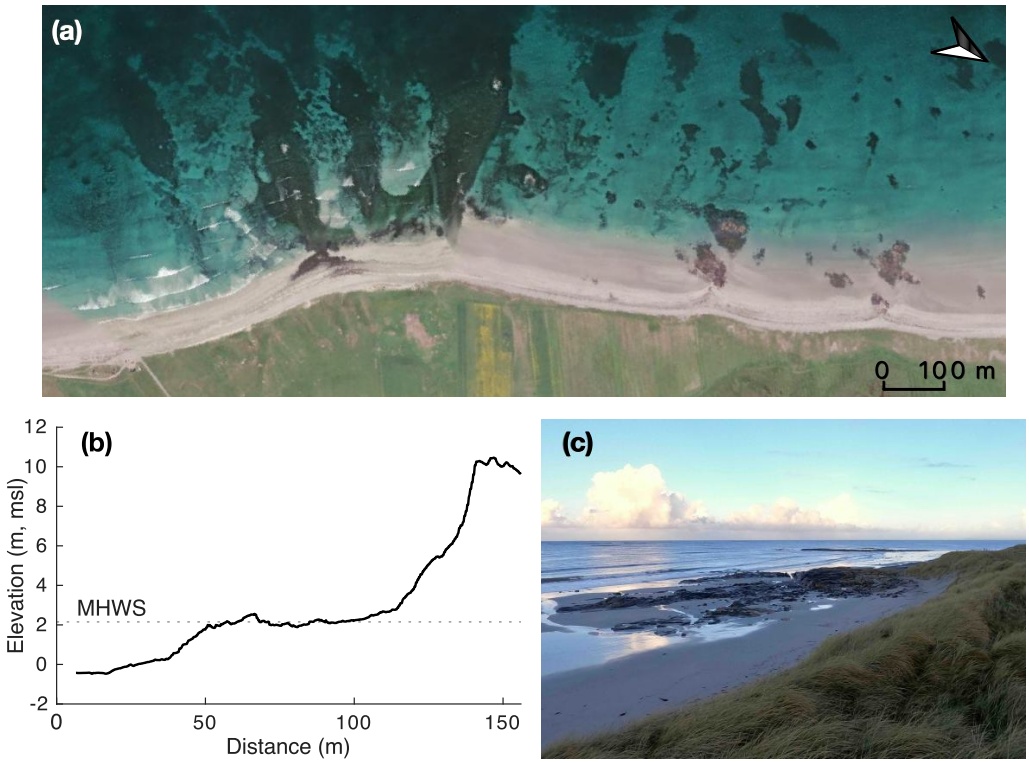

Figure 5.10 Examples of inter- and subtidal rock platforms and outcrops in the Outer Hebrides. **(a)** ESRI satellite image of a barrier showing a sandy barrier fronted by various intertidal rock features. **(b)** Example of a cross-shore profile with an intertidal rock platform that is positioned at ~ 2.1 m corresponding to Mean High Water Springs (MHWS). **(c)** Photograph of the example intertidal rock platform in (b).

5.7 Acknowledgements

Vincent Kümmerer receives funding for his Ph.D. through the Portuguese Foundation of Science and Technology (FCT) grant 2020.07497.BD and from the British Society for Geomorphology BSG-2022-30. This work was additionally supported by FCT, under the projects LA/P/00069/2020 (granted to the Associate Laboratory ARNET) and UID/00350/2020 CIMA.

5.8 Data Availability

XBeach is an open-source model that is made freely available by Deltares (https://oss.deltares.nl/web.xbeach/). Access to the wave data from the Outer Hebrides wave buoy is provided by CEFAS Wavenet (https://wavenet.cefas.co.uk). Wind speed data of the MIDAS weather station 18903 in South Uist are provided by the British Atmospheric Data Centre (BADC) through the CEDA Archive (https://data.ceda.ac.uk). Water level data recorded by the Stornoway gauge are available from the British Oceanographic Data Centre (BODC, https://www.bodc.ac.uk). The bathymetric data are provided by the European Marine Observation and Data Network (EMODnet) and can be accessed online (https://emodnet.ec.europa.eu/en).

5.9 References

Bastos, A.P., Taborda, R., Silva, A.N., Lira, C.P., Andrade, C., Calvão, J.M., 2022. A punctuated equilibrium model for storm response of geologically controlled beaches: Application to western Portuguese beaches. Geomorphology 404, 108184. https://doi.org/10.1016/j.geomorph.2022.108184

Bitterwolf, S.A., Reguero, B.G., Storlazzi, C.D., Beck, M.W., 2024. Shifting sands: The influence of coral reefs on shoreline erosion from short-term storm protection to long-term disequilibrium. Nature-Based Solutions 6, 100174. https://doi.org/10.1016/j.nbsj.2024.100174

Booij, N., Ris, R.C., Holthuijsen, L.H., 1999. A third-generation wave model for coastal regions: 1. Model description and validation. J. Geophys. Res. 104, 7649–7666. https://doi.org/10.1029/98JC02622

Bosserelle, C., Gallop, S.L., Haigh, I.D., Pattiaratchi, C.B., 2021. The Influence of Reef Topography on Storm-Driven Sand Flux. JMSE 9, 272. https://doi.org/10.3390/jmse9030272

Buckley, M.L., Lowe, R.J., Hansen, J.E., Van Dongeren, A.R., Pomeroy, A., Storlazzi, C.D., Rijnsdorp, D.P., Da Silva, R.F., Contardo, S., Green, R.H., 2022. Wave-Driven Hydrodynamic Processes Over Fringing Reefs With Varying Slopes, Depths, and Roughness: Implications for Coastal Protection. JGR Oceans 127, e2022JC018857. https://doi.org/10.1029/2022JC018857

Cohn, N., Ruggiero, P., García-Medina, G., Anderson, D., Serafin, K.A., Biel, R., 2019. Environmental and morphologic controls on wave-induced dune response. Geomorphology 329, 108–128. https://doi.org/10.1016/j.geomorph.2018.12.023

Cooper, J.A.G., Green, A.N., Loureiro, C., 2018. Geological constraints on mesoscale coastal barrier behaviour. Global and Planetary Change 168, 15–34. https://doi.org/10.1016/j.gloplacha.2018.06.006

Cooper, J.A.G., Jackson, D.W.T., Dawson, A.G., Dawson, S., Bates, C.R., Ritchie, W., 2012. Barrier islands on bedrock: A new landform type demonstrating the role of antecedent topography on barrier form and evolution. Geology 40, 923–926. https://doi.org/10.1130/G33296.1

Costa, M.B.S.F., Araújo, M., Araújo, T.C.M., Siegle, E., 2016. Influence of reef geometry on wave attenuation on a Brazilian coral reef. Geomorphology 253, 318–327. https://doi.org/10.1016/j.geomorph.2015.11.001

Da Silva, R.F., Hansen, J.E., Lowe, R.J., Rijnsdorp, D.P., Buckley, M.L., 2023. Dynamics of the Wave-Driven Circulation in the Lee of Nearshore Reefs. JGR Oceans 128, e2022JC019013. https://doi.org/10.1029/2022JC019013

Dean, R.G., 1991. Equilibrium Beach Profiles: Characteristics and Applications. Journal of Coastal Research 7.

Dissanayake, P., Yates, M.L., Suanez, S., Floc'h, F., Krämer, K., 2021. Climate Change Impacts on Coastal Wave Dynamics at Vougot Beach, France. JMSE 9, 1009. https://doi.org/10.3390/jmse9091009

Drost, E.J.F., Cuttler, M.V.W., Lowe, R.J., Hansen, J.E., 2019. Predicting the hydrodynamic response of a coastal reef-lagoon system to a tropical cyclone using phase-averaged and surfbeat-resolving wave models. Coastal Engineering 152, 103525. https://doi.org/10.1016/j.coastaleng.2019.103525

EMODnet Bathymetry Consortium, 2022. EMODnet Digital Bathymetry.

Fanti, V., Loureiro, C. and Ferreira, Ó., 2025. Development of topo-bathymetric continuum profiles for coastal barriers with global open-access data.

Fellowes, T.E., Vila-Concejo, A., Gallop, S.L., Harley, M.D., Short, A.D., 2022. Wave shadow zones as a primary control of storm erosion and recovery on embayed beaches. Geomorphology 399, 108072. https://doi.org/10.1016/j.geomorph.2021.108072

Fox-Kemper, B., H.T. Hewitt, C. Xiao, G. Aðalgeirsdóttir, S.S. Drijfhout, T.L. Edwards, N.R. Golledge, M. Hemer, R.E. Kopp, G. Krinner, A. Mix, D. Notz, S. Nowicki, I.S. Nurhati, L. Ruiz, J.-B. Sallée, A.B.A. Slangen, and Y. Yu, 2021: Ocean, Cryosphere and Sea Level Change. In Climate Change 2021: The Physical Science Basis. Contribution of Working Group I to the Sixth Assessment Report of the Intergovernmental Panel on Climate Change [Masson-Delmotte, V., P. Zhai, A. Pirani, S.L. Connors, C. Péan, S. Berger, N. Caud, Y. Chen, L. Goldfarb, M.I. Gomis, M. Huang, K. Leitzell, E. Lonnoy, J.B.R. Matthews, T.K. Maycock, T. Waterfield, O. Yelekçi, R. Yu, and B. Zhou (eds.)]. Cambridge University Press, Cambridge, United Kingdom and New York, NY, USA, pp. 1211–1362, doi:10.1017/9781009157896.011.

Gallop, S.L., Bosserelle, C., Eliot, I., Pattiaratchi, C.B., 2013. The influence of coastal reefs on spatial variability in seasonal sand fluxes. Marine Geology 344, 132–143. https://doi.org/10.1016/j.margeo.2013.07.016

Gallop, S.L., Bosserelle, C., Eliot, I., Pattiaratchi, C.B., 2012. The influence of limestone reefs on storm erosion and recovery of a perched beach. Continental Shelf Research 47, 16–27. https://doi.org/10.1016/j.csr.2012.08.001

Gallop, S.L., Kennedy, D.M., Loureiro, C., Naylor, L.A., Muñoz-Pérez, J.J., Jackson, D.W.T., Fellowes, T.E., 2020. Geologically controlled sandy beaches: Their geomorphology, morphodynamics and classification. Science of The Total Environment 731, 139123. https://doi.org/10.1016/j.scitotenv.2020.139123

Garner, G. G., T. Hermans, R. E. Kopp, A. B. A. Slangen, T. L. Edwards, A. Levermann, S. Nowikci, M. D. Palmer, C. Smith, B. Fox-Kemper, H. T. Hewitt, C. Xiao, G. Aðalgeirsdóttir, S. S. Drijfhout, T. L. Edwards, N. R. Golledge, M. Hemer, G. Krinner, A. Mix, D. Notz, S. Nowicki, I. S. Nurhati, L. Ruiz, J-B. Sallée, Y. Yu, L. Hua, T. Palmer, B. Pearson, 2021. IPCC AR6 Sea Level Projections. Version 20210809. Dataset accessed 2025-01-22 at https://doi.org/10.5281/zenodo.5914709.

Jackson, D.W.T., Cooper, J.A.G., del Rio, L., 2005. Geological control of beach morphodynamic state. Marine Geology 216, 297–314. https://doi.org/10.1016/j.margeo.2005.02.021

Karimpour, A., Chen, Q., 2017. Wind wave analysis in depth limited water using OCEANLYZ, A MATLAB toolbox. Computers & Geosciences 106, 181–189. https://doi.org/10.1016/j.cageo.2017.06.010

Kenyon, N.H., Pelton, C.D., 1979. Seabed conditions west of the Outer Hebrides (No. 95). Institute of Oceanographic Sciences, Godalming, Surrey, UK.

Kopp, R. E., Garner, G. G., Hermans, T. H. J., Jha, S., Kumar, P., Reedy, A., Slangen, A. B. A., Turilli, M., Edwards, T. L., Gregory, J. M., Koubbe, G., Levermann, A., Merzky, A., Nowicki, S., Palmer, M. D., & Smith, C. (2023). The Framework for Assessing Changes To Sea-Level (FACTS) v1.0: A platform for characterizing parametric and structural uncertainty in future global, relative, and extreme sea-level change. Geoscientific Model Development, 16, 7461–7489. https://doi.org/10.5194/gmd-16-7461-2023

Kümmerer, V., Ferreira, Ó., Fanti, V., Loureiro, C., 2024. Storm identification for high-energy wave climates as a tool to improve long-term analysis. Clim Dyn 62, 2207–2226. https://doi.org/10.1007/s00382-023-07017-w

Kümmerer, V., Loureiro, C., Ferreira, Ó., 2023. Muted morphological response to extreme storms in geologically controlled barrier islands, in: Coastal Sediments 2023. Presented at the Coastal Sediments 2023, WORLD SCIENTIFIC, New Orleans, LA, USA, pp. 44–56. https://doi.org/10.1142/9789811275135_0005

Kümmerer V., Ferreira Ó., Loureiro, C. (2025). Distinct shoreline behaviour along storm-dominated and geologically controlled coastal barriers. Earth Surf Processes Landf 50, e70042. https://doi.org/10.1002/esp.70042.

Laigre, T., Balouin, Y., Villarroel-Lamb, D., De La Torre, Y., 2023. Seasonal to Multi-Decadal Shoreline Change on a Reef-Fringed Beach. Coasts 3, 240–262. https://doi.org/10.3390/coasts3030015

Lavaud, L., Bertin, X., Martins, K., Pezerat, M., Coulombier, T., Dausse, D., 2022. Wave Dissipation and Mean Circulation on a Shore Platform Under Storm Wave Conditions. JGR Earth Surface 127, e2021JF006466. https://doi.org/10.1029/2021JF006466

Lobeto, H., Semedo, A., Lemos, G., Dastgheib, A., Menendez, M., Ranasinghe, R., Bidlot, J.-R., 2024. Global coastal wave storminess. Sci Rep 14, 3726. https://doi.org/10.1038/s41598-024-51420-0

Loureiro, C., Ferreira, O., Cooper, J.A.G., 2014. Non-uniformity of storm impacts on three high-energy embayed beaches. Journal of Coastal Research 70, 326–331. https://doi.org/10.2112/SI70-055.1

Loureiro, C., Ferreira, Ó., Cooper, J.A.G., 2013. Applicability of parametric beach morphodynamic state classification on embayed beaches. Marine Geology 346, 153–164. https://doi.org/10.1016/j.margeo.2013.09.005

Loureiro, C., Ferreira, Ó., Cooper, J.A.G., 2012. Geologically constrained morphological variability and boundary effects on embayed beaches. Marine Geology 329–331, 1–15. https://doi.org/10.1016/j.margeo.2012.09.010

MacMahan, J., Thornton, E., Dressel, S., Cook, M., 2024. Intermediate Wave Scale Rocky Bottom Variability for the Nearshore Along California. Earth and Space Science 11, e2023EA003475. https://doi.org/10.1029/2023EA003475

Marshall, R.J.E., Stephenson, W.J., 2011. The morphodynamics of shore platforms in a micro-tidal setting: Interactions between waves and morphology. Marine Geology 288, 18–31. https://doi.org/10.1016/j.margeo.2011.06.007

Masselink, G., Beetham, E., Kench, P., 2020. Coral reef islands can accrete vertically in response to sea level rise. Sci. Adv. 6, eaay3656. https://doi.org/10.1126/sciadv.aay3656

Masselink, G., McCall, R., Beetham, E., Kench, P., Storlazzi, C., 2021. Role of Future Reef Growth on Morphological Response of Coral Reef Islands to Sea-Level Rise. JGR Earth Surface 126, e2020JF005749. https://doi.org/10.1029/2020JF005749

Masselink, G., van Heteren, S., 2014. Response of wave-dominated and mixed-energy barriers to storms. Marine Geology 352, 321–347. https://doi.org/10.1016/j.margeo.2013.11.004

McCall, R., Masselink, G., Austin, M., Poate, T., Jager, T., 2017. Modelling indicent-band and infragravity wave dynamics on rock shore platforms. Coastal Dynamics.

McCarroll, R.J., Masselink, G., Valiente, N.G., Scott, T., Wiggins, M., Kirby, J.-A., Davidson, M., 2021. A rules-based shoreface translation and sediment budgeting tool for estimating coastal change: ShoreTrans. Marine Geology 435, 106466. https://doi.org/10.1016/j.margeo.2021.106466

McIntire, W.G., Walker, H.J., 1964. Tropical cyclones and coastal morphology in Mauritius. Annals of the Association of American Geographers 54, 582–596. https://doi.org/10.1111/j.1467-8306.1964.tb01786.x

Muñoz-Perez, J.J., Medina, R., 2010. Comparison of long-, medium- and short-term variations of beach profiles with and without submerged geological control. Coastal Engineering 57, 241–251. https://doi.org/10.1016/j.coastaleng.2009.09.011

Nawarat, K., Reyns, J., Vousdoukas, M.I., Duong, T.M., Kras, E., Ranasinghe, R., 2024. Coastal hardening and what it means for the world's sandy beaches. Nat Commun 15, 10626. https://doi.org/10.1038/s41467-024-54952-1

Ogawa, H., Dickson, M.E., Kench, P.S., 2015. Hydrodynamic constraints and storm wave characteristics on a sub-horizontal shore platform. Earth Surf Processes Landf 40, 65–77. https://doi.org/10.1002/esp.3619

Ogawa, H., Dickson, M.E., Kench, P.S., 2011. Wave transformation on a sub-horizontal shore platform, Tatapouri, North Island, New Zealand. Continental Shelf Research 31, 1409–1419. https://doi.org/10.1016/j.csr.2011.05.006

Pearson, S.G., Storlazzi, C.D., Van Dongeren, A.R., Tissier, M.F.S., Reniers, A.J.H.M., 2017. A Bayesian-Based System to Assess Wave-Driven Flooding Hazards on Coral Reef-Lined Coasts. JGR Oceans 122, 10099–10117. https://doi.org/10.1002/2017JC013204

Pile, J., Cooper, J.A.G., Jackson, D.W.T., 2019. Stratigraphy and internal structure of wind-dominated barrier islands (dune and machair) of the Outer Hebrides, Scotland. Earth Surf. Process. Landforms 44, 1482–1493. https://doi.org/10.1002/esp.4579

Poate, T., Masselink, G., Austin, M.J., Dickson, M., McCall, R., 2018. The Role of Bed Roughness in Wave Transformation Across Sloping Rock Shore Platforms: Bed roughness on wave transformation. J. Geophys. Res. Earth Surf. 123, 97–123. https://doi.org/10.1002/2017JF004277

Poate, T., Masselink, G., Austin, M.J., Inch, K., Dickson, M., McCall, R., 2020. Infragravity wave generation on shore platforms: Bound long wave versus breakpoint forcing. Geomorphology 350, 106880. https://doi.org/10.1016/j.geomorph.2019.106880

Portch, C.E., Cuttler, M.V.W., Buckley, M.L., Hansen, J.E., Lowe, R.J., 2023. Wave runup and inundation dynamics on a perched beach. Geomorphology 435, 108751. https://doi.org/10.1016/j.geomorph.2023.108751

Quataert, E., Storlazzi, C., Van Dongeren, A., McCall, R., 2020. The importance of explicitly modelling sea-swell waves for runup on reef-lined coasts. Coastal Engineering 160, 103704. https://doi.org/10.1016/j.coastaleng.2020.103704

Ris, R.C., Holthuijsen, L.H., Booij, N., 1999. A third-generation wave model for coastal regions: 2. Verification. J. Geophys. Res. 104, 7667–7681. https://doi.org/10.1029/1998JC900123

Roelvink, D., Reniers, A., van Dongeren, A., van Thiel de Vries, J., McCall, R., Lescinski, J., 2009. Modelling storm impacts on beaches, dunes and barrier islands. Coastal Engineering 56, 1133–1152. https://doi.org/10.1016/j.coastaleng.2009.08.006

Roelvink, J.A., 1993. Dissipation in random wave groups incident on a beach. Coastal Engineering 19, 127–150. https://doi.org/10.1016/0378-3839(93)90021-Y

Ruessink, B.G., Miles, J.R., Feddersen, F., Guza, R.T., Elgar, S., 2001. Modeling the alongshore current on barred beaches. J. Geophys. Res. 106, 22451–22463. https://doi.org/10.1029/2000JC000766

Sallenger, A.H., Holman, R.A., 1985. Wave energy saturation on a natural beach of variable slope. J. Geophys. Res. 90, 11939–11944. https://doi.org/10.1029/JC090iC06p11939

Salmon, J.E., Holthuijsen, L.H., Zijlema, M., van Vledder, G.Ph., Pietrzak, J.D., 2015. Scaling depth-induced wave-breaking in two-dimensional spectral wave models. Ocean Modelling 87, 30–47. https://doi.org/10.1016/j.ocemod.2014.12.011

Santo, H., Taylor, P.H., Woollings, T., Poulson, S., 2015. Decadal wave power variability in the North-East Atlantic and North Sea. Geophys. Res. Lett. 42, 4956–4963. https://doi.org/10.1002/2015GL064488

Savige, T.R., Kowalczyk, H.E.L., Fellowes, T.E., Kennedy, D.M., 2021. The role of seaward morphology on wave transformation onto and across a microtidal shore platform. Continental Shelf Research 224, 104472. https://doi.org/10.1016/j.csr.2021.104472

Segura, L.E., Hansen, J.E., Lowe, R.J., 2018. Seasonal Shoreline Variability Induced by Subtidal Water Level Fluctuations at Reef-Fringed Beaches. JGR Earth Surface 123, 433–447. https://doi.org/10.1002/2017JF004385

Sherwood, C.R., Van Dongeren, A., Doyle, J., Hegermiller, C.A., Hsu, T.-J., Kalra, T.S., Olabarrieta, M., Penko, A.M., Rafati, Y., Roelvink, D., Van Der Lugt, M., Veeramony, J., Warner, J.C., 2022. Modeling the Morphodynamics of Coastal Responses to Extreme

Events: What Shape Are We In? Annu. Rev. Mar. Sci. 14, 457–492. https://doi.org/10.1146/annurev-marine-032221-090215

Short, A.D., 2010. Role of geological inheritance in Australian beach morphodynamics. Coastal Engineering 57, 92–97. https://doi.org/10.1016/j.coastaleng.2009.09.005

Suanez, S., Cariolet, J.-M., Cancouët, R., Ardhuin, F., Delacourt, C., 2012. Dune recovery after storm erosion on a high-energy beach: Vougot Beach, Brittany (France). Geomorphology 139–140, 16–33. https://doi.org/10.1016/j.geomorph.2011.10.014

Syvitski, J., Ángel, J.R., Saito, Y., Overeem, I., Vörösmarty, C.J., Wang, H., Olago, D., 2022. Earth's sediment cycle during the Anthropocene. Nat Rev Earth Environ 3, 179–196. https://doi.org/10.1038/s43017-021-00253-w

Taborda, R., Ribeiro, M.A., 2015. A simple model to estimate the impact of sea-level rise on platform beaches. Geomorphology 234, 204–210. https://doi.org/10.1016/j.geomorph.2015.01.015

Thornton, E.B., Guza, R.T., 1982. Energy saturation and phase speeds measured on a natural beach. J. Geophys. Res. 87, 9499–9508. https://doi.org/10.1029/JC087iC12p09499

Trenhaile, A.S., 2004. Modeling the accumulation and dynamics of beaches on shore platforms. Marine Geology 206, 55–72. https://doi.org/10.1016/j.margeo.2004.03.013

Van Rijn, L.C., Walstra, D.J.R., Grasmeijer, B., Sutherland, J., Pan, S., Sierra, J.P., 2003. The predictability of cross-shore bed evolution of sandy beaches at the time scale of storms and seasons using process-based Profile models. Coastal Engineering 47, 295–327. https://doi.org/10.1016/S0378-3839(02)00120-5

Velegrakis, A.F., Trygonis, V., Chatzipavlis, A.E., Karambas, Th., Vousdoukas, M.I., Ghionis, G., Monioudi, I.N., Hasiotis, Th., Andreadis, O., Psarros, F., 2016. Shoreline variability of an urban beach fronted by a beachrock reef from video imagery. Nat Hazards 83, 201–222. https://doi.org/10.1007/s11069-016-2415-9

Xu, D., Yan, Y., Wang, X., Qin, Y., 2023. Numerical modelling of the physical response of coral reef Sandy island to sea level rise by considering seasonal patterns. Ocean & Coastal Management 245, 106860. https://doi.org/10.1016/j.ocecoaman.2023.106860

Yao, Y., Li, Z., Zhao, Z., Chen, L., Zhou, B., Han, X., 2025. Study on the morphodynamic response of reef flat with moveable bed to monochromatic waves. Marine Geology 107479. https://doi.org/10.1016/j.margeo.2025.107479

Zimmerman, Z.D., Mulligan, R.P., Storlazzi, C.D., 2024. Hurricane wave energy dissipation and wave-driven currents over a fringing reef. Coral Reefs. https://doi.org/10.1007/s00338-024-02604-7

Chapter 6

Concluding Remarks

Research on the morphological responses of coastal barriers to storms has been typically based on unconstrained and low to medium wave energy coasts. As such, geologically controlled barriers exposed to high wave energy conditions are poorly understood and much remains to be explored to enhance our understanding of storm processes and impacts along such coastlines. The main aim of this work was to assess the relative importance of geological controls on storm processes and impacts in high wave energy coastal barriers. To address this, the analysis framework ranged from large scale offshore storm characterisation to local scale beach morphodynamic processes investigation. This was performed using the Outer Hebrides barrier islands as a case study, and using a wide range of datasets and approaches, including records from monitoring stations and data from climate models, field surveys and observations, satellite imagery analysis and process-based modelling.

Assessing coastal processes and impacts requires the identification and characterisation of storm events that drive coastal morphological impacts. However, thresholds and parameters to define storms are not consistently defined, and in this work, it was found that the identification and characterisation of independent storms in high wave energy coasts differs from those in low to medium wave energy coasts. This led to the development of a storm identification algorithm better suited to energetic storm-dominated environments. The algorithm developed proposes the use of statistically defined criteria to identify independent storms, consistent with regional meteorological processes and timescales. This consistency is particularly important when assessing long-term trends in storminess, as links to the driving meteorological and climate dynamics can improve the predictability of future storms and, thus, of the associated storm impacts. The application of the storm identification algorithm to multidecadal wave reanalysis datasets for the western coast of Scotland, a high-energy coast located in the North

Atlantic storm track, allowed to identify a statistically significant long-term of increasing storm duration, which results in increased storm wave power impacting this coastline.

Quantifying long-term to storm-induced coastal changes often requires a detailed definition of shoreline proxies that are suitable for the area and timescale of interest. However, the combination of very low gradient beach face and large tidal ranges strongly affects the accuracy of widely used shoreline detection algorithms based on waterline indicators. Therefore, the investigation of shoreline changes along the Outer Hebrides barriers relied on the development of a tailored approach that takes advantage of the increasing availability and resolution of satellite imagery. The key elements of the approach implemented were the use of the vegetation line as a shoreline change indicator and the subdivision of the barriers into shorter alongshore sections. These were restricted to the upper beach and vegetated foredune, allowing accurate semi-automatic shoreline delineation. These adjustments resulted in precise satellite-derived shoreline change detection, extending the use of satellite imagery to the study of the morphological evolution of barriers in meso- to macrotidal high-energy coastlines at different time scales (from days to years). A novel framework for incorporating the type of geological control in the configuration of the foreshore into the assessment of shoreline change was also proposed. This revealed that the shoreline change behaviour depends not only on the hydrodynamic forcing mechanisms and the morphology of the barrier, but also on the presence of exposed subtidal to intertidal bedrock surfaces in front of the barrier, with the sediment availability controlling the contemporary shoreline evolution along these sediment-limited coasts.

Results from a field investigation during extreme storm wave conditions that impacted the high-energy barriers of the Outer Hebrides showed a generally muted morphological storm response. Exploratory nearshore wave modelling has also shown that wave dissipation over shallow bedrock surfaces can be significant and therefore control the amount of wave energy reaching the shoreline. This indicated that these high-energy geologically controlled barriers are generally attuned to extreme waves and that a better understanding on the combined role of waves, water levels and coastal geomorphology is required. The correlation of shoreline changes with storm events characterised by both extreme water levels (spring tide plus storm surge) and energetic wave conditions highlights that relevant storm impacts (dune retreat and overwash) only occur when both factors occur simultaneously. In addition, process-based

modelling of the storm response to different forcing conditions with XBeach demonstrated that the variation of the maximum water level driven by the storm surge had a greater influence in determining the morphological barrier response compared to changes on the intensity of the wave forcing. The critical influence of water levels on storm response was considered to be the result of the saturated surfzone environment typical of shallow rocky and reef-fronted coastlines. The morphodynamic modelling also showed that intertidal rocky features such as platforms or outcrops can effectively reduce storm induced dune erosion. However, simulations of different intertidal geological controls and hydrodynamic storm conditions revealed the existence of a critical threshold, related to the vertical difference between total water level and the elevation of the rock surface. Crossing this threshold leads to a shift in the barrier response, changing from being dominated by changes in hydrodynamic forcing to being dominated by geological controls. As this threshold is based on the difference between water levels and intertidal rock features, this may have implications for the coastal management of geologically controlled barriers under sea level rise scenarios.

Overall, the results presented in this thesis demonstrate that non-dynamic geological controls mediate, and in some cases dominate, the storm-induced barrier response on sediment-limited and geologically constrained barriers, contrarily to the observations for sediment rich environments where the contemporary morphological evolution of the barriers is primarily driven by the interaction between hydrodynamic forcing and mobile sediment. This suggests that consideration of variable geological controls, such as the presence of bedrock surfaces and local sediment availability, may improve our understanding of shoreline variability along coastal barriers fronted by topographically complex nearshore environments.

In a changing climate and particularly with sea level rising, the response of coastal barriers to storms in high-energy geologically constrained environments may change, as the severity of storm impacts is highly dependent on water level and the rocky surfaces that determine the geological control will remain at the same elevation. Further research on storm impact thresholds, incorporating the combined effect of future wave and water level conditions, could lead to a better understanding of future trajectories of barrier evolution in high-energy geologically constrained environments and, particularly, on the changes to storm impacts in the future. Additional process-based modelling of storm-induced morphodynamic processes in geologically constrained coasts could lead to the development or adaptation of model

parameters to better integrate the influence of geological controls, thereby contributing to a better understanding of barrier morphodynamics in mixed rock and sedimentary coasts. The quantification of the difference between geologically constrained and unconstrained barriers can be used to develop new resilience concepts adapted to these complex coasts, which is essential to improve their future management.